

Modulation of Piezo1 by lipids and synthetic small-molecules

Adam James Hyman

Submitted in accordance with the requirements for the degree of
Doctor of Philosophy

The University of Leeds
School of Biomedical Sciences

February 2018

The candidate confirms that the work submitted is his own and that appropriate credit has been given where reference has been made to the work of others.

This copy has been supplied on the understanding that it is copyright material and that no quotation from the thesis may be published without proper acknowledgement.

The right of Adam James Hyman to be identified as Author of this work has been asserted by him in accordance with the Copyright, Designs and Patents Act 1988.

© 2018 The University of Leeds and Adam James Hyman.

Acknowledgements

I would like to thank my supervisor, Professor David Beech, for his support, guidance and motivation throughout my PhD. There have been some tough times during the last few years, from lab work to needing crutches, but he has always managed to get the best out of me. I would also like to thank my co-supervisors Dr. Lin-Hua Jiang and Dr. Jing Li for their assistance throughout my PhD.

I would like to thank Beech lab members for their support. Particularly Dr Melanie Ludlow for her help with molecular biology.

I would like to thank Antreas Kalli for his work on the molecular dynamic simulations.

Many thanks to the BBSRC for their generous funding to enable me to undertake this research.

I would like to thank Dr. Peter Webster, Dr. Nick Moss, Dr. Baptiste Rode, Hannah Gaunt, Nicola Blythe, Elizabeth Evans and Katie Musialowski who have helped make this PhD a great experience.

Everyone involved with Leeds Medics and Dentist RUFC who I have shared some great experiences off and on the rugby pitch. The cold and wet away games in the middle of nowhere really helped to refresh the mind. A particular mention to Josh Janvier for thinking he could lift more than me (pre-injury).

My family for their love, support and encouragement in everything I do.

I would especially like to thank Rachel for her love and support throughout my PhD and her help getting me back on my feet so I could complete this PhD.

Abstract

Regulation of Ca²⁺ entry plays important roles in cardiovascular physiology and pathophysiology. Understanding how these processes are altered in pathophysiological states and designing drugs to target Ca²⁺ entry into cells may provide avenues for developing new therapeutic strategies for cardiovascular disease, such as atherosclerosis. The overall aim of this study was to identify mechanisms of regulating the Ca²⁺ permeable ion channel Piezo1 by lipids and synthesised small molecules.

Piezo1 proteins form mechanosensitive non-selective cation channels that have been shown to have important roles in vascular development, endothelial shear stress sensing and regulation of vascular tone. In this study, the impact of cholesterol on Piezo1 was investigated because it is a risk factor in cardiovascular diseases and an important membrane constituent. Piezo1-mediated calcium entry was inhibited by addition and depletion of cholesterol from cell membranes. Cholesterol interaction sites were found within the structure of Piezo1. Mutating these interaction sites reduced Piezo1 sensitivity to cholesterol addition. The data suggest previously unrecognised mechanisms of Piezo1 regulation by cholesterol through interaction sites.

Sphingolipids form a diverse class of signalling lipids. Production of sphingolipids can occur by activation of sphingomyelinase which often occurs in response to inflammatory stimuli, infection or cell stress. Here sphingomyelinase activity is shown to potentiate activation of endothelial Piezo1 by Yoda1, a chemical activator of Piezo1. The mechanism of potentiation occurred through production of sphingosine and subsequent inhibition of protein kinase C, activation of phospholipase C and activation of protein kinase D. These data suggest

endothelial Piezo1 activity may be modulated by inflammatory mediators which may have major roles in cardiovascular disease.

Targeting Piezo1 pharmacologically may provide treatments for diseases in the future. Modifying the activator of Piezo1, Yoda1, revealed a novel activator of Piezo1 with desirable characteristics for compound development.

In summary, this research developed new knowledge and hypotheses about modulation of Piezo1 by lipids and novel small-molecules which may provide better understanding of cardiovascular disease and new treatment strategies.

Table of Contents

Acknowledgements	ii
Abstract	iii
Table of Contents	v
List of Tables	ix
List of Figures	x
List of Publications and Communications	xiii
Abbreviations	xv
Chapter 1 Introduction	1
1.1 Cardiovascular System	1
1.2 Cardiovascular disease	3
1.2.1 Atherosclerosis	4
1.2.2 Ca ²⁺ in atherosclerosis	8
1.3 Ca ²⁺ signalling in the cardiovascular system	9
1.3.1 Ion channels	11
1.3.2 Intracellular Ca ²⁺ release and uptake mechanisms	14
1.3.3 Mechanism of Ca ²⁺ extrusion	14
1.4 Cholesterol regulation of ion channels	16
1.4.1 Mechanisms of cholesterol regulation of ion channels	17
1.4.2 Hypercholesterolaemia and ion channels	20
1.5 Sphingolipid metabolism and signalling	22
1.5.1 Metabolism of Sphingolipids	24
1.5.2 Subcellular compartmentalisation of sphingolipids	25
1.5.3 Sphingolipids as signalling molecules	26
1.5.4 Sphingomyelinases in the cardiovascular system	33
1.7 Piezo1	38
1.7.1 Structure	38
1.7.2 Activation of Piezo1	41
1.7.3 Biophysical properties of Piezo1 ion channel	42
1.7.4 Modulation of Piezo1 activity	45
1.7.5 Functional roles of Piezo1	51
1.7.6 Piezo1 in disease	59
1.8 Aims of the study	62

Chapter 2 Methods and materials	64
2.1 Cell lines and cell culture.....	64
2.1.1 Human Umbilical Vein Endothelial Cells.....	64
2.1.2 Piezo1 tetracycline inducible HEK293 cell line	64
2.1.3 TRPC5 tetracycline inducible HEK293 cell line	64
2.1.4 TRPC4 β tetracycline inducible HEK293 cell line	65
2.1.5 HEK TREx.....	65
2.1.6 Chinese Hamster Ovary cells stably expressing TRPV4	65
2.2 Ionic solutions	66
2.2.1 Dulbecco's Phosphate-Buffered Saline	66
2.2.2 Standard bath solution	66
2.3 Chemical reagents	66
2.3.1 Yoda1 analogues	66
2.4 Cell transfection.....	68
2.5 Molecular Biology techniques	68
2.5.1 DNA constructs	68
2.5.2 Mutagenesis.....	68
2.5.3 Preparation of plasmid DNA	70
2.6 Intracellular Ca ²⁺ measurement.....	72
2.6.1 FlexStation 3	72
2.6.2 Single-cell imaging	75
2.7 Shear stress	76
2.7.1 Cell alignment analysis.....	77
2.8 Cholesterol treatment	79
2.9 Live/Dead cytotoxicity assay	79
2.10 Bioinformatics.....	81
2.11 Computational modelling	81
2.12 Statistical analysis	82
Chapter 3 Regulation of Piezo1 by cholesterol	84
3.1 Introduction	84
3.2 Aims	86
3.3 Results	87
3.3.1 Cholesterol inhibits shear stress-evoked Ca ²⁺ influx.....	87
3.3.2 Exogenous cholesterol inhibits Yoda1 response in HUVECs.....	89

3.3.3	Depletion of cholesterol reduces Yoda1 response in HUVECs.....	91
3.3.4	Exogenous cholesterol reduces Yoda1 response in Piezo1 overexpression system.....	94
3.3.5	Depletion of cholesterol reduces Yoda1 response in Piezo1 overexpression system.....	96
3.3.6	Predicting cholesterol binding sites	98
3.3.7	Computational modelling of Piezo1/cholesterol interactions	101
3.3.8	Mutagenesis of cholesterol binding sites in Piezo1	104
3.4	Discussion.....	107
3.4.1	Cholesterol binding in Piezo1	107
3.4.2	Other possible factors affecting Piezo1 activation	109
3.4.3	Clinical relevance	110
3.5	Summary.....	111
Chapter 4 Sphingolipid modulation of Piezo1 activation in endothelial cells.....		112
4.1	Introduction	112
4.2	Aims	113
4.3	Results	114
4.3.1	Sphingomyelinase potentiates Piezo1 activation in HUVECs.....	114
4.3.2	Sphingomyelinase decreases Yoda1 responses in Piezo1 overexpression system.....	116
4.3.3	Effect of sphingomyelinase on other Ca ²⁺ entry mechanisms.....	117
4.3.4	Effect of Piezo1 inhibitors on SMase potentiation	120
4.3.5	Downstream signalling of sphingomyelinase on Piezo1 activity.....	123
4.3.6	Mechanism of potentiation of Piezo1 by sphingosine	132
4.4	Discussion.....	138
4.4.1	Sphingomyelinase potentiation of Piezo1 in HUVECs	138
4.4.2	Sphingosine mediates potentiation of Piezo1 activation	139
4.4.3	Mechanism of potentiation in HUVECs downstream of sphingosine	140
4.4.4	Cardiovascular function.....	143
4.4.5	Potential role in cardiovascular disease	144
4.5	Summary.....	144

Chapter 5 Novel small-molecule modulators of Piezo1 channels.....	145
5.1 Introduction	145
5.1.1 Piezo1 pharmacology.....	145
5.1.2 Aims.....	147
5.2 Results	148
5.2.1 Structure-activity relationships of Yoda1 analogues	148
5.2.2 Characterisation of hit compounds	159
5.2.3 Effect of Yoda1 analogues on endothelial cell alignment....	170
5.2.4 Endothelial cell death by Yoda1 and analogues	172
5.3 Discussion.....	174
5.3.1 Yoda1 structure activity relationship	174
5.3.2 Selectivity of Piezo1 activators	176
5.3.3 Stability and solubility of Yoda1 analogues.....	177
5.3.4 Piezo1 activators as a therapeutic agents	178
5.3.5 Summary.....	179
Chapter 6 Final summary and future work.....	180
References	187

List of Tables

Table 2.1: List of reagents used.	67
Table 2.2: List of oligonucleotide primers used to generate mutants. .	71
Table 3: Cholesterol binding site mutations and locations.	105
Table 5.1: Structures of dichlorophenyl ring modifications to Yoda1 and summary of results.	150
Table 5.2: Structures of pyrazine ring modifications to Yoda1 and summary of results.....	154
Table 5.3: Structures of thiadiazole linker modifications to Yoda1 and summary of results.....	157
Table 5.4: 3h has a much greater in vitro pharmacokinetic profile than Yoda1 or 2c.	169
Table 8: Cholesterol binding motifs in human Piezo1.	215
Table 9: Cholesterol binding motifs in mouse Piezo1.....	217

List of Figures

Figure 1.1: Schematic of Ca ²⁺ handling in a vascular cell.	10
Figure 1.2: Key reactions and compartmentalisation of the sphingolipid metabolic pathway.....	23
Figure 1.3: Cryo-EM structure of Piezo1 trimer.	40
Figure 2.1: FlexStation 3 (Molecular Devices).	74
Figure 2.2: Method for cell alignment analysis.....	78
Figure 2.3: Schematic of Live/Dead cytotoxicity assay.....	80
Figure 3.1: Cholesterol inhibits shear stress-evoked Ca ²⁺ entry in HUVECs.....	88
Figure 3.2: Exogenous cholesterol reduces Yoda1 response in HUVECs.....	90
Figure 3.3: Depletion of endogenous cholesterol reduces Yoda1 response in HUVECs.	92
Figure 3.4 Alpha cyclodextrin has no effect on Piezo1 activation.	93
Figure 3.5: Exogenous cholesterol reduces Yoda1 response in P1 HEK TREx.	95
Figure 3.6: Depletion of endogenous cholesterol reduces Yoda1 response in P1 HEK TREx.....	97
Figure 3.7: CRAC domains in Piezo1.	100
Figure 3.8: Computational modelling of cholesterol interactions with Piezo1.....	103
Figure 3.9: Cholesterol binding mutants are resistant to exogenous inhibition by exogenous cholesterol.....	106
Figure 4.1: Sphingomyelinase potentiates Yoda1 response in HUVECs.	115
Figure 4.2: Sphingomyelinase reduces Yoda1 response in Piezo1 HEK TREx.	116
Figure 4.3: Sphingomyelinase does not affect ATP response in HUVECs.....	117
Figure 4.4: Sphingomyelinase reduced Ca ²⁺ add-back response in HUVECs.....	119
Figure 4.5: Sphingomyelinase does not affect VEGF response in HUVECs.....	119
Figure 4.6: Potentiation of Yoda1 responses by sphingomyelinase is inhibited by gadolinium.....	121
Figure 4.7: Potentiation of Yoda1 responses by sphingomyelinase is inhibited by ruthenium red but not increases in baseline Ca ²⁺ ...	121

Figure 4.8: Potentiation of Yoda1 responses by sphingomyelinase was reduced by Piezo1 knockdown but increases in baseline Ca²⁺ was not affected.	122
Figure 4.9: Sphingomyelin did not affect Yoda1 responses or baseline Ca²⁺ in HUVECs.....	124
Figure 4.10: Phosphocholine did not affect Yoda1 responses or baseline Ca²⁺ in HUVECs.	124
Figure 4.11: Ceramides did not affect Yoda1 responses or baseline Ca²⁺ in HUVECs.....	126
Figure 4.12: Ceramide-1-phosphate did not affect Yoda1 responses or baseline Ca²⁺ in HUVECs.	127
Figure 4.13: Sphingosine increased Yoda1 responses and baseline Ca²⁺ in HUVECs.....	129
Figure 4.14: Sphingosine-1-phosphate did not affect Yoda1 responses or baseline Ca²⁺ in HUVECs.....	131
Figure 4.15: PKA does not affect sphingomyelinase potentiation of Yoda1 responses or increased baseline Ca²⁺ in HUVECs.	132
Figure 4.16: PKC inhibition potentiated Yoda1-induced Piezo1 activation similar to SMase in HUVECs.	134
Figure 4.17: PKD reduced sphingomyelinase-induced potentiation of Piezo1 activation in HUVECs.	135
Figure 4.18: Phospholipase C inhibition reduced sphingomyelinase-induced baseline Ca²⁺ increases in HUVECs.....	136
Figure 4.19: Inositol-1,4,5-triphosphate receptor inhibition reduced sphingomyelinase-induced baseline Ca²⁺ increases in HUVECs.	137
Figure 5.1: The structure of Yoda1.....	146
Figure 5.2: Methoxy and methyl substitutions of chlorines can be tolerated.	151
Figure 5.3: Pyrazine ring modifications produced a highly active Yoda1 analogue.....	155
Figure 5.4: Modifying the central ring and linker often abolished activity.	158
Figure 5.5: Modifications to dichlorophenyl ring and pyrazine ring produced more potent analogues of Yoda1.	161
Figure 5.6: Yoda1 and its analogues do not activate HEK TREx cells.	163
Figure 5.7: Yoda1 and its analogues do not activate TRPC4 or TRPC5 ion channels.....	164
Figure 5.8: Responses of Yoda1 and hit analogues in CHO-TRPV4 cells.	166

Figure 5.9: Piezo1 knockdown abolishes responses of Yoda1 and its analogues in HUVECs.	168
Figure 5.10: Effect of Yoda1 and hit analogues on HUVEC alignment.	171
Figure 5.11: Yoda1 and its analogues caused cell death in HUVECs.	173
Figure 6.1: Cartoon summarising the data from Chapter 3 and new hypothesis based on the data.....	182
Figure 6.2: Cartoon summarising the data from Chapter 4 and new hypothesis based on the data.....	184
Figure 6.3: Alignment of human and mouse Piezo1 with highlighted highly conserved cholesterol binding motifs.	222

List of Publications and Communications

Published Manuscripts

Li J, Hou B, Tumova S, Muraki K, Bruns A, Ludlow MJ, Sedo A, **Hyman AJ**, McKeown L, Young RS, Yuldasheva NY, Majeed Y, Wilson LA, Rode B, Bailey MA, Kim HR, Fu Z, Carter DA, Bilton J, Imrie H, Ajuh P, Dear TN, Cubbon RM, Kearney MT, Prasad RK, Evans PC, Ainscough JF, Beech DJ. Piezo1 integration of vascular architecture with physiological force. *Nature*. 2014 Nov.

Hyman AJ, Tumova S, Beech DJ. Piezo1 Channels in Vascular Development and the Sensing of Shear Stress. *Current topics in membranes*. 2017 Jan.

Webster PJ, Littlejohns AT, Gaunt HJ, Young RS, Rode B, Ritchie JE, Stead LF, Harrison S, Droop A, Martin HL, Tomlinson DC, **Hyman AJ**, Appleby HL, Boxall S, Bruns AF, Li J, Prasad KR, Lodge JPA, Burke DA, Beech DJ. Upregulated WEE1 protects endothelial cells of colorectal cancer liver metastases. *Oncotarget*. 2017 Jun.

Evans E, Cuthbertson K, Endesh N, Rode B, Blythe NM, **Hyman AJ**, Hall S, Gaunt HJ, Ludlow MJ, Foster R, Beech DJ. Yoda1 analogue (Dooku1) which antagonises Yoda1-evoked activation of Piezo1 and aortic relaxation. *British Journal of Pharmacology*. 2018 Feb.

Manuscripts submitted or in preparation

Hyman AJ, Ludlow MJ, Kalli AC, Beech DJ. Modulation of Piezo1 channel function by cholesterol. In preparation.

Hyman AJ, Beech DJ. Sphingomyelinase potentiation of endothelial Piezo1. In preparation.

Hyman AJ, Cuthbertson K, Endesh N, Myers D, Evans E, Beech DJ. Yoda1 analogue with favourable pharmacokinetic properties. In preparation.

Morley LC, Shi J, Gaunt HJ, **Hyman AJ**, Webster PJ, Williams C, Forbes K, Walker JJ, Simpson NAB, Beech DJ. Piezo1 is required for mechanosensing in human fetoplacental endothelial cells. Submitted to *Molecular Human Reproduction*.

Communications

Hyman AJ, Kalli AC, Beech DJ. Lipid bilayer regulation of Piezo1 in endothelial cells. (Poster presentation). International Union of Physiological Sciences 38th World Congress, Rio De Janeiro, 2017.

Hyman AJ, Hou B, Li J. Shear stress sensing and the alignment of endothelial cells. Postgraduate Symposium, University of Leeds, 2014 and Endothelial Retreat, Lake District, 2014.

Abbreviations

α CD	Alpha cyclodextrin
μ L; mL	microlitre; millilitre
μ m; mm; cm	micrometre; millimetre; centimetre
nM; μ M; mM	nanomolar; micromolar; millimolar
ATP	Adenosine triphosphate
Ca ²⁺	Calcium ion
C-1-P	Ceramide-1-phosphate
CDase	Ceramidase
DAG	Diacylglycerol
DNA	Deoxyribonucleic acid
DNAse	Deoxyribonuclease
DMSO	Dimethyl sulphoxide
EDHF	Endothelium-derived hyperpolarising factor
EDTA	Ethylene diaminetetraacetic acid
EGM	Endothelial growth medium
eNOS	Endothelial nitric oxide synthase
ER	Endoplasmic reticulum
Fura-2 AM	Fura-2-acetoxymethyl ester
Gd ³⁺	Gadolinium ion
GsMTx4	Grammastola spatulata, mechanotoxin 4
GPCR	G-protein coupled receptor
G protein	Guanosine nucleotide-binding protein
HA	Hemagglutinin
HEK	Human embryonic kidney cells
IP ₃	Inositol 1,4,5-triphosphate
IP ₃ R	Inositol 1,4,5-triphosphate receptor

M β CD	Methyl beta cyclodextrin
MCU	Mitochondrial Ca ²⁺ uniporter
MSC	Mechanosensitive channels
NCX	Na ⁺ /Ca ²⁺ exchanger
NO	Nitric Oxide
P2X4	P2X purinoceptor 4
PBS	Phosphate buffered saline
PCR	Polymerase chain reaction
PLC	Phospholipase C
PMCA	Plasma membrane Ca ²⁺ ATPase
PKA	Protein Kinase A
PKC	Protein Kinase C
PKD	Protein Kinase D
ROC	Receptor-operated channel
rpm	Revolutions per minute
RyR	Ryanodine Receptor
S-1-P	Sphingosine-1-phosphate
SBS	Standard Bath Solution
SERCA	Sarcoplasmic endoplasmic Ca ²⁺ ATPase
siRNA	Small interfering ribonucleic acid
SMase	Sphingomyelinase
SOC	Store-operated channel
SK	Sphingosine kinase
TPC	Two-pore channel
TRP	Transient receptor potential
TRPC	Canonical transient receptor potential
TRPV	Vanilloid transient receptor potential
VGCC	Voltage-gated Ca ²⁺ channel

Chapter 1

Introduction

1.1 Cardiovascular System

The cardiovascular system transports nutrients and oxygen to the body, and removes waste products, via blood travelling through a vast network of vessels. Blood provides nutrients and oxygen to each of the body's approximately 75 trillion cells whilst also being a conduit for hormones to be transported throughout the body. The driving force of the movement of blood around the body is the heart. The heart is a muscular organ located in the central thorax which acts as a dual pump for blood.

Blood is carried through specialised tubes called blood vessels. There are five types of blood vessel which differ from each other histologically and functionally. There are arteries, arterioles, capillaries, venules and veins. Arteries transport blood away from the heart and originate from the aorta, which receives blood from the left ventricle of the heart, or the pulmonary artery which receives blood from the right ventricle and transports it to the lungs to be oxygenated. Branches off the aorta form new arteries which transport blood to body tissues. Arteries branch and divide to form smaller vessel called arterioles, which branch further to capillaries. Due to their single-cell wall structure, capillaries allow diffusion of nutrients between the blood and interstitial fluid surrounding cells. Cells generally have a close proximity to capillaries which allows for rapid diffusion. Venules collect deoxygenated blood from capillaries to be transported back to the heart via veins.

The structure of blood vessels largely determines their function. Arteries and veins are constructed with three major wall layers: tunica intima, tunica media and tunica adventitia. The tunica intima lines the lumen of the blood vessel and is in contact with the blood. The main cell type in the tunica intima are endothelial cells, which form a stable monolayer under physiological conditions. Endothelial cells are subjected to shear stress generated by friction of blood flow against the wall, ranging from 1 to 70 dyn.cm⁻² depending on the blood vessel and species (Chiu and Chien, 2011). The tunica intima is surrounded by the tunica media and separated by the internal elastic lamina in large arteries. The tunica media is comprised of a thick layer of smooth muscle cells, elastic tissue and connective tissue in arteries and veins, with arteries having a greater thickness of smooth muscle cells. The tunica media largely controls vessel diameter. The external elastic lamina separates the tunica media from the outermost layer, the tunica adventitia. The tunica adventitia is largely composed of connective tissue. However, nerves are also found in this layer as well as the vasa vasorum, a network of small blood vessels that supplies nutrients to large blood vessels.

The heart generates blood flow by active pumping. However, blood vessels regulate the rate of blood flow internally by altering the lumen diameter appropriately. These changes are vasoconstriction, narrowing of the vessel lumen, and vasodilation. Vasoconstriction is mediated by contractions of smooth muscle cells which can be induced by endogenous pressors, such as ATP, angiotensin II and endothelin (Navar et al., 1996). Vasodilation can be regulated by many factors, such as the release of nitric oxide (NO) from endothelial cells or endothelium-derived hyperpolarising factor (EDHF), which cause smooth muscle cell relaxation (Navar et al., 1996; Ozkor and Quyyumi, 2011). Regulation

of intracellular Ca^{2+} in both endothelial and smooth cells is essential for regulation of the vasculature (Tsoukias, 2011).

1.2 Cardiovascular disease

Cardiovascular disease is an umbrella term for pathologies of the cardiovascular system that include coronary artery disease, cerebrovascular disease, peripheral arterial disease, rheumatic and congenital heart disease, and venous thromboembolism. Cardiovascular diseases accounted for the largest amounts of deaths worldwide, 31% globally in 2015 (WHO, 2017). In England, cardiovascular disease accounted for 34% of deaths in 2012 (Nichols et al., 2012). Additionally, cardiovascular diseases were the leading cause of loss of disability-adjusted life year globally (Perk et al., 2012). The prevalence of cardiovascular diseases is increasing worldwide as the risk factors for cardiovascular diseases are increasing in previously low risk countries.

Premature cardiovascular disease has been shown to be preventable in many cases and the World Health Organisation estimated that approximately 75% of cardiovascular disease cases are preventable (WHO, 2018). Additionally, the WHO have suggested that combatting risk can help reduce the burden of cardiovascular diseases on individuals and healthcare providers. Age has been shown to be a risk factor for cardiovascular disease but pathological evidence suggested that developing cardiovascular diseases is not inevitable.

Risk factors of cardiovascular disease, particularly coronary heart disease, were investigated in the INTERHEART study (Yusuf et al., 2004). Dyslipidaemia, smoking, hypertension, diabetes, abdominal obesity, alcohol consumption and psychosocial factors, such as depression and stress, accounted for most of the

risk of coronary heart disease. However, the consumption of fruits and vegetable, and regular exercise protected against coronary heart disease. Furthermore, the findings of this study were consistent throughout all populations, ethnicities and socioeconomic levels studied, suggesting uniformity of risk factors globally.

1.2.1 Atherosclerosis

In most cases of obstructive coronary diseases and cerebrovascular disease the cause is atherosclerosis. Atherosclerotic vascular diseases progress from early life and can eventually lead to obstructive arterial disease, resulting in acute complications such as ischaemic heart disease, myocardial infarction or stroke (Lusis, 2000). Atherosclerosis results in the formation of a fibrous plaque within the vessel wall which can rupture. There are five key steps in the development of atherosclerotic plaques: endothelial dysfunction, lipoprotein entry and modification, leukocyte recruitment, foam cell formation and degradation of the extracellular matrix.

1.2.1.1 Endothelial dysfunction

The earliest signs of atherosclerosis are the appearance of a fatty streak on the surface of an artery lumen and thickening of the intima. The fatty streak contains accumulations of intracellular and extracellular lipids. Endothelial dysfunction has been suggested to be the primary event which results in the formation of the fatty streak, resulting from multiple risk factors such as hypercholesterolaemia and smoking. In endothelial dysfunction the phenotype of endothelial cells changes to proinflammatory, prothrombotic, impaired barrier function and impaired NO-mediated vasodilation (Endemann and Schiffrin, 2004; Münzel et al., 2008). Lack of NO bioavailability leads to greater expression of vascular cell adhesion molecule 1 (VCAM1) in endothelial cells, increasing monocyte and T

lymphocyte adhesion, resulting in invasion of inflammatory cells in the vessel wall (Khan et al., 1996; Libby, 2012).

1.2.1.2 Lipoprotein entry and modification

The disruption of the endothelial cell barrier due to endothelial dysfunction allows lipoprotein to invade the subintimal space. Proteoglycans in the intima allow for retention and accumulation of lipoproteins by binding to apolipoprotein (ApoB100), an apolipoprotein of low density lipoprotein (LDL) (Borén et al., 1998). Chronic accumulation of lipoproteins results in their chemical modification (Parthasarathy et al., 2010). Lipoproteins can be oxidised to form oxidised LDL (oxLDL) by reactive oxygen species and pro-oxidant enzymes produced by the endothelium and smooth muscle cells. Glycation of lipoprotein can occur due to chronic hyperglycaemia, forming an antigenic and proinflammatory form of lipoprotein. These proinflammatory forms of lipoprotein contribute to the inflammatory phenotype of endothelial dysfunction and induces leukocyte recruitment and foam cell formation in the fatty streak while the atherosclerotic plaque develops (Maiolino et al., 2013).

1.2.1.3 Leukocyte recruitment

Focal recruitment of circulating monocytes and T lymphocytes has been documented as one of the earliest cellular responses in atherogenesis (Libby, 2012). Increased endothelial adhesion molecule expression, such as intercellular adhesion molecule 1 (ICAM1) and VCAM1, by oxLDL promotes leukocyte recruitment. Additionally, chemoattractants such as oxLDL and monocyte chemoattractant protein-1 (MCP-1) must be present (Libby, 2012). MCP-1 attracts both monocytes and T-lymphocytes but not neutrophils and B cells. Endothelial and smooth muscle cells contribute to overexpression of MCP-1 in

atherosclerosis (Deshmane et al., 2009). These molecules allow for transendothelial migration of leukocytes.

1.2.1.4 Foam cell formation

Once in the intima, monocytes differentiate into macrophages and internalise atherogenic lipoproteins via scavenger receptors, including scavenger receptor A (SR-A) and CD36 (de Villiers and Smart, 1999; Moore and Tabas, 2011; Bobryshev, 2006). Due to the lack of down-regulation of scavenger receptors from high cholesterol content, unlike the classic LDL-receptors, macrophages can assimilate lipids without a negative feedback mechanism. The lipid-loaded macrophages form foam cells which continue to internalise lipoprotein until apoptosis occurs, contributing to a destabilised lipid-rich core of the atherosclerotic plaque.

1.2.1.5 Smooth muscle cell migration

Smooth muscle cells proliferate in response to vascular insult and are responsible for healing and repair of arterial injuries. Persistence of atherogenic stimuli and progression of fatty streak formation results in proliferation of intimal smooth muscle cells and migration from the media to the intima (Bennett et al., 2016). If proliferation of smooth muscle cells continues in response to atherogenic stimuli, occlusion of the vessel lumen may occur, disrupting local blood flow. Additionally, smooth muscle cells can become lipid-loaded foam cells, contributing to the destabilised core of the atherosclerotic plaque (Allahverdian et al., 2012). Conversely, smooth muscle cells and the matrix they produce can stabilise atherosclerotic plaques, protecting them from rupture and thrombosis.

1.2.1.6 Plaque rupture

The atherosclerotic plaque is formed by a fibrous cap at the luminal surface with a lipid-rich necrotic core. The fibrous cap contains smooth muscle cells, macrophages and dead foam cells. The lipid-rich necrotic core is an avascular, hypocellular structure devoid of collagen. During the progression of atherosclerosis, endothelial cells, macrophages and smooth muscle cells experience cell death by either necrosis or apoptosis. Death of smooth muscle cells results in a thinner fibrous cap and destabilises the plaque (Geng and Libby, 2002). Additionally, macrophages produce matrix metalloproteases which degrade the extracellular matrix produced by smooth muscle cells (Watanabe and Ikeda, 2004). The plaque may rupture when the fibrous cap becomes too thin and the plaque is unstable. Rupture of the plaque exposes the lipid-rich thrombogenic core to the flowing blood resulting in platelet aggregation and thrombus formation, which is the main cause of coronary artery thrombosis (Moore and Tabas, 2011).

1.2.1.7 Prevention of atherosclerosis

Prevention of atherosclerosis is mainly aimed at reducing risk factors of cardiovascular disease. Increased exercise, diet modification, smoking cessation, reduction in alcohol consumption and maintenance of a body mass index between 20-25 are all recommended for prevention of cardiovascular diseases (Stewart et al., 2017). Medical treatments largely aim to reduce blood lipid levels and lower apoB-LP retention. 3-Hydroxy-3-methyl-glutaryl-coenzyme A reductase inhibitors, commonly referred to as statins, have been used since the 1980s to reduce lipid levels. Statins reduce cholesterol synthesis and have anti-inflammatory effects (Rosenson, 2004). Other lipid lowering therapies are

also used, commonly when statins alone do not improve patient lipid profiles, such as bile acid sequestrants, fibrates and nicotinic acid (Piepoli et al., 2016). These are often used in conjunction with statins due to side-effects and lack of reduction in cardiovascular disease events. New lipid lowering therapies are being developed using monoclonal antibodies for proprotein convertase subtilisin-kexin type 9, such as alirocumab (Robinson et al., 2015). Phase III data suggest alirocumab may be used as a monotherapy or in conjunction with statins with a significant reduction in cardiovascular diseases events. Alternative therapies for cardiovascular disease include aspirin, to reduce platelet aggregation (Ittaman et al., 2014), and anti-hypertensive agents, such as calcium-channel blockers, angiotensin-converting enzyme inhibitors, angiotensin II receptor inhibitors and thiazide diuretics (Stewart et al., 2017).

1.2.2 Ca²⁺ in atherosclerosis

Calcium (Ca²⁺) is a universal second messenger in eukaryotic cells. Ca²⁺ signalling mechanisms in the cardiovascular system can contribute to the development of atherosclerosis. Activation of endothelial nitric oxide synthase (eNOS), and subsequent NO production, can occur in response to Ca²⁺ interacting with calmodulin to form a complex (Lin et al., 2000). Ca²⁺/calmodulin is also involved in the apoptosis of macrophages, smooth muscle cells and endothelial cells in development of the atherosclerotic plaque (Scull and Tabas, 2011). Phosphoinositide 3-kinase (PI3K) signalling is also regulated by Ca²⁺ and has been implicated in atherogenesis (Morello et al., 2008). Ca²⁺ signalling mechanisms have also been reported to be altered in mouse models of atherosclerosis before and after plaque formation which is a mechanism for endothelial dysfunction (Prendergast et al., 2014a; Prendergast et al., 2014b).

1.3 Ca^{2+} signalling in the cardiovascular system

Calcium ions (Ca^{2+}) affect the functions of almost all cellular life processes such as proliferation, migration and apoptosis. In the vascular system Ca^{2+} is required for vasoconstriction and dilation, endothelial permeability and angiogenesis (Munaron and Fiorio Pla, 2009; Sukriti et al., 2014; Jackson, 2000). This divalent cation can change the activity of many proteins by altering their conformational state and electrostatic charge.

The concentration of free intracellular Ca^{2+} is approximately 100 nM with a 20,000-fold difference to the extracellular fluid (approximately 2 mM). This concentration gradient is tightly regulated because elevation of cytoplasmic Ca^{2+} can induce cell death (Clapham, 2007). However, cells evolved to utilise Ca^{2+} as a signalling mechanism. Ca^{2+} cannot be chemically modulated so it must be bound to other molecules, compartmentalised or exported from the cell.

Ca^{2+} is not only present in the cytosol but is compartmentalised into intracellular organelles, such as the endoplasmic reticulum (ER), mitochondria, Golgi and lysosomes. ER is considered the major intracellular store of Ca^{2+} containing up to 75% of total intracellular Ca^{2+} (Berridge, 2002). Mitochondria are intimately connected with the regulation of Ca^{2+} in the ER. Mitochondria can uptake Ca^{2+} released from ER and are involved in stress signals via Ca^{2+} moving from the ER to mitochondria.

Multiple mechanisms regulate Ca^{2+} homeostasis via activation of receptors, ion channels, pumps and exchangers located in organelles and at the plasma membrane. The mechanism by which a cell controls Ca^{2+} homeostasis is summarised schematically in Figure 1.1.

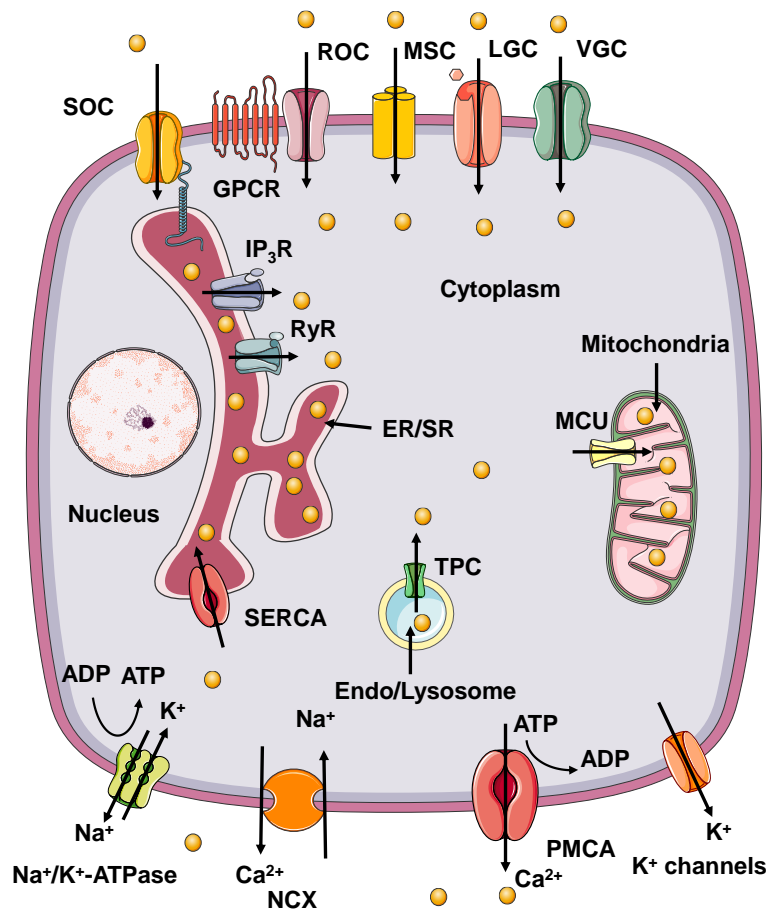


Figure 1.1: Schematic of Ca²⁺ handling in a vascular cell. Intracellular Ca²⁺ stores: endo/sarcoplasmic reticulum (ER/SR), mitochondria. Ca²⁺ entry mechanism: voltage-gated Ca²⁺ channel (VGCC), is activated in response to membrane depolarisation. Receptor-operated Ca²⁺ (ROC) channel, mediate Ca²⁺ entry in response to agonists binding to corresponding G-protein coupled receptors (GPCR). Store-operated Ca²⁺ (SOC) channel, opens in response to depletion of the intracellular Ca²⁺ stores. Ligand-gated Ca²⁺ channel, can be activated by direct agonist binding to the channel. MSC, mechanosensitive Ca²⁺ channel, is activated in response to a wide range of external mechanical stress stimuli. Intracellular Ca²⁺ release and uptake mechanisms: Ca²⁺ release from ER is mainly mediated by two channels, the inositol 1,4,5-trisphosphate receptor (IP₃R) and ryanodine receptor (RyR). The uptake of Ca²⁺ by ER is mediated by Sarco/endoplasmic reticulum calcium ATPase (SERCA) pump. Two pore channel 1/2 (TPC1/2), is required for NAADP-induced Ca²⁺ release from endosomes and lysosomes. The mitochondrial Ca²⁺ uniporter (MCU) is considered to be responsible for mitochondrial Ca²⁺ uptake. Ca²⁺ extrusion mechanism: plasma membrane Ca²⁺-ATPase (PMCA) and Na⁺/Ca²⁺ exchanger (NCX) are responsible for the processes. The Na⁺/K⁺-ATPase maintains the Na⁺ required for NCX activity. K⁺ channels cause hyperpolarisation which creates an electrochemical gradient for Ca²⁺. *Image created through Servier Medical Art.*

1.3.1 Ion channels

Ion channels are transmembrane proteins that enable the movement of ions down their electrochemical gradient in response to a stimulus. The movement of ions across the membrane triggers a rapid response to the stimulus. Some ion channels are selective to specific ions, such as Ca^{2+} , whereas as others discriminate ions only by charge. There are many different types of ion channels that facilitate the movement of Ca^{2+} ions into the cytosol which allow cell to respond appropriately to different stimuli.

1.3.1.1 Voltage-gated Ca^{2+} channels

Voltage-gated ion channels are largely expressed in excitable cell types, such as neurons and muscle. They respond to changes in membrane potential, specifically depolarisation for voltage gated Ca^{2+} channels (VGCC). VGCCs were originally classed into subfamilies dependent on their function and/or inhibition by toxins, L-, N-, P/Q-, R- and T-type VGCC. Since then VGCCs have been categorised into three major subfamilies, Ca_v1 , Ca_v2 and Ca_v3 , according to the gene encoding the pore-forming α_1 subunit (Ertel et al., 2000). In the vasculature VGCCs are largely associated with function in smooth muscle cells, such as contractility and proliferation (Muramatsu et al., 1997; Rodman et al., 2005). However, roles for VGCCs have been suggested for microvascular endothelial cells but not macrovascular endothelial cells (Zhou and Wu, 2006; Zhou et al., 2010; Bossu, Elhamdani, Feltz, et al., 1992; Bossu, Elhamdani and Feltz, 1992). For example, T-type Ca^{2+} channels have been suggested to be responsible for P-selectin surface expression and von Willebrand factor release in pulmonary microvascular endothelial cells (Zhou et al., 2010).

1.3.1.2 Ligand-gated Ca²⁺ channels

Ligand-gated ion channels are activated by binding of an agonist to the channel, triggering activation. P2X receptors are examples of ligand-gated ion channels found in the vasculature. P2X receptors are activated by adenosine 5-triphosphate (ATP), mediating Ca²⁺ entry (Burnstock and Ralevic, 2013). There are seven members of the P2X receptor family: P2X₁₋₇. P2X₁ has been suggested to have a role in the vasoconstriction function of vascular smooth muscles (Vial and Evans, 2002). In endothelial cells, P2X₂ and P2X₄, contribute to shear stress-induced Ca²⁺ entry in response to ATP release contributing to vasodilation (Harrington et al., 2007; Yamamoto et al., 2006).

1.3.1.3 Receptor-operated Ca²⁺ entry

Receptor operated Ca²⁺ entry is mediated by non-selective cation channels that are activated downstream of a G-protein coupled receptors (GPCR). These channels are known as receptor-operated cation channels (ROCC). Activation of GPCRs results in activation of a variety of cell signalling pathways including the synthesis of inositol 1,4,5-triphosphate (IP₃) and diacylglycerol. Several transient receptor potential canonical (TRPC) channels have been shown to be activated downstream of GPCR activation. For example, TRPC3, TRPC6 and TRPC7 have been shown to be activated by DAG (Eder and Groschner, 2008) and TRPC5 may be activated by sphingosine 1-phosphate GPCR activation (Jiang et al., 2011).

1.3.1.4 Store-operated Ca²⁺ entry

Store-operated Ca²⁺ entry (SOCE) occurs in response to depletion of Ca²⁺ stores from the endoplasmic reticulum (ER). SOCE is the most common form of Ca²⁺ entry in non-excitable cells as Ca²⁺ entry across the plasma membrane occurs

infrequently. Two components have been shown to be important in SOCE, stromal interaction molecule 1 (STIM1) and Orai1 (Lewis, 2011). STIM1 is situated in the ER membrane whilst Orai1 is found in the plasma membrane. When ER Ca^{2+} stores have been depleted, STIM1 senses the reduction in ER Ca^{2+} concentration and forms clusters close to the plasma membrane. As a result, the highly-selective Ca^{2+} channel Orai1 allows Ca^{2+} entry into the cytosol and subsequent refilling of the ER Ca^{2+} stores via the SERCA pump. TRPC channels have also been suggested to contribute to SOCE (Salido et al., 2009). SOCE has been shown to be important in endothelial cell tube formation as well as smooth muscle cell proliferation and migration (Li et al., 2008; Li et al., 2011).

1.3.1.5 Mechanically gated ion channels

Mechanically-activated ion channels respond to changes in cell membrane tension caused by cell deformation. Transduction of mechanical signals occurs in many cell types, such as neurons, epithelial cells and endothelial cells, for many forms of mechanical stimuli, such as stretch, touch or fluid flow (Ranade et al., 2015).

There have been many mechanically-activated cation channels proposed, including several TRP channels such as TRPV2, TRPV4, TRPM4, TRPC1, TRPC5, TRPC6 and a TRPP1/ TRPP2 complex (Liu and Montell, 2015). However, the mechanical gating of TRP channels is controversial. TRPV has been suggested to have roles in essential hypertension and pulmonary arterial hypertension due to mechanical activation (Hartmannsgruber et al., 2007). Additionally, TRPV4 has been suggested as a sensor of shear stress in endothelial cells (Köhler and Hoyer, 2007).

Piezo proteins (Piezo1 and Piezo2) have also been shown to be mechanically-activated ion channels (Coste et al., 2010). The properties of Piezo1 and its role in the vascular system are discussed below.

1.3.2 Intracellular Ca²⁺ release and uptake mechanisms

Ca²⁺ stored in the ER can be released by activation of two channels, the IP₃ receptor (IP₃R) and ryanodine receptor (RyR) (Berridge, 2002). IP₃, generated by phospholipase C (PLC) activation, stimulates IP₃R resulting in release of Ca²⁺ from the ER. The RyR is activated by Ca²⁺, physiologically, and may also be activate by caffeine. Ca²⁺ release can also occur from acidic intracellular stores, such endosomes and lysosomes. Nicotinic acid adenine dinucleotide phosphate (NAADP) has been suggested to induce release from these stores via two pore channels (Patel and Docampo, 2010).

The uptake of Ca²⁺ into the ER is mediated by the sarcoendoplasmic reticulum Ca²⁺ ATPase (SERCA) pump (Brini and Carafoli, 2011). For every ATP hydrolysed by the SERCA pump two protons are exchanged into the cytosol and two Ca²⁺ against its concentration gradient. The mitochondria can also uptake Ca²⁺ via the mitochondrial Ca²⁺ uniporter on the organelle's inner membrane (Kirichok et al., 2004).

1.3.3 Mechanism of Ca²⁺ extrusion

Removing Ca²⁺ from the cytosol is important in Ca²⁺ homeostasis. The plasma membrane Ca²⁺ ATPase (PMCA), Na⁺/Ca²⁺ exchanger (NCX) and Na⁺/Ca²⁺-K⁺ exchanger (NCKX) are responsible for extrusion of Ca²⁺ out of the cell (Berridge et al., 2003). The PMCA is located in the plasma membrane. For every ATP hydrolysed by these pumps two protons are exchanged into the cytosol and one

Ca^{2+} . Four isoforms of PMCA have been identified with PMCA1 predominantly expressed in endothelial cells (Szewczyk et al., 2007).

NCX and NCKX are also found on the plasma membrane. These exchangers export Ca^{2+} by utilising the energy between the concentration gradients of Na^+ and K^+ . The $\text{Na}^+/\text{Ca}^{2+}$ exchanger (NCX) exchanges one Ca^{2+} for three Na^+ . Similarly, the $\text{Na}^+/\text{Ca}^{2+}-\text{K}^+$ exchanger (NCKX) exchanges one Ca^{2+} and one K^+ for four Na^+ ions. Three isoforms of NCX have been determined (NCX1-3) with NCX1 expressed in endothelial and vascular smooth muscle cells (Szewczyk et al., 2007). Four isoforms of NCKX (NCKX1-4) have been found with NCKX3-4 expression shown in vascular smooth muscle cells (Dong et al., 2006).

These mechanisms set up and maintain the large gradient between the cytosol and the extracellular fluid. This gradient is important to allow Ca^{2+} signalling via fluxes of Ca^{2+} concentration caused by the activation of ion channels.

1.4 Cholesterol regulation of ion channels

Cholesterol is an essential component of eukaryotic cell membranes comprising up to 45% of the molar proportion compared to other lipids. Physiological cholesterol maintains membrane thickness, fluidity and compartmentalisation of lipid domains that serve as scaffolds for signalling platforms (Krause and Regen, 2014). Alterations in membrane cholesterol may underlie cellular and tissue dysfunction that contribute to the pathophysiology of diseases resulting from hypercholesterolaemia or reductions in cholesterol synthesis such as in Smith-Lemli-Opitz syndrome.

Alterations in membrane content has been shown to affect the activity of many ion channels. The effects of cholesterol on ion channels vary greatly with cholesterol depletion increasing activity of some channels whilst decreasing the activity of other channels. Suppression of channel activity was the most common effect of cholesterol on ion channels including decrease in the open probability, unitary conductance and or the number of active channels on the membrane (Rosenhouse-Dantsker et al., 2012). These effects have been observed in multiple K⁺ channels, including inwardly-rectifying K⁺ channels (Romanenko et al., 2002), Ca²⁺-sensitive K⁺ channels and voltage-gated K⁺ channels (Hajdú et al., 2003; Abi-Char et al., 2007), as well as voltage-gated Na⁺ and Ca²⁺ channels (Lundbæk et al., 2004), volume-regulated anion channels (Romanenko et al., 2004) and TRPV channels (Picazo-Juarez et al., 2011). Some channels have been suggested to require cholesterol to function, in a similar manner to some ion channels requiring PIP₂ to function, such as nicotinic acetylcholine receptor (nAChR) (Barrantes, 2007) and GABA_A receptors (Sooksawate and Simmonds,

2001). The effects of cholesterol on ion channels may differ even within a sub-family of channels.

1.4.1 Mechanisms of cholesterol regulation of ion channels

Two general methods of regulation of ion channels by cholesterol have been proposed. The first is direct interaction of cholesterol with transmembrane domains of the channel protein (Marsh and Barrantes, 1978). Secondly, cholesterol has been proposed to affect ion channel activity by modulation of membrane viscosity (Lundbæk et al., 1996; Lundbæk and Andersen, 1999). This will increase the energy required for a change in conformational state of the ion channel. Indirect mechanisms have also been suggested by affecting different signalling cascades and membrane properties.

1.4.1.1 Direct interaction of cholesterol with ion channels

The first model of direct interaction between cholesterol and nAChR suggested that cholesterol may be part of a lipid belt surrounding the immediate environment of the ion channel (Marsh and Barrantes, 1978). This model is supported by studies showing that ion channel regulation by sterols is dependent on the chiral nature of the sterol analogue (Romanenko et al., 2002). This suggests a specific protein-sterol interaction. Additionally, cholesterol binding motifs have been suggested in ion channels. The most well-known motif is the cholesterol recognition amino acid consensus (CRAC) motif, which is -L/V-(X₁₋₅)-Y-(X₁₋₅)-R/K- where (X₁₋₅) represents between one and five residues of any amino acid (Li and Papadopoulos, 1998; Epanand, 2006). Cholesterol binding requires a branched apolar residue (leucine or valine), the aromatic tyrosine and a basic residue (lysine or arginine). The predictive value of the CRAC motif for cholesterol binding sites has come under scepticism due to its variability (Epanand,

2006). However, the motif has been found in many proteins and cholesterol interaction with CRAC sites has been confirmed. An inverted CRAC motif, the CARC motif has also been identified (Fantini and Barrantes, 2013). The motif is the reversal of the CRAC motif. However, the tyrosine residue may be substituted for a phenylalanine resulting in a motif of R/K-(X₁₋₅)-Y/F-(X₁₋₅)-L/V.

1.4.1.1.1 CRAC motifs in ion channels

CRAC motifs have been described in large conductance calcium-activate K⁺ (BKCa), nAChR, Kir2.1 and Orai1 channels. Seven CRAC motifs have been found in BKCa (Singh et al., 2012). Mutations of CRAC motifs resulted in decreased sensitivity to cholesterol. CRAC motifs in nAChR and Kir2.1 channels were found in extracellular domains and cytosolic domains of the channels, respectively, suggesting that these domains are not energetically favourable for cholesterol binding (Fantini and Barrantes, 2013; Rosenhouse-Dantsker et al., 2013). Orai1 was found to have a single CRAC motif after depletion of membrane cholesterol reduced activity (Derler et al., 2016). Mutating the leucine and tyrosine residues of the CRAC motif reduced sensitivity to cholesterol depletion and enhanced activation in control conditions.

1.4.1.1.2 CARC motifs in ion channels

CARC motifs have been identified in the transmembrane domains of TRPV1, nAChR and Kir2.1. In TRPV1 a CARC motif was found in the S5 transmembrane helix of the channel (Picazo-Juárez et al., 2011). Mutations of the characteristic CARC residues reduced the sensitivity of TRPV1 to cholesterol. CARC motifs were identified in AChR subunits by docking of cholesterol to TM1, TM3 and TM4. Each site of cholesterol docking corresponded to CARC motifs (Fantini and Barrantes, 2013). Kir2.1 was found to have two CARC motifs at the

transmembrane-cytosolic interface (Rosenhouse-Dantsker et al., 2013). Mutation of one residue of the R67-F73-V77 motif (V77I) resulted in loss of sensitivity towards cholesterol. Mutating the other residues in this motif resulted in loss of channel function. Mutating the second CARC motif did not affect sensitivity to cholesterol, suggesting that the existence of a cholesterol binding motif does not necessarily imply cholesterol binding.

1.4.1.2 Non-specific membrane effects

Changes in physical properties of membranes was first shown to alter the activity of voltage-gated Na⁺ channels (Lundbæk et al., 2004). Depletion of cholesterol in HEK293 cells overexpressing Nav1.4 resulted in a hyperpolarising shift in current inactivation. This effect was replicated by Triton X-100 and β -octyl glucoside which are known to alter lipid bilayer properties. It was proposed that altering the intermolecular interactions between membrane lipids results in changes in membrane curvature and bilayer elasticity, resulting in changes in the required energy for channel gating. This effect was also seen in gramicidin channels where changes in membrane stiffness altered channel activity, with increased cholesterol increasing membrane stiffness and reducing channel activity (Lundbæk et al., 1996). Additionally, the effect of structurally distinct amphiphiles on bilayer elastic properties was shown to be characterised by changes in a bilayer spring constant. The voltage-dependent inactivation of Nav channels was shown to be a function of this bilayers spring constant (Lundbaek et al., 2010).

1.4.1.3 Cholesterol-rich domains

The lipid composition of the plasma membrane has great variability with over 2000 lipid species thought to be involved in its formation (Barenholz, 2000).

Cholesterol-rich membrane domains, often called lipid rafts form with sphingolipids and phospholipids with saturated acyl tails, creating heterogeneous distribution of cholesterol in the membrane (Pike, 2003). Many ion channels have been shown to associate with lipid rafts. Ion channels may be modulated directly by cholesterol in these rafts, by mechanisms discussed above, or indirectly by affecting channel trafficking and interaction with signalling complexes localised to lipid rafts. Caveolae are the most distinct form of lipid raft where caveolin proteins form flask-shaped pits in cholesterol and sphingolipid enriched membranes (Patel et al., 2008). Disruption of caveolar rafts by cholesterol depletion and caveolin-3 knockout has been shown to reduce activation of $Ca_v1.1$ in response to β -adrenergic signalling and activation of cAMP/PKA pathways in cardiomyocytes (Balijepalli et al., 2006; Calaghan and White, 2006). Interaction of K_{ATP} channels and eNaC (epithelial sodium channel) has also been shown to be affected by caveolin-1 dependent internalisation (Jiao et al., 2008; Lee et al., 2009). Additionally, $Nav1.5$ has been shown to be recruited to the plasma membrane by caveolin-3 following activation of β -adrenergic receptors (Balijepalli and Kamp, 2008).

1.4.2 Hypercholesterolaemia and ion channels

Hypercholesterolaemia models of atherosclerosis have been shown to alter activity of ion channels in the vasculature. Ca^{2+} activated K^+ , K_v and K_{ir} channels have all been shown to be affected by hypercholesterolaemia. Several Ca^{2+} -activated K^+ channels are expressed in vascular smooth muscle cells and endothelial cells and are important in regulation of vascular functions (Ledoux et al., 2006). $K_{Ca1.1}$ was shown to be inhibited in endothelial and smooth muscle cells (X. L. Wang et al., 2005; Bolotina et al., 1989). Contrasting results of diet-

induced hypercholesterolaemia in rabbits with both enhancement and impairment endothelium-dependent vasodilation mediated by Ca^{2+} -activated K^+ reported (Najibi et al., 1994; Najibi and Cohen, 1995; Jeremy and McCarron, 2000). However, these responses were measured in different vessel beds. Depletion of cholesterol was shown to enhance vasodilation in intact pig and rat arteries that was dependent on $\text{K}_{\text{Ca}2}$ (Absi et al., 2009). Furthermore, $\text{K}_{\text{Ca}3.1}$ was found to be upregulated in apolipoprotein E knockout ($\text{ApoE}^{-/-}$) mice, one of the most predominant models of atherosclerosis (Toyama et al., 2008). Blockers of $\text{K}_{\text{Ca}3.1}$ reduced development of atherosclerosis.

Kv channel activation was reduced in aortic smooth muscle cells in hypercholesterolaemic ApoE and low density lipoprotein receptor (LDLR) null mice ($\text{ApoE}^{-}/\text{LDLR}^{-}$ mice) (Jiang et al., 1999). Additionally, blockade of Kv channels inhibited acetylcholine-dependent relaxation in rabbit cerebral arteries. However, this response was abolished in diet-induced hypercholesterolaemia rabbits, indicating impairment of Kv channel-mediated vasodilation (Ghanam et al., 2000). Furthermore, Kv -dependent vasodilation was impaired in hypercholesterolaemic pig with reduction in smooth muscle cell Kv currents (Heaps et al., 2005).

Kir currents in porcine hypercholesterolaemia models have been shown to be reduced in aortic endothelial cells (Fang et al., 2006). Additionally, hypercholesterolaemia in the same model showed depolarisation of endothelial cells and loss of flow-mediated vasodilation in the femoral artery (Fang et al., 2006). The suppression of Kir currents was proposed to impair flow-induced vasodilation due to reports of endothelial Kir channels sensing shear stress (Olesen et al., 1988; Jacobs et al., 1995).

1.5 Sphingolipid metabolism and signalling

Sphingolipids are a major class of lipids that are ubiquitously found in eukaryotic membranes. Originally the primary role sphingolipids was thought to be structural in the formation of membranes. However, research into the metabolism and functions of the sphingolipid family revealed they are bioactive lipids with an increasing number of biological actions occurring, such as modulation of the cell cycle, angiogenesis, stress and inflammatory responses. Sphingolipids have also been shown to have effects on membrane sterols, helping to form lipid microdomains to form hubs for effective signal transduction. Sphingolipid signalling is complex due to the mechanisms of generation, degradation, conversion and compartmentalisation of the molecules. The sphingolipid metabolism pathways and their compartmentalisation are represented schematically in Figure 1.2.

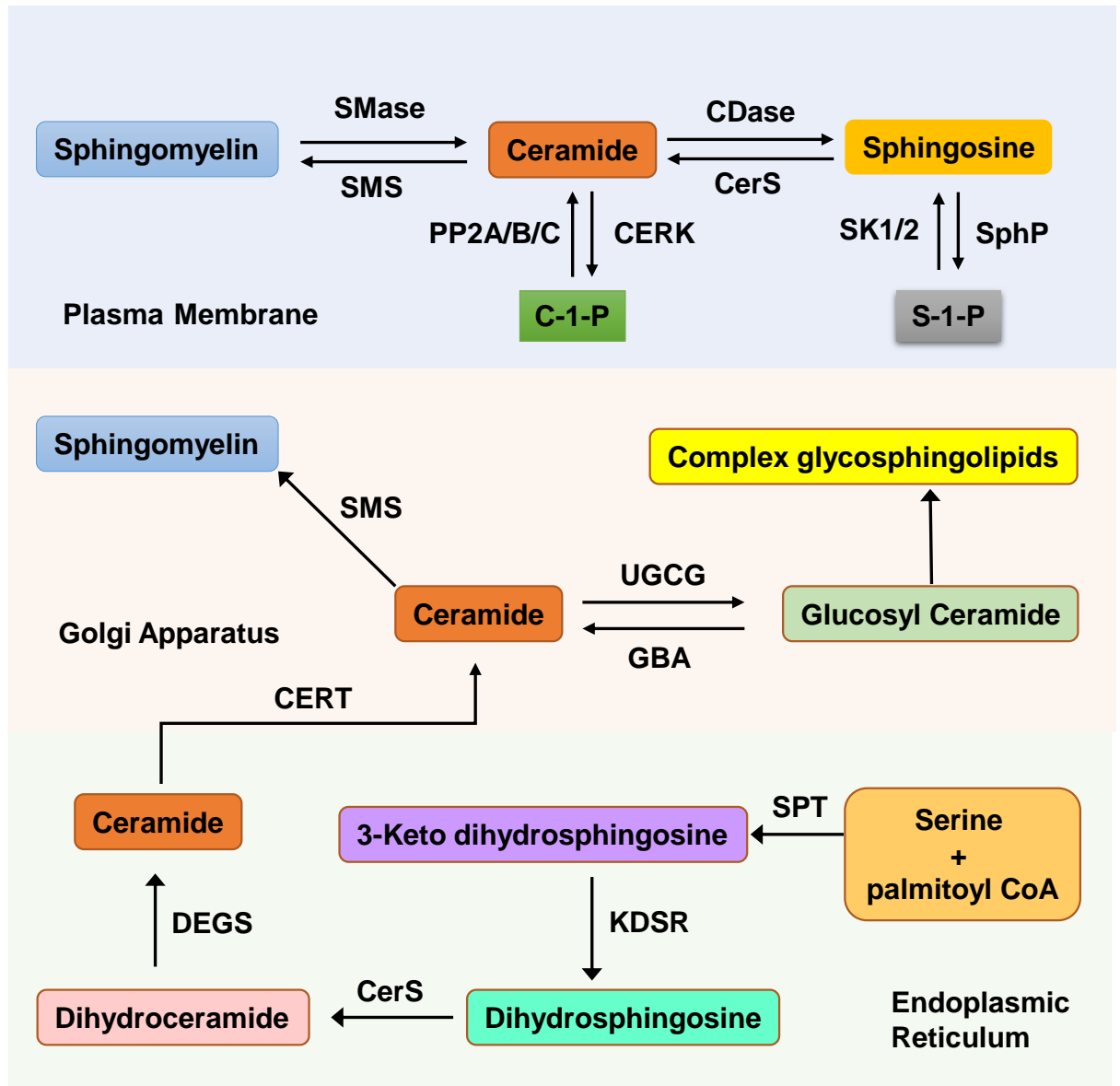


Figure 1.2: Key reactions and compartmentalisation of the spingolipid metabolic pathway.

Ceramide is produced in the endoplasmic reticulum and later transported to the Golgi for further conversion to complex spingolipids. In addition to de novo synthesis, ceramide is also generated by hydrolysis of sphingomyelin. Ceramide is subject to conversion to various other spingolipid metabolites like ceramide-1-phosphate (C-1-P), sphingosine, and sphingosine-1-phosphate (S-1-P). Compartments are highlighted in coloured boxes. CDase: ceramidase; CERK: ceramide kinase; CerS: ceramide synthase; CERT: ceramide transfer protein; DEGS: dihydroceramide desaturase; GBA: glucosyl ceramidase; KDSR: 3-keto dihydrosphinganine reductase; PPAP2A/B/C: phosphatidic acid phosphatase 2A/B/C; SMS: sphingomyelin synthase; SPP: sphingosine-1-phosphate phosphatase; SMase: sphingomyelin phosphodiesterase; SK1/2: sphingosine kinase 1/2; SPT: serine palmitoyl transferase; UGCG: UDP-glucose ceramide glucosyltransferase.

1.5.1 Metabolism of Sphingolipids

Sphingolipid metabolism forms an intricate network of reactions, containing many enzymatic reactions to form many types of sphingolipid. Central to this sphingolipid network is ceramide which is key to sphingolipid biosynthesis and metabolism. Ceramide can be synthesized *de novo* or from the hydrolysis of complex sphingolipids, such as sphingomyelin.

1.5.1.1 De novo sphingolipid pathway

The *de novo* pathway of ceramide production is initiated by the condensation of serine and palmitoyl-CoA which is catalysed by serine palmitoyl transferase, which results in the production of 3-keto-dihydrosphingosine. 3-keto-dihydrosphingosine is then reduced to dihydrosphingosine, which is then *N*-acylated by dihydro-ceramide synthase (Mandon et al., 1992). Ceramide is produced from the desaturation of dihydroceramide by dihydro-ceramide desaturase (Michel and van Echten-Deckert, 1997). Ceramide can be phosphorylated by ceramide kinase to form ceramide-1-phosphate, or glycosylated by glucosyl or galactosyl ceramide synthase (Ichikawa and Hirabayashi, 1998; Sugiura et al., 2002). However, the majority of ceramide formed in the sphingolipid biosynthetic pathway is primarily used for production of sphingomyelin. Sphingomyelin is formed by transferring a phosphocholine headgroup from phosphatidylcholine due to the action of sphingomyelin synthases, which also results in the production of diacylglycerol (Tafesse et al., 2006).

1.5.1.2 Hydrolytic pathway

Ceramide can also be produced from hydrolysis of complex glycosphingolipids. Specific hydrolases remove terminal hydrophilic portions to form

glucosylceramide and galactosylceramide which can then be hydrolysed β -glucosidases and galactosidases to release ceramide (Tettamanti, 2003).

Ceramide can also be produced from the hydrolysis of sphingomyelin releasing phosphocholine. This reaction can be catalysed by one of many sphingomyelinases which are characterised by their optimal pH and subcellular localisation: lysosomal acid sphingomyelinase, zinc-dependent secretory sphingomyelinase, neutral magnesium-dependent sphingomyelinase and alkaline sphingomyelinase (Marchesini and Hannun, 2004).

Ceramide is catabolised by ceramidases, which remove the amide-linked fatty acid portion of the molecule to form sphingosine (Mao and Obeid, 2008). Sphingosine seems to have one of two fates. Sphingosine may be recycled into sphingolipid pathways by conversion back into ceramide by ceramide synthases or phosphorylation by one of two sphingosine kinases (SK1 or SK2) to form sphingosine-1-phosphate (Hait et al., 2006). Sphingosine-1-phosphate may then be dephosphorylated by S1P-phosphatases or irreversibly cleaved to form ethanolamine phosphate and hexadecenal (Johnson et al., 2003; Bandhuvula and Saba, 2007).

1.5.2 Subcellular compartmentalisation of sphingolipids

Certain sphingolipids are localised to particular subcellular locations as many enzymes involved in sphingolipid metabolism are localised to specific cellular apparatus. The location of these enzymes has a profound effect on the functions of the sphingolipids produced. The de novo synthesis pathway of ceramide production occurs on the cytosolic leaflet of the ER membrane (Michel and van Echten-Deckert, 1997). Ceramide is subsequently transported to the Golgi by CERT where sphingomyelin will be produced by sphingomyelin synthases

(Yamaji et al., 2008; Villani et al., 2008). Sphingomyelin is then transported to the plasma via vesicular trafficking (Deng et al., 2016). At the plasma membrane sphingomyelin may be metabolised by SMases to ceramide and further to sphingosine and sphingosine 1-phosphate. Additionally, sphingolipids may be recirculated into the cell through the endosomal pathway where sphingomyelin can be metabolised in lysosomes to form ceramide and subsequently sphingosine via acid ceramidase. Sphingosine may leave the liposome and due to solubility in the cytosol, return to the ER where it can be salvaged (Riboni et al., 1998).

Due to the solubility limitations of most sphingolipids in cells there are restrictions to where sphingolipids can function. Without specific trafficking mechanisms for the sphingolipid, they are likely to remain at the site of synthesis. Some sphingolipids, such as ceramide which is composed of neutral hydrophobic chains may flip-flop between membrane leaflets but are still restricted to their compartment of synthesis (López-Montero et al., 2005). However, sphingosine and sphingosine-1-phosphate may defy compartmentalisation. As they are single-chain lipids these molecules have sufficient aqueous solubility to move between membranes. At a physiological pH, approximately 70% of sphingosine has been estimated to be incorporated in membranes and the remaining 30% is in aqueous solution (Khan et al., 1991). Therefore, these molecules can rapidly equilibrate between membranes.

1.5.3 Sphingolipids as signalling molecules

The complexity of sphingolipid metabolic pathways enables cells to determine cellular responses by regulating sphingolipid interconversions. Cellular levels of different bioactive sphingolipids exert various effects on cell function. In most cell

types sphingomyelin concentrations are an order of magnitude higher than that of ceramide. Furthermore, ceramide is often detected at concentrations greater than an order of magnitude higher than those of sphingosine. Therefore, sphingosine concentrations can be doubled by only 3-10% of ceramide hydrolysis. Subsequently, phosphorylation of 1-3% sphingosine may double the concentration of sphingosine-1-phosphate (Bielawski et al., 2006).

1.5.3.1 Sphingomyelin

Sphingomyelin has a largely structural role in biological membranes with little involvement in downstream signalling mechanisms (van Meer et al., 2008). However, sphingomyelin has also been suggested to regulate the activity of ion channels and enzymes located in the membrane. Voltage-gated potassium channels, Kv2.1 and Kv, were shown to be regulated by sphingomyelin as cleavage of choline from sphingomyelin resulted in a shift of the conductance-voltage relationship resulting in activation of channels at negative potentials (Ramu et al., 2006). A similar relationship was also found in Kv1.3 channels and voltage-dependent Na⁺ and Ca²⁺ channels (Combs et al., 2013). The effect of sphingomyelin cleavage was suggested to be caused by interactions of the channel's voltage sensing domain with sphingomyelin's phosphoryl headgroup (Xu et al., 2008; Milescu et al., 2009). Furthermore, sphingomyelinase D was shown to inhibit Orai1 channels in T-lymphocytes independent of sphingomyelin metabolites (Combs and Lu, 2015). Accumulation of sphingomyelin has also been suggested to inhibit PMCA. In the murine model of Niemann Pick Type A, where acid sphingomyelinase is knocked out, high intracellular Ca²⁺ levels were found to be due to this mechanism (Pérez-Cañamás et al., 2017). Sphingomyelin has also been suggested to inhibit secretory phospholipase A₂ (Nakamura et al., 2015). In CHO cells lacking NPC1 (Niemann Pick disease, type C1), a protein

that mediates intracellular cholesterol trafficking, sphingomyelin concentrations were lower in the plasma membrane compared to the parent cell line. The reduced plasma membrane sphingomyelin was correlated with an increased release of arachidonic acid induced by secretory phospholipase A₂. Furthermore, addition of exogenous sphingomyelin reduced the release of arachidonic acid.

1.5.3.2 Ceramide

Ceramide has largely been reported to regulate cell processes regarding cell growth, differentiation, senescence, necrosis, proliferation and apoptosis. Ceramide can produce its functions by affecting membranes. Additionally, direct effectors of ceramide have also been identified. Ceramide has been shown to enhance the autophosphorylation of kinase suppressor of Ras (KSR-1) which modulates the activation of Raf by Ras (Zhang et al., 1997). Furthermore, ceramide has been shown to have a concentration-dependent effect on PKC ζ , either stimulating it or inhibiting it (Müller et al., 1995). Activation of PKC ζ has been implicated in the regulation of membrane potential, inhibition of Akt and pro-apoptotic functions (Bourbon et al., 2002; Ramström et al., 2004; G. Wang et al., 2005). Ceramide has also been shown to activate a mix-lineage kinase (MLK) mediating the TNF α 's effect on JNK (Sathyanarayana et al., 2002). Cathepsin B and cathepsin D have also been shown to interact with ceramide (Liu et al., 2016). Activation of cathepsin D by ceramide results in activation of Bcl-2 family members, including Bid, leading to pro-apoptotic events (Heinrich et al., 2004). Protein phosphatases PP1A and PP2A are also activated by ceramide (Chalfant et al., 1999). Activation of PP2A by ceramide has been suggested to result in the dephosphorylation of eNOS resulting in vascular dysfunction in mice (Bharath et al., 2015).

Ceramide has been shown to inhibit several types of ion channels, including Kv1.3 channels and HERG. The mechanisms of inhibition of these ion channels is not clear in all cases. However, it has been suggested that Kv1.3 channels are inhibited in Jurkat T lymphocytes due to formation of large ceramide-enriched membrane platforms (Bock et al., 2003). The inhibition of HERG channels by ceramide is controversial. Chapman showed that HERG channels stably expressed in HEK293 cells were inhibited due to rapid reduction in cell surface expression upon exposure to C₆-ceramide (Chapman et al., 2005). However, Ganapathi suggested that C₆-ceramide induced a hyperpolarising shift that resulted in the inhibition of HERG channels (Ganapathi et al., 2010). Additionally, ceramide also caused translocation of HERG channels into cholesterol rich domains which altered the gating mechanism of HERG channels (Ganapathi et al., 2010).

1.5.3.3 Ceramide-1-phosphate

Ceramide-1-phosphate has largely been implicated in cell growth, cell survival and inflammatory responses (Arana et al., 2010). Ceramide-1-phosphate was initially found to have mitogenic properties in rat and mouse fibroblasts (Gomez-Muñoz et al., 1995; Gomez-Muñoz et al., 1997). Further investigation into the mitogenic properties of ceramide-1-phosphate in macrophages revealed that Ceramide-1-phosphate mediated this response via activation of the mitogen-activated protein kinase kinase (MEK)/Extracellular regulated kinases 1-2 (ERK1-2), phosphatidylinositol 3-kinase (PI3-K)/Protein Kinase B (PKB) and c-Jun terminal kinase (JNK) pathways (Gangoiti et al., 2008). Activation of these pathways enhances cell survival by stimulation of the transcription factor NF-κB. Ceramide-1-phosphate was found to stimulate NF-κB DNA binding activity in primary mouse macrophages promoting cell survival. Ceramide-1-phosphate

has also been shown to have anti-apoptotic activity in bone marrow-derived macrophages. This anti-apoptotic effect was found to be due to direct inhibition of acid sphingomyelinase activity by ceramide-1-phosphate and subsequent reduction in cellular ceramide accumulation (Gómez-Muñoz et al., 2004).

The first report of ceramide-1-phosphate in inflammatory responses showed that ceramide-1-phosphate was responsible to arachidonic acid release and prostanoid synthesis in A549 lung adenocarcinoma cells (Pettus et al., 2003). Subsequently, this response was shown to be due to direct activation of Phospholipase A₂ and was shown to enhance the binding of Phospholipase A₂ to phosphatidylcholine (Pettus et al., 2004; Subramanian et al., 2005). Ceramide-1-phosphate has also been implicated in other inflammatory processes such as phagocytosis of neutrophils and degranulation of mast cells (Hinkovska-Galcheva et al., 1998; Hinkovska-Galcheva et al., 2005; Mitsutake et al., 2004).

1.5.3.4 Sphingosine

Sphingosine has been implicated in similar cell processes as ceramide signalling such as inducing cell cycle arrest and apoptosis. Many enzyme targets of sphingosine have been suggested in various cell types as well as direct modulation of ion channels. Sphingosine has been shown to be a potent inhibitor of protein kinase C, which inhibits the interaction between protein kinase C and its substrate (Smith et al., 2000). The inhibition of protein kinase C by sphingosine has been suggested to reverse growth inhibition of vascular smooth muscles and contribute to apoptosis of human promyelocytic leukaemia cells (Weiss et al., 1991; Ohta et al., 1995). Sphingosine has also been shown to inhibit calmodulin-dependent kinases and Src kinases (Jefferson and Schulman, 1988; Igarashi et al., 1989). Activation of kinases by sphingosine has also been

demonstrated. Protein kinase A (PKA) has been shown to be activated by sphingosine in Balb/3T3 cells resulting in phosphorylation of 14-3-3 protein, which is important in the modulation of cell signalling pathways (Ma et al., 2005). Activation of casein kinase II, p21-activated kinase 1 and 3-phosphoinositide-dependent kinase 1 have also been shown to be activated by sphingosine (McDonald et al., 1991; Bokoch et al., 1998; King et al., 2000). Furthermore, sphingosine has been suggested to activate phospholipase D in bovine pulmonary artery endothelial cells and human fibroblasts, with exogenous treatment of sphingosine and treatment with bacterial sphingomyelinase resulting in activation in human fibroblasts (Natarajan et al., 1994; Meacci et al., 1996). Additionally, isolated phospholipase lipase C δ 1 has been shown to be activated by sphingosine (Matecki and Pawelczyk, 1997).

Direct modulation of ion channels by sphingosine has also been reported. Store operated Ca^{2+} release activate Ca^{2+} channels have been suggested to be inhibited directly by extracellular sphingosine in rat basophilic leukaemia cells (Mathes et al., 1998). Furthermore, TRPM7 and TRPM6 channels have been inhibited by sphingosine when overexpressed in HEK293 by reduction in open probability but not single channel conductance (Qin et al., 2013). Sphingosine derivatives, such as FTY720, also inhibited TRPM6 and TRPM7 channels but not metabolites of sphingosine such as ceramides or S-1-P. Conversely, TRPM3 channels have been shown to be activated by sphingosine when the channels were overexpressed in HEK293 cells (Grimm et al., 2005).

1.5.3.5 Sphingosine-1-Phosphate

Sphingosine-1-phosphate has opposing signalling functions to sphingosine and ceramide. S-1-P has been implicated in regulation of proliferation, cell growth,

cell survival, cell migration, inflammation, angiogenesis, vasculogenesis and resistance to apoptosis (Spiegel and Milstien, 2003). S-1-P has been proposed to act as both an extracellular mediator and as an intracellular second messenger. Five closely related G-protein couple receptors of S-1-P have been identified, S1P₁₋₅, with high affinities for S-1-P (Rosen et al., 2013). S-1-P receptors have a diverse range of signalling responses due to their association with different G_α subunits. S1P₁ has been shown to couple with G_{i/o}, whereas S1P₂ and S1P₃ can couple through G_{i/o}, G_q and G_{12/13} (Windh et al., 1999; Jiang et al., 2007; Takashima et al., 2008). S1P₄ and S1P₅ can couple through G_{i/o} and G_{12/13} (Malek et al., 2001; Gräler et al., 2003). The responses of cells to S-1-P depends on the expression of subtypes in each tissue. Endothelial cells and vascular smooth muscle cells predominantly express S1P₁, S1P₂, and S1P₃ at various levels depending on vessel type and tissue of origin (Takuwa et al., 2008). S1P₄ and S1P₅ are predominantly expressed in the immune system and the nervous system, respectively (Gräler et al., 1999; Im et al., 2000). Knockout of S1P₁ alone results in embryonic lethality due to defects in vascular development (Liu et al., 2000). Knockout of S1P₂ and S1P₃ receptors did not produce significant phenotype in mice (Kono et al., 2004). Signalling through S1PRs has been associated with diverse vascular functions including vascular permeability activation of PI3K and Rac to enhance endothelial barrier function (Singleton et al., 2005), cell migration via Rho-dependent activation of α_vβ₃- and β₁-containing integrins (Paik et al., 2001), cell-cell adhesion via Rho and Rac-coupled adherens junction assembly (Lee et al., 1999), survival (Lee et al., 1998) and tumour angiogenesis (Chae et al., 2004).

Intracellular signalling mechanisms have also been suggested for S-1-P through production of S-1-P by sphingosine kinases. Sphingosine Kinase 2 can be found

in the nucleus of many cell types in a repressor complex with histone H3 and histone deacetylases (HDACs) that regulates gene transcription (Hait et al., 2009). S-1-P was shown to bind to HDAC1 and HDAC2. This inhibition has been suggested to affect epigenetic regulation of cyclin-dependent kinase inhibitor *p21* and the transcriptional regulator *c-fos* (Hait et al., 2009). S-1-P has also been shown to be important in the activation of NF- κ B in response to TNF α via TNF receptor-associated factor 2 (TRAF2) and the ubiquitination of RIP1 (Xia et al., 2002). S-1-P was shown to be a cofactor required for the E3 ligase activity of TRAF2 resulting in the ubiquitination of RIP1 (Alvarez et al., 2010). S-1-P has also been suggested to be important in the function of mitochondria. Sphingosine kinase 2 was shown to localise with mitochondria and sphingosine kinase 2 knockout mice had reduced activity of complex IV of the electron transport chain. The effect of sphingosine kinase 2 knockout was determined to be due to loss of S-1-P production and its interaction with Prohibitin 2 that regulated mitochondrial assembly and function (Strub et al., 2011).

1.5.4 Sphingomyelinases in the cardiovascular system

Various tissue extracts were found to have sphingomyelinase activity in 1940 (Thannhauser and Reichel, 1940). However, a specific enzyme with sphingomyelinase activity was not identified until 1966 (Kanfer et al., 1966). From here different sphingomyelinases have been identified that fall into three main classes- acid, alkaline and neutral- which corresponds to the optimal pH for each enzyme family (Goñi and Alonso, 2002). Alkaline sphingomyelinase expression is confined to the intestinal mucosa and liver in human (Duan, 2006). However, acid sphingomyelinases and neutral sphingomyelinases have been

shown to have crucial roles in cardiovascular physiology and pathophysiology (Pavoine and Pecker, 2009).

1.5.4.1 Acid Sphingomyelinases

The first sphingomyelinase identified had optimal activity at pH 5 and was found to be encoded by the *Smpd1* gene (Gatt, 1963; Schuchman et al., 1992). Deficiency in acid sphingomyelinase activity was attributed to the lysosomal storage disorder, Niemann-Pick disease, which resulted in accumulation of sphingomyelin in lysosomes (Brady et al., 1966). The protein product of this was found to form two distinct forms of acid sphingomyelinase through differential trafficking of a 75 kDa protein precursor (Schissel et al., 1996). The acid sphingomyelinase located to either lysosomes (lysosomal acid sphingomyelinase; L-aSMase) or the Golgi secretory pathway (secretory acid sphingomyelinase; S-aSMase). L-aSMase is a 70 kDa glycoprotein containing a mannose 6-phosphate residue that is essential for lysosomal targeting via the mannose 6-receptor. S-aSMase has complex N-linked oligosaccharide post modifications. Both isoforms of aSMase require zinc for activity. However, L-aSMase is tightly bound to zinc and does not require exogenous zinc for activity, whereas S-aSMase requires exogenous zinc for optimal activation (Tabas, 1999; Smith and Schuchman, 2008). The amount of each isoform produced has been suggested to be due to cytokine exposure to cells. For example, human coronary artery endothelial cells secrete large amounts of S-aSMase in response to interferon- γ and interleukin-1 β (Marathe et al., 1998). An increase in S-aSMase is linked to a decrease in L-aSMase activity suggesting a shunting of the common precursor away from the lysosomal trafficking pathway (Marathe et al., 1998; Tabas, 1999).

1.5.4.1.1 L-aSMase in vascular tone

L-aSMase can translocate to extracellular surface of the plasma membrane from lysosomes. This was first shown in human lymphocytes in response to receptors belonging to the TNF family and mediators of apoptosis (Grassme et al., 2001). Translocation of L-aSMase occurs in response to phosphorylation by PKC δ (Zeidan et al., 2008). L-aSMase produces increased ceramide in the intracellular leaflet of the plasma membrane and the formation of ceramide-rich domains which may serve as a hub for apoptosis signalling (Gulbins, 2003). In vascular smooth muscle cells and endothelial cells, the formation of ceramide-rich domains by L-aSMase has been shown to contribute to Fas-ligand impairment of vasodilation and muscarinic-1 receptor-mediated coronary artery constriction (Jin et al., 2008; Zhang et al., 2007; Jia et al., 2008). Both of these are factors in atherosclerosis development.

1.5.4.1.2 S-aSMase in atherosclerosis

Endothelial cells that cover the atherosclerotic lesions secrete S-aSMase due to enhanced proinflammatory atherogenic cytokine exposure (Marathe et al., 1998). The secretion of S-aSMase has been suggested to contribute to vascular smooth muscle cell proliferation via production of ceramides (Augé et al., 1996). Additionally, S-aSMase has been shown to act on lipoprotein particles containing sphingomyelin resulting in fusion and subendothelial aggregation of lipoprotein particles leading to foam cell formation (Schissel et al., 1998; Goldschmidt-Clermont et al., 2007). S-aSMase has been found in atherosclerotic lesions in human and experimental models (Marathe et al., 1999; Hojjati et al., 2005). When hyperlipidaemic knockout mice models of atherosclerosis, *Apoe*^{-/-} and *Ldlr*^{-/-}, were crossed onto aSMase deficient mice, *Asm*^{-/-}, atherosclerotic lesion

development and arterial lipoprotein aggregation was reduced (Devlin et al., 2008).

1.5.4.2 Neutral Sphingomyelinases

Neutral sphingomyelinase activity was first described in fibroblasts from Niemann-Pick disease patients and knockout mice models of *Smpd1* (Horinouchi et al., 1995; Levade et al., 1991). Sphingomyelinase activity was preserved at a neutral pH in these cells indicating the existence of a distinct enzyme with a different optimal pH to aSMase and generated from a separate gene. Characterisation of this enzyme determined a membrane bound protein, dependence for Mg^{2+} and an optimal pH of 7.4 (Rao and Spence, 1976; Liu et al., 1998; Gatt, 1976). Three nSMase genes have now been cloned (*Smpd2*, *3* and *4*) (Tomiuk et al., 1998; Hofmann et al., 2000; Krut et al., 2006). Knockout of nSMase1 (*Smpd2*) gene in mice does not display any functional phenotype (Zumbansen and Stoffel, 2002). Additionally, overexpression of nSMase1 in cells did not modify sphingomyelin metabolism but acted as a lyso-platelet activating factor phospholipase C (Sawai et al., 1999). nSMase2 has been shown to have ubiquitous expression in mammalian tissues and is essential for growth and skeletal development (Stoffel et al., 2007). The nSMase3 gene (*Smpd4*) has high expression in cardiac tissues and is an integral part of TNF α receptor 1 and FAN (factor associated with nSMase activation) signalling (Krut et al., 2006).

Mechanotransduction and nSMase activation have reported to have overlaps in function in endothelial cells. Inhibition of nSMase by scyphostatin in bovine aortic endothelial cells resulted in reduced phosphorylation of MEK1/2 in response to shear stress (Czarny and Schnitzer, 2004). This inhibition of shear stress responses was recovered by exogenous treatment of ceramides and bacterial

nSMase. In microvascular lung endothelial cells nSMase was shown to be activated by shear stress and resulted in ceramide production at caveolae (Czarny et al., 2003; Rizzo et al., 1998). Additionally, isolated arteries have been shown to relax in response to exogenous bacterial nSMase via activation of eNOS, independent of increases in intracellular Ca^{2+} (Mogami et al., 2005). However, nSMase activation in ageing rat arteries has been shown to decrease eNOS activation via ceramide-activated protein phosphatase 2A activity, decreasing vasomotor activity (Smith et al., 2006).

Activation of nSMase has been implicated in the pathophysiology of atherosclerosis. Vascular smooth muscle cell death has been shown to be induced by apoC-1 enriched HDLs which activate nSMase in vitro (Kolmakova et al., 2004). ApoC-1 content appears as an early marker of coronary artery disease in patients and has been identified in areas of plaque rupture in Watanabe hyperlipidaemic rabbits (Björkegren et al., 2002; Steen et al., 2007). These suggest a link between activation of nSMase in vitro and in vivo. Furthermore, oxidised LDLs have been shown to induce proliferation of vascular smooth muscle cells in vitro, which may trigger progression of atherosclerosis and plaque rupture (Auge et al., 2004; Auge et al., 2002).

1.7 Piezo1

The Piezo family of proteins form mechanically-activated non-selective cation channels. Discovered in a siRNA screen against mechanically activated currents in a glioblastoma cell line in 2010 (Coste et al., 2010), the functions and molecular mechanisms of Piezo proteins are starting to emerge. The family consists of two proteins, Piezo1 and Piezo2. Both proteins assemble to form channels which independently confer mechanically activated non-selective cation currents with relatively fast kinetics and inactivation when overexpressed in heterologous systems (Coste et al., 2010). Piezo proteins have widespread expression throughout mechanically active tissues, however, Piezo2 was most obviously localised to sensory neurons and Piezo1 to the lung and kidney (Coste et al., 2010). There is evidence to suggest Piezo2 has roles in touch and pain sensation (Kim et al., 2012; Faucherre et al., 2013). Piezo1 has been shown to be involved in sensation of interstitial pressure and urinary flow in the kidneys (Miyamoto et al., 2014). Piezo1 may have roles other than mechanosensation with roles in cell migration and proliferation (McHugh et al., 2010).

1.7.1 Structure

The structure of Piezo1 is striking when compared to other ion channels. The Piezo1 monomer is of a similar size to a sodium channel from *Electrophorus Electricus* at 286 kDa (Noda et al., 1984). However, the sodium channel contains repeating sequences in its protein structure whereas Piezo1 does not, suggesting that Piezo1 must multimerise to form the functional ion channel. Initial structural analysis suggested that Piezo1 formed a tetramer. This was achieved using cross-linking using paraformaldehyde and a four-stage bleaching of fluorescent-tagged Piezo1 (Coste et al., 2012). However, the complete 3

dimensional structure, resolved to 4.8 Å using cryo-electron microscopy, determined that Piezo1 formed a trimeric structure in a propeller-like fashion (Ge et al., 2015). The C-terminal regions of the protein come together to form a central pore region with a large extracellular cap and the peripheral N-terminal regions are like blades of a propeller (Figure 1.3). Bioinformatic analysis of the Piezo1 protein suggested hydrophobic regions which may have formed 28-32 transmembrane domains. However, the initial cryo-EM structure of Piezo1 determine there are approximately 18 transmembrane domains, most of which are located in the N-terminal blade structures. More recently, higher-resolution cryo-EM structures have been found to have 24 transmembrane helices in the N-terminal blade structures which were arranged as six repeated 4-transmembrane structures (Guo and MacKinnon, 2017; Saotome et al., 2017). Furthermore, a 38 transmembrane domain structure of Piezo1 has been resolved with 9 repetitive units consisting of 4 transmembrane domains which form a highly-curve blade structure (Zhao et al., 2018). The blade structures have been suggested to bend the local lipid environment to form 'dome' structures (Guo and MacKinnon, 2017). It was proposed that flattening of the membrane due to an increase membrane tension may flatten the dome structure and activate Piezo1. The N-terminal repeats are connected to the inner and outer helices of the central pore domains by the anchor region. Additionally, a beam structure on the intracellular region of Piezo1 has been suggested to associate with the C-terminal domain and the third repeat of the transmembrane domains in blade structure. This blade region may be involved in the gating mechanism of Piezo1 (Saotome et al., 2017; Zhao et al., 2018). Furthermore a lipid pocket has been suggested between the anchor domain and the first repeat of the blade transmembrane domain clusters (Saotome et al., 2017).

Using electrophysiological patch clamp techniques with mutated and chimeric Piezo1 channels, the C-terminal region has been shown to be important in the gating and ion selectivity of the channel (Gnanasambandam et al., 2015; Coste et al., 2015; Zhao et al., 2016). However, the N-terminal ‘blade’ regions of the protein are important for mechanical activation. When a chimeric channel of the N-terminal region of Piezo1 and an ASIC, which is not normally mechanically activated, is subjected to mechanical force a mechanically-activated current is evoked (Zhao et al., 2016). However, the function of the N-terminal blades conferring mechanical activation onto an ASIC has been disputed with suggestion that this response is from native Piezo1 expression in the heterologous system used (Dubin et al., 2017).

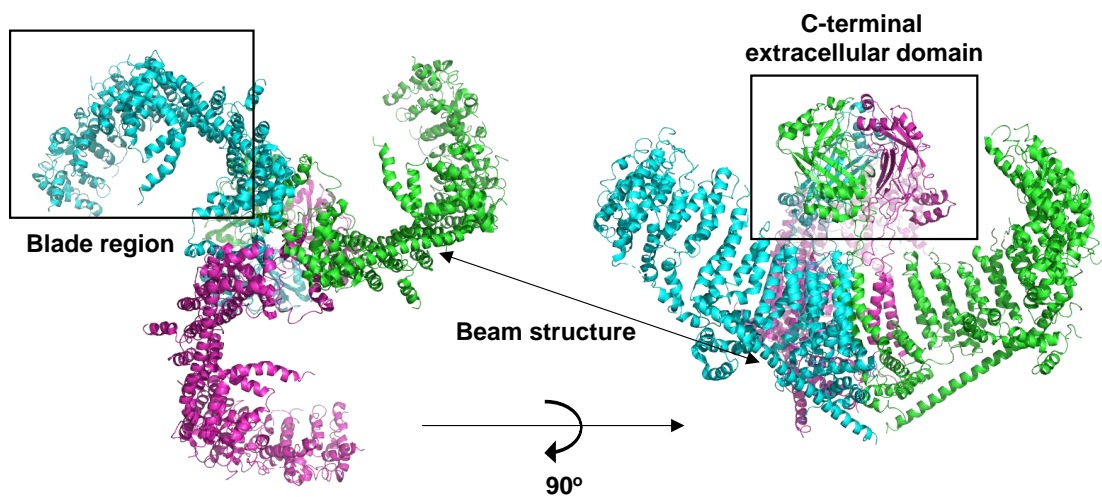


Figure 1.3: Cryo-EM structure of Piezo1 trimer. Left, an intracellular view of Piezo1. Right, the structure of left rotated 90° around the x-axis. Key structure of Piezo1 are highlighted. PDB: 5Z10, 3.97 Å (Zhao et al., 2018).

1.7.2 Activation of Piezo1

The activation of mechanosensitive ion channels in response to mechanical force requires transmission of the force to the channel to cause a conformational change in the protein. Two models have been proposed for force transmission, the force-from-lipids principle and the force-from-filament principle. The force-from-lipid principle argues that mechanical forces are transmitted to mechanosensitive ion channels via deformation of the lipid bilayer (Martinac et al., 1990; Kung, 2005). The force-from-filament principle suggests that mechanosensitive ion channels receive mechanical forces by being tethered to the cytoskeleton or extracellular elements (Katta et al., 2015; Zhang et al., 2015). Cox et al. (2016) have argued that the force-from-lipid principle is more applicable to Piezo1 compared to the force-from-filament principle.

1.7.2.1 The Force-from-Lipids Principle

The force-from-lipid principle was proposed due to the activation of bacterial mechanosensitive ion channels in *Escherichia Coli* spheroplasts by amphipaths (Martinac et al., 1990). Amphipaths have also been shown to activate eukaryotic mechanosensitive ion channels such as TREK-1, TRAAK and Piezo1 (Maingret et al., 2000; Syeda et al., 2015). Additionally, mechanosensitive ion channels have been shown to retain mechanosensitivity after the purified protein was reconstituted in artificial bilayers (Häse et al., 1995; Brohawn et al., 2014; Dong et al., 2015). This suggests that these mechanosensitive ion channels do not require any other cellular components than the lipid bilayer to be activated.

1.7.2.2 Force-from-Lipids principle and Piezo1

Evidence for mechanical activation of Piezo1 by transmission of force from lipids was apparent when activity was observed in HEK293 cell membrane blebs (Cox

et al., 2016). Membrane blebs are protrusions of the cell membrane that are detached from the cortical cytoskeleton. This allowed Piezo1 to be studied in a native cell membrane without influence of the cytoskeleton. Pharmacological disruption of the cytoskeleton using colchicine and cytochalasin D also does not abolish mechanical activation of Piezo1. This suggests that Piezo1 does not require the cytoskeleton for activation.

To prove that Piezo1 can be activated by force from lipids the purified protein may be reconstituted into artificial bilayers and mechanically activated (Coste et al., 2012; Syeda et al., 2016; Syeda et al., 2015). However, when purified mouse Piezo1 was reconstituted in diphytanoylphosphocholine (DPhPC) bilayers with one leaflet containing the conically shaped lipid phosphatidic acid (DOPA) only spontaneous activity has been observed. Additionally, this spontaneous activity requires asymmetric bilayers as no activity was recorded in symmetrical artificial bilayers. Obtaining mechanically activated Piezo1 activity when reconstituted in an artificial bilayer would prove that Piezo1 is inherently mechanosensitive.

1.7.3 Biophysical properties of Piezo1 ion channel

The unitary conductance and inactivation kinetics of Piezo1 have been shown to be determined by the C-terminal pore region of the protein (Coste et al., 2015). Detailed reports of the kinetics of Piezo1 channels have been achieved by using whole cell, cell-attached and outside-out patch clamp configuration on HEK cells transfected with Piezo1 (Gottlieb et al., 2012; Bae et al., 2013; Gnanasambandam et al., 2015; Coste et al., 2010). Currents were evoked by indentation of the membrane using a glass probe or stretching of the membrane by negative pressure. Piezo1 current fit a 3-state model with the channel either closed, open or inactivated.

1.7.3.1 Activation of Piezo1

Activation of Piezo1 has been shown to be pressure-dependent with the half-maximal pressure (P_{50}) reported at -31.2 mmHg during cell-attached stretch (Coste et al., 2010). Maximal current during these conditions was reported at -43 pA and a holding potential of -80 mV. Activation of Piezo1 is dependent on bilayer tension, similar to other mechanically activated channels such as MscL and TREK-1 (Cox et al., 2016; Lewis and Grandl, 2015; Berrier et al., 2013; Häse et al., 1995). Tether-based activation, such as what is involved in the activation of mechanosensitive channels in cochlear hair cells, does not appear to activate Piezo1. However, cytoskeleton-disrupting agents can affect the activation of Piezo1 by altering bilayer stress (Cox et al., 2016; Gottlieb et al., 2012). Inactivation of Piezo1 is not affected by the lipid bilayer tension. However, inactivation of Piezo1 is voltage-dependent (Gottlieb et al., 2012).

1.7.3.2 Inactivation of Piezo1

Inactivation of Piezo1 was determined by discriminating against adaptation of force transmission or inactivation of the channel causing desensitisation of currents (Gottlieb et al., 2012). A two-step staircase stimulus resulted in no response from the second stimulus, suggesting that Piezo1 inactivates. The inactivation rate of Piezo1 is varied across the literature but was originally reported at ~16 ms at -80 mV. Repeated activation resulted in an irreversible loss of inactivation which occurred simultaneously rather than channel-by-channel. Furthermore, it has been suggested that repeated mechanical stimulation may lead to dynamic structural changes in the cytoskeleton which may cause the variability of inactivation rates. Depolarisation of membrane

potential has been shown to slow the inactivation rate of Piezo1. However, there has not been a mechanism suggested for this event.

1.7.3.3 Domains affect Piezo1 kinetics

The cell membrane does not have a uniform composition. In regions where there are differences in composition between membrane leaflets, through lipids or membrane proteins, domains are formed. These domains provide a different environment for an ion channel with varying physical properties, such as fluidity, deformability and tension (Jacobson et al., 1995). Membrane tension may alter the state of ion channel open/closed/inactivated states.

Inactivation was lost when Piezo1 was repeatedly stimulated. This has been suggested to occur due to Piezo1 channels existing in their own spatial domains where they can only inactivate when interacting with each other (Gottlieb et al., 2012; Gottlieb and Sachs, 2012). Rupturing these domains by repeated mechanical stimuli may allow the channels to diffuse away from each other, losing the ability to inactivate. Furthermore, when Piezo1 channels were reconstituted into lipid bilayers they could be activated but would not inactivate, possibly due to the lack of spatial domains formed in these artificial membranes. Additionally, Piezo1-1591-GFP transfected into HEK cells formed clusters of Piezo1 channels (Cox et al., 2016). This supports the argument that Piezo1 exists in spatial domains. The lack of a credible Piezo1 antibody has not allowed for the discovery of these clusters in native Piezo1 expressing cells.

1.7.3.4 Permeation and selectivity of Piezo1

The selectivity of mouse and human Piezo1 has been shown to be typical of non-selective cation channels (Gnanasambandam et al., 2015). Piezo1 is permeable to monovalent and some divalent cations, particularly Ca^{2+} and Mg^{2+} , except for

Mn²⁺. The permeability of Piezo1 is $P_K > P_{Cs} \approx P_{Na} > P_{Li}$ (1.0: 0.88: 0.82: 0.71). This is similar to the conductance of the monovalent cations. However, Li⁺ has a much lower conductance. The concentration conductance relationship of K⁺ has a parabolic increase which is saturated at 45-50 pS. Organic monovalent cations, such as tetramethyl ammonium and tetraethyl ammonium (TEA⁺) can move through the channel pore. Due to the size of TEA⁺ the narrowest part of the Piezo1 pore has been suggested to be ~8 Å in diameter.

The unitary conductance of the divalent cations Ba²⁺, Ca²⁺ and Mg²⁺ at 90 mM are ~25 pS (-80 mV), ~15 pS (-80 mV), and ~10 pS (-50 mV), respectively. Piezo1 is not Ca²⁺ selective like Orai or voltage-gated Ca²⁺ channels. However, Coste *et al.*, (2010) suggested that Piezo1 prefers Ca²⁺ over other divalent cations.

1.7.4 Modulation of Piezo1 activity

1.7.4.1 Inhibitors

1.7.4.1.1 Small molecular inhibitors

Piezo1 has no specific pharmacological antagonists. Blockers of cation channels, such as ruthenium red and streptomycin block Piezo1 (Coste *et al.*, 2010). Ruthenium red blocks Piezo1 in a voltage-dependent manner, which is common for a pore blocker that depends of ion flow directionality. Ruthenium red blocks inward ion currents but not outward current. When ruthenium red was applied to the extracellular surface of Piezo1 reconstituted in an artificial bilayer, it blocked mechanically activated currents. However, no block by ruthenium red occurred when it was applied to the intracellular surface of Piezo1. Furthermore, ruthenium red has a species-specific blockade of Piezo1. Human and mouse

Piezo1 have been shown to be blocked by ruthenium red, whereas *D. melanogaster* Piezo1 is not affected by ruthenium red.

1.7.4.1.2 Peptides

GsMTx4 (Grammostola Spatulata Mechanotoxin 4) is a peptide isolated from the venom of the Chilean Rose tarantula (*Grammostola Spatulata*) (Suchyna et al., 2000). The peptide is 34 amino acids long that can be chemically synthesised and folded with a globular structure. Both enantiomers of GsMTx4 inhibited endogenous mechanically activated currents, suggested that inhibition occurred by positioning itself between at the interface between the ion channel and lipid bilayer (Suchyna et al., 2004). Both human and mouse Piezo1 channels have been shown to be inhibited by GsMTx4 by reducing mechanically activated currents in overexpression systems (Bae et al., 2011).

1.7.4.1.3 Proteins

Mechanically activated currents can be altered by the activity of other proteins. In the renal proximal convoluted tubule, Piezo1-dependent mechanically activated currents were found. These currents were modulated by the expression of Polycystine-2, also known as TRPP2 (Peyronnet et al., 2013). TRPP2 caused reduction of Piezo1 current. Immunoprecipitation of Piezo1 and TRPP2 suggests direct modulation of Piezo1 by TRPP2.

Additionally, Piezo1 has been found to be directly regulated by the SERCA2 protein (Zhang et al., 2017). In the N2A cell line endogenous SERCA2 and Piezo1 was shown to interact by co-immunoprecipitation and co-localisation. Using a fragment of the Piezo1 protein SERCA2 was shown to interact with the anchor domain of Piezo1. SERCA2 was also shown to inhibit Piezo1-dependent mechanically activated currents when co-expressed in HEK293T cells and

overexpressed in N2A cells. Furthermore, disruption of SERCA2 expression potentiated mechanically-activated currents in N2A cells and HUVECs. The inhibition of Piezo1 was suggested to be due to suppression of mechanosensitivity by regulating gating of Piezo1 at the linker. In HUVECs the SERCA2-Piezo1 interaction was suggested to regulate cell migration and eNOS phosphorylation.

1.7.4.2 Cytoskeleton and cell membrane

1.7.4.2.1 STOML3

Stomatin-like protein-3 (STOML3) was shown to be critical for touch in mouse. However, the mechanism by which STOML3 contributes to mechanotransduction was unknown. Therefore, STOML3 was investigated to determine whether there was a relationship between it and Piezo1. Initially, Poole *et al.*, (2014) isolated sensory neurons and grew them on pillars which, when deflected by approximately 13 nm, activated mechanically activated currents. Neurons from STOML3 knockout mice required much higher amounts of pillar deflection to be activated. This suggested a relationship between STOML3 and mechanically activated currents. To focus on the relationship between STOML3 and Piezo1 the same experiment was repeated with the N2A cell line. Pillar deflection also produced mechanically-activated currents which were ablated when cells were treated with siRNA targeting Piezo1, reducing its expression. Overexpression of STOML3 subsequently increased the magnitude of mechanically activated currents in these cells. Conversely, depleting STOML3 increased the stimulus required to activate mechanically-activated currents. When STOML3 was overexpressed with either Piezo1 or Piezo2 in HEK293 cells, sensitivity to mechanically stimulation was also increased. This suggested

that STOML3 could fine tune Piezo1 sensitivity possibly by affecting the local environment of the channel.

Qi *et al.*, (2015) determined that STOML3 facilitates membrane stiffness by associating with cholesterol and forming lipid rafts. Removing cholesterol and abolishing STOML3 expression resulted in reduced mechanical responses of Piezo1. The attenuation of Piezo1 activation was attributed to a decrease in membrane stiffness and loss of association with lipid rafts.

1.7.4.2.2 Filamin A

A relationship between Piezo1 and Filamin A was revealed when investigating arterial remodelling in caudal arteries due to hypertension (Retailleau *et al.*, 2015). A conditional knockout mouse of Piezo1 was generated which had no mechanically activated current in vascular smooth muscle cells compared to control mice. In the Piezo1 knockout mice hypertension-induced vascular remodelling did not occur. When filamin A was knocked out, an elevation in intracellular Ca^{2+} was observed. However, when both Piezo1 and filamin A were knocked out this elevation in Ca^{2+} did not occur. This suggests that the increase in intracellular Ca^{2+} was due to Piezo1 and filamin A modulating Piezo1 activity. Furthermore, mechanically activated currents were potentiated in the filamin A conditional knockout mouse. This was thought to occur due to filamin A reducing tension in the membrane domain in which Piezo1 is located.

1.7.4.3 Protonation

When measured at different pHs, human Piezo1 currents were found to be decreased at lower pH levels, with a reduction of >80% whole-cell current amplitude at pH 6.5 compared to pH 7.3 (Bae *et al.*, 2015). Additionally, there was a loss of currents in response to sequential stimuli at pH 6.5 which could be

reversed when pH was returned to pH 7.3. Plotting the loss of mean function as a function of pH produced a Hill coefficient of 3 ± 1.0 , suggesting positive cooperativity and at least two sites of protonation in Piezo1. When tested on an inactivating double mutant of Piezo1 (M2225R and R2456K) pH had no effect. This suggested that protonation stabilises the inactivation state of Piezo1. These findings suggest that Piezo1 may be affected in pathophysiological environments where pH is reduced, such as ischaemia or the tumour microenvironment.

1.7.4.4 Cell signalling pathways

Regulation of ion channels by intracellular signalling pathways has been demonstrated for many ion channel families. For Piezo channels, the focus has been on modulation of Piezo2 activity in sensory neurons. Piezo2 activity was shown to be potentiated by activation of protein kinase C (PKC) and protein kinase A (PKA) in mouse dorsal root ganglion neurons following activation of bradykinin receptors (Dubin et al., 2012). Additionally, Piezo2 activity has been shown to be potentiated by cyclic adenosine monophosphate (cAMP) via exchange protein directly activate by cAMP (EPAC) in human DRG neurons using cAMP analogues (Eijkelkamp et al., 2013).

Modulation of Piezo1 by intracellular signalling mechanisms was found in conjunction with modulation of Piezo2 via TRPV1 (Borbiro et al., 2015). In TRPV1 expressing neurons, treatment with TRPV1 agonist capsaicin abrogated mechanically-activated currents. Co-expressing either Piezo1 or Piezo2 with TRPV1 in HEK cells resulting in inhibition of mechanically-activated currents after application of capsaicin. This inhibition was dependent on the presence of extracellular Ca^{2+} highlighting the importance of Ca^{2+} in the mechanism of inhibition. Ca^{2+} influx via TRPV1 had been linked to activation of PLC δ and leads

to a decrease in PI(4,5)P₂ and PI(4)P levels at the plasma membrane (Lukacs et al., 2007; Lukacs et al., 2013). Intracellular application of PI(4,5)P₂ or PI(4)P in whole cell patch configuration reduced the inhibition of Piezo1 by TRPV1 activation. Inhibition of Piezo1 also occurred in response to treatment with pseudojanin which dephosphorylates PI(4,5)P₂ and PI(4)P. Furthermore, rundown of mechanically-activated Piezo1 currents in excised patches was observed. This phenomenon often occurs in channels dependent on PI(4,5)P₂ for activity (Rohacs, 2014).

Carbachol activates G_q-coupled M1 muscarinic acetylcholine receptors and a decrease in PI(4,5)P₂ and PI(4)P in the plasma membrane (Borbiro et al., 2015). However, when carbachol was used to determine inhibition of Piezo1 the effect was marginal compared to the inhibitory effect of TRPV1. The depletion of PI(4,5)P₂ and PI(4)P was greater after TRPV1 activation, with PI(4)P decrease at much greater levels, compared to M1 activation. When ATP was removed from the intracellular pipette solution to remove restoration of phosphoinositide levels carbachol induced a much greater level on inhibition of Piezo1. This suggests that Piezo1 is affected by phosphoinositides in the plasma membrane, requiring them for activation.

1.7.4.5 Chemical activation of Piezo1

Recently, a specific agonist for Piezo1 has been discovered called Yoda1 (Syeda et al., 2015). Yoda1 was discovered in a screen of approximately 3 million small molecular weight compounds targeting calcium influx via Piezo1 and Piezo2. Yoda1 was shown to activate Piezo1 over Piezo2. The biophysical properties of Piezo1 were altered by Yoda1 compared to mechanically activated Piezo1 in the cell-attached patch clamp configuration. There was a slowing of channel

inactivation, a decrease in pressure required to activate the channel and spontaneous channel opening without applied pressure. The changes in biophysical properties are consistent with the changes found in mutations of Piezo1 that cause hereditary xerocytosis. This mutation is located in the C-terminal region near the pore domain (Bae, Gnanasambandam, et al., 2013). This suggests that Yoda1 may bind to the C-terminal region of Piezo1, opening the pore. To determine whether Yoda1 directly activates Piezo1 the channel was reconstituted into a lipid bilayer and single channel currents were recorded. At 1 μ M Yoda1 activated single channels with multiple channels opening at higher concentrations. Chemically-modified Yoda1-like compounds did not activate Piezo1 suggesting direct interaction between Yoda1 and Piezo1. Yoda1 has subsequently been used as an agonist of Piezo1 to determine possible physiological roles of Piezo1 channels (Wang et al., 2016; Cahalan et al., 2015).

1.7.5 Functional roles of Piezo1

Since the discovery of Piezo1 many functional roles have been determined in different cell types. McHugh et al. showed that Piezo1 is responsible for integrin activation in cells and the same group also showed that reduced expression of Piezo1 in lung epithelial cells decreased adherence and increased migration of these cells (McHugh et al., 2010; McHugh et al., 2012). However, contrasting results have been found in zebrafish epithelial cells and gastric cancer cells when compared to the studies by McHugh et al. Disruption of the Piezo1 gene decreased epithelial cell extrusion and increased epithelial cell masses in zebrafish (Eisenhoffer et al., 2012). Furthermore, knockdown of Piezo1 decreased gastric cancer cell migration (Yang et al., 2014). Aside from roles in cell migration and proliferation, Piezo1 channels have been shown to function as

a sensor of pressure and fluid flow. In the kidneys, inhibition of Piezo1 reduced stretch-activated currents in proximal convoluted tube epithelial cells, suggesting Piezo1 has a role in sensing urinary flow and changes in intraluminal pressure (Miyamoto et al., 2014). Furthermore, Piezo1 has been shown to be important in shear stress sensing in endothelial cells, which is critical for vascular development (Li et al., 2014; Ranade et al., 2014). Overall, these studies suggest that Piezo1 is important in different tissues to function as a mechanical sensor of their environment.

1.7.5.1 Piezo1 in vascular functions

The physiological force of shear stress has been shown to be essential for vascular functions from development to maintenance of health. Although there have been many proposed shear stress sensing mechanisms, a direct mechanism of shear stress sensing remained elusive. However, Piezo1 was found to be a direct sensor of shear stress and regulated many endothelial cell functions (Li et al., 2014; Ranade et al., 2014).

1.7.5.1.1 Vascular development

Piezo1 has been shown to be important in vascular development (Li et al., 2014; Ranade et al., 2014). Global knockout of the Piezo1 gene results in embryonic lethality at E9.5 in murine models. However, homozygous negative murine embryos did not develop vascular networks in the yolk sac or embryo which resulted in the embryo being absorbed. Heterozygous Piezo1 murine embryos survived and allowed study of the vascular development of mice with haploinsufficiency. Vascular development in the heterozygous yolk sac showed considerable disruption in the organisation of the vascular network due to an inability to remodel vessels in response to shear stress. Endothelial-specific

knockout, without stopping the heartbeat also caused similar vascular defects during development showing the importance of endothelial Piezo1 in this process (Li et al., 2014). Depletion of Piezo1 using siRNA in HUVECs suppressed endothelial cell tube formation and cell migration towards VEGF. This suggests that Piezo1 is important for vascular remodelling and angiogenesis in the embryo and is essential for embryonic survival.

1.7.5.1.2 Shear stress-evoked Ca²⁺ entry

Piezo1 was also discovered to be important in shear stress-evoked calcium entry into endothelial cells (Li et al., 2014). Knocking down the expression of Piezo1 with siRNA or blocking with GsMTx4 reduced shear stress-evoked calcium events. Introducing Piezo1 to cells that do not usually respond to shear stress (HEK293 cells) also produced these shear stress-evoked calcium events and cationic currents. This suggests that Piezo1 is a direct sensor of shear stress.

1.7.5.1.3 Endothelial cell alignment

Alignment of endothelial cells is important in the maintenance of healthy vasculature. Endothelial cells align to the polarity of blood flow in response to shear stress. Areas of low shear stress, that is atherogenic, have a reduction in the alignment of endothelial cell alignment to flow. Depletion of Piezo1 in endothelial cells abolishes alignment in vitro and in vivo (Li et al., 2014). The mechanism behind Piezo1-dependent alignment is calcium-dependent activation of calpain which in-turn digests focal adhesions to allow changes in cell morphology and alignment of endothelial cells.

1.7.5.1.4 Regulation of eNOS

Piezo1 has also been shown to regulate the expression of eNOS (Li et al., 2014). Activation of eNOS by VEGF stimulation was reduced in both HUVECs depleted

of Piezo1 and haploinsufficient endothelial cells. Additionally, there was a reduction in total eNOS in HUVECs depleted of Piezo1. This mechanism may lead to the reduction in endothelial cell migration and tube formation.

1.7.5.1.5 Cardiovascular homeostasis during exercise

Piezo1 was shown to be important in the redistribution of blood flow during exercise (Rode et al., 2017). An endothelial-specific Piezo1 knockout mouse, using Cre deletion driven by the Tie2 promoter, was used to investigate endothelial Piezo1 in exercise. These knockout mice had no obvious superficial differences to control mice. However, isometric tension recordings of second-order mesenteric arteries displayed an anti-endothelium-derived hyperpolarising (factor) (EDH(F)) effect. Combining toxin inhibitors, apamin and charybdotoxin, of two K⁺ channels which are responsible for EDH(F) reduced acetylcholine-induced relaxation in Piezo1-null mesenteric arteries but had little effect on control vessels.

Due to the effect on mesenteric arteries and their relevance to peripheral resistance, blood pressure was monitored during rest and activity. During rest there was no difference between control and the knockout mice. However, during exercise the mice with no endothelial Piezo1 had a reduction in the increase in blood pressure in response to exercise.

Piezo1 was shown to be responsible for sensing shear stress in endothelial cells freshly isolated from mesenteric arteries which resulted in depolarisation of the endothelial cells in response to flow. This depolarisation was coupled to the vascular smooth muscle cells of the mesenteric artery which resulted in activation of voltage-gated Ca²⁺ channels which resulted in vasoconstriction. Blocking voltage-gated Ca²⁺ channels with nifedipine reduced contraction in

response to flow in similar fashion to knockout of endothelial Piezo1 in mesenteric arteries.

The effect of endothelial Piezo1 in the mesentery was suggested to have a role in exercised induced redistribution of blood from the gut to skeletal muscles. There was a reduction in activity bouts recorded on a voluntary running wheel over five nights in endothelial Piezo1 null mice compared to control mice. Additionally, in saphenous and carotid arteries, which would normally dilate to provide more blood flow to skeletal muscles or the brain during exercise, Piezo1 did not have an anti-EDH(F) effect. This suggests that Piezo1 functions differently depending on the vascular bed which is optimised for physical performance.

1.7.5.1.6 Hypertensive remodelling

As discussed above, filamin A was shown to modulate Piezo1 activity in vascular smooth muscle cells. Filamin A was shown to reduce Piezo1 activity in these cells and when filamin A was conditionally knocked out remodelling occurred even without hypertension. Furthermore, when Piezo1 was knocked out hypertension-induced remodelling of caudal arteries was abolished. This suggests that remodelling of vascular smooth muscle cells during hypertension is dependent on Piezo1.

1.7.5.2 Piezo1 in cell motility

The first functional discovery of the Piezo1 gene (FAM38A) was discovered in epithelial cells (McHugh et al., 2010). Fam38a was shown to induce integrin activation via R-Ras and calpain, suggesting its involvement in cell adhesion to the extracellular matrix. Knockdown of Fam38a by siRNA resulted in reduced

activation of integrin $\beta 1$ and R-Ras signalling. Cells with reduced Fam38a displayed reduced cell migration (McHugh et al., 2012).

Due to the potential link between Piezo1 and cell migration breast cancer cell lines were investigated for expression of Piezo1 (Li et al., 2015). MCF-7 and MCF-10a cell lines were compared. The more malignant MCF-7 cell line displayed a higher level of Piezo1, detected by patch clamp, than MCF-10a cell line. GsMTx4 reduced motility of the MCF-7 cell line, suggesting a possible role for Piezo1 in the cell line's increased malignancy. These results contrast the depletion of Piezo1 increasing epithelial cell motility. This may be due to Piezo1 activating different signalling pathways in the specialised cells.

1.7.5.3 Piezo1 in cell-to-cell contact

The extracellular environment has a significant impact on cell function. This may involve interaction of opposing cells or the extracellular matrix. These interactions produce traction forces therefore Piezo1 has been investigated as a sensor of this force and transducing it into appropriate cell functions.

The role of Piezo1 in sensing the extracellular environment of cells has largely been investigated in neural and epithelial cells. In neural cells, Piezo1 was shown to sense substrate stiffness which resulted in the differentiation of Neural stem cells into neurons over astrocytes at higher levels of stiffness (Pathak et al., 2014). Ca^{2+} fluxes were reported in hNSPC as a result of the traction forces exhibited on the cells. Reducing Piezo1 with siRNA reduced these Ca^{2+} fluxes. Additionally, Yap and Taz transcription factors have been shown to translocate from the cytoplasm to the nucleus in response to higher substrate stiffness. Piezo1 knockdown by siRNA excluded Yap from the nucleus suggesting that Piezo1 senses substrate stiffness. To determine Piezo1's role in hNSPC

differentiation the cells were grown in increasing levels of substrate stiffness and analysed neuron/astrocyte composition. Both treatment with GsMTx4 and Piezo1 siRNA resulted in an increase of astrocytes over neurons in stiffer substrates compared to control conditions. These data suggested that Piezo1 senses substrate stiffness and is important in neural stem cell differentiation.

In epithelial cells, Piezo1 has been suggested to maintain cell homeostasis by allowing extrusion of live cells from the epithelial cell layer (Eisenhoffer et al., 2012). Epithelial cells maintain a constant density of cells in a layer by matching the number of dividing cells with lost cells. Epithelial cells grown to confluence on a stretched silicone membrane, which was then released resulting in increased cell density, returned to confluency after 6 hours due to cell extrusion. A marker for apoptosis, caspase-3, was not always apparent in extruded cells indicating a live cell extrusion pathway. Gd^{3+} and photocleavable morpholino probes used to knockdown Piezo1 expression reduced extrusion of epithelial cells in vitro and in zebrafish, resulting in the formation of masses of cells. Piezo1 has also been shown to trigger epithelial cell division (Gudipaty et al., 2017). Stretching epithelial cells results in cell division at low density. Knockdown of Piezo1 by siRNA reduced stretch-induced mitosis which was recovered by transfection with Piezo1-GFP. Ca^{2+} entry via Piezo1 was shown to result in downstream activation of ERK1/2 and cyclin B transcription resulting in mitosis.

1.7.5.4 Piezo1 in nociception

Piezo1 was shown to have a role in the avoidance response to noxious mechanical stimuli of *Drosophila* larvae (Kim et al., 2012). Expression of Piezo1 was found in adult and larvae *Drosophila melanogaster* in neuronal cells and other tissues. When Piezo1 knockout larvae were produced they were tested for

the avoidance response with von Frey filaments. At a stimulus of 45 mN 80% of wild-type larvae responded. However, only approximately 34% of Piezo1 knockout larvae responded to the same stimulus. Responses to noxious heat and light touch were not affected between wild-type and knockout larvae.

1.7.5.5 Ca²⁺ influx and ATP release

Stimulation of Piezo1 resulting in Ca²⁺ influx and subsequent ATP release has been reported in three different cell types, urothelial cells, erythrocytes and endothelial cells. Initially, (Miyamoto et al., 2014) showed that Piezo1 is expressed in mouse urothelium and cultured urothelial cells. When Piezo1 expression was reduced by treatment with siRNA, stretch-induced Ca²⁺ influx and ATP release was diminished.

Secondly, Cinar et al. (2015) revealed that Piezo1 plays a similar role in erythrocytes. Shear stress was used to stimulate Ca²⁺ influx and subsequent ATP release. GsMTx4, Gd³⁺ and ruthenium red all reduced shear-induced Ca²⁺ influx and ATP release. However, these pharmacological treatments are not specific for Piezo1. Therefore, red blood cells from patients with Xerocytosis were compared to red blood cells from healthy patients. Xerocytosis has been linked with a mutation of Piezo1 which results in slower inactivation and latency to activation of the channel. Xerocytosis cells displayed reduced Ca²⁺ influx and ATP release compared to control cells which suggest more involvement of Piezo1 in this mechanism. The mechanism of ATP release was suggested to be from Pannexin-1 using the inhibitor carbenoxolone, which diminished ATP release from red blood cells. Treatment with both GsMTx4 and carbenoxolone decreased ATP release further, suggesting a link between mechanically-activated ion channels and Pannexin-1.

Finally, (Wang et al., 2016) observed that Piezo1 was responsible for Ca^{2+} influx and ATP release from human umbilical arterial endothelial cells. Knockdown of Piezo1 expression by siRNA reduced Ca^{2+} influx and ATP release after activation by both shear stress and Yoda1. Pannexins were also attributed to the release of ATP as siRNA targeting Pannexin-1 and -2 reduced shear- and Yoda1-induced ATP release. However, other mechanisms of ATP release may also occur as ATP release was not completely abolished.

1.7.6 Piezo1 in disease

1.7.6.1 Lymphatic dysplasia

Loss of function mutations of Piezo1 have been associated with generalised lymphatic dysplasia (Fotiou et al., 2015; Lukacs et al., 2015). The disease is autosomal recessive and affects the ability of lymphatic system to perform its function. The lymphatic system is independent of the circulatory system but transports fluid in a similar manner to blood. Lymph transported by lymphatic vessels is extracellular fluid rich in proteins containing antigens that are delivered to lymph nodes as part of the immune system. Lymphatic vessels are also lined by endothelial cell which have distinct cell surface markers and transcription factors from their circulatory system counterparts. Initially, the lymphatic endothelial cells are leaky but larger collecting vessels have tighter cell-to-cell junctions and are surrounded by lymphatic smooth muscle. The contractile smooth muscle cells conduct lymph flow. The contractions of lymphatic vessels are sensitive to mechanically-associated Ca^{2+} signalling pathways which can be regulated by VEGF-C, endothelin, nitric oxide, and other ligands (Padera et al., 2016). Failure of the lymphatic system to effectively drain interstitial fluid back to the blood results in lymphoedema. Lymphoedema is a chronic condition that

causes swelling in body tissues which can lead to local inflammation, adipose hypertrophy and progressive fibrosis. Lymphoedema can be primary, caused by genetic mutations, or secondary, caused by damage to lymphatic vessels.

Piezo1 mutations have been described in families with nonimmune hydrops fetalis secondary to generalised lymphatic dysplasia (Fotiou et al., 2015; Lukacs et al., 2015). There have been 12 mutations found with all documented or predicted to be loss-of-function. The characterised mutations, G2029R and S1153Wfs21, are located in the anchor region and peripheral helices of Piezo1 respectively (Lukacs et al., 2015). Both mutations were tested for Ca^{2+} elevations in response to negative pressure or Yoda1 in erythrocytes from the heterozygous parents as a control and affected compound heterozygotes. Compared to the control, the mutants displayed reduced Ca^{2+} elevations in response to both negative pressure and Yoda1. The G2029R mutant was over expressed in HEK293 cells for further characterisation. The overexpressed mutant produced less response to Yoda1, minimal mechanically activated currents and reduced cell surface expression in comparison to wild-type Piezo1. The loss-of-function of Piezo1 by these mutants are thought to cause lack of lymphatic endothelial development, with Piezo1 contributing to lymphatic endothelial cell development in healthy physiology.

1.7.6.2 Hereditary Xerocytosis

Gain-of-function mutations of Piezo1 have been shown to cause hereditary xerocytosis, also known as dehydrated stomatocytosis (Albuisson et al., 2013; Andolfo et al., 2013; Andolfo et al., 2017; Zarychanski et al., 2012). Hereditary xerocytosis is an autosomal dominant haemolytic anaemia where red blood cells are characterised by the properties of erythrocyte dehydration: increased mean

corpuscular haemoglobin concentration, resistance to osmotic lysis and increased red cell density (Andolfo et al., 2016). Currently 24 mutations of Piezo1 have been reported in patients with hereditary xerocytosis. The most characterised mutations are the M2225R and R2456H mutations in human Piezo1. These mutations slowed the inactivation of Piezo1 currents in both whole cell and cell-attach patch configurations when overexpressed in HEK cells (Bae, Gnanasambandam, et al., 2013; Bae, Gottlieb, et al., 2013). Additionally, the mutations caused latency of activation in response to mechanical stimuli. To identify the mechanism of Piezo1's involvement in red blood cell dehydration in hereditary xerocytosis Yoda1 was used (Cahalan et al., 2015). On wild-type red blood cells, Ca^{2+} influx occurred in response to Yoda1 treatment which resulted in activation of a Ca^{2+} -activated K^+ channel. When Piezo1 was knocked out of red blood cells swelling and overhydration occurred. This suggested that Piezo1 was responsible for red blood cell volume homeostasis and gain-of-function mutations resulted in excessive activation of Ca^{2+} -activated K^+ channels which resulted in osmotic loss of water from the cell.

1.8 Aims of the study

The overall aim of this work was to develop a better understanding of mechanisms that regulate Piezo1 activity. The focus was on Ca²⁺ entry via Piezo1 and how this mechanism can be modulated by cholesterol, sphingolipid signalling mechanisms or synthetic small molecules.

First it was hypothesised that cholesterol may have an important relationship with Piezo1 activation by directly regulating the channel. The objectives of the study were: 1) to determine the effects of cholesterol-loading on shear stress responses in endothelial cells; 2) to determine the effects of cholesterol-loading and cholesterol depletion on Piezo1 activation by Yoda1 in endothelial cells and HEK293 cells conditionally over-expressing Piezo1; 3) to determine the mechanism of the effects of cholesterol on Piezo1; 4) to determine cholesterol binding sites within Piezo1 that regulation Piezo1 sensitivity to cholesterol.

The second aim was to determine the effects of sphingolipids on Piezo1 activation in endothelial cells. Inflammatory mechanisms have been shown to alter Piezo1 activity in other cell types. Therefore it was hypothesised that sphingomyelinase, which is involved in inflammatory signalling mechanisms, may affect Piezo1 activation in endothelial cells. The objectives of the study were: 1) to determine the effects of sphingomyelinase on Piezo1 activation by Yoda1 in endothelial cells; 2) to determine sphingolipid metabolites that affect Piezo1 activation; 3) to determine targets of sphingolipid signalling that affects Piezo1 activation.

The final aim was to develop synthetic small molecules to modulate Piezo1 by modifying the structure of the known agonist, Yoda1. The objectives were: 1) to determine the structure-activity relationship of Yoda1 analogues on Piezo1 over-

expressed in HEK cells; 2) determine the characteristics of hit compounds, such as potency, selectivity and solubility compared to Yoda1; 3) to determine the functional effects of hit compounds on Piezo1-dependent endothelial cell functions.

Chapter 2

Methods and materials

2.1 Cell lines and cell culture

2.1.1 Human Umbilical Vein Endothelial Cells (HUVECs)

Human Umbilical Vein Endothelial Cells (HUVECs) were purchased from Lonza and cultured in Endothelial Cell Basal Medium (EBM-2) supplemented with 2% foetal calf serum (FCS) and the following growth factors: 10 ng.ml⁻¹ vascular endothelial growth factor (VEGF), 5 ng.ml⁻¹ human basic fibroblast growth factor, 1 µg.ml⁻¹ hydrocortisone, 50 ng.ml⁻¹ gentamicin, 50 ng.ml⁻¹ amphotericin B and 10 µg.ml⁻¹ heparin. These growth factors were supplied as a bullet kit (BulletKit™, Lonza). Experiments were performed on cells from passage 2-5.

2.1.2 Piezo1 tetracycline inducible HEK293 cell line (P1 HEK TREx)

HEK T-REx™ cells which overexpress Piezo1 upon induction with tetracycline were made as described in Rode et al., (2017). Expression was induced by treating the cells for 24 hours with 10 ng.mL⁻¹ tetracycline (Sigma). Cells were cultured in Dulbecco's modified Eagle's medium-F12 GlutaMAX (Invitrogen, Paisley, UK) supplemented with 10% foetal calf serum (Sigma) and 1% Pen/Strep (Sigma-Aldrich). Subsequently, cells were treated with 10 µg.mL⁻¹ blasticidin and 200 µg.mL⁻¹ zeocin (Invitrogen, Thermo Fisher Scientific) to select for stably transfected cells.

2.1.3 TRPC5 tetracycline inducible HEK293 cell line (HEK-TRPC5)

Human TRPC5 was over-expressed in HEK293 cells using cDNA encoding TRPC5 channels under the control of a tetracycline-regulated expression

system. The addition of $1 \mu\text{g.mL}^{-1}$ tetracycline (Tet+) induced expression of TRPC5 channels (Zeng, 2004). Cells were cultured in Dulbecco's modified Eagle's medium-F12 GlutaMAX (Invitrogen, Paisley, UK) supplemented with the selection antibiotics $5 \mu\text{g.mL}^{-1}$ blasticidin and $400 \mu\text{g.mL}^{-1}$ zeocin (Invitrogen).

2.1.4 TRPC4 β tetracycline inducible HEK293 cell line (HEK-TRPC4)

Human TRPC4 was over-expressed in HEK293 cells using cDNA encoding TRPC5 channels under the control of a tetracycline-regulated expression system (Akbulut et al., 2015). The addition of $1 \mu\text{g.ml}^{-1}$ tetracycline (Tet+) for 24 hours induced expression of TRPC4 channels. Cells were cultured in Dulbecco's modified Eagle's medium-F12 GlutaMAX (Invitrogen, Paisley, UK) supplemented with the selection antibiotics $5 \mu\text{g.mL}^{-1}$ blasticidin and $400 \mu\text{g.mL}^{-1}$ zeocin (Invitrogen).

2.1.5 HEK TREx

Tetracycline-Regulated Expression (T-REx) cell line stably expressing the tetracycline repressor derived from HEK293 cells. T-RExTM-293 cells were purchased from ThermoFisher. Cells were cultured in Dulbecco's modified Eagle's medium-F12 GlutaMAX (Invitrogen, Paisley, UK) supplemented with the antibiotic $5 \mu\text{g.mL}^{-1}$ blasticidin (Invitrogen).

2.1.6 Chinese Hamster Ovary (CHO) cells stably expressing TRPV4

CHO K1 cells stably expressing human TRPV4 were maintained in Ham's F12 (ThermoFisher Scientific) in the presence of 1 mg.mL^{-1} G418 (Sigma-Aldrich).

All cells were grown at 37°C and in 5% CO_2 in a humidified incubator.

2.2 Ionic solutions

2.2.1 Dulbecco's Phosphate-Buffered Saline (DPBS)

DPBS purchased from Gibco contained 1,000 mg.L⁻¹ D-glucose and 36 mg.L⁻¹ sodium pyruvate, 36mg.L⁻¹ calcium, and 36 mg.L⁻¹ magnesium.

2.2.2 Standard bath solution (SBS)

SBS contained: NaCl 135 mM, KCl 5 mM, MgCl₂ 1.2 mM, CaCl₂ 1.5 mM, D-glucose 8 mM and HEPES 10 mM. pH was titrated to 7.4 using 4M NaOH and the osmolality was ~290 mOsm/kg. Ca²⁺-free SBS contained the same components as normal SBS except containing 0.4mM EGTA and containing no CaCl₂. 7.5 mM CaCl₂ was used for Ca²⁺ add-back experiments for a final concentration of 1.5 mM Ca²⁺.

2.3 Chemical reagents

All general salts and solutions were purchased from Sigma. Other chemicals are summarised in Table 2.1.

2.3.1 Yoda1 analogues

Analogues of Yoda1 were synthesised by Kevin Cuthbertson, School of Chemistry, University of Leeds. All synthesised chemicals were purified by column chromatography or trituration and determined as >97% pure by ¹H NMR (proton nuclear magnetic resonance) and ¹³C NMR (carbon-13 nuclear magnetic resonance).

Table 2.1: List of reagents used.

Name	Company	Solvent	Storage	Description
Yoda1	Tocris	DMSO	10 mM -20°C	Piezo1 activator
H89	Sigma	DMSO	10mM -20°C	PKA inhibitor
BIM	Sigma	DMSO	10 mM -20°C	PKC inhibitor
SC-9	Tocris	DMSO	10 mM -20°C	PKC activator
Ceranib-1	Tocris	DMSO	10 mM -20°C	Ceramidase inhibitor
U71332	Tocris	DMSO	5 mM -20°C	PLC inhibitor
CRT0066101	Cayman Chemical	DMSO	10 mM -20°C	PKD inhibitor
4 α -phorbol 12,13-decanoate	Sigma	DMSO	10 mM -20°C	TRPV4 activator
(-)-Englerin A	PhytoLab	DMSO	10 mM -80°C	TRPC4/5 activator. *
Sphingosine	StressMarq	DMSO	50 mM -20°C	*
Sphingomyelin	FLUKA	Methanol	100 mM -20°C	*
Sphingomyelinase from Staphylococcus Aureus	Sigma	Buffered aqueous glycerol solution	4°C	
N-Acetyl-D-Sphingosine (C ₂ -ceramide)	Alfa Aesar	Ethanol	10 mM -20°C	*
N-Hexanoyl-D-Sphingosine (C ₆ -ceramide)	Sigma	Ethanol	10 mM -20°C	*
C ₁₆ -ceramide	LKT Laboratories	Ethanol	50 mM -20°C	*
C ₈ Ceramide 1-phosphate	Cayman Chemical	Ethanol	10 mM -20°C	*
Sphingosine 1-phosphate	Sigma	Methanol	2.5 mM -20°C	*
Phosphocholine chloride calcium salt tetrahydrate	Santa Cruz Biotechnology, Inc.	dH ₂ O	50 mM -20°C	*
Pico 145	Synthesis by School of Chemistry	DMSO	30 μ M -20°C	
Thapsigargin	Sigma	DMSO	2 mM -20°C	SERCA inhibitor

*0.01% pluronic acid included in experimental solutions as dispersing agent.

2.4 Cell transfection

HUVECs, HEK TReX and CHO-TRPV4 cells were transfected with 20 nM siRNA or 400 ng cDNA using Lipofectamine 2000 in OptiMEM (Gibco) as per the manufacturer's instructions (Invitrogen). Medium was replaced after 4-5 hr and cells were used for experimentation 48 hours post transfection. siRNA was purchased from ambion. The sequence for Piezo1 is GCCUCGUGGUCUACAAGAUtt. Control siRNA was obtained from Dharmacon (<http://dharmacon.gelifesciences.com/sirna/on-targetplus-non-targeting-control-pool/>).

2.5 Molecular Biology techniques

2.5.1 DNA constructs

Mouse Piezo1-IRES-GFP in pcDNA3 was obtained from Ardem Patapoutian's group (Coste et al., 2010). Mouse Piezo1-IRES-GFP was cloned into pcDNA4/TO by Dr Melanie Ludlow. A truncated mouse Piezo1 plasmid was cloned containing cDNA sequence 5858-7641 to facilitate mutagenesis within this region.

2.5.2 Mutagenesis

For single residue mutations standard site-directed mutagenesis was performed. Mutagenesis primers were designed using PrimerX software, purchased from Sigma and reconstituted in H₂O to 125 ng.μL⁻¹ (Table 2.2). Mutagenesis reactions were composed of 1 x Buffer, 50 ng template, 125 ng forward and reverse primers, 200 μM dNTP, 1.25 U of PrimeSTAR HS DNA polymerase (TaKaRa) and H₂O, with a final volume of 50 μL. Thermal cycling encompassed

an initial 2 mins at 98 °C, followed by 18 cycles of 10 sec at 98 °C, 5 sec at 58 °C, 2 mins 30 sec at 72 °C, then a final extension of 5 mins 72 °C. Subsequently the input template was degraded by the addition of 15 U DpnI (NEB) at 37°C for 2 hours. Prior to transformation into bacteria, the restriction enzyme was denatured by 10 mins incubation at 80 °C.

For double and triple residue mutations overlap extension PCR was used. Primers, containing the desired mutation(s), were designed using NetPrimer software, purchased from Sigma and reconstituted in H₂O to 10 µM (Table 2.2). Firstly, overlapping PCR products were amplified using 30 cycles of 10 sec at 98 °C, 5 sec at 58 °C, 45 sec at 72 °C. Reactions were composed of 1 x Buffer, 1 ng template, 0.25 µM forward and reverse primers, 200 µM dNTP, 1.25 U of PrimeSTAR HS DNA polymerase (TaKaRa) and H₂O, with a final volume of 50 µL. Secondly, 1 µl of each of the two reaction mixes containing the overlapping products was used as the template in a subsequent round of PCR. For the first three thermal cycles primers were omitted, allowing the overlapping PCR products to anneal to each other and extend to yield 'full length' DNA. Then primers, binding to the 5' and 3' ends of this 'full length' product, were introduced and 30 further thermal cycles used to facilitate its amplification. Gibson Assembly (NEB) was used to introduce the PCR product into EcoRV digested pcDNA4/TO. Finally, for all mutants, the truncated mouse Piezo1 sequence was inserted into the full length construct using Gibson Assembly (NEB) of overlapping PCR amplified products.

DNA constructs were sequenced by GENEWIZ using customs primers.

Mutagenesis was performed by Dr. Melanie Ludlow.

2.5.3 Preparation of plasmid DNA

Stellar competent cells (TaKaRa) were transformed with plasmid DNA at a volume ratio of 50:1 by heat shock at 42 °C for 45 seconds followed by 2 minutes on ice. A 9x volume of SOC medium was added and the bacteria incubation at 37 °C, 200 rpm for 60 minutes. After incubation transformed bacteria were plated onto agar plates containing 50 µg.mL⁻¹ ampicillin and incubated overnight at 37 °C. Single colonies were grown up in 5 ml LB medium containing 50 µg.mL⁻¹ ampicillin at 37 °C, 200 rpm agitation until saturated, typically overnight. Bacterial broths were pelleted at 6800 x g, 3 mins at RT, supernatants removed and bacteria cell pellets either stored at -20 °C or processed immediately. DNA was extracted by alkaline lysis and purified by anion-exchange using a QIAprep Spin Miniprep kit (Qiagen).

Table 2.2: List of oligonucleotide primers used to generate mutants.

Mutation	Primer pair 5' – 3'
R2126A + F2130S	GGTTCGCTCTAGTGCCGTCCCTGGTGGAGCTGCGGG - Forward GGACGGCACTAGAGCGAACCCTGGAAAAGGAAGAG - Reverse
F2130S + R2135A	CCCTGGTGGAGCTGGCGGCCGTCATGGACTGGG - Forward CGCCAGCTCCACCAGGACGGCACTAGACGGAACCC - Reverse
R2126A + F2130S + R2135A	CTAGTGCCGTCCCTGGTGGAGCTGGCGGCCGTCATGGACTGGG - Forward CCACCAGGGACGGCACTAGAGCGAACCCTGGAAAAGGAAGAG - Reverse
M2190A + F2198S	GCGGGAGGCCTCATTATCCTCTCCCTCATCGCCATCATCTGGTTCCT - Forward GGATAATGAGGCCTCCCGCACCATCTGACAATTTTCTTCTTCTC - Reverse
F2205A + M2210A	TCCCCTCTGCTCTTCGCG TCACTGATCCGCTCTGTGGTC - Forward CGCGAAGAGCAGAGGGGACCAGATGATGGCGATGAGG - Reverse
Y2470S + K2479S	CCATCGTGTGGTGGTGGCGCGTTTGTGCGGGGCTTCTTCA - Forward CCAACCACCAGCAGATGGAGACGGACAGCCCCACAATCCCGTAG - Reverse
R2482A + F2484S	GTGGCGGGCTCCTTCAGCGAGATCTCTCACTCC - Forward CTGAAGGAGCCCGCCACAAACTTGCCAACCACCAG - Reverse
R2482A + F2485S	GCAAGTTTGTGGCGGGCTTCTCCAGCGAGATCTCTCACTCCATC - Forward GCTGGAGAAGCCCGCCACAAACTTGCCAACCACCAG - Reverse
R2482A + F2484S + F2485S	GTGGCGGGCTCCTTCAGCGAGATCTCTCACTCCA - Forward GCTGGAGGAGCCCGCCACAAACTTGCCAACCACCAG - Reverse
R2126A	CCTTTTCCAGGGTTTCGCTCTAGTGCCGTTCCTG - Forward CAGGAACGGCACTAGAGCGAACCCTGGAAAAGG - Reverse
F2130S	CCGTCTAGTGCCGTCTCTGGTGGAGCTGCG - Forward CGCAGCTCCACCAGAGACGGCACTAGACGG - Reverse
F2130A	GTTCCGTCTAGTGCCGGCCCTGGTGGAGCTGCGG - Forward CCGCAGCTCCACCAGGCGCGCACTAGACGGAAC - Reverse
R2135A	GTTCCGTGGTGGAGCTGGCGGCCGTCATGGACTGG - Forward CCAGTCCATGACGGCCGCGCTCCACCAGGAAC - Reverse

2.6 Intracellular Ca²⁺ measurement

2.6.1 FlexStation 3

Ca²⁺ indicator dyes are tools used for measuring intracellular Ca²⁺ concentration. Fura-2 is a ratiometric Ca²⁺ indicator dye which permits the measurement of intracellular Ca²⁺. It is excited at 340 nm and 380 nm and the ratio of emission at 510 nm calculated. Once bound to Ca²⁺ there is a spectral shift in Fura-2 absorption which is proportional to the intracellular concentration of Ca²⁺, increasing emission from excitation at 340 nm and decreasing emission from excitation at 380 nm at higher Ca²⁺ concentrations. This causes a change in the ratio which can be measured ($\Delta F_{340/380}$). Fluo-4 is a single wavelength Ca²⁺ indicator dye. It was excited at 485 nm and emitted light collected at 525 nm. Increasing concentrations of Ca²⁺ increase emission intensity which are shown as absolute fluorescence in arbitrary units.

Measurements were made at room temperature on a FlexStation 3 (Molecular Devices, California) bench-top fluorometer controlled by Softmax Pro software v5.4.5 (Figure 2.1). HEK293 and CHO cells were plated in poly-d-lysine coated 96-well plates (Corning, NY, USA) and HUVECs in clear 96-well plates (Corning, NY, USA) at a confluence of 90%, 24 hours before experimentation. Cells were incubated with fura-2AM (2 μ M) (Molecular Probes™), or fluo-4-am (4 μ M) (Molecular Probes™) for CHO cells, in SBS containing 0.01% pluronic acid (Thermo Fisher Scientific) for 60 min at 37 °C. For recordings with fluo-4, 2.5 mM probenecid (Sigma Aldrich) was included in the SBS throughout the experiment. Cells were washed with SBS for 30 min at room temperature. All cholesterol, sphingomyelinase and sphingolipid treatments were added prior to the 30 min wash, for 30 min at 37 °C, and were present during Ca²⁺ measurements. Yoda1

analogues tested as antagonists were added during the 30 min wash at room temperature. A compound plate was prepared containing drugs to be tested (Yoda1/Yoda1 analogues, VEGF, ATP) at twice or five times the final concentration in Ca^{2+} -SBS. The FlexStation 3 was set to add 80 μL (2x concentration) or 20 μL (5x concentration) of the compound solution to each well on the test plate containing 80 μL of recording buffer. Baseline fluorescence ratios were recorded before the addition of the compound solution to the cell plate after 30 or 60 seconds, with regular recordings thereafter for a total of 150-300 seconds.

Peak Ca^{2+} responses were measured by subtracting the average of the baseline fluorescence ratio from the greatest ratio value post compound addition. This was used for each well to take into account different baseline fluorescence after pre-treatment conditions. Amplitudes of responses between timepoints were measured by subtracting the average of the baseline fluorescence ratio from the average ratio value between the timepoints specified.

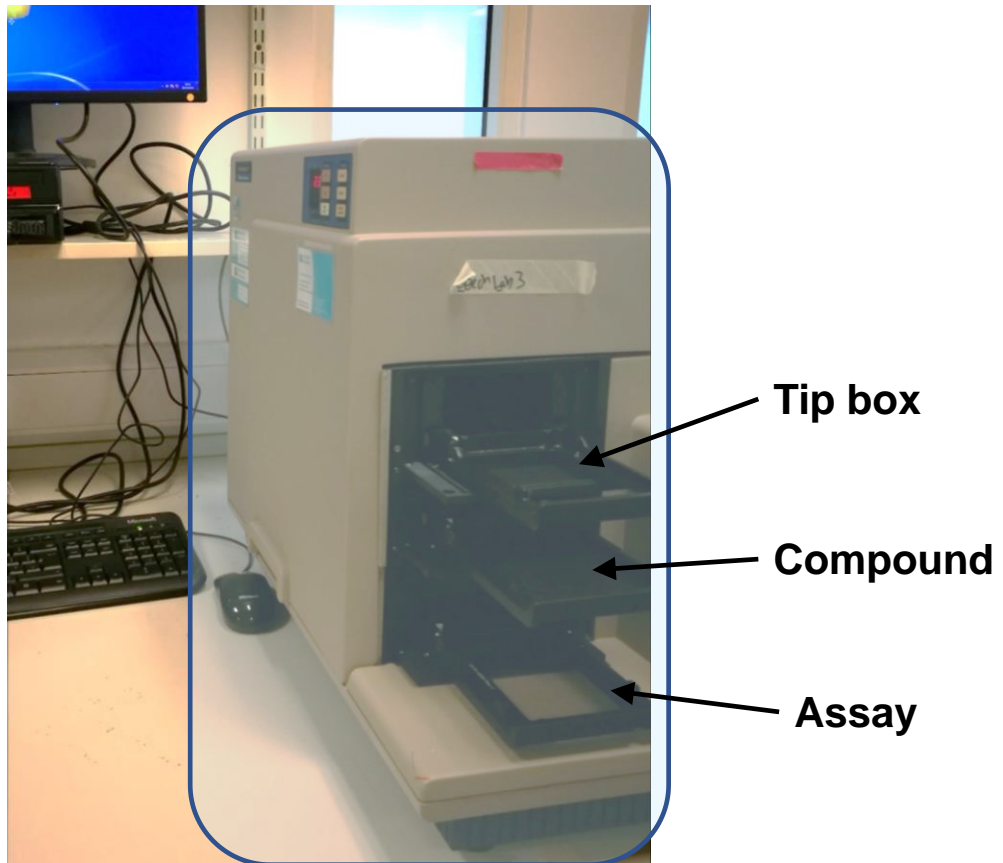


Figure 2.1: FlexStation 3 (Molecular Devices). Flexstation 3 device with areas of interest highlighted. The assay plate consisted of a confluent monolayer of cells loaded with the intracellular Ca^{2+} indicator dyes. The tip box area contained pipette tips that transferred drugs from the compound plate to the assay plate. The SoftMax Pro program was used to acquire data.

2.6.2 Single-cell imaging

Shear stress-evoked Ca^{2+} signals were measured using Zeiss Axiovert fluorescent microscope equipped with x20 (NA 0.75) Fluar objective. While the FlexStation 3 reads the fluorescence from an area containing multiple cells, the fluorescent microscope allows single-cell Ca^{2+} measurements. Excitation light is from a xenon lamp, and the wavelength is selected by a filter wheel (Ludl Electronic Products). Emitted light is collected through an emission filter and images captured by an Retiga EXi digital camera (QImaging).

HUVECs and LECs were seeded on Ibidi μ -Slide VI^{0.4} (Ibidi treated) 4 hours before the experiments. Cells were loaded with Fura-2 AM with the same protocol as that for FlexStation 3 experiments except 2 $\text{ng}\cdot\text{ml}^{-1}$ VEGF was included in SBS during the entire experiment. Volocity 6.3 (Perkin Elmer) software was used to collect data.

2.7 Shear stress

Shear stress was achieved in microfluidic chambers, Ibidi μ -Slide VI^{0.4} (<http://ibidi.com/>). The intensity of shear stress was controlled using PumpControl software for the system.

For generating shear stress in microfluidic chambers, an Ibidi pump system was used. The Ibidi Pump System has two main components: The Ibidi Pump (software controlled air pump) and the Fluidic Unit (holder for cell media perfusion set, μ -Slide, and electrically controlled valve set). The PumpControl software controls the air pressure, and consequently the shear stress acting on the cells in the chambers. In order to save medium, liquid was pumped back and forth between the two media reservoirs. For Ca²⁺ imaging experiments, HUVECs were seeded on Ibidi μ -Slide VI^{0.4} 4 hours prior to experiments. To better characterize the full range of the responses, incrementing shear stresses were applied (10, 20 and 30 dyn.cm⁻²).

For generating shear stress using an orbital shaker, HUVECs were plated on a 6-well plate at 70 % confluence 4 hours before being subjected to shear stress generated by the orbital shaker (SSM1, Stuart) rotating at 153 rpm with an orbit of 16 mm for 24 hours. Drugs were added to the medium 30 minutes before the shear stress was applied. Cells were cultured in 2 mL medium, so that the shear stress at the edge of the wells was ~10-15 dyn.cm⁻² (Dardik et al., 2005; Warboys et al., 2014). Cells were then imaged using the Incucyte microscope. The method for analysing the EC alignment is described in the next section.

2.7.1 Cell alignment analysis

To estimate the orientation of endothelial relative to flow images were analysed using ImageJ software (NIH, Bethesda, Maryland, USA). Images were processed using a 'Difference of Gaussian' operator to highlight the edge of individual cells. This was achieved by using the 'Difference of Gaussians' ImageJ plugin from the University of Sussex (<http://www.sussex.ac.uk/gdsc/intranet/microscopy/imagej/utility>). The settings used for phase contrast images were Sigma1=20, Sigma2=1.5. Enhance Contrast was applied. Automated quantification of cell orientation relative to flow was determined using an ImageJ plugin, OrientationJ, as described by Rezakhaniha et al. (2012). OrientationJ produced a histogram of local angles. Using OriginPro 2017 Gauss distribution curves were fitted the histograms. The baseline-adjusted frequency at the mode of each curve compared between experimental groups. OrientationJ software is available for download from <http://bigwww.epfl.ch/demo/orientation/>. The protocol for analysis is summarised in Figure 2.2.

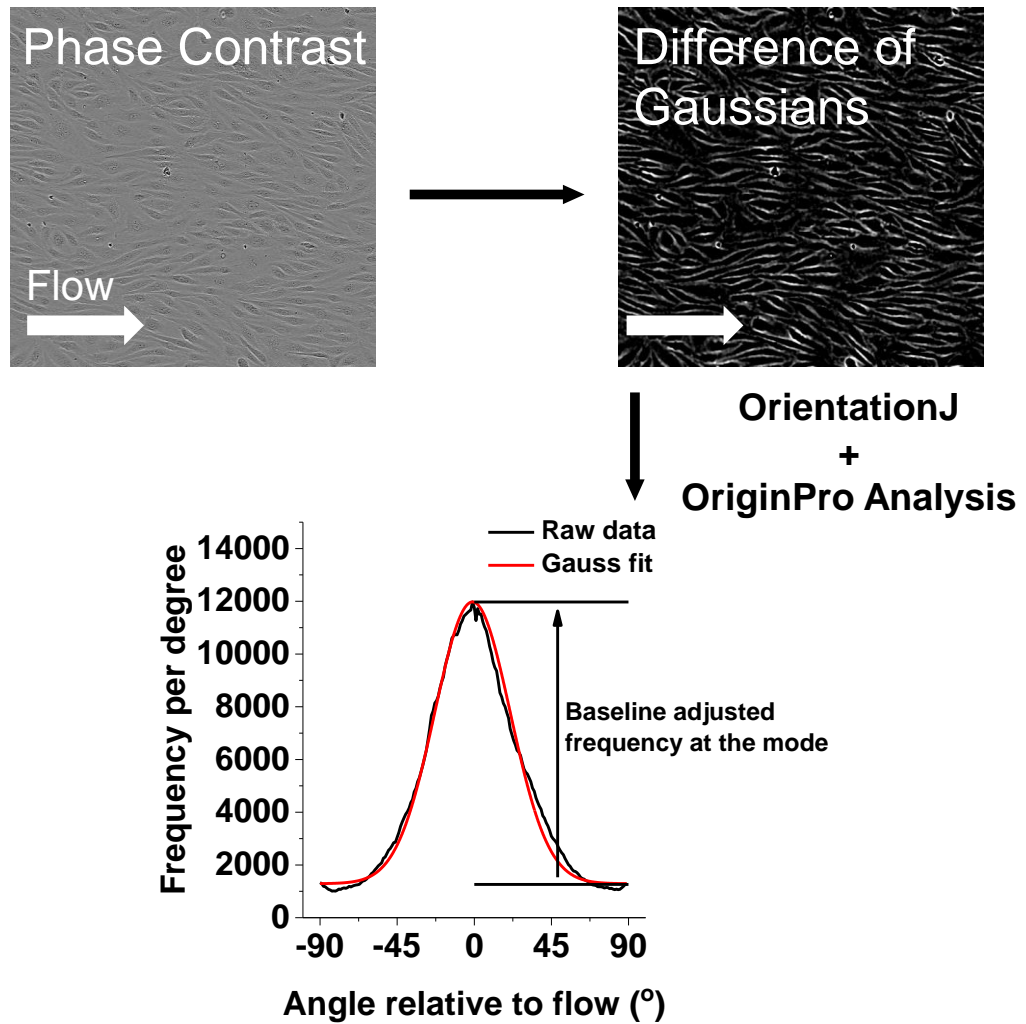


Figure 2.2: Method for cell alignment analysis. Phase-contrast image is processed using Difference of Gaussians function in ImageJ software to define the cell edge. Orientations of the HUVECs are quantified using OrientationJ software, a plugin for ImageJ. The software returns the frequency of cells at each degree. The frequency of the aligned edges in the direction of flow are used for comparison.

2.8 Cholesterol treatment

Water soluble cholesterol in complex with methyl β cyclodextrin (cholesterol at 40mg/g. 3.6 mg of complex into 1 mL solution = 0.5 mM cholesterol) and methyl β cyclodextrin were purchased from Sigma. Alpha cyclodextrin used as negative control to methyl β cyclodextrin was also purchased from Sigma. Cells were incubated with cholesterol enriching or depleting agents for 30 minutes, 37 °C, 0% CO₂ in SBS.

2.9 Live/Dead cytotoxicity assay

HUVEC cell death was measured using a LIVE-DEAD™ Viability/Cytotoxicity Kit for mammalian cells (Molecular Probes). HUVECs were seeded (Corning, NY, USA) at a confluence of 90%, 24 hours before experimentation. Prior to experiment EGM-2 media was replaced with 0.5% FCS EGM-2 for 1 hour at 37°C, 5% CO₂. Afterwards, Yoda1 analogues were incubated in 0.5% FCS EGM-2 for 30 mins at 37°C, 5% CO₂. HUVECs were then washed with DPBS. Cells were incubated with 100 μ L staining solution containing 1 μ M calcein AM and 2 μ M ethidium homodimer in DPBS at room temperature. Live cells are determined by the presence of esterase activity which converts the cell permeable non-fluorescent calcein-AM into highly fluorescent calcein. Calcein is retained within live cells producing green fluorescence (excitation/emission ~495 nm/~515 nm). Ethidium homodimer enters cells with damaged membranes and increases fluorescence upon binding to nucleic acids, producing a red fluorescence in dead cells (excitation/emission ~495 nm/~635 nm). Ethidium homodimer is excluded from cells with intact plasma membrane. The plate was imaged on an Incucyte™ Kinetic Imaging System (Essen Bioscience, Michigan) in phase-contrast and

fluorescence mode using a x10 objective. The total number of fluorescent cells in each well was calculated using inbuilt algorithms.

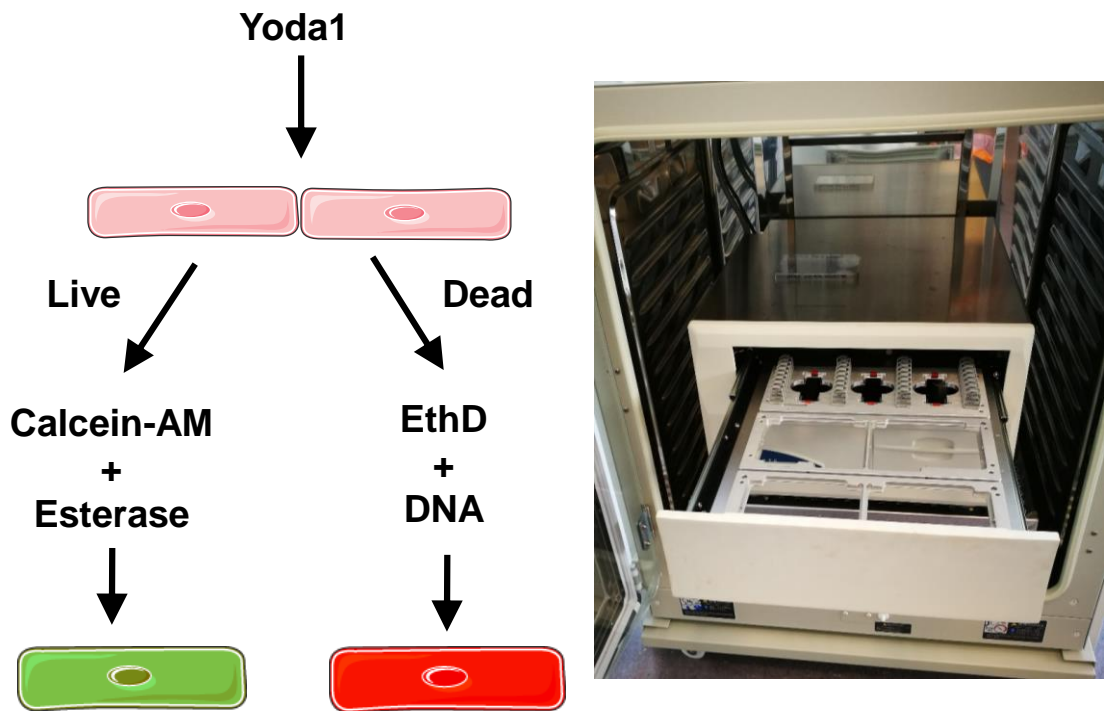


Figure 2.3: Schematic of Live/Dead cytotoxicity assay. Left, Schematic of Live/Dead cell assay. Calcein-AM is converted to calcein by esterases in live cells producing green fluorescent cells. Ethidium homodimer (EthD) enters cells with damaged membranes and increases fluorescence upon binding to nucleic acids, producing a red fluorescence in dead cells. The Incucyte™ Kinetic Imaging System (right) consists of a microscope inside an incubator and permits phase contrast and green/red fluorescence live content imaging of cells.

2.10 Bioinformatics

FuzzPro (<http://www.bioinformatics.nl/cgi-bin/emboss/fuzzpro>) was used to search for Cholesterol Recognition/interaction Amino Acid Consensus sequences (CRAC) - L/V-X₁₋₅-Y-X₁₋₅-R/K – and CARC sequences - R/K-X₁₋₅-Y-X₁₋₅-L/V – in the full human and mouse Piezo1 protein sequences. Protein Family Alignment Annotation Tool (PFAAT) 2.0 was used to determine conservation of amino in Piezo1 sequences in 68 orthologues of the gene found on Ensembl (Caffrey et al., 2007). Conservation score was determine using Von Neumann Entropy. Multiple sequence alignment figures were produce using MUSCLE.

2.11 Computational modelling

To elucidate the interactions of Piezo1 with cholesterol molecular dynamics (MD) simulations were used. These simulations allow us to study the motion and dynamics of proteins in their native environment (Stansfeld and Sansom, 2011). In this study we have used a modification of classical MD simulations, namely coarse-grained molecular dynamics (CG-MD) simulations (Marrink and Tieleman, 2013). In CG-MD simulations atoms are grouped into particles thus reducing the resolution of the system. This reduced representation allows simulations of larger systems for longer time-scales.

The Martini 2.2 force-field (de Jong et al., 2012; Monticelli et al., 2008) and GROMACS 4.6 (Hess et al., 2008) were used to performed the CG-MD simulations. For the simulations, the pore region of the Piezo1 EM structure (PDB: 3JAC)(Ge et al., 2015) was used. Missing unstructured regions from the EM structure were added using Modeller (Fiser and Šali, 2003). Firstly, a POPC

bilayer was self-assembled around the Piezo1 pore region. At the end of the simulation the POPC lipids were exchanged using a locally written script (Koldsø et al., 2014). Four different systems with the protein inserted in complex symmetric bilayer were created: 1) 80% POPC -20% CHOL, 2) 85% POPC - 15% CHOL, 3) 90% POPC -10% CHOL, and 75% POPC - 20% CHOL – 5% PI(4,5)P₂ (Koldsø et al., 2014). The protein/lipid systems were solvated and ~150 nM of NaCl was added to neutralize the systems. The systems were then energy minimized and equilibrated. 5 repeat simulations for 5 μs were performed for each system. An elastic network using a cut-off distance of 7 Å was used to restrain the protein secondary and tertiary structure.

During the simulations, the protein diffused in the bilayer and dynamically interacted with the different lipid types. Using the trajectories from the simulations we calculated the distribution of lipids around the protein. This enabled us to identify how often each lipid type interacted with different regions of the protein. A lipid was considered to interact with a protein region if the distance between the lipid headgroup and the protein region was less than 5.5 Å.

MD simulations and data analysis was performed by Dr. Antreas Kalli.

2.12 Statistical analysis

OriginPro 9.1 was used for data analysis and graph production. Averaged data are presented as mean±s.e.mean. Most data were produced in pairs (test and control) and these data pairs were compared statistically using Student *t* tests. One-way ANOVA followed by Tukey posthoc test was used for comparing multiple groups. Statistically significant difference is indicated by * ($P<0.05$) and no significant difference by NS ($P>0.05$). The number of independent

experiments is indicated by 'n'. For multiwell assays, the number of replicate wells is indicated by 'N'.

Chapter 3

Regulation of Piezo1 by cholesterol

3.1 Introduction

The Piezo protein family consists of two proteins that form mechanically-activated non-selective cation channels. Piezo proteins have widespread expression throughout mechanically active tissues (Coste et al., 2010). The structure of Piezo1 is striking when compared to other ion channels. The initial structure was solved by cryo-electron microscopy at a resolution of 4.8 Å and determined that Piezo1 monomers come together to form a trimer with a total weight of 858 kDa (Ge et al., 2015). The trimer forms a propeller-like structure with three N-terminal blade regions. More recently, a 38 transmembrane domain structure of Piezo1 has been resolved with 9 repetitive units consisting of 4 transmembrane domains which form a highly-curve blade structure (Zhao et al., 2018). The curvature of the N-terminal blades are thought to deform the membrane to form a dome structure (Guo and MacKinnon, 2017). The N-terminal repeats are connected to the C-terminal region by the anchor domain. A lipid binding pocket has been suggested between the anchor domain and the first N-terminal transmembrane repeats (Saotome et al., 2017). The C-terminal regions of the protein come together to form a central pore region with a large extracellular cap which is important for ion selectivity and gating of the channel (Gnanasambandam et al., 2015; Coste et al., 2015; Zhao et al., 2016). The peripheral N-terminal regions are similar in structure to blades of a propeller. These N-terminal 'blade' regions of the protein were proposed to be important

for mechanical activation. When a chimeric channel of the N-terminal region of Piezo1 and an ASIC, which is not normally mechanically activated, is subjected to mechanical force a mechanically-activated current is evoked (Zhao et al., 2016). However, the effects of the chimeric have come under scrutiny and the responses of the chimeric channel has been proposed to be due to endogenous Piezo1 expression (Dubin et al., 2017). The sensitivity of Piezo1 activation by mechanical force is related to membrane tension and stiffness which can be affected by the lipid composition of the membrane (Qi et al., 2015; Lewis and Grandl, 2015).

Piezo1 is not exclusively activated by mechanical stimuli. A specific agonist for Piezo1 has been discovered called Yoda1 (Syeda et al., 2015). Yoda1 has been shown to activate Piezo1 and not Piezo2 when each is expressed in cells genetically-modified to express no Piezo1.

Piezo1 has been shown to be important in shear stress sensing in endothelial cells, which is critical for vascular development (Li et al., 2014; Ranade et al., 2014). Global knockout of the Piezo1 gene results in embryonic lethality at E9.5 in murine models due to reduced ability of embryonic blood vessels to remodel in response to the initiation of the heartbeat. Furthermore, Piezo1 was also discovered to be important in shear stress-evoked Ca^{2+} entry in endothelial cells and senses shear stress directly.

Shear stress, the frictional force of blood flow against endothelial cells, varies greatly in the cardiovascular system and different intensities of shear stress produce vastly different responses by endothelial cells. Higher intensities of shear stress are associated with laminar blood flow patterns. This induces endothelial cell quiescence which is characterised by endothelial cell growth

arrest, alignment and nitric oxide production. Alternatively, low shear stress evokes an inflammatory response and proliferation of endothelial cells which is largely regulated by Nuclear Factor- κ B. Low shear stress is largely associated with vascular diseases such as atherosclerosis. Atherosclerosis is also affected by risk factors such as smoking, diabetes and hypercholesterolemia.

Levels of membrane cholesterol content are important for cell viability and survival but also for the activity of membrane proteins such as ion channels. The impact of cholesterol on ion channels is highly heterogeneous with effects such as decreasing activity in several types of K^+ channel, voltage gated Na^+ and Ca^{2+} channels and Orai1 (Derler et al., 2016; Romanenko et al., 2002; Hajdú et al., 2003; Wu et al., 1995). However, there are instances where depletion of membrane cholesterol also decrease channel activity, such as in epithelial Na^+ channels and certain members of the transient receptor potential (TRP) family (Beech et al., 2009; Balut et al., 2006). Regulatory effects of cholesterol on mechanosensitive channels have been investigated in human leukaemia cells however, the molecular identity of the channel is not reported (Morachevskaya et al., 2007; Chubinskiy-Nadezhdin et al., 2011).

3.2 Aims

Due to the importance of cholesterol and shear stress in the pathogenesis of atherosclerosis it was important to determine if there was a relationship between these factors. The importance of Piezo1 in shear stress sensing and its activity-relationship with membrane tension, which can be altered by cholesterol, made it a prime candidate to provide a link for this relationship.

3.3 Results

3.3.1 Cholesterol inhibits shear stress-evoked Ca²⁺ influx

To determine the effects of cholesterol on shear stress responses in HUVECs, Ca²⁺ events upon shear stress activation were measured. Ca²⁺ influx has been found to be an endogenous shear stress response of endothelial cells that is dependent on Piezo1 (Li et al., 2014). Incubating HUVECs with 1 mM cholesterol inhibited shear stress-evoked Ca²⁺ at 20 dyn.cm⁻² (Figure 3.1A, B). Cholesterol reduced the proportion of HUVECs that responded positively to shear stress over 10, 20 and 30 dyn.cm⁻² (Figure 3.1C). These data suggest that cholesterol affects shear stress sensing. Due to the importance of Piezo1 in endothelial shear stress sensing, the effect of cholesterol on chemical activation of Piezo1 was investigated.

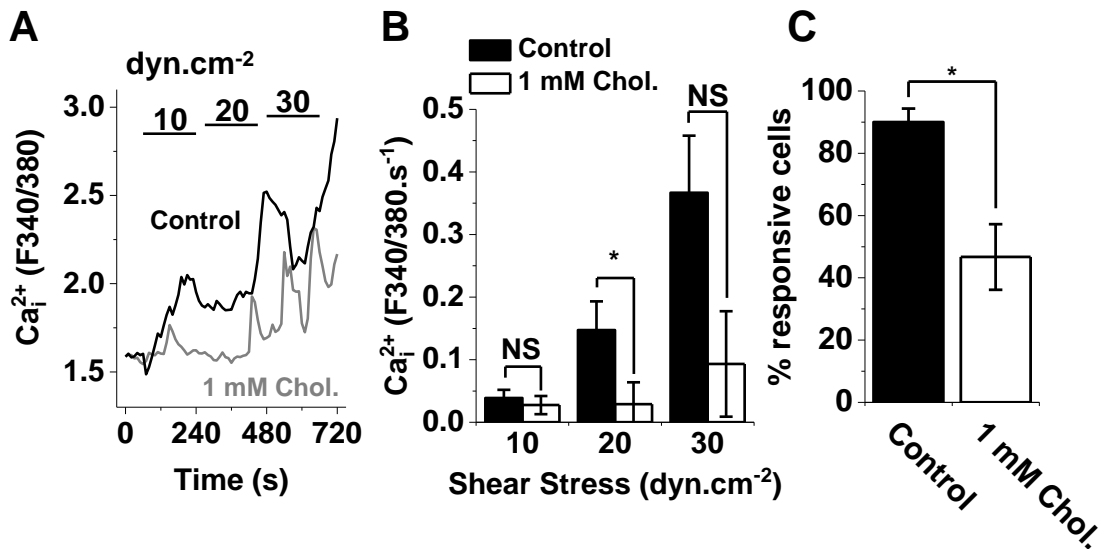


Figure 3.1: Cholesterol inhibits shear stress-evoked Ca²⁺ entry in HUVECs.

A, an example measurement of the intracellular Ca²⁺ concentration in response to shear stress in single HUVECs treated with cholesterol or not. **B**, Mean data of total Ca²⁺ entry per second from experiments represented in **A**. n/N=3/15. * = P < 0.05. **C**, mean percentage of cells that responded positively with Ca²⁺ influx over 10, 20 and 30 dyn.cm⁻². * = P < 0.05. n/N=4/15.

3.3.2 Exogenous cholesterol inhibits Yoda1 response in HUVECs

Due to cholesterol reducing shear stress-evoked Ca^{2+} influx in HUVECs (Figure 3.1) the effect of exogenous cholesterol on Yoda1 responses was investigated. Treating HUVECs with exogenous cholesterol reduced increases in intracellular Ca^{2+} in response to 1 μM Yoda1 in HUVECs (Figure 3.2A). The IC_{50} of cholesterol was 0.31 mM (Figure 3.2B). However, due to the limited solubility of cholesterol, higher concentrations of cholesterol were not tested even though they may have given a more complete block of Yoda1 responses. Furthermore, the sustained response of Yoda1 was inhibited by cholesterol with an IC_{50} of 0.04 mM (Figure 3.2C). This suggested that cholesterol may have an effect on the kinetics of Piezo1 responses. The rate of intracellular Ca^{2+} rise and decay was analysed to determine if there was an effect on the kinetics of Yoda1 response. The initial rising phase was analysed at 65-90 seconds of the experiment time after Yoda1 application as this was the timeframe in which Yoda1 reached a peak response in control conditions. The first time point where Yoda1 was applied to the cells (60 seconds) was not used due to a rapid decrease in fluorescence which was an artefact. There was a trend towards increased rate of rise but there were no statistically significant changes in the rate of rise upon treatment with cholesterol (Figure 3.2D). However, the rate of decay was significantly increased by cholesterol at 0.05 to 0.5 mM with the greatest rate of decay at 0.1 mM cholesterol (Figure 3.2E). The rate of decay appears to slow again at 1 mM cholesterol. The data suggest that exogenous cholesterol causes a dose-dependent reduction in Piezo1 activation to Yoda1 and increased rate of decay.

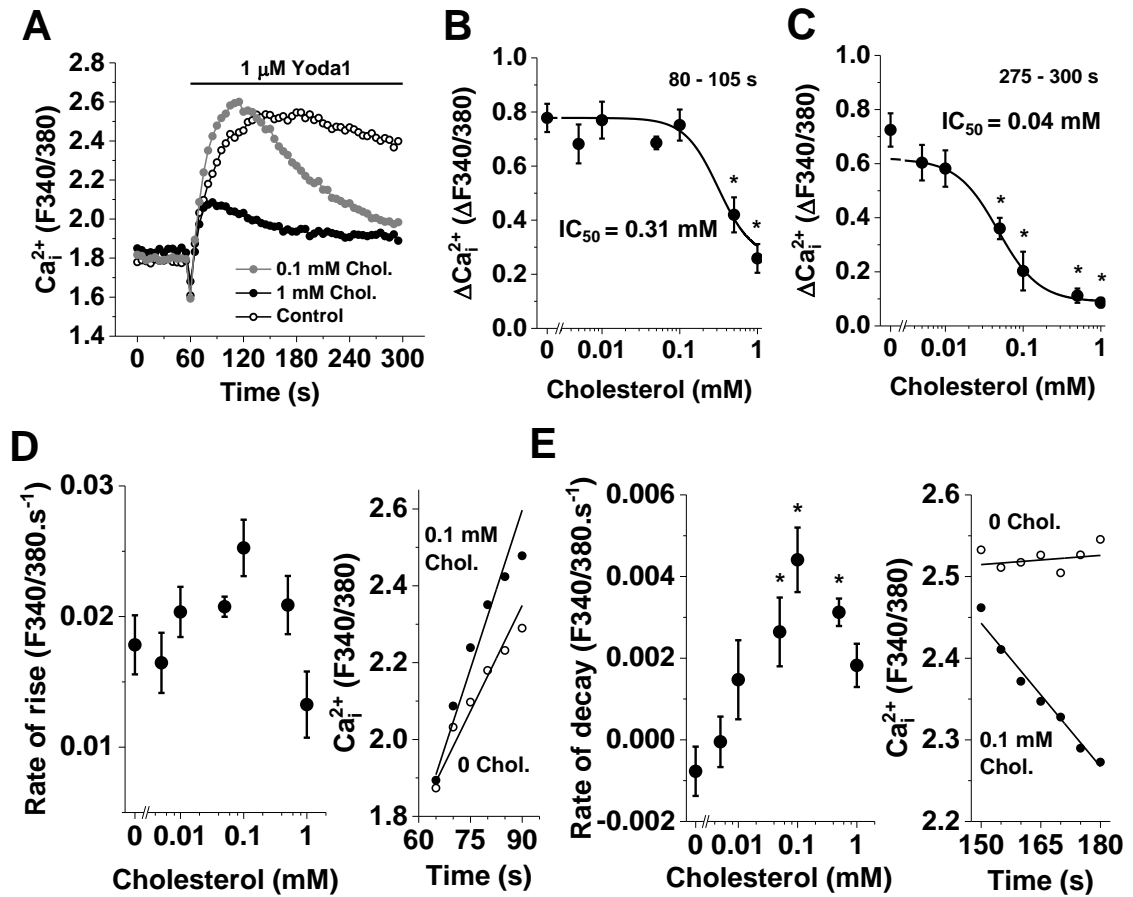


Figure 3.2: Exogenous cholesterol reduces Yoda1 response in HUVECs. **A**, an example measurement of the change in intracellular Ca^{2+} concentration evoked by 1 μ M Yoda1 in HUVECs pre-treated with 0 (control), 0.1 and 1 mM cholesterol. **B**, mean data of the amplitudes of HUVEC responses between 80 – 105 seconds after start of experiment to varying doses of cholesterol (0.005-1 mM) displayed as a Hill Equation indicating the 50 % inhibitory effect (IC_{50}) at 0.31 mM. $n/N=4/4$. * = $P < 0.05$. **C**, mean data of the amplitudes of HUVEC responses between 275 – 300 seconds after start of experiment to varying doses of cholesterol (0.005-1 mM) displayed as a Hill Equation indicating the 50 % inhibitory effect (IC_{50}) at 0.04 mM. $n/N=4/4$. * = $P < 0.05$. **D**, left, mean data of the rate of the rising phase of intracellular Ca^{2+} , measured between 65-90 seconds after start of the experiment, in response to 1 μ M Yoda1 in HUVECs as in **A**. On the right, an example of analysis of intracellular Ca^{2+} rise from a response to 1 μ M Yoda1 after 0 and 0.1 mM cholesterol treatment. Data points are fitted with a linear fit to determine the gradient. $n/N=4/4$. **E**, on the left, mean data of the rate of the decay phase of intracellular Ca^{2+} , measured between 150-180 seconds after start of the experiment, from responses to 1 μ M Yoda1 in HUVECs as in **A**. On the right, an example of analysis of intracellular Ca^{2+} decay from a response to 1 μ M Yoda1 after 0 and 0.1 mM cholesterol treatment. Data points are fitted with a linear fit to determine the gradient. $n/N=4/4$. * = $P < 0.05$.

3.3.3 Depletion of cholesterol reduces Yoda1 response in HUVECs

As additional cholesterol had an inhibitory effect on Piezo1 activation the endogenous effect of cholesterol in HUVEC membranes was investigated. This was achieved by chemically depleting membrane cholesterol using a sequestering agent M β CD. High concentrations of M β CD reduced the amplitude of Yoda1 responses in HUVECs with an IC₅₀ of 0.61 mM (Figure 3.3A-B). However, there was no increase in Yoda1 responses at low concentrations of M β CD that may have been expected if endogenous cholesterol was inhibiting Piezo1 intrinsically. Furthermore, the sustained Yoda1 responses was also inhibited by M β CD with an IC₅₀ of 0.39 mM. Additionally, the baseline concentration of intracellular Ca²⁺ was greatly increased after treatment with 5 mM M β CD (Figure 3.3A). This may suggest a lack of viability of cells treated with 5 mM M β CD. The rate of rise appeared to increase at 0.1 mM M β CD and decrease at 1 mM M β CD. However, this effect was not statistically significant (Figure 3.3C). The decay of intracellular Ca²⁺ in response to Yoda1 also appeared to increase between 0.1-1 mM M β CD. However this was also not statistically significant (Figure 3.3D).

α cyclodextrin (α CD) was used as a negative control to M β CD. α CD has a smaller binding pocket compared to M β CD and does not remove cholesterol from cell membranes (Szente and Fenyvesi, 2017). Pre-treating HUVECs with up to 1 mM α CD had no effect on the response to 1 μ M Yoda1 (Figure 3.4). This suggests that the effect of M β CD was due to depletion of membrane cholesterol.

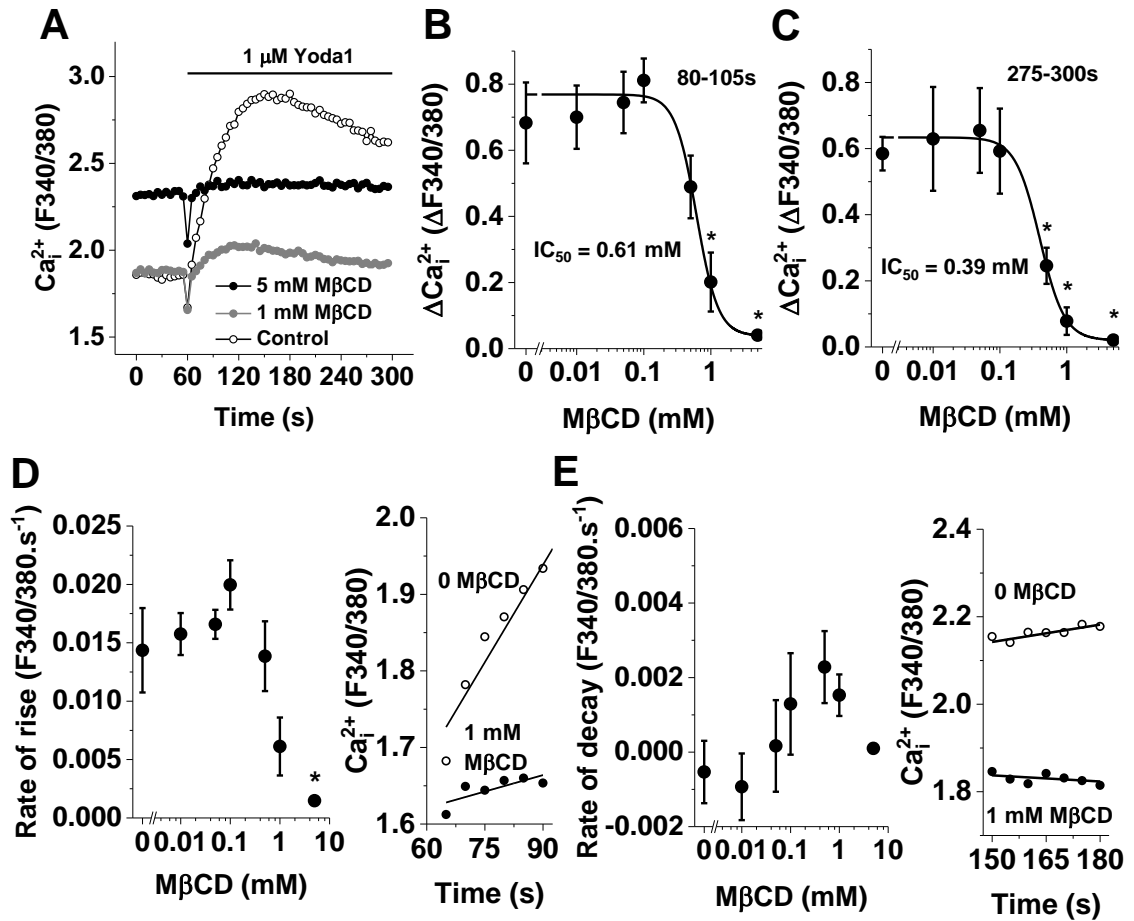


Figure 3.3: Depletion of endogenous cholesterol reduces Yoda1 response in HUVECs. **A**, an example measurement of the change in intracellular Ca^{2+} concentration evoked by $1 \mu\text{M}$ Yoda1 in HUVECs pre-treated with 0 (control), 1 and 5 mM $\text{M}\beta\text{CD}$. **B**, mean data of the amplitude of Yoda1 responses between 80 – 105 seconds post initiation of experiment after pre-treatment with 0.01 - 5 mM $\text{M}\beta\text{CD}$. $n/N=4/4$. * = $P < 0.05$. **C**, mean data of the amplitude of Yoda1 responses between 275 – 300 seconds post initiation of experiment after pre-treatment with 0.01 - 5 mM $\text{M}\beta\text{CD}$. $n/N=4/4$. * = $P < 0.05$. **D**, on the left, mean data of the rate of the rising phase of intracellular Ca^{2+} , measured between 65-90 seconds after start of the experiment, responses to $1 \mu\text{M}$ Yoda1 in HUVECs as in **A**. On the right, an example of analysis of intracellular Ca^{2+} rise from a response to $1 \mu\text{M}$ Yoda1 after 0.1 mM $\text{M}\beta\text{CD}$ treatment. Data points are fitted with a linear fit to determine the gradient. $n/N=4/4$. * = $P < 0.05$. **E**, on the left, mean data of the rate of the decay phase of intracellular Ca^{2+} , measured between 150-180 seconds after start of the experiment, from responses to $1 \mu\text{M}$ Yoda1 in HUVECs as in **A**. On the right, an example of analysis of intracellular Ca^{2+} decay from a response to $1 \mu\text{M}$ Yoda1 after 0.1 mM $\text{M}\beta\text{CD}$ treatment. Data points are fitted with a linear fit to determine the gradient. $n/N=4/4$.

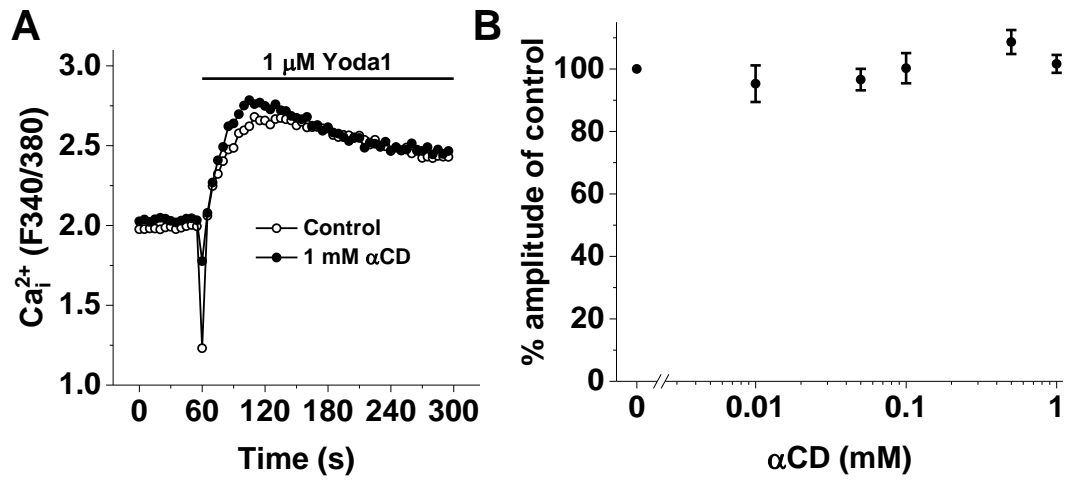


Figure 3.4 Alpha cyclodextrin has no effect on Piezo1 activation. **A**, an example measurement of the change in intracellular Ca²⁺ concentration evoked by 1 μ M Yoda1 in HUVECs pre-treated with 0 (control) and 1 mM α CD. **B**, mean data of peak amplitudes of HUVEC responses to increasing doses of α CD (1-0.01 mM). n/N=3/4.

3.3.4 Exogenous cholesterol reduces Yoda1 response in Piezo1 overexpression system

The effects of cholesterol on Piezo1 was then investigated in an overexpression system. TRex HEK 293 cells with conditional human Piezo1 expression were used (P1 HEK TRex).

Similar to HUVECs, exogenous cholesterol decreased Ca^{2+} entry in a dose-dependent manner with an IC_{50} of approximately 3.72 mM (Figure 3.5A-B). The sustained Yoda1 response was also inhibited with an IC_{50} of approximately 0.15 mM (Figure 3.5C). The rate of rise was also similarly unaffected by application of cholesterol (Figure 3.5D). Furthermore, the rate of decay increased in response to 0.5 mM cholesterol application (Figure 3.5D). Therefore, these data suggest cholesterol affects overexpressed Piezo1 channels similarly to endogenous endothelial Piezo1 channels.

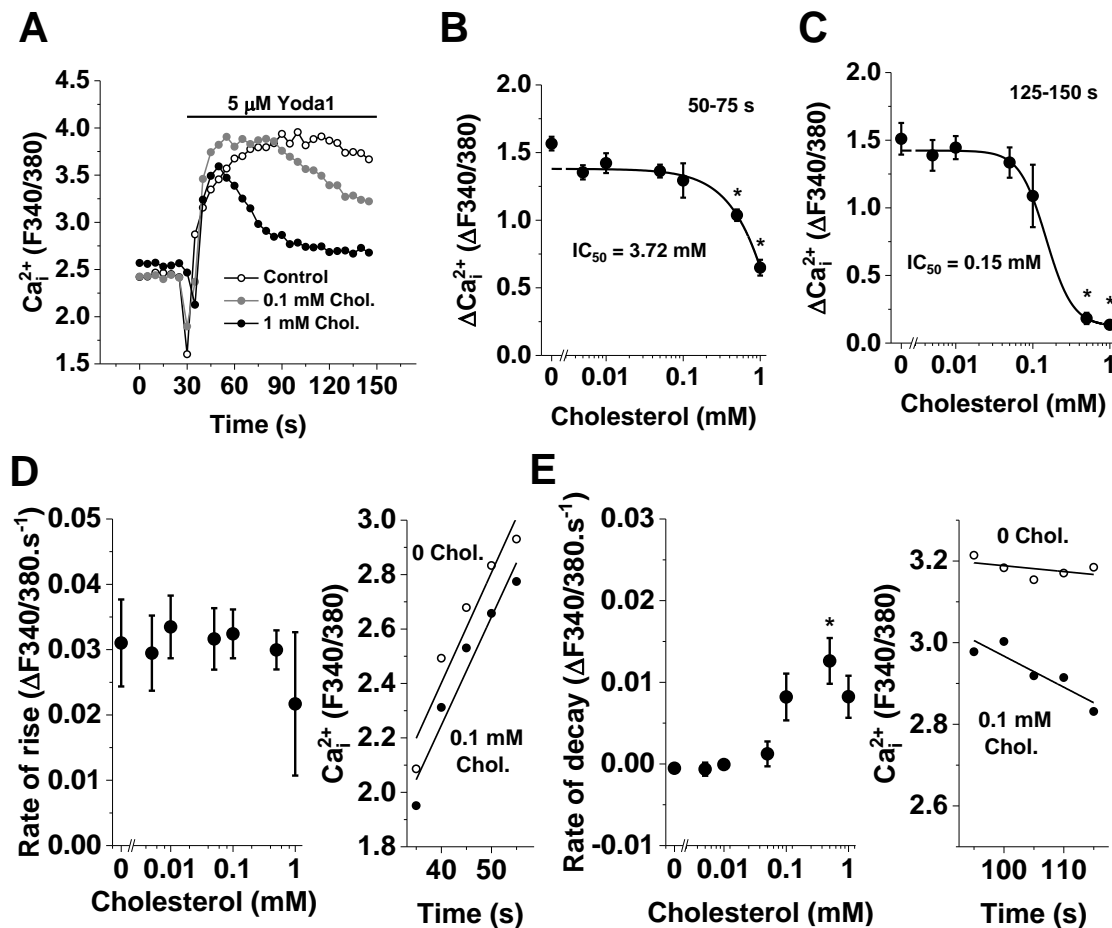


Figure 3.5: Exogenous cholesterol reduces Yoda1 response in P1 HEK TREx. **A**, an example measurement of the change in intracellular Ca^{2+} concentration evoked by 5 μ M Yoda1 in P1 HEK TREx pre-treated with 0 (control), 0.1 and 1 mM cholesterol. **B**, mean data of the amplitude of Yoda1 responses between 50 – 75 seconds post initiation of experiment after pre-treatment with 0.005 - 1 mM Cholesterol. $n/N=4/4$. * = $P < 0.05$. **C**, mean data of the amplitude of Yoda1 responses between 125 – 250 seconds post initiation of experiment after pre-treatment with 0.005 - 1 mM Cholesterol. $n/N=4/4$. * = $P < 0.05$. **D**, mean data of the rate of the rising phase of intracellular Ca^{2+} , measured between 35-60 seconds after start of the experiment, responses to 5 μ M Yoda1 in P1 HEK TREx as in **A**. On the right, an example of analysis of intracellular Ca^{2+} rise from a response to 5 μ M Yoda1 after 0.1 mM cholesterol treatment. Data points are fitted with a linear fit to determine the gradient. $n/N=4/4$. **E**, on the left, mean data of the rate of the decay phase of intracellular Ca^{2+} , measured between 95-115 seconds after start of the experiment, from responses to 5 μ M Yoda1 in P1 HEK TREx as in **A**. right, an example of analysis of intracellular Ca^{2+} decay from a response to 1 μ M Yoda1 after 0.1 mM cholesterol treatment. Data points are fitted with a linear fit to determine the gradient. $n/N=4/4$. * = $P < 0.05$.

3.3.5 Depletion of cholesterol reduces Yoda1 response in Piezo1 overexpression system

Depleting cholesterol content of cells overexpressing Piezo1 also had similar effects to HUVECs. M β CD reduced the amplitude of Ca²⁺ entry in response to 5 μ M Yoda1 in P1 HEK TRex. Depletion of cholesterol reduced Yoda1 responses in a dose-dependent manner. The IC₅₀ was approximately 0.58 mM M β CD for the initial peak of Ca²⁺ influx (Figure 3.6B). Additionally, the sustained response to Yoda1 was inhibited with an IC₅₀ of 1.12 mM. Similar to HUVECs the rate of rise and decay of Ca²⁺ entry were not affected by treatment with M β CD (Figure 3.6D-E). However, there was a trend for reduced rate of influx after pre-treatment 1 mM M β CD but this was not statistically significant.

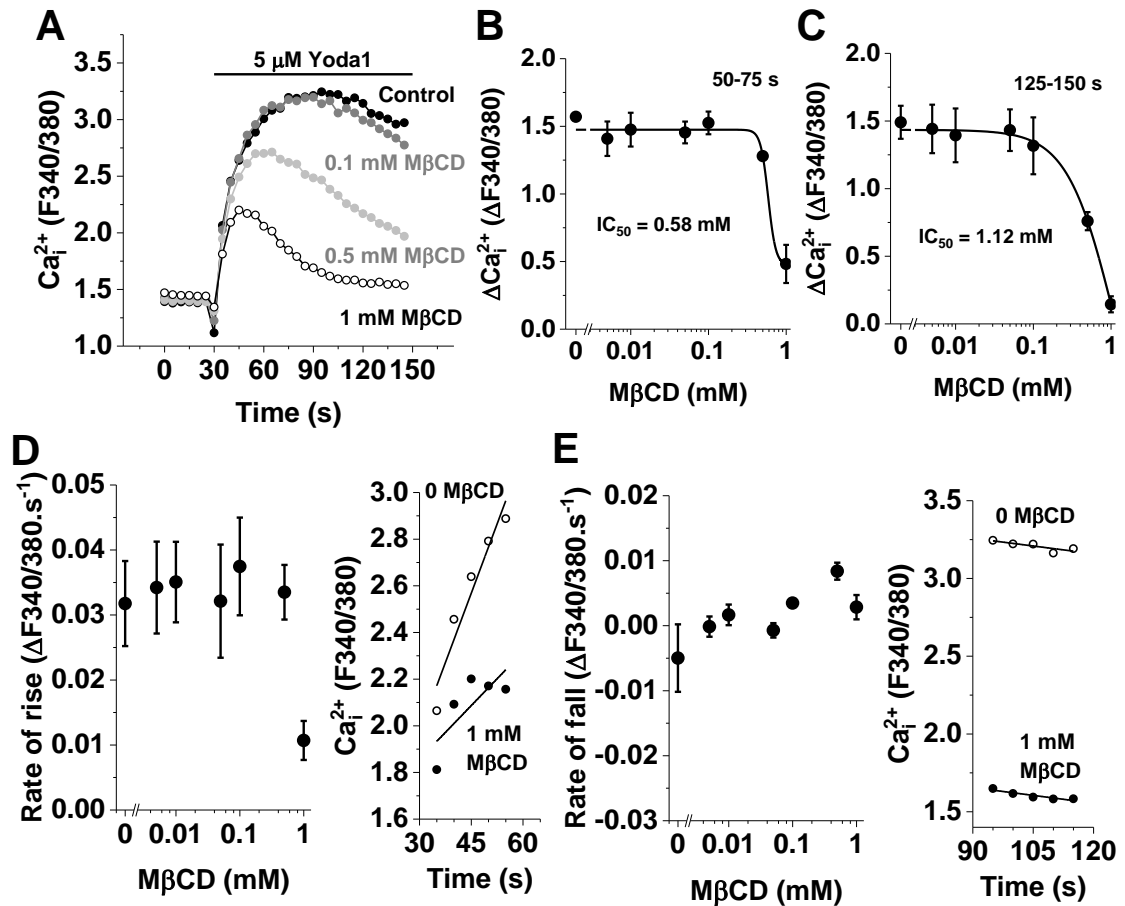


Figure 3.6: Depletion of endogenous cholesterol reduces Yoda1 response

in P1 HEK TREx. **A**, an example measurement of the change in intracellular Ca^{2+} concentration evoked by 5 μM Yoda1 in P1 HEK TREx pre-treated with 0 (control), 0.1, 0.5 mM and 1 mM M β CD. **B**, mean data of the amplitude of Yoda1 responses between 50 – 75 seconds post initiation of experiment after pre-treatment with 0.005 - 1 mM M β CD. $n/N=4/4$. * = $P < 0.05$. **C**, mean data of the amplitude of Yoda1 responses between 125 – 250 seconds post initiation of experiment after pre-treatment with 0.005 - 1 mM M β CD. $n/N=4/4$. * = $P < 0.05$. **D**, left, mean data of the rate of the rising phase of intracellular Ca^{2+} , measured between 35-60 seconds after start of the experiment, responses to 5 μM Yoda1 in P1 HEK TREx as in **A**. On the right, an example of analysis of intracellular Ca^{2+} rise from a response to 5 μM Yoda1 after 1 mM M β CD treatment. Data points are fitted with a linear fit to determine the gradient. $n/N=4/4$. **E**, on the left, mean data of the rate of the decay phase of intracellular Ca^{2+} , measured between 95-115 seconds after start of the experiment, from responses to 5 μM Yoda1 in P1 HEK TREx as in **A**. On the right, an example of analysis of intracellular Ca^{2+} decay from a response to 1 μM Yoda1 after 0.1 mM M β CD treatment. Data points are fitted with a linear fit to determine the gradient. $n/N=4/4$.

3.3.6 Predicting cholesterol binding sites

Cholesterol binding sites have been shown to affect the activity of different proteins, including ion channels such as Orai1. A common sequence of amino acids known as the Cholesterol recognition/interaction amino acid consensus sequences or CRAC motif (L/V-X₁₋₅-Y-X₁₋₅-R/K) has been widely reported as an interaction site of proteins with cholesterol. Modifications of this motif also have been found to bind to cholesterol including the CARC motif (R/K-X₁₋₅-Y/F-X₁₋₅-L/V), which is the reverse of the CRAC motif and CRAC- and CARC-like motifs where the tyrosine is replaced with a phenylalanine residue.

3.3.6.1 Cholesterol binding sites in Piezo1

Pattern recognition software, FuzzPro, was used to determine the abundance and location of possible cholesterol binding sites in human and mouse Piezo1. Mouse Piezo1 was also investigated as its structure had been elucidated by cryo-EM. Many CRAC and CARC like domains were found in both human and mouse Piezo1 amino acid sequences (Figure 3.7). 65 potential cholesterol binding motifs were found in human Piezo1 and 61 cholesterol binding motifs were found in mouse Piezo1 (Appendix A, Table 8 and Table 9). In human Piezo1 22 CRAC and 43 CARC motifs were discovered. However, 19 CRAC motifs and 42 CARC motifs were found in mPiezo1. These motifs were not located in any specific region of the mouse Piezo1 structure or the aligned structure of human Piezo1. Therefore the conservation of the amino acids in each cholesterol binding motif was determined.

To determine which of these binding sites may be important, the conservation of each site was calculated using multiple sequence alignment software PFAAT

using a BLOSUM62 matrix. 95 Piezo1 orthologue sequences were obtained from ensemble.org for analysis (ENSG00000103335). Conservation scores of each amino acid was given between 0-1. The average score of each cholesterol interaction motif was calculated across all amino acids in the motif. For both human and mouse Piezo1 15 cholesterol interaction motifs were found to have amino acid conservation scores equal to or greater than 0.8. Each of these 15 cholesterol interaction sites corresponded to aligned sequences between mouse and human Piezo1 (Appendix, Figure 6.3). 13 of the 15 highly conserved motifs were located between transmembrane helix (TH) 34 and the C-terminal domain, with motifs included in the anchor region, outer helix of the pore region and the C-terminal extracellular domain. Between TH34 and the anchor region has been suggested to be a lipid binding pocket that has been suggested to have arginine residues that are essential for Piezo1 activation. The R2035 residue reported in the lipid binding pocket (Saotome et al., 2017) was found to be located in CARC domain (R2035-L2044) of mPiezo1 which corresponds to a CARC domain in hPiezo1 (R2019-L2028).

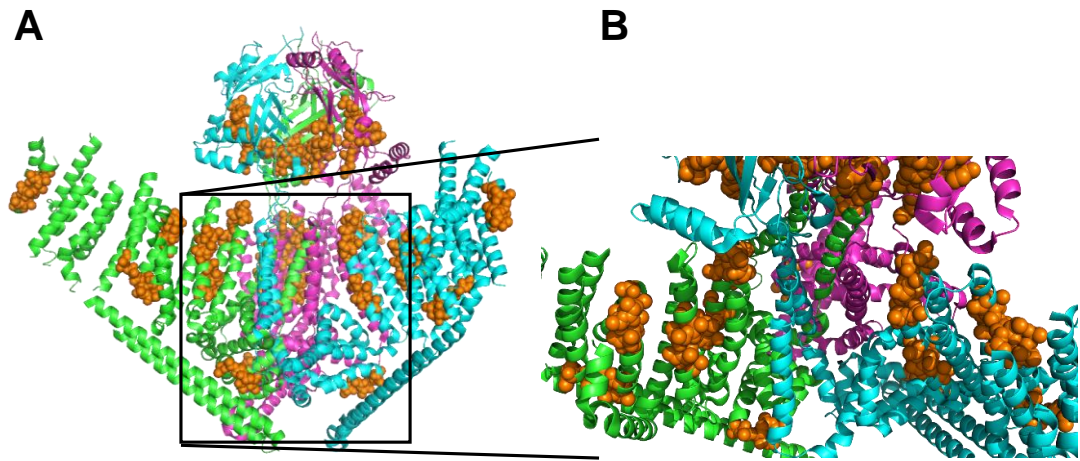


Figure 3.7: CRAC domains in Piezo1. **A**, Structure of mPiezo1 with all predicted CRAC motifs highlighted as orange spheres in the available structure (PDB: 3JAC). **B**, CRAC motifs highlighted near the C-terminal domain and ion pore suggested in the mPiezo1 structure.

3.3.7 Computational modelling of Piezo1/cholesterol interactions

Due to the amount of potential cholesterol interaction sites, computational modelling was used to further indicate cholesterol interaction sites with the available Piezo1 structure. The Cryo-EM structure of mouse Piezo1 was used in dynamic simulations of Piezo1 in a model lipid bilayer. Amino acid residues 1992-2545 of mPiezo1 were used for the modelling as other amino acid positions had not been assigned in the N-terminal blade structures (Figure 3.8A). 1-Palmitoyl-2-oleoyl-sn-glycerol-3-phosphocholine (POPC) membranes were modelled with increasing percentages of cholesterol content (10, 15, 20% and 20% + 5% PIP₂). The probability of cholesterol interaction was calculated for each simulation condition with a possible score of 1 for each simulation condition. Residues with a score above 2.3 for cholesterol interaction were considered to be highly likely to interact with the Piezo1 protein.

Five regions of the transmembrane domains were suggested to interact with cholesterol (Figure 3.8D). In the first region residues H2001, T2005, I2007, A2008, L2011 and Q2015 were suggested to bind to cholesterol. However, this does not correspond to any CRAC or CARC motifs determined above. According to the structure proposed by Zhao et al. (2018) H2001, T2005 and I2007 are contained within TH33. A2008 and L2011 are located between TH33 and TH34. The second region with amino acids scoring above 2.3 had three residues, Y2038, K2041 and L2044. These residues were contained in a CARC motif in TH34 of mPiezo1. This region has recently been suggested to be near a lipid binding pocket. The third region contained residues F2125, V2128 and V2123, which also correspond to a CARC motif in the alpha helix of the anchor domain of Piezo1. Furthermore, this CARC domain was located with the proposed lipid

binding pocket. The fourth region contained residues V2187, K2188, M2191, G2192, I2195, I2196, L2199, I2202, P2206 and L2207. These residues corresponded with a CARC motif found in the outer helix of the pore domain that is highly conserved. The final region contained residues V2471, V2474, L2475 and G2478. These residues were identified as an cholesterol interaction motifs. However, these residues are located within the Inner Helix of the pore region.

Surprisingly, the dynamic molecular simulation determined that the C-terminal extracellular domain could move to interact with the lipid bilayer (Figure 3.8B). However, the probability of amino acids in this structure interacting with cholesterol was very low.

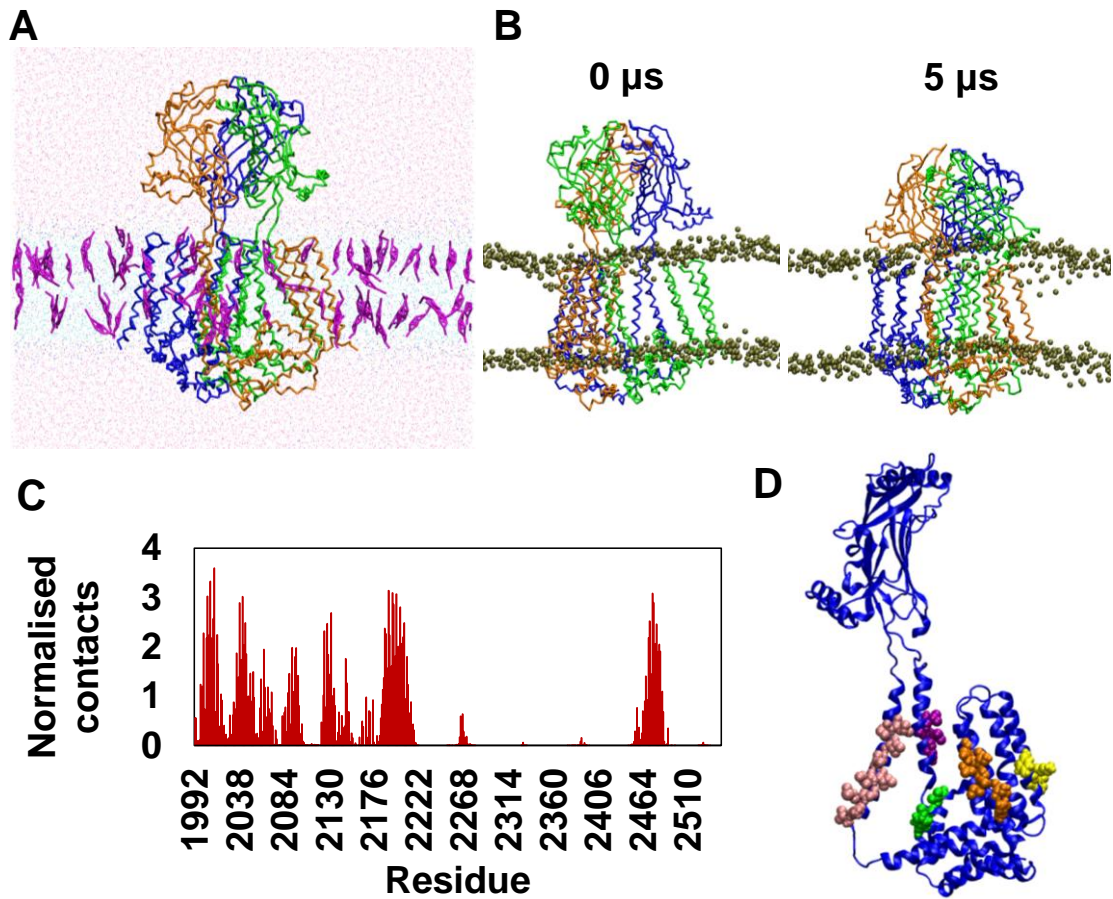


Figure 3.8: Computational modelling of cholesterol interactions with Piezo1. **A**, C-terminal structure within model with cholesterol shown in magenta. **B**, Simulation of Piezo1 in a lipid bilayer starting at 0 μ s (left) to 5 μ s (right). **C**, Cumulative probability of cholesterol for each amino residue in four modelling simulation with a cholesterol content of 10%, 15%, 20% and 20% + 5 % PIP₂. **D**, Regions of predicted cholesterol interaction sites. Orange (2001-2015), yellow (2038-2044), green (2125-2132), pink (2187-2207) and magenta (2471-2478). Computational modelling and binding site predictions were conducted by Dr. Antreas Kalli.

3.3.8 Mutagenesis of cholesterol binding sites in Piezo1

To determine whether the predicted cholesterol binding sites affect Piezo1 sensitivity to cholesterol, mutants of the binding sites were created (Table 3). Mutants were focussed on the predicted binding sites of the inner helix, outer helix and anchor domain due to the current suggestion of the C-terminal region being responsible for gating of Piezo1.

Single, double and triple mutations of potential cholesterol interaction sites were generated in the anchor domain, outer helix and inner helix of Piezo1. Mutating more than one residue in the anchor domain or outer helix produced non-functional Piezo1 mutants (Table 3). However, mutations in the inner helix and single point mutations produced active channels. Wild-type and mutants of Piezo1 were inhibited by addition and depletion of cholesterol (Figure 3.9G, H). However, the percentage inhibition by 1 mM cholesterol in mutants #7, #8, #9, #10 and #13 was significantly less compared to wild-type Piezo1 upon the initial activation of Piezo1 (Figure 3.9G). However, cholesterol still maintained inhibition of sustained Yoda1 responses in these mutants. Effects of M β CD were not significant in mutants compared with wildtype channel (Figure 3.9H). However, there was no inhibition of mutants #8, #10 and #13 by 1 mM M β CD. This suggests that exogenous cholesterol may exert its effects on Piezo1 by interacting at least partly with sites involving R2126 and R2135 in the anchor domain and R2482, R2484 and F2485 in the inner helix domain.

Table 3: Cholesterol binding site mutations and locations. Comparison of activation was to 2 μ M Yoda1 responses with vector control subtracted. Mutations were created and tested by Dr. Melanie Ludlow.

Name	Mutation	Location	Activation Compared to WT
#1	R2126A + F2130S	Anchor	No response
#2	F2130S + R2135A	Anchor	No response
#3	R2126A + F2130S + R2135A	Anchor	No response
#4	M2190A + F2198S	Outer Helix	70-80% decrease
#5	F2205A + M2210A	Outer Helix	70-80% decrease
#6	Y2470S + K2479S	Inner Helix	No response
#7	R2482A + F2484S	Inner Helix	10-30% increase
#8	R2482A + F2485S	Inner Helix	20-30% increase
#9	R2482A + F2484S + F2485S	Inner Helix	10-30% increase
#10	R2126A	Anchor	30% decrease
#11	F2130S	Anchor	No response
#12	F2130A	Anchor	No response
#13	R2135A	Anchor	50% decrease

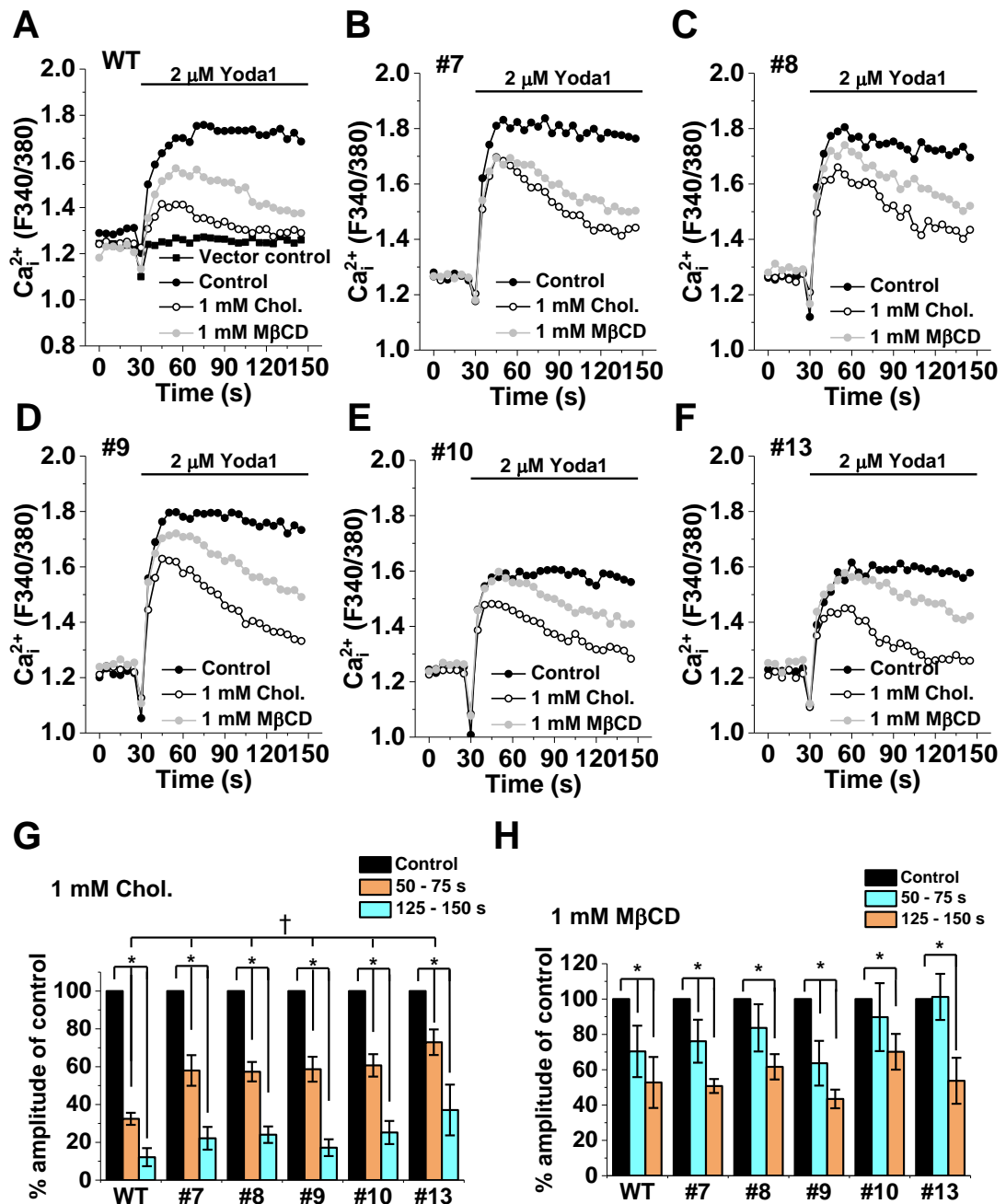


Figure 3.9: Cholesterol binding mutants are resistant to exogenous inhibition by exogenous cholesterol. **A-F**, example intracellular Ca^{2+} measurements from active cholesterol binding mutants of mPiezo1 and wild-type (WT) mPiezo1 after treatment with control, 1 mM cholesterol or 1 mM M β CD in response to 2 μ M Yoda1. **G**, average amplitudes of Yoda1 response of mutants pre-treated with control or 1 mM cholesterol. Amplitude was measured between 50-75 seconds (orange) and 125-150 seconds (blue). * = $P < 0.05$ against control at the timepoints measured. † = $P < 0.05$ against percentage inhibition of WT at 50-75 s. **H**, average amplitudes of Yoda1 response of mutants pre-treated with control or 1 mM cholesterol. Amplitude was measured between 50-75 seconds (orange) and 125-150 seconds (blue). * = $P < 0.05$ against control at the timepoints measured.

3.4 Discussion

This study reveals the ability of cholesterol to inhibit chemical activation of endothelial Piezo1 and overexpressed Piezo1 by Yoda1. Depletion of cholesterol also reduced Piezo1 activation suggesting that cholesterol in the plasma membrane was essential for Piezo1 activation. To probe the mechanism of inhibition by cholesterol addition and depletion, cholesterol interaction sites were found in Piezo1 by searching for motifs in the amino acid sequence of Piezo1 and by computational modelling of Piezo1 in a lipid bilayer. Mutating potential cholesterol binding sites in the anchor and inner helix reduced Piezo1 sensitivity to cholesterol during activation but did not completely abolish it.

3.4.1 Cholesterol binding in Piezo1

Cholesterol binding motifs have been demonstrated in ion channels such as Orai1, TRPV1, BK, nAChR and Kir2.1 channels (Derler et al., 2016; Picazo-Juarez et al., 2011; Singh et al., 2012; Fantini and Barrantes, 2013; Rosenhouse-Dantsker et al., 2013). In many cases mutating the residues in these predicted cholesterol interaction sites reduced sensitivity of the channel to the effects of cholesterol, such as with Orai1 and Kir2.1 (Derler et al., 2016; Rosenhouse-Dantsker et al., 2013). However, not all cholesterol interaction motif mutations reduced channel sensitivity to cholesterol and in some cases has produced non-functional forms of the channel (Rosenhouse-Dantsker et al., 2013). Here many potential cholesterol binding motifs were discovered in the protein sequences of human and mouse Piezo1. Additionally, many of these CRAC and CARC domains were found to be highly conserved. Coarse Grain molecular dynamics modelling of Piezo1 in a lipid bilayer containing cholesterol also suggested cholesterol interaction with some of these motifs. Mutations to these motifs often

produced inactive forms of Piezo1. Five mutations produced active forms of Piezo1 but with modified activity compared to wild-type mPiezo1. The response of each mutant to Yoda1 was reduced by cholesterol and M β CD. However, the inhibition of Yoda1 responses by addition of cholesterol was reduced by these mutants. However, the inhibition of sustained activation by Yoda1 was not affected. This suggests that cholesterol interaction with Piezo1 may affect gating of the channel. R2482, F2484 and F2845 was not in a predicted CRAC or CARC motif. R2126 was proposed to be adjacent to a CARC motif, with R2135 within this CARC motif. R2135A was previously reported to produce a non-functional Piezo1 in response to negative pressure applied to the cell membrane (Coste et al., 2015). However, Yoda1 was able to activate Piezo1 with this mutation. Additionally, this residue has been suggested to form a lipid-binding pocket between the anchor domain and the first repeat of Piezo1 transmembrane clusters (Saotome et al., 2017). Double and triple mutations of the proposed binding region between R2126 and R2135 produced non-functional mutants of Piezo1 in response to Yoda1. This suggests that these amino acids are essential for Piezo1 activity possible through cholesterol binding at these sites. The mechanism of regulation has not been determined for cholesterol binding. However, due to the importance of the location of cholesterol interaction sites mutated in gating, cholesterol may reduce the flexibility of the anchor and channel domain helices, attenuating opening of the channel.

To investigate direct binding of cholesterol to these sites multiple methods may be used. Fluorescence Resonance Energy Transfer (FRET) has been used to suggest binding between a fluorescent analogue of cholesterol, such TopFluor Cholesterol, and the Orai1 channel (Derler et al., 2016; Sezgin et al., 2016). The cholesterol binding motif mutants could be used to determine cholesterol binding

compared to wild type Piezo1 using this method. Additionally, displacement of cholesterol using similar sterols has also been a method of suggesting direct interaction between a protein and cholesterol (Bukiya et al., 2011). Epicholesterol and *ent*-cholesterol have similar effects to cholesterol on membrane fluidity and on the formation of lipid domains but have been shown to have different effects on ion channels, such as nAChR (Addona et al., 2003; Gimpl et al., 1997; Xu and London, 2000; Rychnovsky and Mickus, 1992; Mickus et al., 1992; Westover and Covey, 2004).

3.4.2 Other possible factors affecting Piezo1 activation

Piezo1 activity has previously been shown to be affected by membrane tension independent of the cytoskeleton (Lewis and Grandl, 2015; Cox et al., 2016). Additionally, the cholesterol content of membranes has been shown to affect biophysical membrane properties, such as membrane tension, affecting ion channel activity. Membrane elasticity could be investigated using similar methods to investigate membrane stiffness on Nav1.4 channel activation by using Triton X-100 or β -octyl-glucoside to alter the physical properties of the membrane (Lundbæk et al., 2004). Furthermore, membrane tension can be calculated using atomic force microscopy. The change in membrane tension caused by cholesterol may correlate with Piezo1 activation by Yoda1.

The modulation of Piezo1 by stiffness of the membrane has been suggested to be to occur by STOML3 in neurons (Qi et al., 2015). STOML3 was suggested to associate with and be important in the formation of cholesterol-rich lipid rafts. This suggests that Piezo1 may be associated with lipid rafts. Disruption of these lipid rafts by M β CD may be a mechanism for inhibition of Piezo1. However, direct identification of Piezo1 in lipid rafts by isolation of lipid rafts has not been shown.

Cell surface expression of ion channels has also been shown to be affected by membrane cholesterol content. Depletion of membrane cholesterol by M β CD has been shown to induce internalisation of nicotinic acetylcholine receptors (Borroni et al., 2007). Depletion or addition of cholesterol to the membrane of both HUVECs and over-expressed Piezo1 may have affected trafficking of the channel to the cell surface. To determine the effects of cholesterol depletion of Piezo1 on cell surface expression cell surface biotinylation or immunofluorescence imaging could be used. However, due to the lack of a specific primary antibody for Piezo1, this would have to be conducted on Piezo1 with a tag motif in the structure, such as a hemagglutinin tag.

3.4.3 Clinical relevance

Cholesterol plays a major role in endothelial cell dysfunction (Steinberg et al., 1997). Endothelial dysfunction and cholesterol also lead to the progression of vascular diseases such as atherosclerosis. A functional connection between endothelial Piezo1 and phosphorylation of endothelial nitric oxide synthase (eNOS) has been reported which was important for regulation of blood pressure (Wang et al., 2016). Due to the inhibition of Piezo1 by exogenous cholesterol this may provide a link between hypercholesterolemia and low shear stress causing atherosclerosis. To investigate this further *in vivo*, endothelial-specific Piezo1 knockout mice crossed with ApoE knockout mice may be used and fed a high-fat diet. We would expect that these mice would have a higher susceptibility to atheroma formation due to loss of shear stress sensing ability and high cholesterol.

3.5 Summary

Piezo1 activation can be inhibited by increasing or decreasing membrane cholesterol content. The regulation of activity by cholesterol may be due to cholesterol binding to Piezo1. Piezo1 has many cholesterol binding motifs in its structure and potential interaction sites close the C-terminus, which is important for gating. Single point mutations of Piezo1 can reduce the sensitivity of cholesterol inhibiting Piezo1 activation but not the depletion of cholesterol. This suggests that direct interactions between cholesterol may regulate Piezo1 activity, however, other factors such as membrane tension may also contribute to the effects of cholesterol on Piezo1.

Chapter 4

Spingolipid modulation of Piezo1 activation in endothelial cells.

4.1 Introduction

Spingolipids have been shown to affect downstream signalling pathways in various cell types with a range of different responses. Ceramide and spingosine have been suggested to play roles in apoptosis (Woodcock, 2006), whereas spingosine 1-phosphate and ceramide 1-phosphate have been shown to have opposing effects (Gómez-Muñoz et al., 2013; Maceyka et al., 2012). The effects of spingolipids are dependent on activation of particular enzymes, such as spingomyelinases, which break down spingomyelin into ceramide and phosphocholine; ceramidases, which convert ceramides into spingosine; or spingosine kinases, which phosphorylate spingosine to form spingosine 1-phosphate (Hannun and Obeid, 2008).

Spingomyelinases have been shown to contribute to endothelial dysfunction by reducing endothelium-dependent vasodilation (Bao et al., 2010; Murohara et al., 1996). Additionally, spingomyelinase activation increased the expression of the atherogenic marker ICAM-1 in endothelial cells contributing to T Cell migration (Lopes Pinheiro et al., 2016). Furthermore, activation of spingomyelinase has been suggested in shear stress dependent endothelial cell responses (Czarny et al., 2003; Czarny and Schnitzer, 2004).

Piezo1 has been shown to be important for endothelial cell functions such as shear stress-evoked Ca^{2+} entry, cell alignment and migration (Li et al., 2014). Furthermore, Piezo1 has been shown to regulate overall vascular functions in vivo, such as vascular tone (Rode et al., 2017; Wang et al., 2016). Piezo1 has been shown to activate molecules downstream of activation via Ca^{2+} entry in endothelial cells, such as calpain (Li et al., 2014). However, modulation of Piezo1 in endothelial cells by cell signalling pathways has not been investigated. Piezo1 activity has been shown to be affected by PIP_2 depletion in neural cells and when overexpressed in HEK cells after activation of TRPV1 (Borbiro et al., 2015). However, Piezo2, a mechanosensitive channel of the same family of Piezo1, has been shown to have enhanced activity after activation of protein kinases A and C (Dubin et al., 2012).

4.2 Aims

In this chapter the effects of sphingomyelinase, and downstream products, were investigated on the activation of Piezo1 by Yoda1. Due to the effects of sphingomyelinase in inflammatory responses in the cardiovascular system this may implicate Piezo1 in cardiovascular disease mechanisms and reveal mechanisms to target this response.

4.3 Results

4.3.1 Sphingomyelinase potentiates Piezo1 activation in HUVECs

The effect of sphingolipids on Piezo1 activity as initially investigated by exposing HUVECs to bacterial sphingomyelinase. When sphingomyelin was digested using exogenous sphingomyelinase Piezo1 activation was increased in response to Yoda1 at 1 μM . The amplitude of Ca^{2+} influx in response to Yoda1 increased to 160% of the control amplitude (Figure 4.1B). This potentiation of Piezo1 activation in HUVECs was preceded by an increase in baseline intracellular Ca^{2+} concentration, indicated by an increase in fluorescence ratio prior to addition of Yoda1 in sphingomyelinase treated HUVECs. The baseline was increased by 0.15 fluorescence ratio units (Figure 4.1C). When sphingomyelinase was pre-inactivated, by heating the enzyme at 100°C for 30 minutes, the effects on Ca^{2+} and baseline Ca^{2+} were abolished. These data suggest that sphingomyelinase potentiates Piezo1 activity in HUVECs. This may be achieved through altering the membrane composition by digestion of sphingomyelin or downstream products of sphingomyelinase digestion affecting Piezo1 activity.

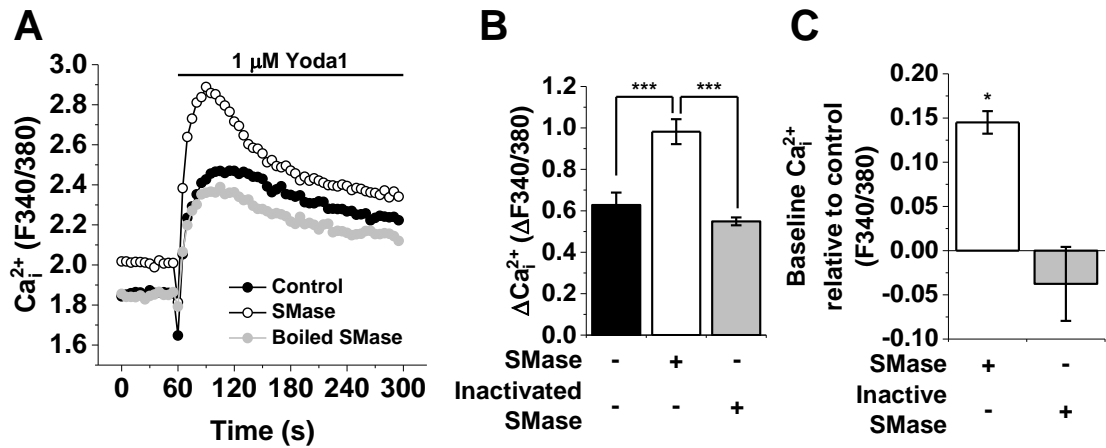


Figure 4.1: Spingomyelinase potentiates Yoda1 response in HUVECs. **A**, Typical Ca²⁺ response to 1 μM Yoda1 of HUVECs when pre-treated with sphingomyelinase (SMase) at 0.5 U/mL or boiled inactivated SMase for 30 minutes at 37°C compared to control. **B**, Average amplitude of Yoda1 response influx of conditions in **A**. *** = P < 0.01. n/N = 3/4. **C**, Average baseline intracellular Ca²⁺ of conditions in **A**. * = P < 0.05. n/N = 3/4.

4.3.2 Sphingomyelinase decreases Yoda1 responses in Piezo1 overexpression system

To determine whether the potentiation of endothelial Piezo1 also occurred with constituted Piezo1, hP1 HEK TREx cells were treated with sphingomyelinase. Unexpectedly the response to Yoda1 in sphingomyelinase-treated P1 HEK TREx cells was markedly decreased to 55% of control (Figure 4.2). Additionally, there was no change in baseline intracellular Ca^{2+} concentrations prior to Yoda1 addition. These data suggest that sphingomyelinase has different effects on human Piezo1 activity native to endothelial cells or over-expressed in HEK293 cells. Such a difference could be due to different cell signalling machinery available in these cells.

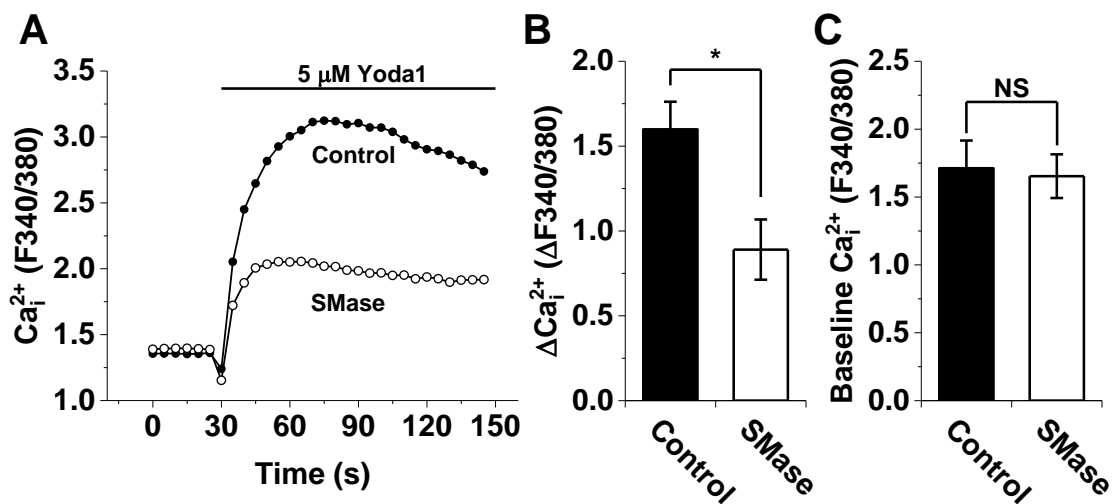


Figure 4.2: Sphingomyelinase reduces Yoda1 response in Piezo1 HEK TREx. **A**, Typical Ca^{2+} response to 5 μM Yoda1 of Piezo1 HEK TREx when pre-treated with sphingomyelinase (SMase) at 0.5 U/mL for 30 minutes at 37°C compared to control. **B**, Average amplitude of Yoda1 response of conditions in **A**. * = $P < 0.05$. n/N = 4/4. **C**, Average baseline intracellular Ca^{2+} of conditions in **A**. NS = $P > 0.05$. n/N = 4/4.

4.3.3 Effect of sphingomyelinase on other Ca²⁺ entry mechanisms

To determine the specificity of sphingomyelinase on Piezo1 activity, other Ca²⁺ entry mechanisms were investigated.

4.3.3.1 ATP

ATP induces both Ca²⁺ entry via ionotropic P2X receptors and Ca²⁺ release via activation of metabotropic P2Y receptors and subsequent activation of IP₃ receptors. Therefore, the effect of sphingomyelinase on Ca²⁺ flux by ATP was investigated in HUVECs. After pre-treatment with 0.5 U/mL sphingomyelinase the amplitude of Ca²⁺ rise was not affected when compared to control in response to 20 μM ATP (Figure 4.3). However, the effect of increased baseline Ca²⁺ still occurred suggesting that SMase was active for these experiments.

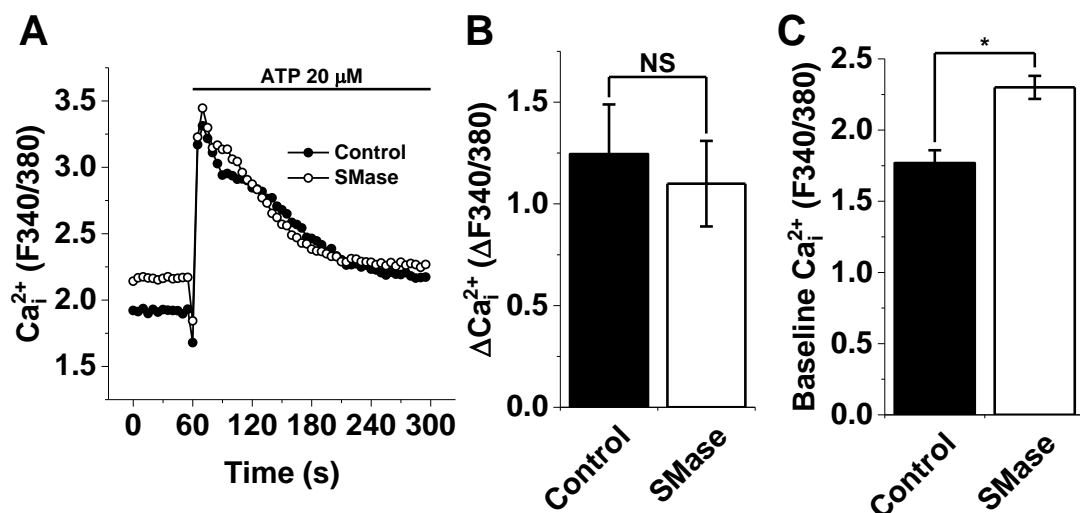


Figure 4.3: SpHINGOMYELINASE does not affect ATP response in HUVECs. A, Typical Ca²⁺ response of HUVECs to 20 μM ATP when pre-treated with sphingomyelinase (SMase) at 0.5 U/mL for 30 minutes at 37°C compared to control. **B,** Average amplitude of calcium influx of conditions in **A**. NS = not significant. n/N = 3/4. **C,** Average baseline intracellular Ca²⁺ of conditions in **A**. * = P < 0.05. n/N = 3/4.

4.3.3.2 Store-operated Ca²⁺ Entry

Store-operated Ca²⁺ entry occurs in response to depletion of ER Ca²⁺ stores and subsequent activation of Orai1 channels. To investigate the effect of sphingomyelinase on SOC responses, 2 μM thapsigargin in 0 Ca²⁺ SBS was used to deplete ER Ca²⁺ stores. 1.5 mM Ca²⁺ was added back to the solution for Ca²⁺ influx to occur via Orai1. Sphingomyelinase reduced SOC responses amplitudes in HUVECs (Figure 4.4). However, there was no increase in baseline Ca²⁺, suggesting that the elevated baseline seen in the previous experiments depended on extracellular Ca²⁺ or thapsigargin-sensitive Ca²⁺ release.

4.3.3.3 VEGF-mediated Ca²⁺ entry

Vascular endothelial growth factor has been shown to activate receptor operated calcium channels, such as TRPC3 and TRPC6 (Cheng et al., 2006), as well as Orai1 (Li et al., 2011). VEGF-induced Ca²⁺ responses in HUVECs were not affected by SMase in HUVECs (Figure 1.5). These data suggest sphingomyelinase does not affect VEGF responses in HUVECs.

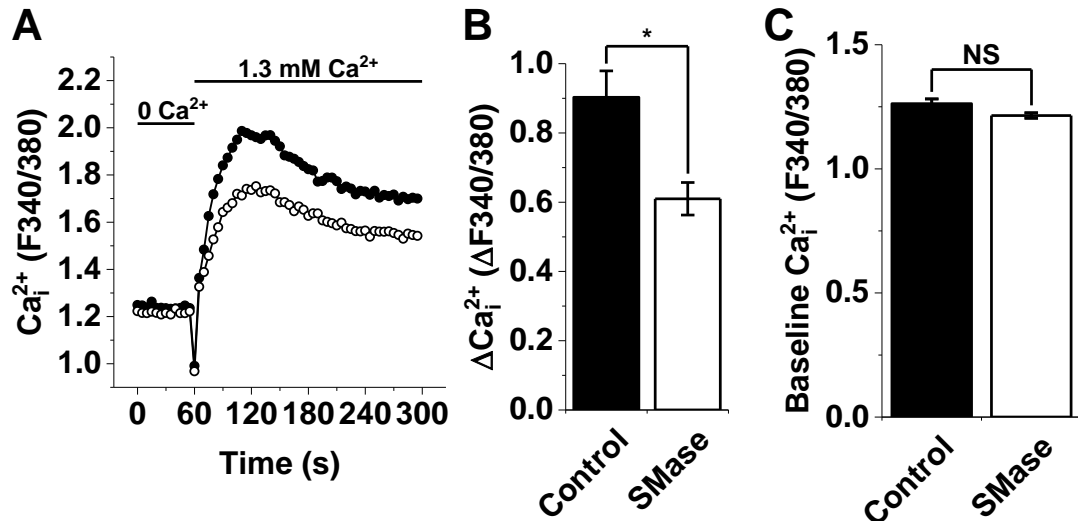


Figure 4.4: SpHINGOMYELINASE reduced Ca²⁺ add-back response in HUVECs. **A**, Typical Ca²⁺ response of HUVECs to Ca²⁺ add-back when pre-treated with sphingomyelinase (SMase) at 0.5 U/mL or boiled inactivated SMase for 30 minutes at 37°C compared to control. Depletion of intracellular was induced by treatment with 2 μM thapsigargin for 30 minutes in 0 Ca²⁺ SBS. **B**, Average amplitude of Ca²⁺ influx of conditions in **A**. * = P < 0.05. n/N = 3/4. **C**, Average baseline intracellular Ca²⁺ of conditions in **A**. * = P < 0.05. n/N = 3/4.

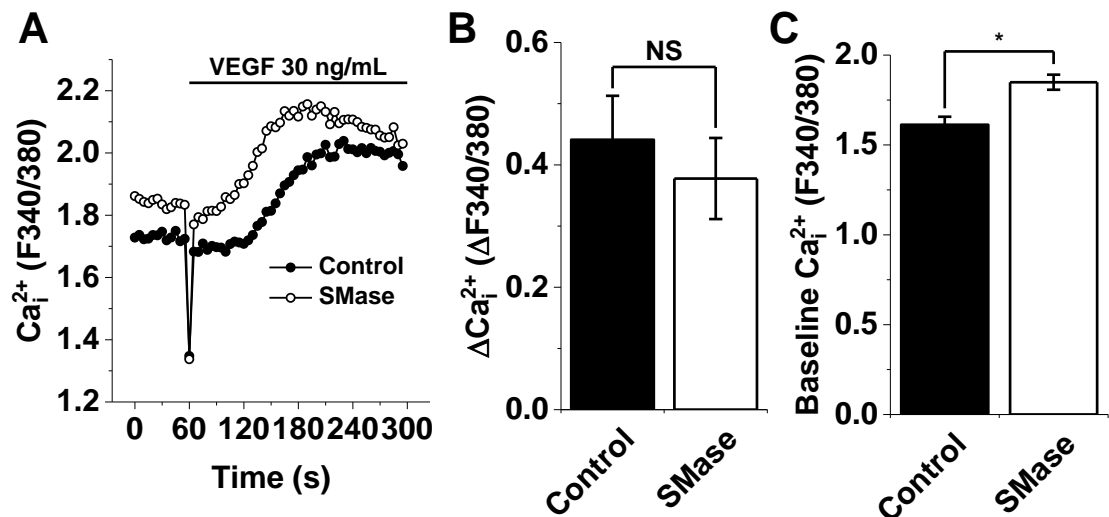


Figure 4.5: SpHINGOMYELINASE does not affect VEGF response in HUVECs. **A**, Typical Ca²⁺ response of HUVECs to 30 ng/mL VEGF when pre-treated with sphingomyelinase (SMase) at 0.5 U/mL for 30 minutes at 37°C compared to control. **B**, Average amplitude of VEGF response of conditions in **A**. NS = not significant. n/N = 3/4. **C**, Average baseline intracellular Ca²⁺ of conditions in **A**. * = P < 0.05. n/N = 3/4.

4.3.4 Effect of Piezo1 inhibitors on SMase potentiation

Piezo1 activation may have contributed to the increase in intracellular Ca^{2+} after incubation with SMase. To determine whether Piezo1 was activated by SMase known inhibitors gadolinium and ruthenium red were used alongside knockdown of Piezo1 expression using siRNA targeting Piezo1.

4.3.4.1 Gadolinium

Gadolinium was used as an inhibitor of Piezo1. Gadolinium abolished Yoda1 responses and SMase-potentiated Yoda1 responses in HUVECs (Figure 4.6A-B). Furthermore, gadolinium reduced baseline Ca^{2+} with or without SMase pre-treatment (Figure 4.6). These data suggest that Piezo1 channels may have been activated by SMase incubation. However, gadolinium is not specific for Piezo1 channels. Therefore, another inhibitor of Piezo1 channels, ruthenium red, was investigated.

4.3.4.2 Ruthenium Red

Ruthenium Red abolished Yoda1 responses and SMase-potentiated Yoda1 responses in HUVECs (Figure 4.7). However, Ruthenium Red increased baseline Ca^{2+} level with or without SMase pre-treatment compared to control. Due to the lack of specificity, and potential effects of fluorescence of ruthenium red, Piezo1 knockdown was used to determine whether SMase activates Piezo1.

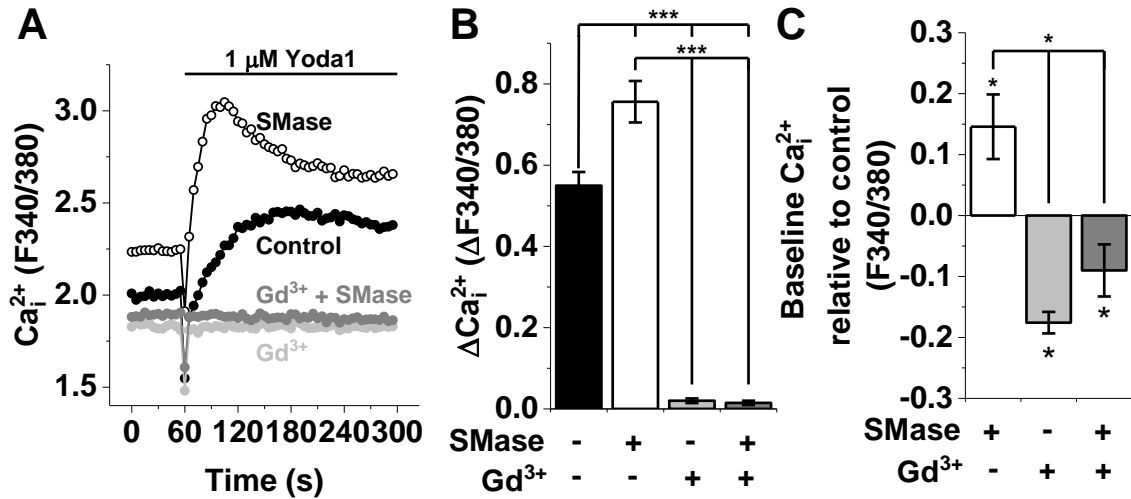


Figure 4.6: Potentiation of Yoda1 responses by sphingomyelinase is inhibited by gadolinium. **A**, Typical Ca_i^{2+} response of HUVECs to 1 μM Yoda1 when pre-treated with sphingomyelinase (SMase) at 0.5 U/mL or 100 μM gadolinium (Gd^{3+}) for 30 minutes at 37°C compared to control. The concentration of Gd^{3+} was maintained throughout the experiment. **B**, Average amplitude of Yoda1 in conditions in **A**. *** = $P < 0.01$. $n/N = 3/4$. **C**, Average baseline intracellular Ca_i^{2+} of conditions in **A**. * = $P < 0.05$. $n/N = 3/4$.

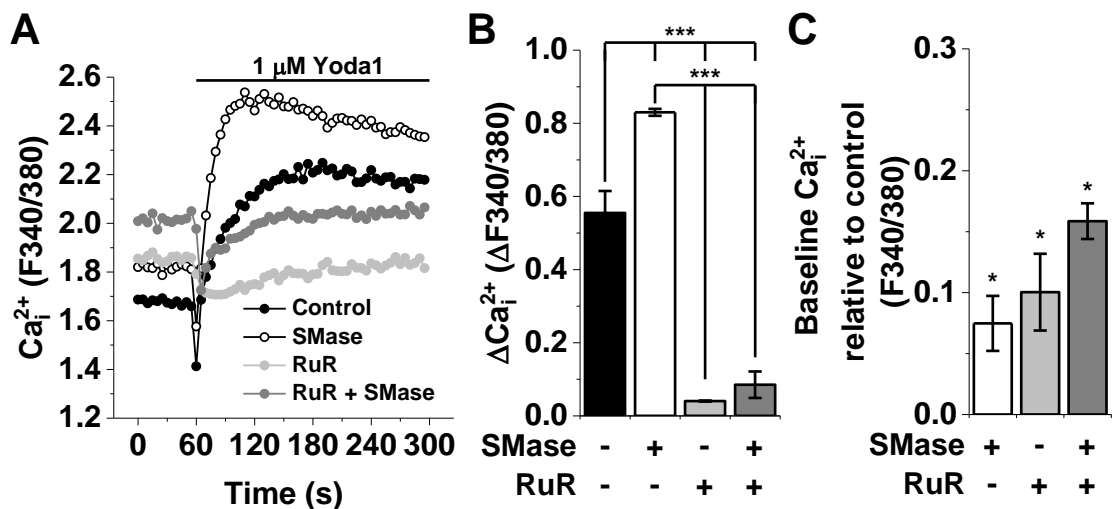


Figure 4.7: Potentiation of Yoda1 responses by sphingomyelinase is inhibited by ruthenium red but not increases in baseline Ca_i^{2+} . **A**, Typical Ca_i^{2+} response of HUVECs to 1 μM Yoda1 when pre-treated with sphingomyelinase (SMase) at 0.5 U/mL or 50 μM ruthenium red (RuR) for 30 minutes at 37°C compared to control. The concentration of RuR was maintained throughout the experiment. **B**, Average amplitude of Yoda1 response in conditions in **A**. *** = $P < 0.01$. $n/N = 3/4$. **C**, Average baseline intracellular Ca_i^{2+} of conditions in **A**. * = $P < 0.05$. $n/N = 3/4$.

4.3.4.3 Piezo1 knockdown

To determine whether Piezo1 was being activated by SMase pre-treatment, Piezo1 siRNA was used to reduce expression of Piezo1. Piezo1 siRNA treated cells had significantly lower Yoda1 responses compared to HUVECs treated with scrambled siRNA. Additionally, the potentiation of Piezo1 activation by SMase treatment was abolished by Piezo1 depletion (Figure 4.8). However, SMase-induced increases in baseline Ca^{2+} levels were not affected by Piezo1 depletion, suggesting that Piezo1 activation does not contribute to the increase in baseline Ca^{2+} caused by SMase.

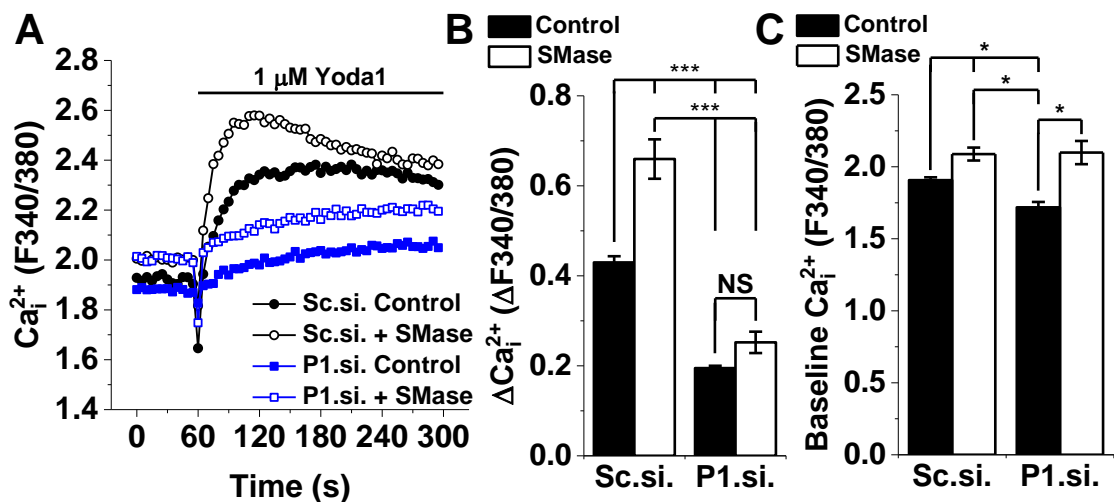


Figure 4.8: Potentiation of Yoda1 responses by sphingomyelinase was reduced by Piezo1 knockdown but increases in baseline Ca^{2+} was not affected. **A**, Typical Ca^{2+} response of HUVECs to 1 μM Yoda1 when pre-treated with sphingomyelinase (SMase) at 0.5 U/mL for 30 minutes at 37°C compared to control. Sc.si denotes cells pre-treated with negative control scrambled siRNA. P1.si denotes cells pre-treated with siRNA targeting Piezo1. **B**, Average amplitude of Yoda1 response of conditions in **A**. *** = $P < 0.01$. $n/N = 3/4$. **C**, Average baseline intracellular Ca^{2+} of conditions in **A**. * = $P < 0.05$. $n/N = 3/4$.

4.3.5 Downstream signalling of sphingomyelinase on Piezo1 activity

Due to the differing effects of sphingomyelinase on Piezo1 activity in HUVECs versus P1 HEK TReX cells, the downstream products of sphingomyelinase digestion were investigated. Sphingomyelin is digested to form ceramides and a choline group. Ceramides can be phosphorylated to form ceramide-1-phosphate or hydrolysed to form sphingosine. Sphingosine can also be phosphorylated to form sphingosine-1-phosphate. These reactions form the sphingomyelinase cycle, which is commonly associated with cell death and proliferation.

4.3.5.1 Sphingomyelin

The effect of endogenous regulation of Piezo1 by sphingomyelin was investigated. Pre-treatment with 100 μ M sphingomyelin to increase membrane sphingomyelin had no effect on Piezo1 activation by Yoda1 (Figure 4.9). Furthermore, sphingomyelin did not affect baseline Ca^{2+} levels of HUVECs after pre-treatment. This suggests that Piezo1 activity in HUVECs is not affected by sphingomyelin itself.

4.3.5.2 Phosphocholine

Digestion of sphingomyelin produces phosphocholine and ceramides. Therefore, phosphocholine was investigated to determine an effect on Piezo1. Piezo1 activation by Yoda1 was not affected by pre-treatment of 50 μ M phosphocholine (Figure 4.10). Furthermore, baseline Ca^{2+} levels were not affected after pre-treatment with phosphocholine. This suggests that phosphocholine was not playing a role in the potentiation of Yoda1-induced Piezo1 activation in HUVECs after SMase pre-treatment.

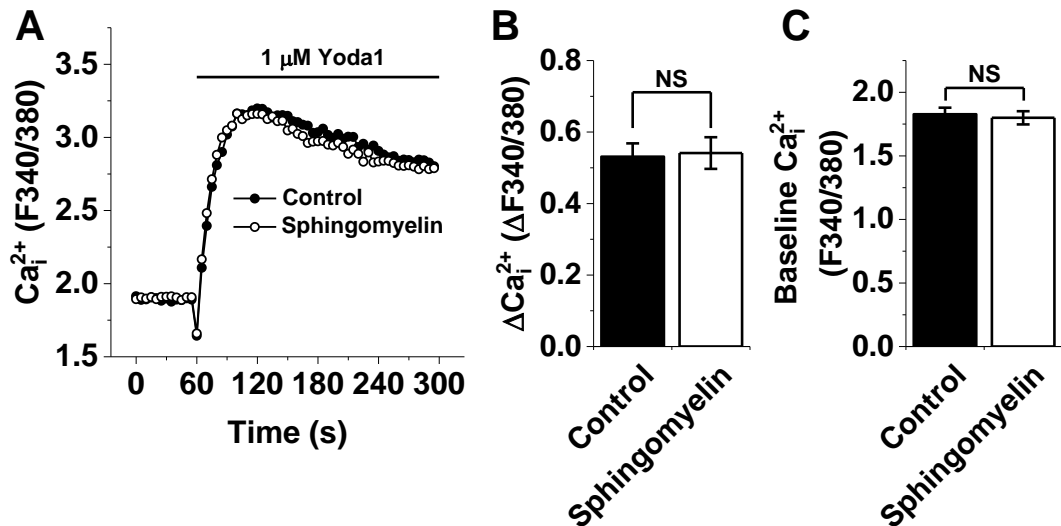


Figure 4.9: SpHINGOMYELIN did not affect Yoda1 responses or baseline Ca^{2+} in HUVECs. **A**, Typical Ca^{2+} response of HUVECs to 1 μM Yoda1 when pre-treated with spHINGOMYELIN at 100 μM for 30 minutes at 37°C compared to control. **B**, Average amplitude of Yoda1 response of conditions in **A**. NS = not significant. $n/N = 4/4$. **C**, Average baseline intracellular Ca^{2+} of conditions in **A**. NS = not significant. $n/N = 4/4$.

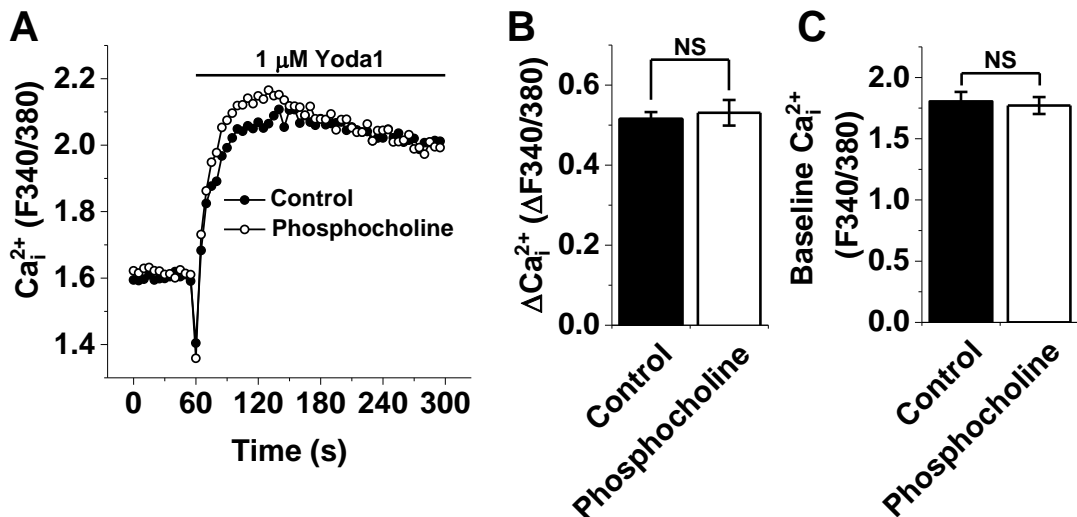


Figure 4.10: Phosphocholine did not affect Yoda1 responses or baseline Ca^{2+} in HUVECs. **A**, Typical Ca^{2+} response of HUVECs to 1 μM Yoda1 when pre-treated with phosphocholine at 50 μM for 30 minutes at 37°C compared to control. **B**, Average amplitude of Yoda1 response of conditions in **A**. NS = not significant. $n/N = 4/4$. **C**, Average baseline intracellular Ca^{2+} of conditions in **A**. NS = not significant. $n/N = 4/4$.

4.3.5.3 Ceramides

Ceramides are commonly known to affect membrane properties and activate cell signalling pathways depending on the length of their lipid chain. 16, 6 and 2 carbon (C₁₆-, C₆-, and C₂-, respectively) forms of ceramide were investigated against activation of Piezo1 by Yoda1 in HUVECs. C₁₆ ceramide is not membrane permeable however, whereas the shorter C₆- and C₂-ceramide are membrane permeable. Piezo1 activation was not affected by pre-treatment with 50 µM of any chain length of ceramide (Figure 4.11). Additionally, ceramides did not affect baseline intracellular Ca²⁺ levels. These data suggest that ceramides were not responsible in the potentiation of Yoda1-induced Piezo1 activation in HUVECs after SMase pre-treatment.

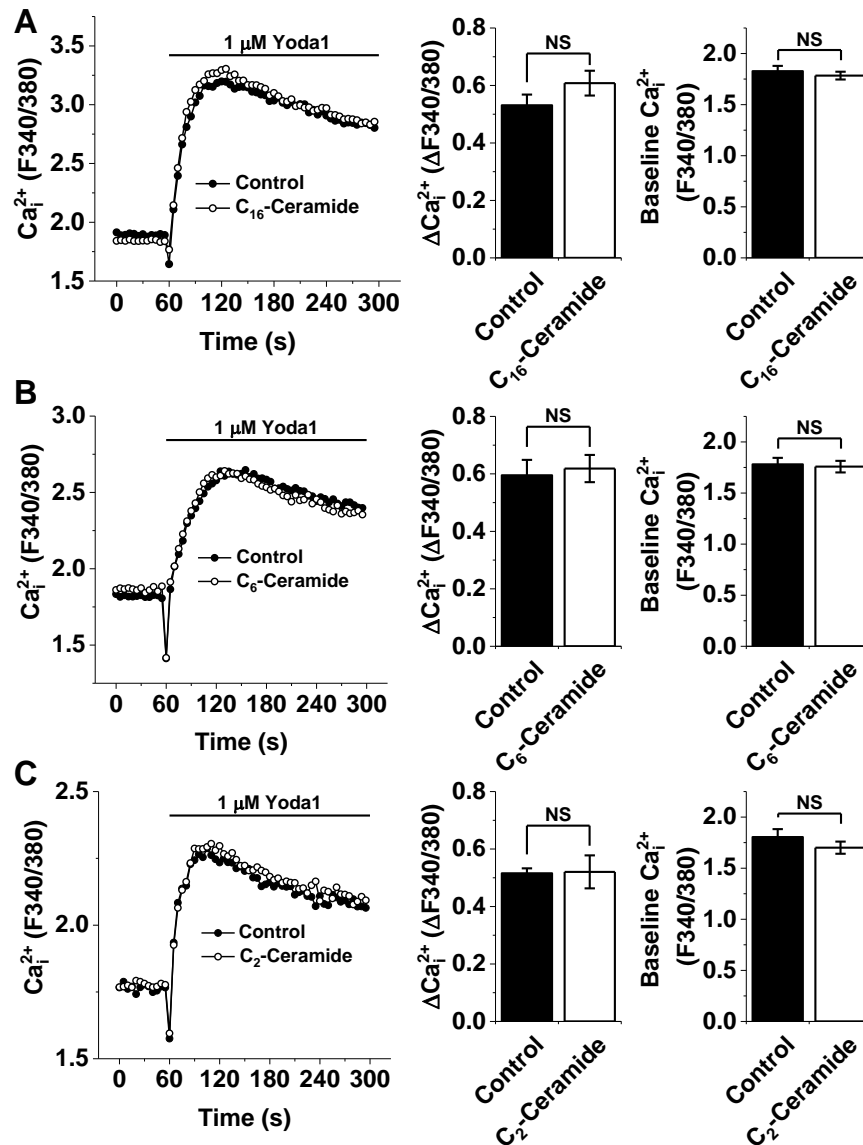


Figure 4.11: Ceramides did not affect Yoda1 responses or baseline Ca^{2+} in HUVECs. **A**, Left Panel. Typical Ca^{2+} response of HUVECs to 1 μM Yoda1 when pre-treated with C_{16} -ceramide at 50 μM for 30 minutes at 37°C compared to control. Middle Panel, Average amplitude of calcium influx of conditions in the left panel. NS = not significant. n/N = 4/4. Right Panel, Average baseline intracellular Ca^{2+} of conditions in the left panel. NS = not significant. n/N = 4/4. **B**, Left Panel. Typical Ca^{2+} response of HUVECs to 1 μM Yoda1 when pre-treated with C_6 -ceramide at 50 μM for 30 minutes at 37°C compared to control. Middle Panel, Average amplitude of calcium influx of conditions in the left panel. NS = not significant. n/N = 4/4. Right Panel, Average baseline intracellular Ca^{2+} of conditions in the left panel. NS = not significant. n/N = 4/4. **C**, Left Panel. Typical Ca^{2+} response of HUVECs to 1 μM Yoda1 when pre-treated with C_2 -ceramide at 50 μM for 30 minutes at 37°C compared to control. Middle Panel, Average amplitude of calcium influx of conditions in the left panel. NS = not significant. n/N = 4/4. Right Panel, Average baseline intracellular Ca^{2+} of conditions in the left panel. NS = not significant. n/N = 4/4.

4.3.5.4 Ceramide-1-phosphate

Ceramides are readily phosphorylated in cells forming ceramide-1-Phosphate. Therefore, ceramide-1-phosphate was investigated as a modulator of Piezo1 activity in HUVECs. Treatment with 10 μM ceramide-1-phosphate had no effect on Piezo1 activity in HUVECs in response to Yoda1 (Figure 4.12). Additionally, no change in baseline Ca^{2+} was observed after treatment with ceramide-1-phosphate. These data suggest that ceramides and ceramide-1-phosphate have no effect on Piezo1. The results pointed to sphingosine or sphingosine-1-phosphate as mediators of Piezo1 potentiation by sphingomyelinase.

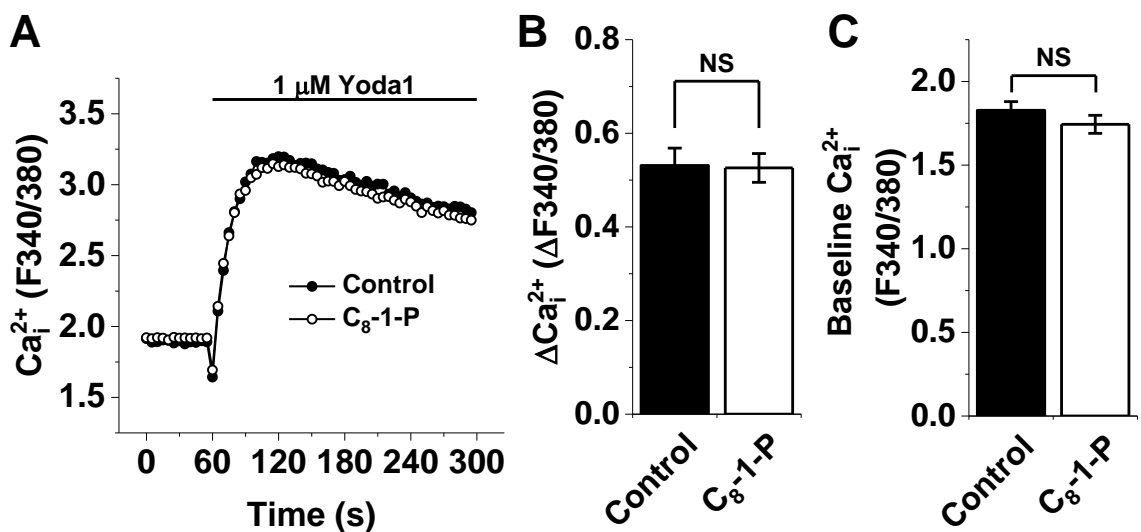


Figure 4.12: Ceramide-1-phosphate did not affect Yoda1 responses or baseline Ca^{2+} in HUVECs. **A**, Typical Ca^{2+} response of HUVECs to 1 μM Yoda1 when pre-treated with ceramide-1-phosphate (C-1-P) at 10 μM for 30 minutes at 37°C compared to control. **B**, Average amplitude of calcium influx of conditions in **A**. NS = not significant. n/N = 4/4. **C**, Average baseline intracellular Ca^{2+} of conditions in **A**. NS = not significant. n/N = 4/4.

4.3.5.5 Sphingosine

To investigate the effect of sphingosine on activation of Piezo1, HUVECs were pre-treated with 50 μM sphingosine. Sphingosine exerted both increases in baseline intracellular Ca^{2+} and potentiation of Yoda1-induced Piezo1 activation (Figure 4.13), effects which were similar to those of sphingomyelinase (Figures 1.1 and 1.6). This suggested that sphingosine may be the molecule key to producing the potentiating effect of sphingomyelinase on Piezo1 activation. To determine whether it is the sphingosine produced by conversion of ceramides after sphingomyelinase activity, ceranib-1, an inhibitor of ceramidases (Draper et al., 2011), was used. Ceranib-1 inhibited both the potentiating effect of sphingomyelinase on the Yoda1 response and the increase in baseline Ca^{2+} . Strikingly, the Yoda1 response and baseline were rescued when sphingosine was incubated with sphingomyelinase and ceranib-1 (Figure 4.13B). These data suggest that sphingosine produced by conversion of the ceramides, downstream of their production after sphingomyelin digestion, was responsible for the potentiation of Piezo1.

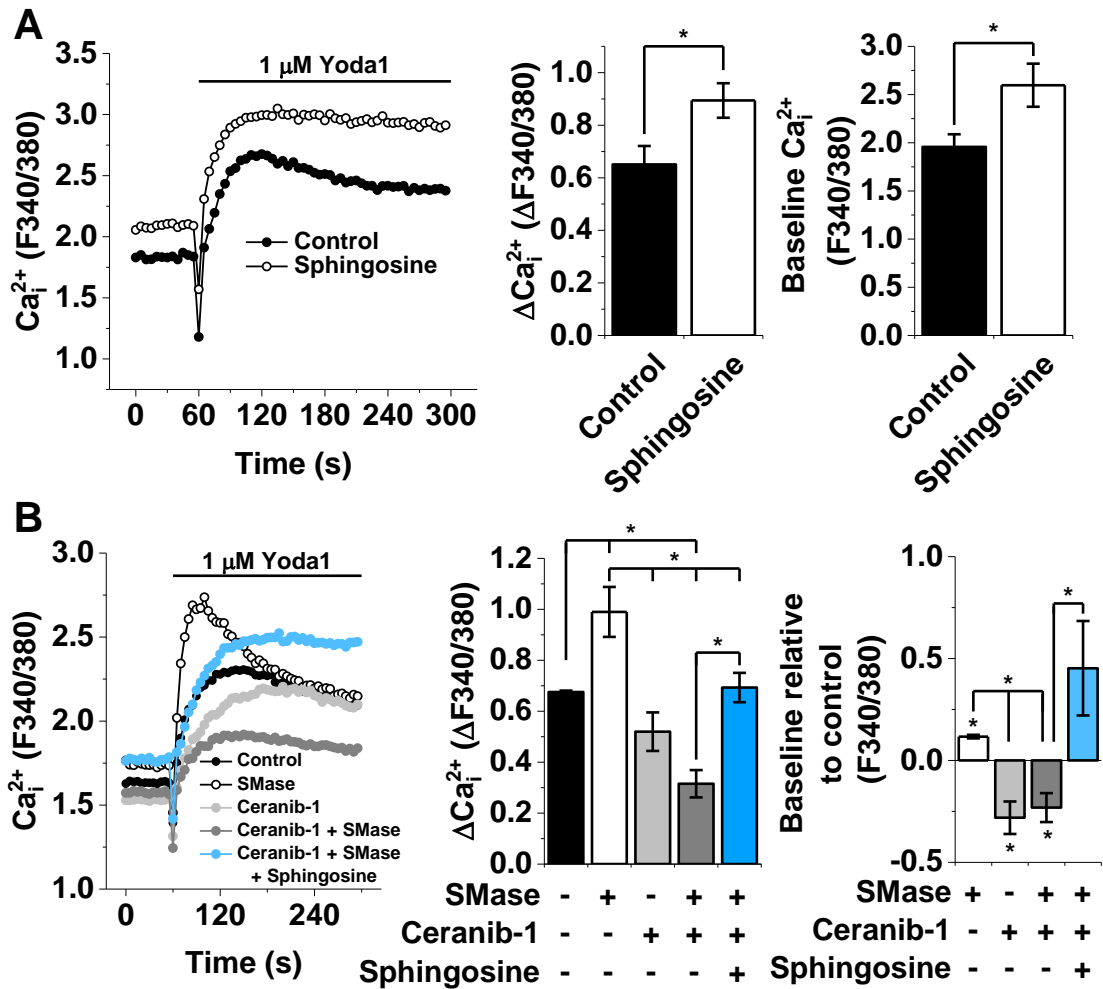


Figure 4.13: Spingosine increased Yoda1 responses and baseline Ca^{2+} in HUVECs. **A**, Left Panel. Typical Ca^{2+} response of HUVECs to 1 μM Yoda1 when pre-treated with Spingosine at 50 μM for 30 minutes at 37°C compared to control. Middle Panel, Average amplitude of calcium influx of conditions in the left panel. * = $P < 0.05$. $n/N = 4/4$. Right Panel, Average baseline intracellular Ca^{2+} of conditions in the left panel. * = $P < 0.05$. $n/N = 4/4$. **B**, Left Panel. Typical Ca^{2+} response of HUVECs to 1 μM Yoda1 when pre-treated with SMase at 0.5 U/mL, ceranib-1 (10 μM) and spingosine (50 μM) for 30 minutes at 37°C compared to control. Middle Panel, Average amplitude of calcium influx of conditions in the left panel. * = $P < 0.05$. $n/N = 4/16$. Right Panel, Average baseline intracellular Ca^{2+} of conditions in the left panel. * = $P < 0.05$. $n/N = 4/4$.

4.3.5.6 Sphingosine-1-phosphate

Sphingosine 1-phosphate (S-1-P) has been shown to activate Ca^{2+} permeable channels as well as many other cell signalling pathways via G-protein coupled receptors. Therefore, HUVECs were exposed S-1-P to determine whether its production downstream of sphingosine may produce the potentiation of Piezo1 activation by SMase. S-1-P did not show any effect on Piezo1 activity or baseline Ca^{2+} levels (Figure 4.14). Additionally, Pico-145 a blocker of TRPC5 channels that can be activated by S-1-P, had no effect on the effects of sphingomyelinase treatment on Piezo1 activation in HUVECs.

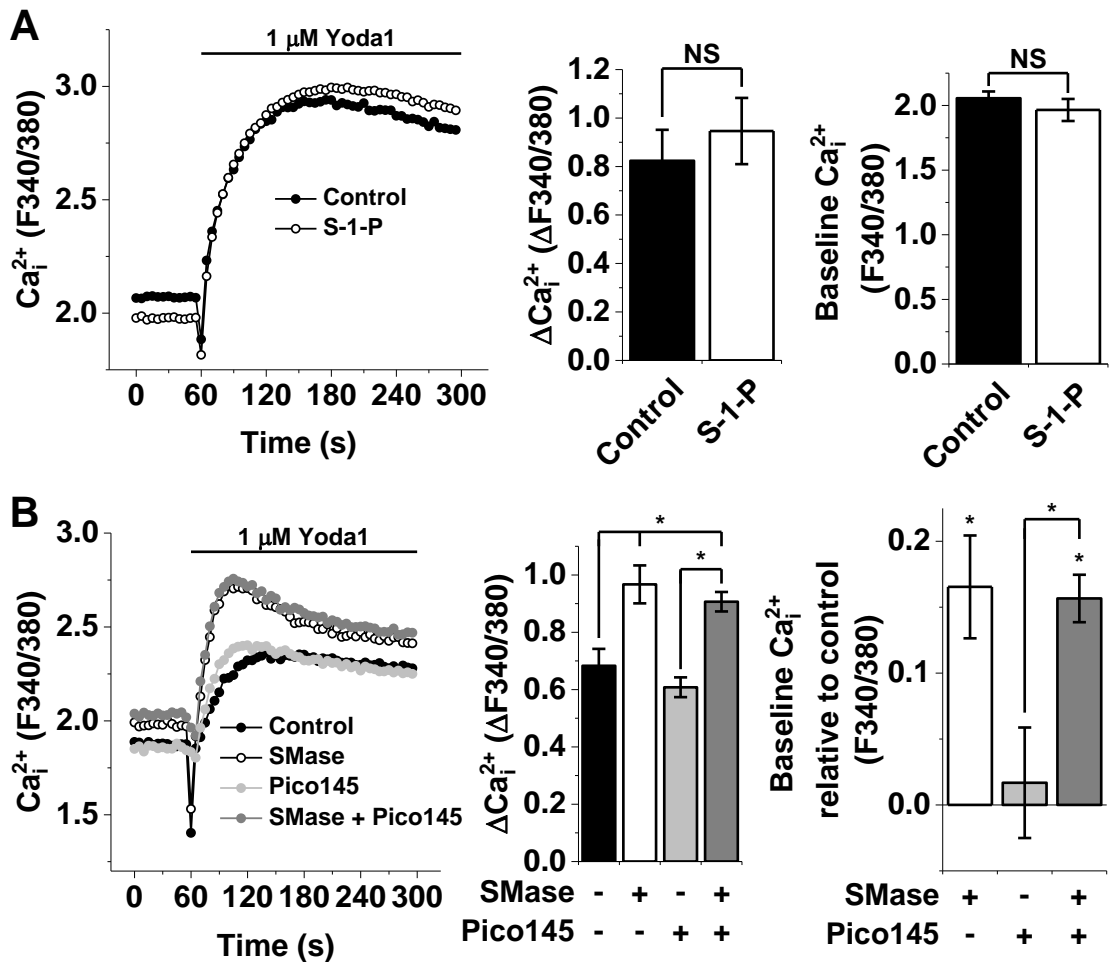


Figure 4.14: Spingosine-1-phosphate did not affect Yoda1 responses or baseline Ca²⁺ in HUVECs. **A**, Left Panel. Typical Ca²⁺ response of HUVECs to 1 μ M Yoda1 when pre-treated with sphingosine-1-phosphate (S-1-P) at 10 μ M for 30 minutes at 37°C compared to control. Middle Panel, Average amplitude of calcium influx of conditions in A. * = P < 0.05. n/N = 4/4. Right Panel, Average baseline intracellular Ca²⁺ of conditions in A. * = P < 0.05. n/N = 4/4. **B**, Left Panel. Typical Ca²⁺ response of HUVECs to 1 μ M Yoda1 when pre-treated with SMase at 0.5 U/mL or Pico145 (30 nM) for 30 minutes at 37°C compared to control. Middle Panel, Average amplitude of calcium influx of conditions in A. NS = not significant. n/N = 4/16. Right Panel, Average baseline intracellular Ca²⁺ of conditions in A. NS = not significant. n/N = 4/16.

4.3.6 Mechanism of potentiation of Piezo1 by sphingosine

The data so far suggested that sphingosine mediated the SMase potentiation of Piezo1-mediated Yoda1 responses in HUVECs. Therefore, known targets of sphingosine were targeted pharmacologically to determine the mechanism of sphingosine's action.

4.3.6.1 PKA

PKA has been suggested to be activated by sphingosine. Therefore, inhibition of PKA was investigated against the potentiation of Piezo1 by sphingomyelinase. H89, an inhibitor of PKA, at 10 μM had no effect on Piezo1 activation by Yoda1 in HUVECs. Additionally, the potentiation by sphingomyelinase was not affected by H89 (Figure 4.15). Sphingomyelinase-induced increases in baseline Ca^{2+} were also not affected by H89. These data suggest that PKA does not affect Piezo1 activity or play a role in the potentiation of Piezo1 activation by sphingomyelinase.

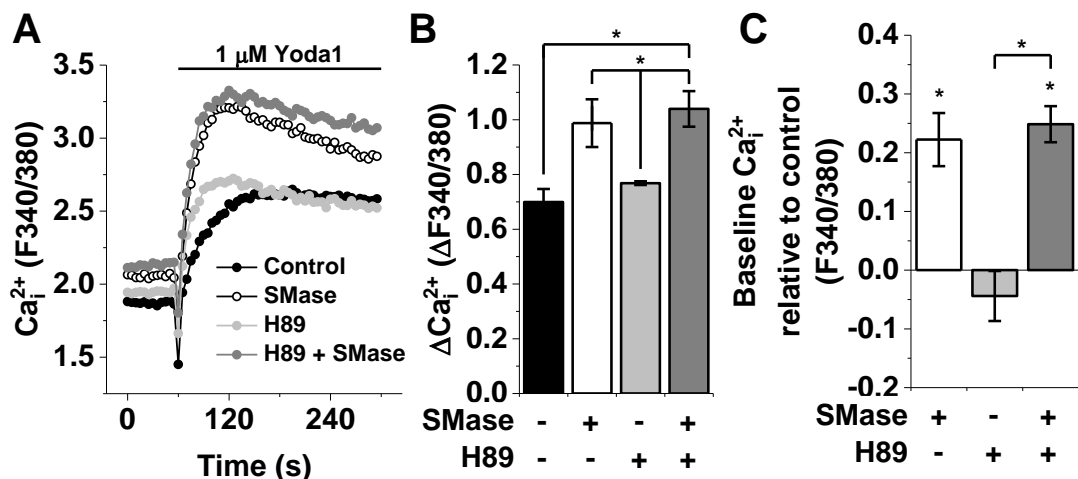


Figure 4.15: PKA does not affect sphingomyelinase potentiation of Yoda1 responses or increased baseline Ca^{2+} in HUVECs. **A**, Typical Ca^{2+} response of HUVECs to 1 μM Yoda1 when pre-treated with SMase (0.5 U/mL) and H89 (10 μM) for 30 minutes at 37°C compared to control. **B**, Average amplitude of calcium influx of conditions in **A**. * = $P < 0.05$. n/N = 4/16. **C**, Average baseline intracellular Ca^{2+} of conditions in **A**. * = $P < 0.05$. n/N = 4/16.

4.3.6.2 PKC

Sphingosine has been shown to inhibit PKC (Igarashi et al., 1989). Therefore, other PKC inhibitors were used as an attempt to mimic the potentiation of Piezo1 responses to Yoda1 by sphingomyelinase. Bisindolylmaleimide I (BIM), an inhibitor of PKC without selectivity to any isoform, was used at 10 μ M. Pre-treatment with BIM alone increased Yoda1-induced Piezo1 activation similar to pre-treatment with SMase (Figure 4.16). However, the amplitude of Yoda1 responses after combined pre-treatment with BIM and SMase was not greater than either of them alone. BIM reduced baseline Ca^{2+} relative to both control and SMase treated HUVECs. However, this may have been due to the fluorescent properties of BIM interfering with Fura2 fluorescence (Nakazono et al., 2007). These data suggest that potentiation of Piezo1 activation occurred through inhibition of PKC by sphingosine.

Due to the effects of inhibiting PKC, activation of PKC was investigated in an attempt to reverse the effect of SMase on Piezo1 activation. SC-9 at 10 μ M was used to activate PKC, which acts as a substitute for phosphatidylserine to activate PKC (Nishino et al., 1986). The amplitude of Ca^{2+} influx in response to Yoda1 was reduced by SC-9 when treated with SMase or without (Figure 4.16). Additionally, the amplitude of Yoda1 response was not different between treatment SC-9 or SC-9 with SMase. Similar to BIM, baseline Ca^{2+} levels were decreased after pre-treatment with SC-9.

These data suggest the potentiation of Yoda1 responses by sphingomyelinase is due to inhibition of PKC.

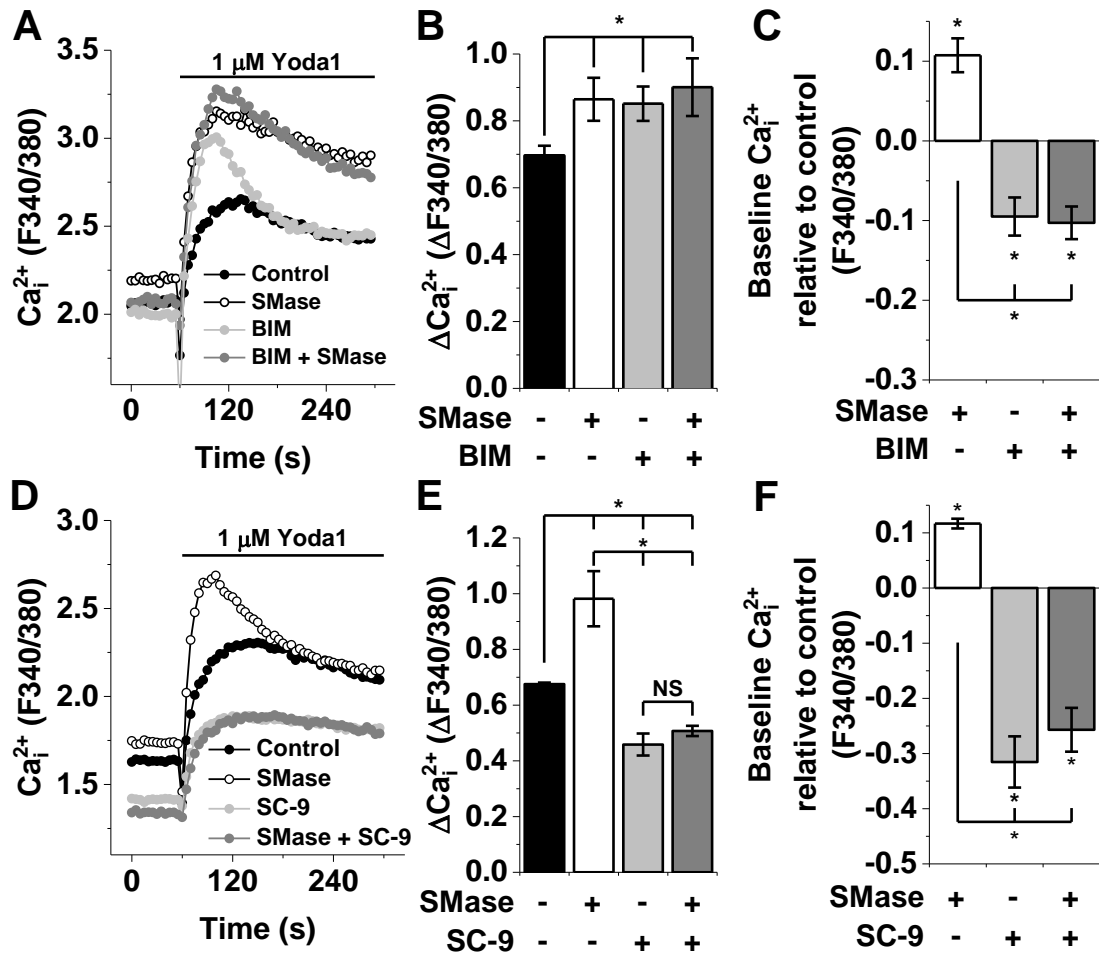


Figure 4.16: PKC inhibition potentiated Yoda1-induced Piezo1 activation similar to SMase in HUVECs. **A**, Typical Ca²⁺ response of HUVECs to 1 μM Yoda1 when pre-treated with SMase at 0.5 U/mL or Bisindolylmaleimide I (BIM) at 10 μM for 30 minutes at 37°C compared to control. **B**, Average amplitude of calcium influx of conditions in the left panel. * = P < 0.05. n/N = 4/4. **C**, Average baseline intracellular Ca²⁺ of conditions in the left panel. * = P < 0.05. n/N = 4/4. **D**, Typical Ca²⁺ response of HUVECs to 1 μM Yoda1 when pre-treated with SMase at 0.5 U/mL or SC-9 at 10 μM for 30 minutes at 37°C compared to control. **E**, Average amplitude of calcium influx of conditions in the left panel. * = P < 0.05. n/N = 4/4. **F**, Average baseline intracellular Ca²⁺ of conditions in the left panel. * = P < 0.05. n/N = 4/4.

4.3.6.3 PKD

PKC isoforms have been shown to activate PKD. Due to the effects of inhibiting PKC, the inhibition of PKD was hypothesised to have a similar result if it is involved. Therefore, the PKD inhibition was investigated to determine whether it is involved in the potentiation of Piezo1 activation by sphingomyelinase. CRT0066101, 10 μM , was used to inhibit PKD and had no effect on control Yoda1 responses. However, CRT0066101 reduced SMase-induced potentiation of Piezo1 activation (Figure 4.17). Increases in baseline Ca^{2+} were not affected by CRT0066101 in control and SMase treated HUVECs. This data suggests that PKD may be activated downstream of SMase activity, contributing the potentiation of Piezo1 activation.

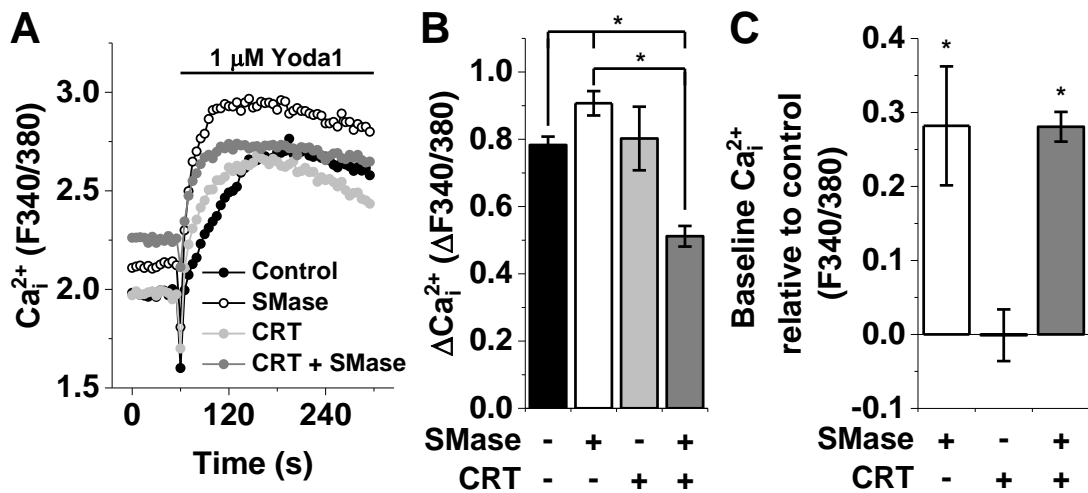


Figure 4.17: PKD reduced sphingomyelinase-induced potentiation of Piezo1 activation in HUVECs. **A**, Typical Ca^{2+} response of HUVECs to 1 μM Yoda1 when pre-treated with SMase (0.5 U/mL) and CRT0066101 (CRT) at 10 μM for 30 minutes at 37°C compared to control. **B**, Average amplitude of calcium influx of conditions in **A**. * = $P < 0.05$. $n/N = 4/4$. **C**, Average baseline intracellular Ca^{2+} of conditions in **A**. * = $P < 0.05$. $n/N = 4/4$.

4.3.6.4 Phospholipase C

Sphingosine has been shown to activate phospholipase C (PLC) $\delta 1$ (Matecki and Pawelczyk, 1997). Additionally, PLC-induced production of diacylglycerol has been shown to be important in the activation of PKC and PKD. Therefore, PLC was investigated for mechanisms of the potentiation of Yoda1 responses and increased baseline Ca^{2+} due to sphingomyelinase activity. U73122, an inhibitor of PLC (Smith et al., 1990; Bleasdale et al., 1990), at 5 μM decreased baseline Ca^{2+} after incubation with sphingomyelinase with no effect on control baseline conditions (Figure 4.18). Furthermore, U73122 increased Yoda1 response with and without SMase incubation. However, there was no difference in Yoda1 responses after U73122 pre-treatment with or without SMase. This suggests that PLC activity may be involved in the potentiation of Piezo1 activity by SMase but PLC also regulates Piezo1 itself.

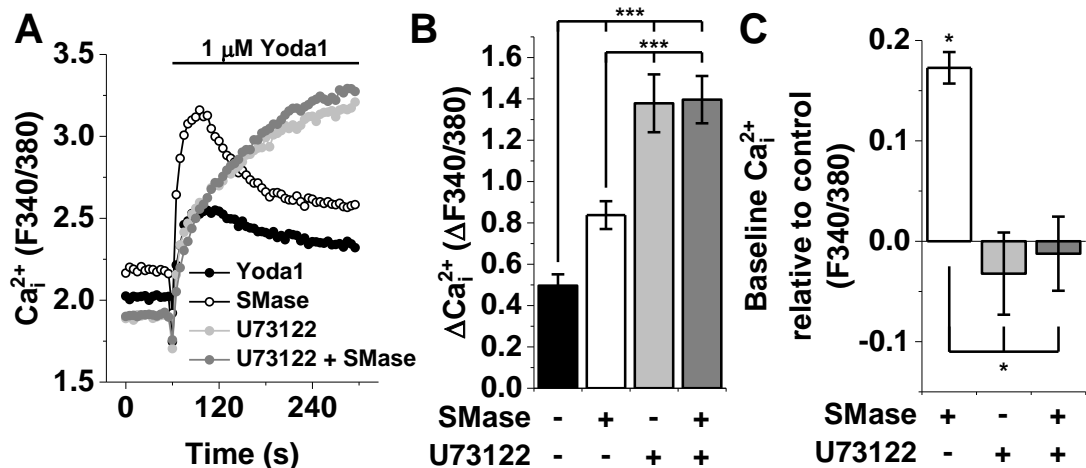


Figure 4.18: Phospholipase C inhibition reduced sphingomyelinase-induced baseline Ca^{2+} increases in HUVECs. **A**, Typical Ca_i^{2+} response of HUVECs to 1 μM Yoda1 when pre-treated with SMase at 0.5 U/mL or U73122 (5 μM) for 30 minutes at 37°C compared to control. **B**, Average amplitude of calcium influx of conditions in **A**. *** = $P < 0.01$. $n/N = 4/4$. **C**, Average baseline intracellular Ca_i^{2+} of conditions in **A**. * = $P < 0.05$. $n/N = 4/4$.

4.3.6.5 Inositol-1,4,5-triphosphate

Phospholipase C cleaves PIP₂ to form DAG and IP₃. IP₃ activates the IP₃ receptor which release Ca²⁺ from ER stores. Therefore, the IP₃R was inhibited using Xestospongin C to determine whether this contributes to the effects of sphingomyelinase on the potentiation of Piezo1 activity. Xestospongin C had no effect on the amplitude of Yoda1 responses of control or post-incubation with sphingomyelinase (Figure 4.19). However, the increased baseline Ca²⁺ caused by sphingomyelinase incubation showed a trend to be reduced by Xestospongin C. However, this was not significantly different compared sphingomyelinase pre-treatment. These data suggest that IP₃ receptors are not involved in potentiation of the Yoda1 response but may contribute to the increase in baseline Ca²⁺.

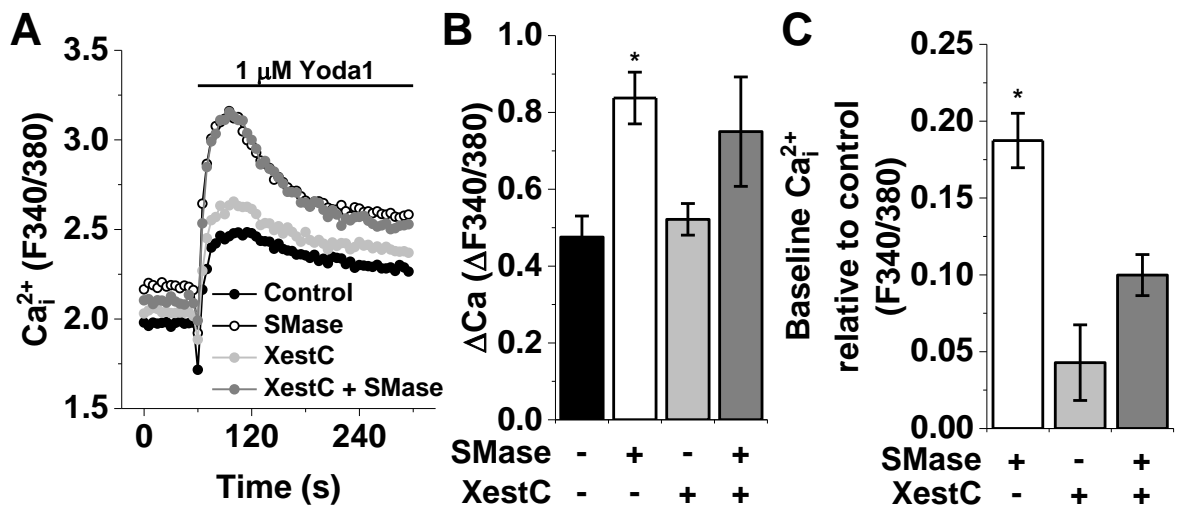


Figure 4.19: Inositol-1,4,5-triphosphate receptor inhibition reduced sphingomyelinase-induced baseline Ca²⁺ increases in HUVECs. **A**, Typical Ca²⁺ response of HUVECs to 1 μM Yoda1 when pre-treated with SMase at 0.5 U/mL or Xestospongin C (XestC) at 2 μM for 30 minutes at 37°C compared to control. **B**, Average amplitude of calcium influx of conditions in **A**. * = P < 0.05. n/N = 4/4. **C**, Average baseline intracellular Ca²⁺ of conditions in **A**. * = P < 0.05. n/N = 4/4.

4.4 Discussion

Here SMase was shown to potentiate activation of endothelial Piezo1 by Yoda1. The action of sphingomyelinase was shown to be due to downstream signalling pathways by the production of sphingosine. Inhibition of PKC, activation of PLC and activation PKD were shown to contribute to the potentiation of Piezo1 by SMase.

4.4.1 Sphingomyelinase potentiation of Piezo1 in HUVECs

Sphingomyelinase activity has been shown to alter ion channel activity and contribute to inflammatory responses in cardiovascular disease. Here exogenous bacterial SMase was shown to potentiate Piezo1 activation by Yoda1. This was contrasted by reductions of responses to Yoda1 in P1 HEK TREx cells. The difference in response may be due to difference in cellular machinery found in HEK TREx compared to HUVECs. The products of sphingomyelin digestion may not have the same targets in HEK-TREx compared to HUVECs providing different effects of SMase. Negligible native ceramidase (Hwang et al., 2005) or ceramide kinase (Sugiura et al., 2002) activity has been detected in HEK293 cells. However, ceramidase (Romiti et al., 2001) and ceramide kinase (Hankins et al., 2013) activity has been reported in endothelial cells. Endogenous activity of sphingosine kinase 1 and 2 has been reported in HEK293 cells (Hait et al., 2005) and endothelial cells (Limaye, 2008). Furthermore, endogenous expression of potential downstream targets of sphingolipid metabolites have been suggested to be expressed in HEK293 cells, such as PKA (Norum et al., 2005), PKC (Xu et al., 2003) and PKD (Franz-Wachtel et al., 2012). Reduction of Yoda1 responses after SMase treatment in P1 HEK TREx cells may be due to effects of SMase on membrane composition.

SMase has been shown to affect the plasma membrane composition and morphology of erythrocytes (Dinkla et al., 2012). Additionally, SMase has been shown to affect gating of ion channels by removing interaction with sphingomyelin (Ramu et al., 2006; Combs and Lu, 2015). Production of ceramide by SMase can result in the production of ceramide enriched platforms which have been shown to inhibit Kv1.3 channel (Bock et al., 2003). Furthermore, ceramide has been suggested to exclude cholesterol from pre-formed lipid rafts (Megha and London, 2004). The opposing response in HUVECs to SMase suggested that a downstream product of sphingomyelin digestion was responsible.

4.4.2 Sphingosine mediates potentiation of Piezo1 activation

To determine the downstream product of SMase, each molecule was tested to assess whether they could induce a response. The only downstream product to have an effect on Piezo1 activation was sphingosine. Application of exogenous sphingosine has been shown to be readily converted to ceramides in Neuro2A cells (Riboni et al., 1998). However, sphingosine accumulation was reported at higher concentration of sphingosine exposure suggesting ceramide synthase could be saturated. Downstream production of sphingosine was shown to be responsible for potentiation of Piezo1 activation by inhibition of ceramidases by ceranib-1, which has been shown to reduce intracellular sphingosine (Draper et al., 2011). However, ceranib-1 also produced an intracellular accumulation of ceramide species when incubated over 24 hours in SKOV3 ovarian cancer cell line (Draper et al., 2011). Incubation of ceramides had no effect on Yoda1 responses in HUVECs suggesting sphingosine, or a downstream product of sphingosine, was the effector for potentiation of Piezo1 activation. Sphingosine phosphorylation produces S-1-P which has been shown to modulate ion channel

activity via its G-protein coupled receptor family. However, there was no effect on Piezo1 after pre-treatment with S-1-P. For further validation, a sphingosine kinase inhibitor, such as MP-A08 which has been shown to reduce S-1-P while increasing sphingosine in cells (Pitman et al., 2016), could have been used in conjunction with SMase treatment. This suggested that sphingosine mediated the potentiation of Piezo1 activation by SMase in HUVECs. Sphingosine has been shown to affect ion channels, inhibiting TRPM7 (Qin et al., 2013) and Ca²⁺ release-activate Ca²⁺ channels (Mathes et al., 1998), and activating TRPM3 channels (Grimm et al., 2005). Due to the opposing effects of SMase on HUVECs and P1 HEK TREx it was unlikely that sphingosine is acting directly on the Piezo1 channel. Therefore, signalling molecules known to interact with sphingosine were investigated as mechanisms of potentiating Piezo1 activation in HUVECs.

4.4.3 Mechanism of potentiation in HUVECs downstream of sphingosine

4.4.3.1 PKA

PKA has been shown to be activated directly by sphingosine (Ma et al., 2005). PKA has been shown to modulate ion channel activity of glutamate receptors, L-type Ca²⁺ channels and Ca²⁺-activated K⁺ channels (Gray et al., 1998). Here inhibition of PKA by H89 did not have an effect on Piezo1 activation by Yoda1 or the potentiation of Piezo1 by SMase. This suggests that another mechanism was required for SMase potentiation of Piezo1 activation.

4.4.3.2 PKC

Here inhibition of PKC was shown to have a similar effect on the potentiation of Piezo1 by sphingomyelinase. However, inhibiting and activating PKC reduced baseline intracellular Ca²⁺ which may have been due to fluorescent artefacts

caused by the PKC modulators used. Therefore, the involvement on PKC on the increase in baseline Ca^{2+} was inconclusive. PKC has widely been reported to be inhibited by sphingosine (Bazzi and Nelsestuen, 1987). Modulation of Piezo1 by PKC has not been reported before. However, PKC has been suggested to modulate Piezo2, a mechanosensitive ion channel of the same family as Piezo1 (Dubin et al., 2012). Reports of PKC modulation of Piezo2 are contradictory. Initially activation of PKA and PKC was shown to potentiate Piezo2 activation (Dubin et al., 2012). However, the potentiation of Piezo2 by PKA and PKC activators was not found by Eijkelkamp *et al.* (2013), exchange protein directly activated by cAMP 1 (Epac1) was reported to potentiate Piezo2 instead.

The mechanism of PKC regulation of Piezo1 remains elusive. However, PKC has been shown to alter the activity of other ion channels. PKC may interact with Piezo1 directly and phosphorylate the channel to regulate its gating. Phosphorylation of TRPV1 by PKC has been shown to be responsible for the sensitisation of the channel to heat and chemical activation after exposure to ATP (Numazaki et al., 2002). Many Piezo1 phosphorylation sites have been suggested, with 33 reported on PhosphositePlus for human Piezo1 (<https://www.phosphosite.org/uniprotAccAction?id=Q92508>) (Hornbeck et al., 2015). However, the function of the phosphorylation is currently unknown with regards to gating of Piezo1. To determine whether PKC interacts directly with FRET, fluorescently tagged Piezo1 and PKC could be utilised to suggest direct interaction. Co-immunoprecipitation could also be utilised. However, due to lack of reliable primary antibodies for endogenous probing of Piezo1, it would only be achieved by editing a tag into the protein similar to the experiments carried out determining association of Piezo1 with SERCA2 (Zhang et al., 2017). Direct

interaction may occur with a constitutively active membrane-bound isoform of PKC which suppresses Piezo1 activation.

4.4.3.3 Phospholipase C

Inhibition of phospholipase C also showed modulation of Piezo1 activity. Additionally, U73122 abolished increases in intracellular Ca^{2+} and potentiation of Piezo1 after SMase incubation. This suggests that phospholipase C might have been activated by sphingosine downstream of SMase action. Phospholipase C has been shown to be activated by sphingosine (Matecki and Pawelczyk, 1997). Phospholipase C digests PIP_2 to form DAG and IP_3 . Regulation of Piezo1 by phosphoinositides has been reported. Ca^{2+} influx after activation of TRPV1 in DRG neurons was shown to deplete $\text{PI}(4,5)\text{P}_2$ resulting in inhibition of Piezo1-dependent mechanically-activated currents and that Piezo1 requires $\text{PI}(4,5)\text{P}_2$ for activity (Borbiro et al., 2015). Conversely, potential depletion of $\text{PI}(4,5)\text{P}_2$ after SMase treatment resulted in potentiation of Piezo1 activation. To confirm an effect of SMase on $\text{PI}(4,5)\text{P}_2$ levels in the plasma membrane, phosphoinositide measurements may be used. Phospholipase C may modulate Piezo1 activity via downstream mechanisms.

A possible mechanism downstream of PLC activation is activation of PKD. Inhibiting PKD with CRT0066101 resulted in the loss of SMase-induced potentiation of Piezo1 activation. PKD can be activated by DAG and PKC (Wang, 2006). Due to the effects of PKC inhibition it is likely that PKD was activated by DAG. PKD has been linked to regulation of ion channels via phosphorylation, such as with Polycystin-2 (Streets et al., 2010). Determination of direct interaction between PKD and Piezo1 would require further investigation, such as FRET and co-immunoprecipitation. Another mechanism of Piezo1 modulation by

PKD may be through modification of the cytoskeleton via F-actin reorganisation (Eiseler et al., 2009). Modification of the cytoskeleton has been reported to affect the mechanical activation of Piezo1 by changing membrane properties (Nourse and Pathak, 2017).

Production of DAG downstream of PLC activation may not be the only source of DAG. Activation of phospholipase D has also been shown to result in an increase in DAG production which may play a role in downstream signalling of SMase and potentiating Piezo1 activation. Furthermore, phospholipase D activation by sphingosine has been observed in endothelial cells (Natarajan et al., 1994). Additionally, activation of phospholipase D and production of DAG is responsible for TRPC ion channel activation in rat ear artery myocytes (Albert et al., 2005). To investigate whether PLD is involved in potentiation of Piezo1 by SMase a pharmacological blocker such as fluoro-2-indolyl des-chlorohalopemide may be used.

4.4.4 Cardiovascular function

Sphingomyelinase activity and sphingolipid metabolites have been shown to occur in physiological responses by endothelial cells. Sphingomyelinase and subsequent production of sphingosine has been suggested to play a role in vasomotor responses in porcine coronary artery (Murohara et al., 1996). Endothelial Piezo1 has recently been shown to be involved in vasomotor responses with different effects dependent on the vascular bed. These effects may be due to modulation of Piezo1 by sphingomyelinases expressed in these vascular beds affecting Piezo1 activation. Shear stress has been suggested to activate native neutral sphingomyelinase in endothelial cells which may sensitise

Piezo1 to shear stress activation (Czarny et al., 2003). However, the effects of SMase on activation of Piezo1 by shear stress would have to be investigated.

4.4.5 Potential role in cardiovascular disease

Activators of sphingomyelinase have been implicated in atherosclerotic development and progression (Pavoine and Pecker, 2009). The activation of sphingomyelinases may contribute to modulation of Piezo1 activity and endothelial cell responses resulting in atherosclerotic plaque formation. Apoptosis of endothelial cells has been described as an important mechanism in inflammatory disease, such as atherosclerosis (Winn and Harlan, 2005). Furthermore, activation of acid and neutral sphingomyelinases have been shown to induce endothelial cell apoptosis (Niaudet et al., 2017; Yang et al., 2004). Potentiation of Piezo1 activation by sphingomyelinase may contribute to apoptosis and cell death by influx of Ca^{2+} . However, this would need to be investigated.

4.5 Summary

Sphingomyelinases have been associated with transduced signals in the physiology and pathophysiology of the cardiovascular system. Here sphingomyelinase activity was shown to potentiate activation of endothelial Piezo1 by Yoda1. Potentiation occurred due to sphingosine production with inhibition of PKC and activation of PKD suggested to increase Piezo1 activity. Yoda1 was used as a substitute for shear stress. Modulation of Piezo1 may contribute to the effects of sphingomyelinases on cardiovascular physiology and pathophysiology. However, further investigation into the effects of sphingomyelinase on Piezo1-mediated endothelial cell functions are required.

Chapter 5

Novel small-molecule modulators of Piezo1 channels

5.1 Introduction

5.1.1 Piezo1 pharmacology

The pharmacology of Piezo1 is limited. Known inhibitors of Piezo1 are generic non-selective cation channels inhibitors, Gd^{3+} and Ruthenium Red, which block the pore of the ion channels (Coste et al., 2010). Additionally, the toxin from *Grammostola Spatulata*, GsMTx4, has been found to inhibit Piezo1 (Bae et al., 2011). The mechanism of action for GsMTx4 is thought to be due to manipulation of the membrane surrounding the ion channel (Suchyna et al., 2004). Consequently GsMTx4 is not specific for Piezo1 and inhibits other mechanically activated ion channels.

Yoda1 is the only known chemical activator of Piezo1 (Syeda et al., 2015). Yoda1 was discovered by the Patapoutian group at the Scripps Institute in 2015 as a result of a screening campaign with approximately 3.25 million compounds tested. Yoda1 was shown to be specific for Piezo1 over Piezo2 and did not produce a response in HEK cells that had Piezo1 expression abolished using CRISPR technology. Yoda1 activated purified Piezo1 protein reconstituted in an artificial bilayer. Therefore, Yoda1-evoked Piezo1 activation was membrane delimited. Activation in fluorescence assays was reduced in when Ca^{2+} chelator EGTA was present in the extracellular solution however, there was no effect on the response when cells were pre-treated with thapsigargin to deplete ER Ca^{2+}

stores. This suggested that Yoda1-induced Ca^{2+} influx into Piezo1 transfected cells was due to Piezo1 activation at the plasma membrane of the cells. Additionally, mechanical activation of Piezo1 was potentiated by Yoda1 pre-treatment, suggesting that Yoda1 may modulate mechanical gating of Piezo1. The EC_{50} of Yoda1 was reported at 26.6 μM for human Piezo1 and 17.1 μM for mouse Piezo1. However, precipitation of Yoda1 was reported in aqueous solution at concentrations above 20 μM , suggesting poor solubility of Yoda1. Syeda et al. (2015) suggested that the dichloro-phenyl ring and thioether linker of Yoda1 was essential for Piezo1.

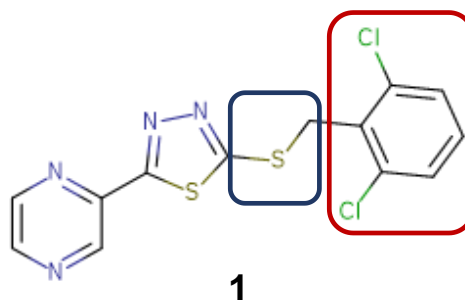


Figure 5.1: The structure of Yoda1. The functional groups suggested by Syeda et al. (2015) are highlighted in red (dichlorophenyl) and blue (thioether).

5.1.2 Aims

Yoda1 is the first known chemical modulator of Piezo1. Therefore, Yoda1 was used as the basis for development of new chemical modulators of Piezo1. Small modifications were created to reveal structure-activity relationship of Yoda1. Modifications were focussed to the three ring structures of Yoda1: dichlorophenyl ring, the central thiodiazole linker and ring, and the pyrazine ring. Hit compounds were characterised and tested as modulators of endothelial cell alignment. The solubility and stability of hit compounds was also investigated to determine any improvement compared to Yoda1.

5.2 Results

Analogues of Yoda1 were tested for Piezo1 activation in a tetracycline-inducible Piezo1 HEK-TREx cell line. Analogues were tested for activation of Piezo1 by measuring Ca^{2+} flux in response to an acute 10 μM addition of the analogue in comparison to 10 μM Yoda1. The percentage activation of the analogues was calculated as the peak elevation in Ca^{2+} compared to that of Yoda1. The Yoda1 analogues were also tested as inhibitors of Yoda1-induced Piezo1 activation by pre-treatment with 10 μM of the analogue for 30 minutes followed by an acute addition of 2 μM Yoda1 to activate Piezo1.

5.2.1 Structure-activity relationships of Yoda1 analogues

The discovery of Yoda1 suggested that there were two main chemical groups that were crucial for Piezo1 activation in the compound, the chlorine atoms in the dichlorophenyl ring and the sulphur in the thioether linker. Modifications were made to these chemical groups in Yoda1 and also the thiadiazole central ring structure and the pyrazine ring.

5.2.1.1 Phenyl modifications to Yoda1

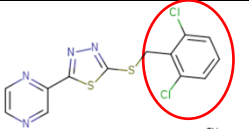
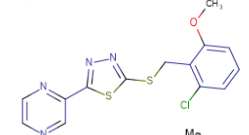
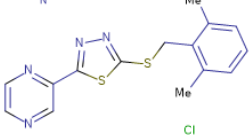
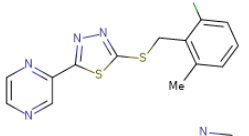
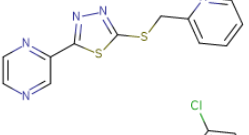
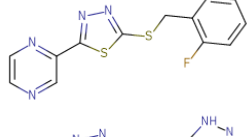
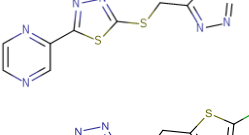
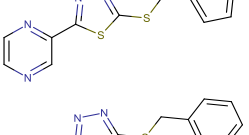
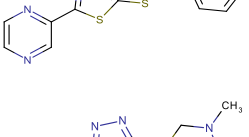
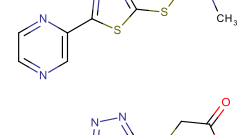
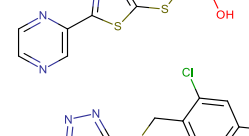
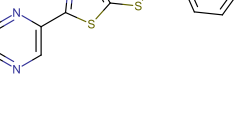
To investigate the importance of the dichlorophenyl group further modifications were made to the ring by substituting the chlorine atoms with different chemical groups and moving the chlorine atoms to different positions in the ring.

To determine whether it is the chlorines themselves that are important for activating with Piezo1 they were substituted with methyl or methoxy groups (**2c**, **2a**). The 2-chloro-6-methyl pattern (**2c**) showed similar activation to Yoda1 at 92% of the control Yoda1 while inhibiting Yoda1 to 20.5% of control (Figure 5.2). The 2-chloro-6-methoxy analogue (**2a**) gave a similar agonist response to **2c**

(89%) and maintained a similar level of inhibition of Yoda1 responses Yoda1 (22%). Substituting both chlorine atoms with methyl groups (**2b**) also produced similar levels of activation (80%) and inhibition (21%) (Figure 5.2). The 2-chloro-6-fluoro analogue had reduced activation compared to Yoda1 (**2e**) (28%). The 2-4-chloro analogue gave the smallest activation response (**2k**) (7%) and a reduction of Yoda1 activity to 57%. These data suggest that modifications to the chlorines of the dichlorophenyl ring can be tolerated to produce activation of Piezo1 channels.

Replacing the dichlorophenyl group with other changes to the phenyl ring were not tolerated (**2d-2j**). No precipitation of these analogues was observed. Replacement of the dichlorophenyl with a pyridine ring (**2d**), phenyl ring (**2h**), dimethylamine (**2i**) or carboxylic acid (**2j**) gave poor responses in the activation assay (26%, 12%, 10%, 4% respectively). Replacing the phenyl ring with a tetrazole (**2f**) produced low activation (12%) and the 5-chloro-thiophen-2-yl group (**2g**) was completely inactive (2%). Replacing the phenyl ring with a tetrazole (**2f**) resulted in low activation (12%) and the 5-chloro-thiophen-2-yl group (**2g**) was completely inactive (2%). Both compounds were intended to exploit any cation interactions, either through a salt bridge (**2f**) or a cation-pi interaction (**2g**).

Table 5.1: Structures of dichlorophenyl ring modifications to Yoda1 and summary of results. The percentage activation of 10 μM of analogues is compared to 10 μM Yoda1. The relative activation of Yoda1 is the response of 2 μM Yoda1 after pre-treatment with 10 μM of analogues compared to DMSO pre-treatment

Drug	Structure	Activation (%)	Relative Yoda1 activation (%)
Yoda1 (1)		100	100 (DMSO)
2a		89.5 \pm 21.5	22.3 \pm 6.8
2b		80.1 \pm 13.3	21.4 \pm 10.3
2c		92.9 \pm 13.7	20.5 \pm 7.5
2d		16.4 \pm 2.7	111.2 \pm 15.0
2e		27.8 \pm 8.8	49.9 \pm 8.3
2f		11.6 \pm 3.0	136 \pm 13.7
2g		2.4 \pm 0.4	71.1 \pm 10.8
2h		12.7 \pm 1.2	88.4 \pm 9.3
2i		10.2 \pm 0.5	129 \pm 23.4
2j		4.2 \pm 2.6	109.1 \pm 16.3
2k		7.6 \pm 3.6	57.5 \pm 0.2

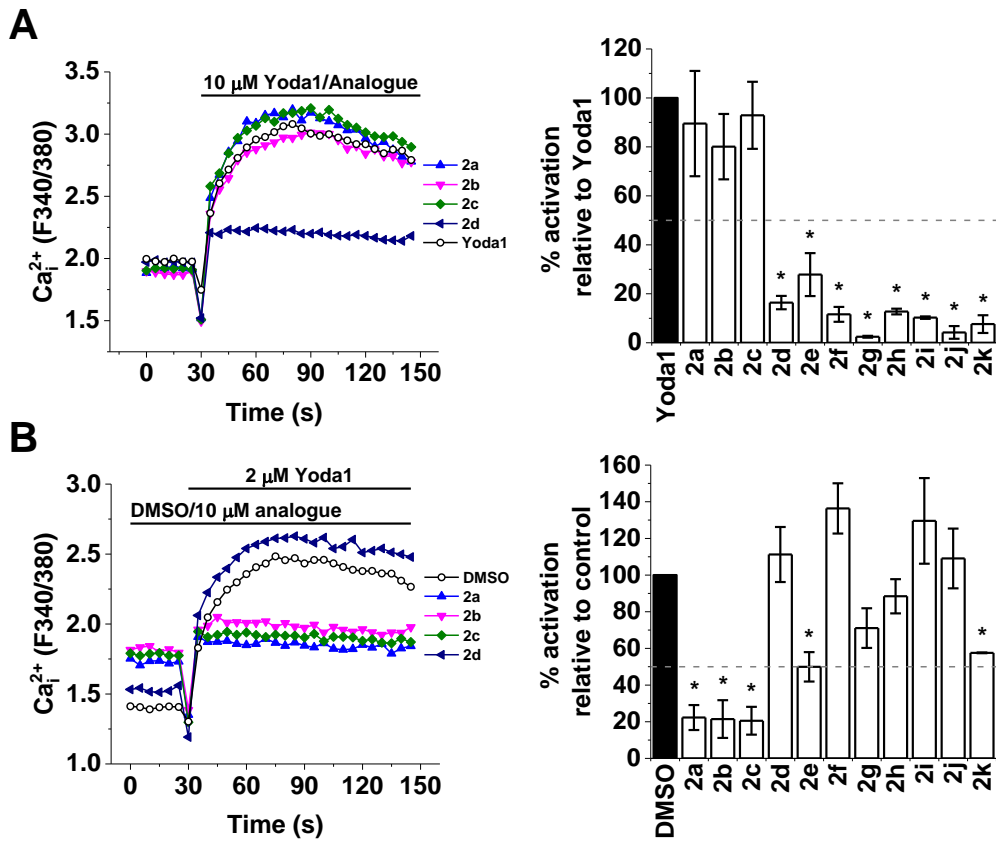


Figure 5.2: Methoxy and methyl substitutions of chlorines can be tolerated.

A, left panel, a typical response of the analogues tested for acute activation of Piezo1 at 10 μM . Tetracycline-positive Piezo1 HEK TREx were used. Right panel, average data from experiment in left panel. $n/N = 3/3$. * = $P < 0.05$ compared to Yoda1. **B**, left panel, a typical response of the analogues tested for inhibition of Yoda1-induced Piezo1 activation. Pre-treatment of 10 μM analogues at RT for 30 mins prior to reading. Tetracycline-positive Piezo1 HEK TREx were used. Right panel, average data from experiments in left panel. $n/N = 3/3$. * = $P < 0.05$ compared to DMSO.

5.2.1.2 Pyrazine modifications to Yoda1

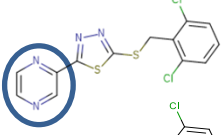
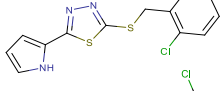
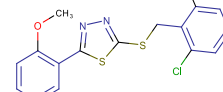
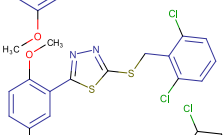
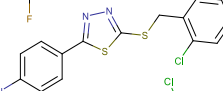
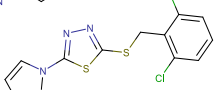
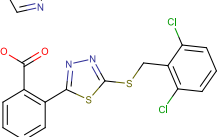
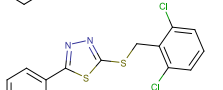
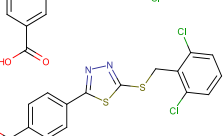
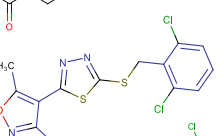
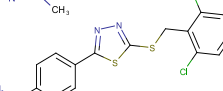
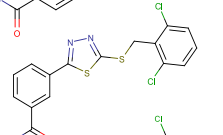
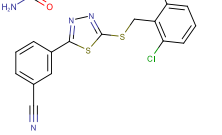
Modifications to the pyrazine group of Yoda1 were not reported in the original publication of Yoda1 (Syeda et al., 2015). Substituting H-bond acceptors of the pyrazine ring with donors (**3a**, **3d**) reduced activation. The pyrrole (**3a**) demonstrated low activation of Piezo1 (19%) and inhibition of Yoda1 to 51% of control. The 4-aminophenyl analogue (**3d**) showed modest activation (41%) but strong antagonist activity (12% response compared to control). The phenyl-3-carboxamide and phenyl-4-carboxamide (**3j** and **3k**) showed reduced activation (37% and 19%, respectively) but modest antagonist activity (39% and 51% respectively). These data suggest that the nitrogens of the pyrazine ring of Yoda1 accepting hydrogen are important for functional modulation as hydrogen bond donating amines abolish activation.

The 2,5-dimethoxyphenyl ring (**3b**) and the 2-methoxy-5-fluorophenyl (**3c**) were both inactive (7% and 10%, respectively). However, **3b** was found to reduce activation by Yoda1 to 57%. **3e** had reduced activation compared to Yoda1 (45%) and displayed almost no inhibition of Yoda1 with 85% of response compared to control. **3i** had activation almost abolished (5%) and displayed little inhibition of Yoda1 with 73% of response compared to control. **3l** had reduced activation compared to Yoda1 (17%) but had a slow linear activation. Furthermore, **3l** inhibited of Yoda1 with 23% of response compared to control suggesting some interaction with Piezo1.

Replacing the pyrazine ring with either a 2-benzoic acid (**3f**), 3-benzoic acid (**3g**) or 4-benzoic acid (**3h**) produced opposing effects. **3f** and **3g** had reduced activation compared to Yoda1 (15% and 17% respectively), with only **3g** reducing Yoda1 activity to 11% compared to Yoda1 retaining 96% activity after

pre-treatment with **3f**. However, **3h** produced Ca^{2+} responses similar to Yoda1 (104%) (Figure 5.3). Furthermore, Yoda1 activation was reduced to 16% compared to control by **3h**. This suggests that benzoic acid modifications may interact with Piezo1 with different effects depending on the position of the carboxylic acid group due drastic differences between 2-, 3- or 4- benzoic acid substitutions.

Table 5.2: Structures of pyrazine ring modifications to Yoda1 and summary of results. The percentage activation of 10 μ M of analogues is compared to 10 μ M Yoda1. The relative activation of Yoda1 is the response of 2 μ M Yoda1 after pre-treatment with 10 μ M of analogues compared to DMSO pre-treatment

Drug	Structure	Activation (%)	Relative Yoda1 activation (%)
Yoda1 (1)		100	100 (DMSO)
3a		2.5 \pm 0.5	60.0 \pm 22.1
3b		7.2 \pm 5.7	57.0 \pm 4.8
3c		10.4 \pm 1.3	82.1 \pm 2.2
3d		40.9 \pm 3.1	11.9 \pm 1.8
3e		45.0 \pm 10.3	85.1 \pm 0.8
3f		15.9 \pm 15.0	96.6 \pm 5.8
3g		17.5 \pm 10.3	11.7 \pm 1.6
3h		104.6 \pm 4.8	16.4 \pm 2.6
3i		5.3 \pm 0.1	75.3 \pm 11.0
3j		19.0 \pm 18.0	51.0 \pm 6.5
3k		37.0 \pm 11.4	39.4 \pm 28.0
3l		17.9 \pm 0.1	23.3 \pm 2.7

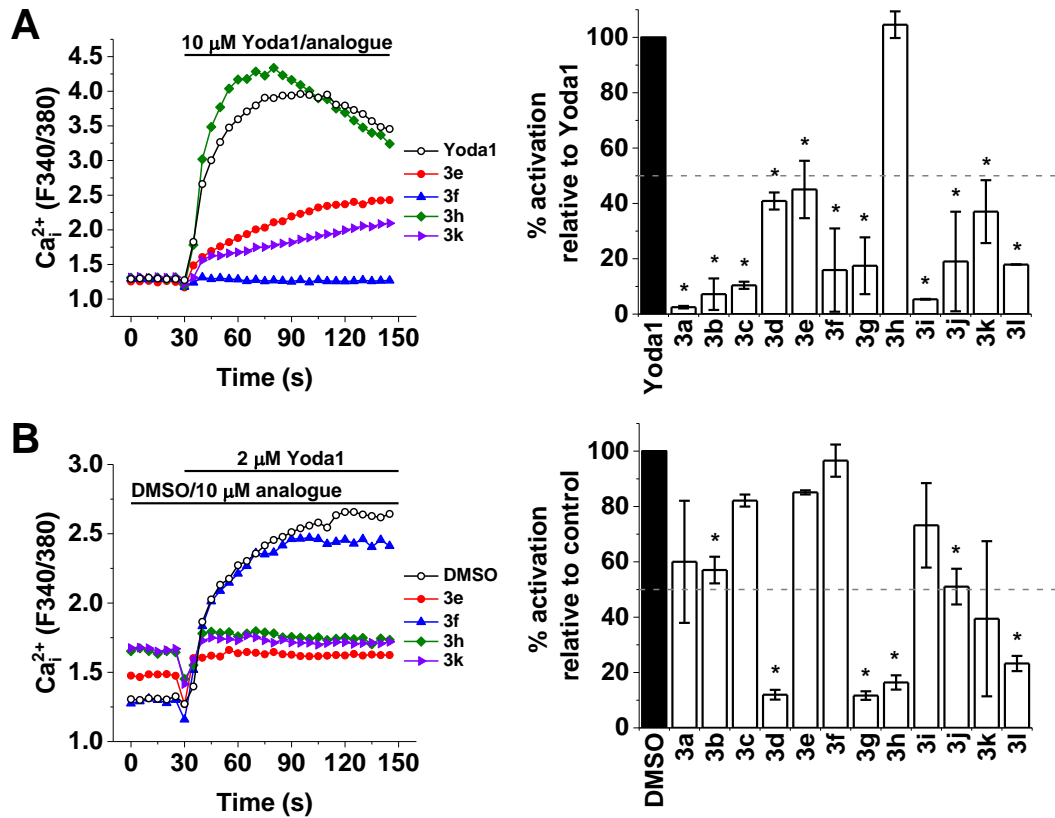


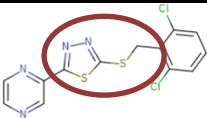
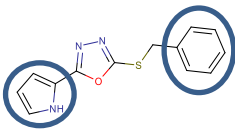
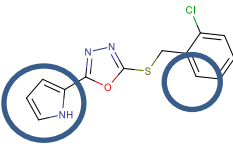
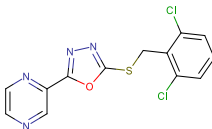
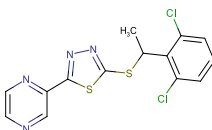
Figure 5.3: Pyrazine ring modifications produced a highly active Yoda1 analogue. **A**, left panel, a typical response of the analogues tested for acute activation of Piezo1 at 10 μM . Tetracycline-positive Piezo1 HEK TREx were used. Right panel, average data from experiment in left panel. $n/N = 3/3$. * = $P < 0.05$ compared to Yoda1. **B**, left panel, a typical response of the analogues tested for inhibition of Yoda1-induced Piezo1 activation. Pre-treatment of 10 μM analogues at RT for 30 mins prior to reading. Tetracycline-positive Piezo1 HEK TREx were used. Right panel, average data from experiments in left panel. $n/N = 3/3$. * = $P < 0.05$ compared to DMSO.

5.2.1.3 Modification of central ring and linker

SAR around the central thiadiazole ring and thioether linker of Yoda1 was investigated. Adding a methyl group in the benzylic position of the linker (**4d**) produced an inactive compound which nevertheless showed inhibition of Yoda1 (65%), implying some binding.

Isosteric replacement of the thiadiazole to a oxadiazole (**4c**) produced an analogue with comparable efficacy to Yoda1 (104%) (Figure 5.4). However, there was large variation in responses possibly due to poor stability or solubility of the compound. Activity was lost when the dichlorophenyl ring was substituted with either a phenyl (**4a**) or 2-chlorophenyl (**4b**) and the pyrazine was substituted for a pyrrole alongside the addition of the oxadiazole (3% and 1%, respectively). Additionally, **4a** and **4b** displayed increased responses of Yoda1 after pre-treatment (134% and 150%, respectively) (Figure 5.4). However, these responses were very variable and not statistically significant. The cause of this effect is unknown but is unlikely to be due to fluorescent or off-target effects due to the lack of response upon acute addition.

Table 5.3: Structures of thiadiazole linker modifications to Yoda1 and summary of results. The percentage activation of 10 μM of analogues is compared to 10 μM Yoda1. The relative activation of Yoda1 is the response of 2 μM Yoda1 after pre-treatment with 10 μM of analogues compared to DMSO pre-treatment. Additional modifications are also highlighted.

Drug	Structure	Activation (%)	Relative activation of Yoda1 (%)
Yoda1 (1)		100	100 (DMSO)
4a		3.5 \pm 0.6	134.5 \pm 29.2
4b		1.4 \pm 0.3	150.1 \pm 60.6
4c		107.1 \pm 24.6	51.9 \pm 14.6
4d		4.2 \pm 1.2	64.9 \pm 5.1

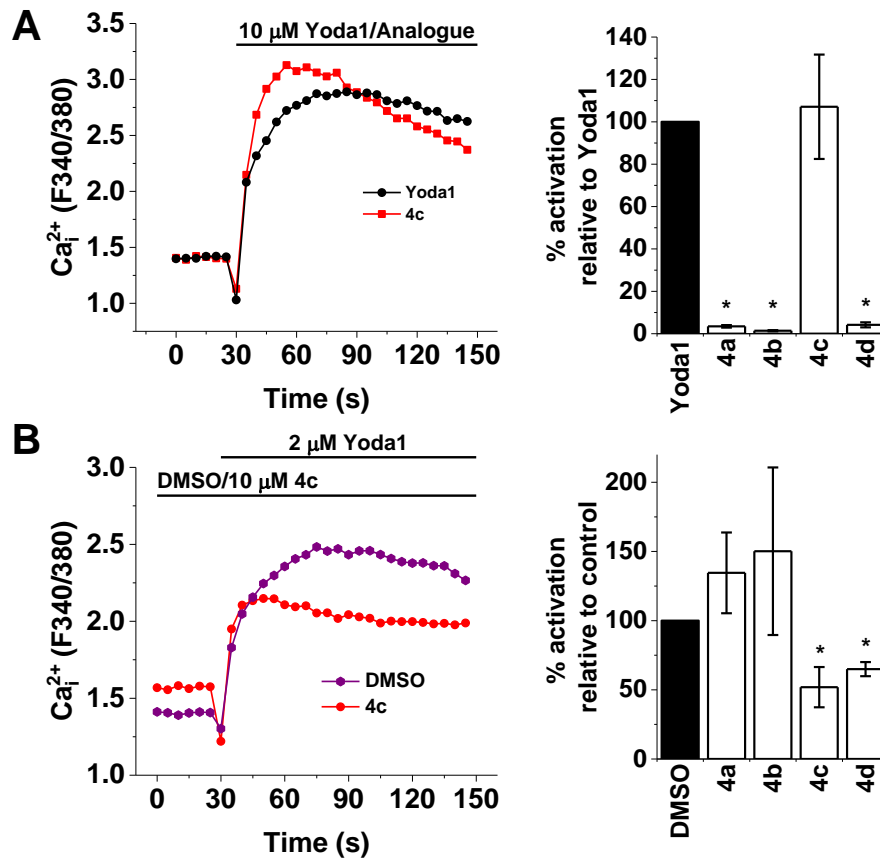


Figure 5.4: Modifying the central ring and linker often abolished activity. A, left panel, a typical response of the analogues tested for acute activation of Piezo1 at 10 μ M. Tetracycline-positive Piezo1 HEK TREx were used. Right panel, average data from experiment in left panel. n/N = 3/3. * = P < 0.05 compared to Yoda1. **B,** left panel, a typical response of the analogues tested for inhibition of Yoda1-induced Piezo1 activation. Pre-treatment of 10 μ M analogues at RT for 30 mins prior to reading. Tetracycline-positive Piezo1 HEK TREx were used. Right panel, average data from experiments in left panel. n/N = 3/3. * = P < 0.05 compared to DMSO.

5.2.2 Characterisation of hit compounds

The above screening of Yoda1 analogues revealed five compounds that also seemed to activate Piezo1. Three of these compounds had changes to the phenyl ring of Yoda1 (**2a**, **2b** and **2c**) where the chlorines were replaced by methyl groups. One compound had modifications to the central of Yoda1, **4c**, and the final compound had a modification to the pyrazine ring of Yoda1, **3h**. To determine the difference between these compounds and Yoda1 the potency of these compounds was determined in Piezo1 HEK-TREx cells. Additionally, the hit compounds were tested for selectivity upon the activation of other Ca²⁺ permeable ion channels. Furthermore, these compounds were tested to determine whether they can modulate the shear stress response of HUVECs.

5.2.2.1 Potency of hit compounds compared to Yoda1

Yoda1 displayed an EC₅₀ of 25.54 µM in Piezo1 HEK TREx cells (Figure 5.5A), however there was no saturation of response at high concentrations therefore the EC₅₀ was not accurate. The compounds with phenyl ring modifications all had reduced EC₅₀s in both Piezo1 HEK TREx (i.e. better apparent potency relative to Yoda1). The importance of the dichlorophenyl structure for efficacy was highlighted by Syeda et al. (2015). However, it is not essential for Piezo1 activation as replacing the chlorines with methyl or methoxy groups also resulted in activation of Piezo1. **2a**, **2b** and **2c** all had lower EC₅₀s compared to Yoda1 in Piezo1 HEK TREx at 8.87, 11.35 and 7.73 µM respectively (Figure 5.5B-D).

Modifying the central ring structure of Yoda1 reduced the potency in Piezo1 HEK-TREx cells. The EC₅₀ of **4c** was 37.78 µM in Piezo1 HEK TREx (Figure 5.5F).

Replacing the pyrazine ring with a 4-benzoic acid group in **3h** potentially increased the potency of compound compared to Yoda1. The EC₅₀ of **3h** was 5.65 μ M in Piezo1 HEK-TREx (Figure 5.5E). However, higher concentrations would need to be tested to create a full dose-response curve.

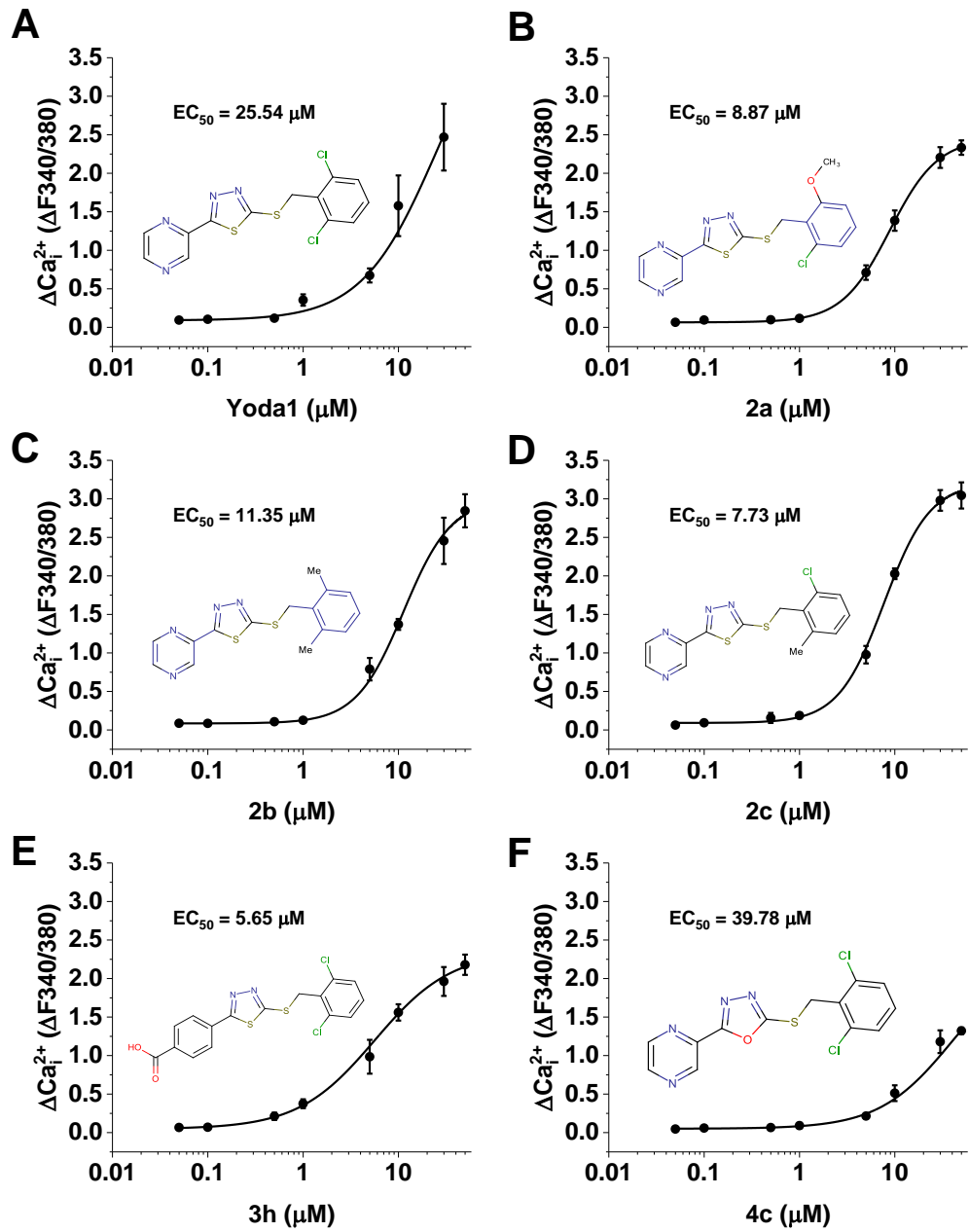


Figure 5.5: Modifications to dichlorophenyl ring and pyrazine ring produced more potent analogues of Yoda1. A-F, dose-response curve of Yoda1 (A), 2a (B), 2b (C), 2c (D), 3h (E), 4c (F), from 50 μM to 0.05 μM , except for Yoda1 where concentration ranged from 30 μM to 0.05 μM . n/N = 3/4. Tetracycline-positive Piezo1 HEK TREx were used throughout.

5.2.2.2 Selectivity of hit compounds

The hit compounds produced large responses in tetracycline treated Piezo1 HEK-TREx cells and HUVECs. However, these compounds may still activate other ion channels and Ca²⁺ entry mechanisms. The hit compounds were tested in other expression systems of Ca²⁺ permeable ion channels and in HUVECs treated with Piezo1 siRNA to reduce Piezo1 expression.

5.2.2.2.1 Responses in HEK-TREx cells

The hit compounds were tested at 10 µM in HEK-TREx that did not contain the human Piezo1 plasmid used to create the tetracycline-inducible Piezo1 expressing cell line. Yoda1 produced very small increases in intracellular Ca²⁺ concentration upon acute treatment with the cells. The response was negligible compared to the Piezo1 overexpression system. Furthermore, **2a**, **2b**, **2c**, **3h** and **4c** also did not produce a response in HEK-TREx cells compared to the Piezo1 overexpression system (Figure 5.6). This suggests that the hit compounds are activating Piezo1 in the Piezo1 HEK-TREx cell line and not natively expressed channels.

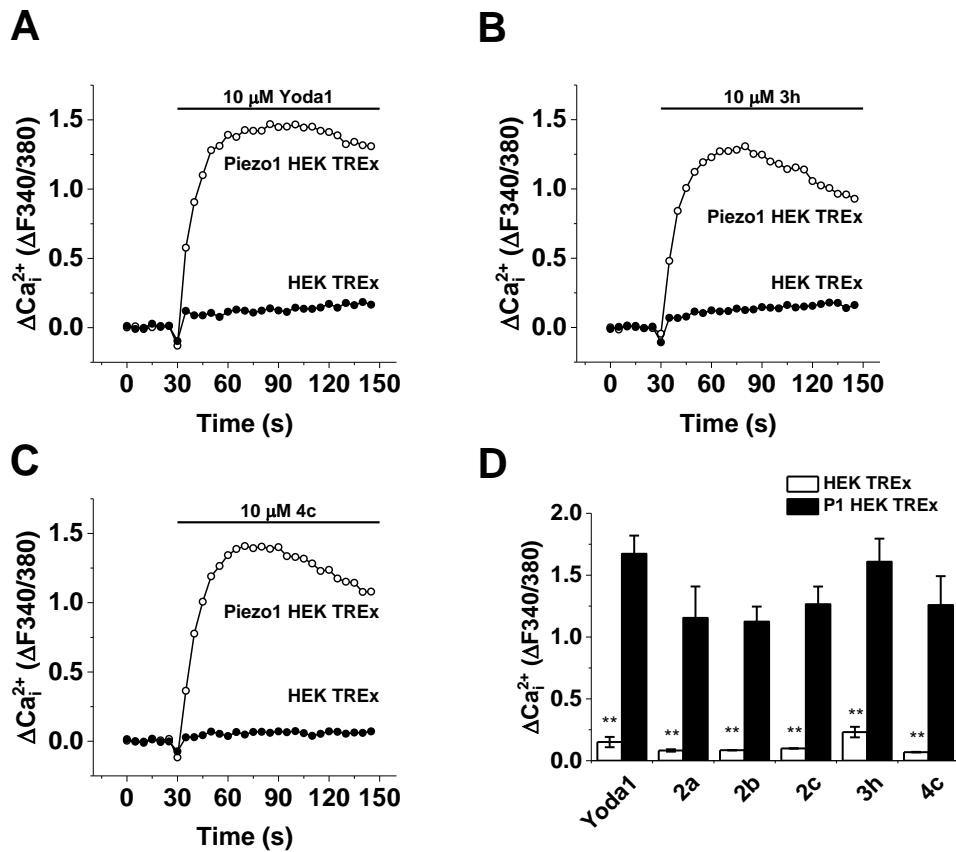


Figure 5.6: Yoda1 and its analogues do not activate HEK TREx cells. A-C, example responses of HEK TREx Tet⁺ and Piezo1 HEK TREx Tet⁺ in response to Yoda1 (A), 3h (B) and 4c (C). **D,** Average data for amplitude of response from hit compounds in HEK TREx Tet⁺ and Piezo1 HEK TREx Tet⁺. n/N = 3/3. * = P < 0.05.

5.2.2.2.2 TRPC4/5 channels

To determine if the hit compounds had any effect on TRPC4 and TRPC5 channels tetracycline-inducible HEK TREx cells were used for the respective channels. Englerin A (-(-)EA) is a nanomolar potency activator of TRPC4 and TRPC5 channels (Akbulut et al., 2015). Compared to 100 nM (-)EA Yoda1 analogues had negligible effect on TRPC4 or TRPC5 overexpressing cells (Figure 5.7). The responses of Yoda1 analogues in TRPC4 and TRPC5 HEK TREx were comparable to response in HEK TREx cells. These data suggest that Yoda1 and its analogues do not activate TRPC4 or TRPC5 channels.

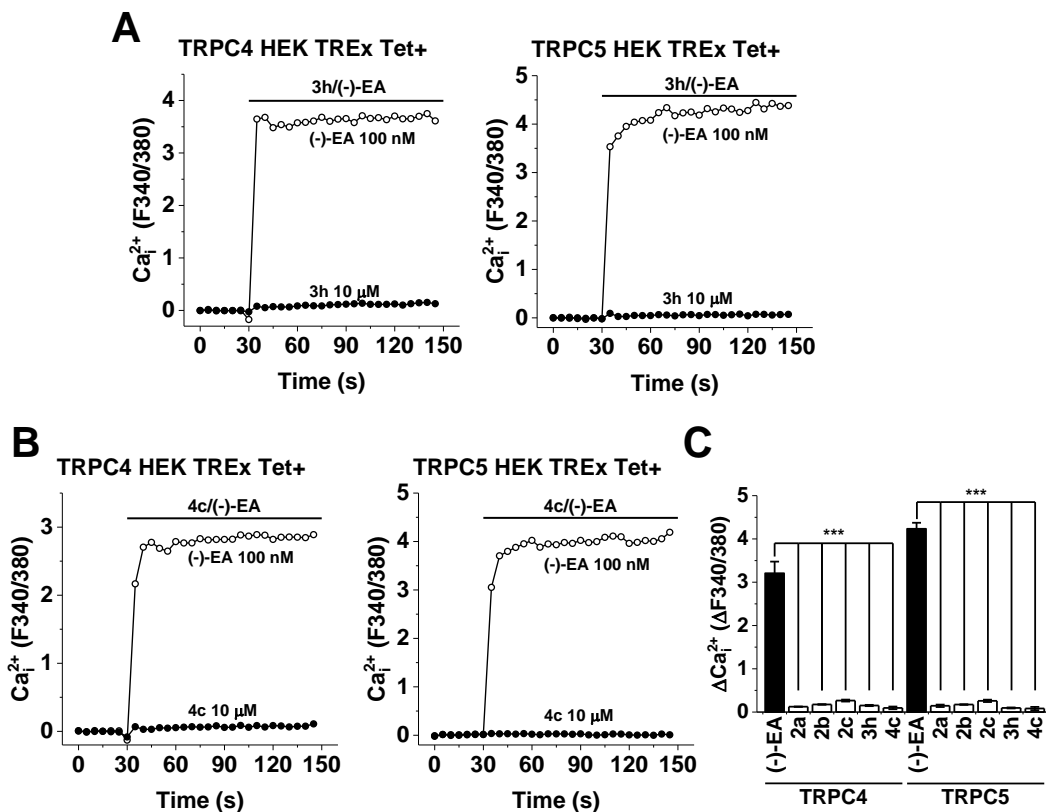


Figure 5.7: Yoda1 and its analogues do not activate TRPC4 or TRPC5 ion channels. A-B, example responses of TRPC5 HEK TREx Tet+ (left panel) and TRPC4 HEK TREx Tet+ (right panel) in response to Yoda1 analogues 3h (**A**) and 4c (**B**) and (-)EA positive control. **C,** Average data for amplitude of response from hit compounds in TRPC5 or TRPC4 HEK TREx Tet+ compared to (-)EA responses. $n/N = 3/3$. *** = $P < 0.01$.

5.2.2.2.3 TRPV4 channels

To determine whether Yoda1 and the hit analogues activate TRPV4 channels Chinese Hamster Ovary (CHO) cells overexpressing TRPV4 were used. 4 α PDD was used as an activator of TRPV4. Yoda1 produced large Ca²⁺ responses in TRPV4-CHO cells as well as 4 α PDD (Figure 5.8A-B). This suggested that Yoda1 may have an effect of TRPV4. However, Piezo1 expression has been reported in CHO cells (McHugh et al., 2010). Therefore, TRPV4-CHO cells were treated with Piezo1 siRNA in an attempt to reduce Yoda1 responses. Yoda1 responses were reduced by Piezo1 siRNA compared to scrambled siRNA suggesting a reduction in Piezo1 expression (Figure 5.8B). Additionally, 4 α PDD responses were not affected by Piezo1 siRNA treatment (Figure 5.8A). This suggested that the Yoda1 responses in CHO-TRPV4 was due to native Piezo1 expression in CHO cells. Hit analogues of Yoda1 also produced responses which were reduced in Piezo1 siRNA treated cells (Figure 5.8E). However, **4c** was the exception. **4c** had negligible responses in CHO-TRPV4 cells treated with either scrambled or Piezo1 siRNA (Figure 5.8D). This may have been due to the lower potency of **4c** compared to Yoda1 and the other analogues. These data suggest that Yoda1 and its analogues do not activate TRPV4.

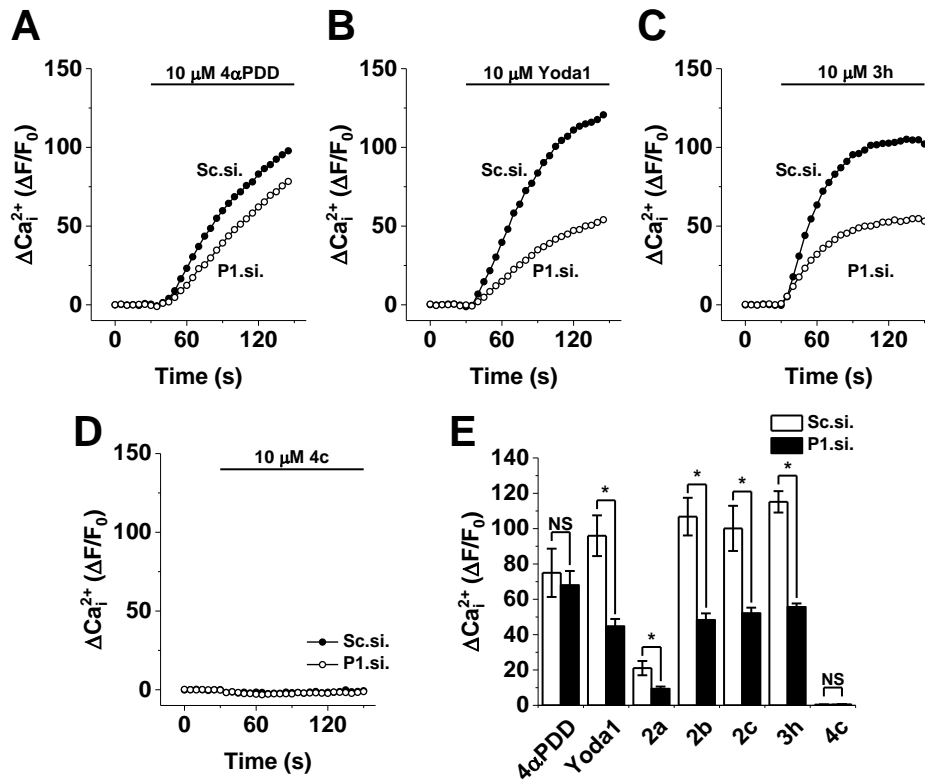


Figure 5.8: Responses of Yoda1 and hit analogues in CHO-TRPV4 cells. A-D, example responses of CHO-TRPV4 cells treated with scrambled siRNA (Sc.si.) or Piezo1 siRNA (P1.si.) and activated with 4aPDD (**A**), Yoda1 (**B**), 3h (**C**) or 4c (**D**). **E**, Average data for amplitude of response from hit compounds in CHO-TRPV4 cells treated with Sc.si. or P1.si. n/N = 4/4. * = $P < 0.05$. NS = not significant.

5.2.2.2.4 Piezo1 knockdown in HUVECs

HUVECs express many Ca²⁺ permeable ion channels, including those from the P2X, Orai and TRP families (Wong and Yao, 2011; Ralevic, 2012; Abdullaev et al., 2008). Reducing Piezo1 expression with siRNA in HUVECs reduced Yoda1-induced Ca²⁺ increases (Figure 5.9A). Hit compounds were tested at 2 µM in HUVECs treated with Piezo1 siRNA or negative control scrambled siRNA. Piezo1 siRNA abolished all increases in intracellular Ca²⁺ in response to treatment with the hit compounds (Figure 5.9C). This suggests that the Yoda1 analogues are not activating other ion channels present in HUVECs and have specificity for Piezo1 activation.

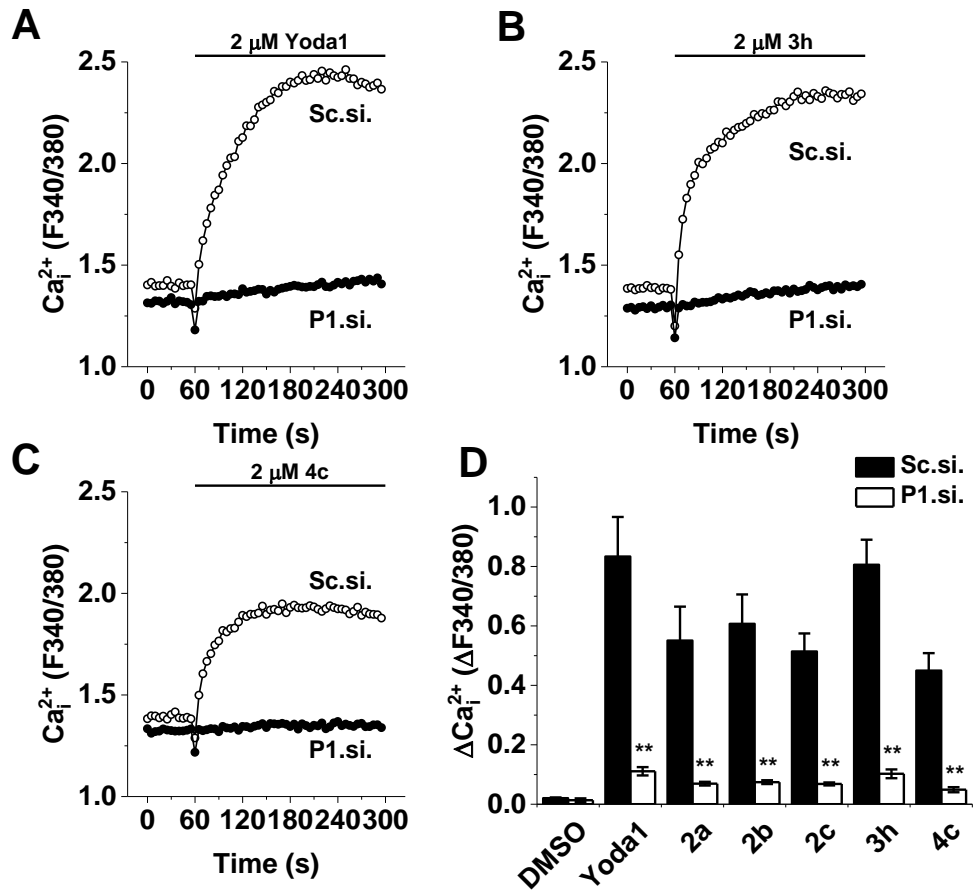


Figure 5.9: Piezo1 knockdown abolishes responses of Yoda1 and its analogues in HUVECs. A-C, example responses of HUVECs treated with scrambled siRNA (Sc.si.) or Piezo1 siRNA (P1.si.) and activated with Yoda1 (A), 3h (B) or 4c (C). D, Average data for amplitude of response from hit compounds in HUVECs treated with Sc.si. or P1.si. n/N = 3/4. ** = P < 0.01.

5.2.2.3 Solubility and stability of 2c and 3h

Most of the compounds had similar solubility issues to Yoda1, where precipitation could be observed at concentrations higher than 20 μM . However, **3h** showed much higher solubility compared to Yoda1 forming a colourless solution even at 50 μM . Therefore, **3h** was sent for in vitro absorption, distribution, metabolism, and excretion (ADME) analysis by Concept Life Sciences along with **2c** due to similar their potencies. Compared to Yoda1 and **2c**, **3h** had much greater kinetic solubility at 76.6 μM , which is the concentration that **3h** was observed to precipitate in aqueous solution (Table 5.4). Furthermore, mouse microsomal stability data showed **3h** had a half-life almost 40-times greater than Yoda1 and 20-times greater than **2c**. Clearance of **4c** was almost 35-times lower than Yoda1 (Table 5.4). These data suggest that **3h** has greater solubility and stability compared to Yoda1 which would make it a more ideal template for drug or tool compound development.

Table 5.4: 3h has a much greater in vitro pharmacokinetic profile than Yoda1 or 2c. ADME data was obtained by Concept Life Sciences.

Drug	Kinetic solubility (μM)	Mouse Microsomal Stability	
		Clearance ($\mu\text{L}/\text{min}/\text{mg}$)	$t_{1/2}$ (min)
Yoda1	0.2	678.1	1.0
2c	1.4	359.1	1.9
3h	76.6	18.6	37.2

5.2.3 Effect of Yoda1 analogues on endothelial cell alignment

Piezo1 has been shown to be crucial for endothelial cell alignment. Yoda1 and the hit analogues of Yoda1 were tested to determine whether they affect endothelial cell alignment. Yoda1 sensitised mechanically activated Piezo1-dependent currents, therefore it was hypothesised that Yoda1 analogues may increase endothelial cell alignment. Confluent HUVECs were treated with 1 μ M of Yoda1, **2a**, **2b**, **2c**, **3h** or **4c** for 30 minutes in reduced serum media to minimize serum binding. The cells were then exposed to shear stress for 24 hours. When imaged at 24 hours, few HUVECs were found after treated with Yoda1 (Figure 5.10). **2a**, **2b**, **2c** and **3h** also caused reduced cell number (Figure 5.11). However, cells remained confluent and aligned to shear stress when treated with **4c**. After treatment with **4c** HUVECs showed a trend to be more aligned compared to the DMSO control (Figure 5.10). This suggests that activators may be able to modulate shear stress responses in endothelial cell by increasing the sensitivity to shear stress. Additionally, the reduced cell number was likely caused by Piezo1 activation.

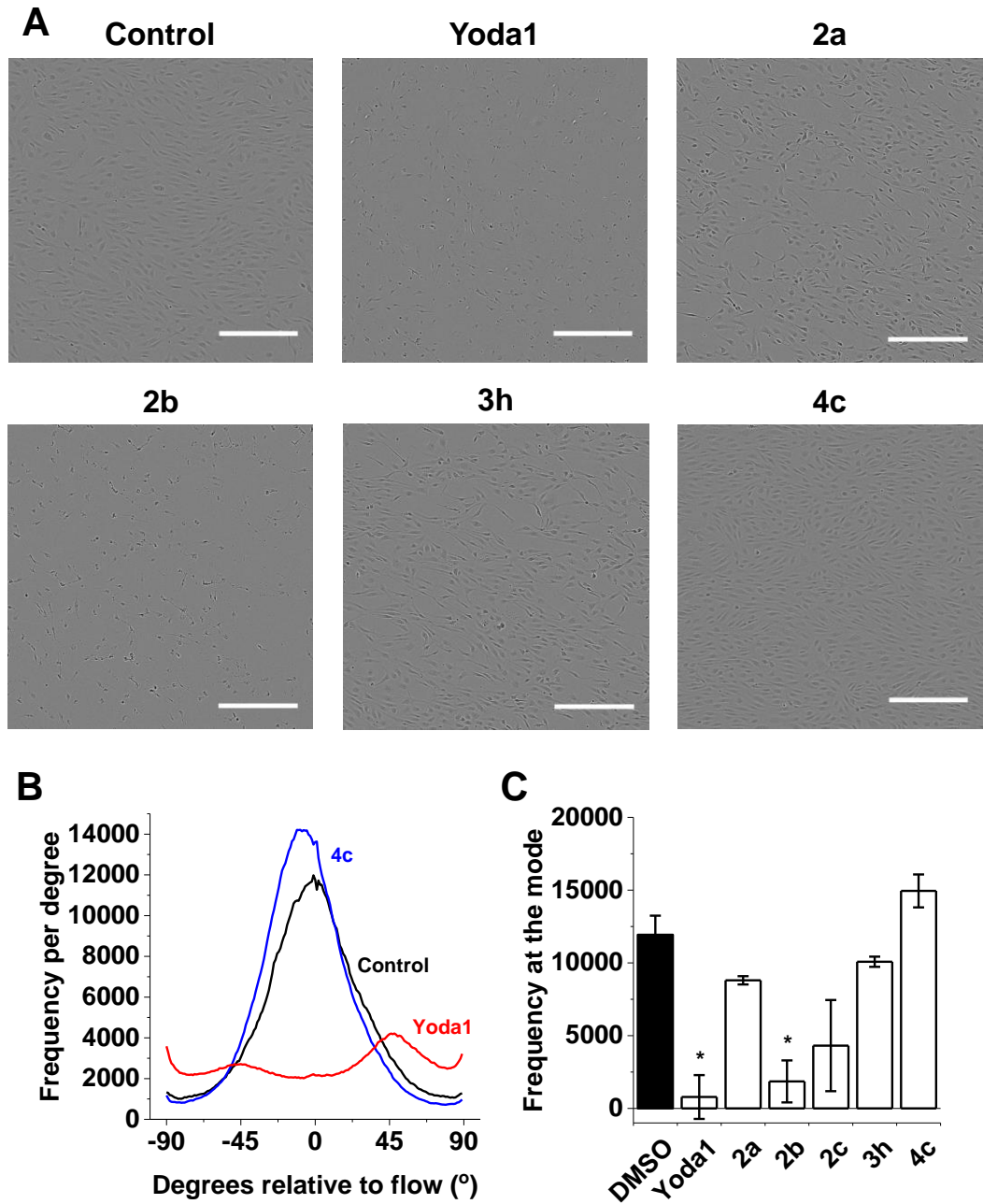


Figure 5.10: Effect of Yoda1 and hit analogues on HUVEC alignment. A, Example phase contrast images of HUVECs subjected to shear stress on an orbital shaker at 153 rpm for 24 hours. HUVECs were treated with DMSO control, Yoda1 or analogue at 1 μ M for 30 minutes prior to exposure to shear stress. Scale bar 300 μ m. **B,** typical distribution of alignment of HUVECs after exposure to shear stress and treated with Yoda1, 4c or control. **C,** Average alignment of HUVECs after treatment with 1 μ M Yoda1, hit analogues or DMSO. Alignment was measured by the height of the peak at the mode of the Gaussian distribution curve. $n = 4$. 3 images were used for analysis per well. * = $P < 0.05$.

5.2.4 Endothelial cell death by Yoda1 and analogues

Due to the cells lost during the shear stress alignment assay, HUVEC death was investigated. Confluent HUVECs were treated with 1, 5 or 10 μM concentrations of Yoda1 or the hit analogues in reduced serum media for 1 hour. Yoda1 caused the HUVECs to round up and die even at 1 μM . At 10 μM significant cell death occurred for all compounds (Figure 5.11). These data suggest that activators of Piezo1 may cause endothelial cell death.

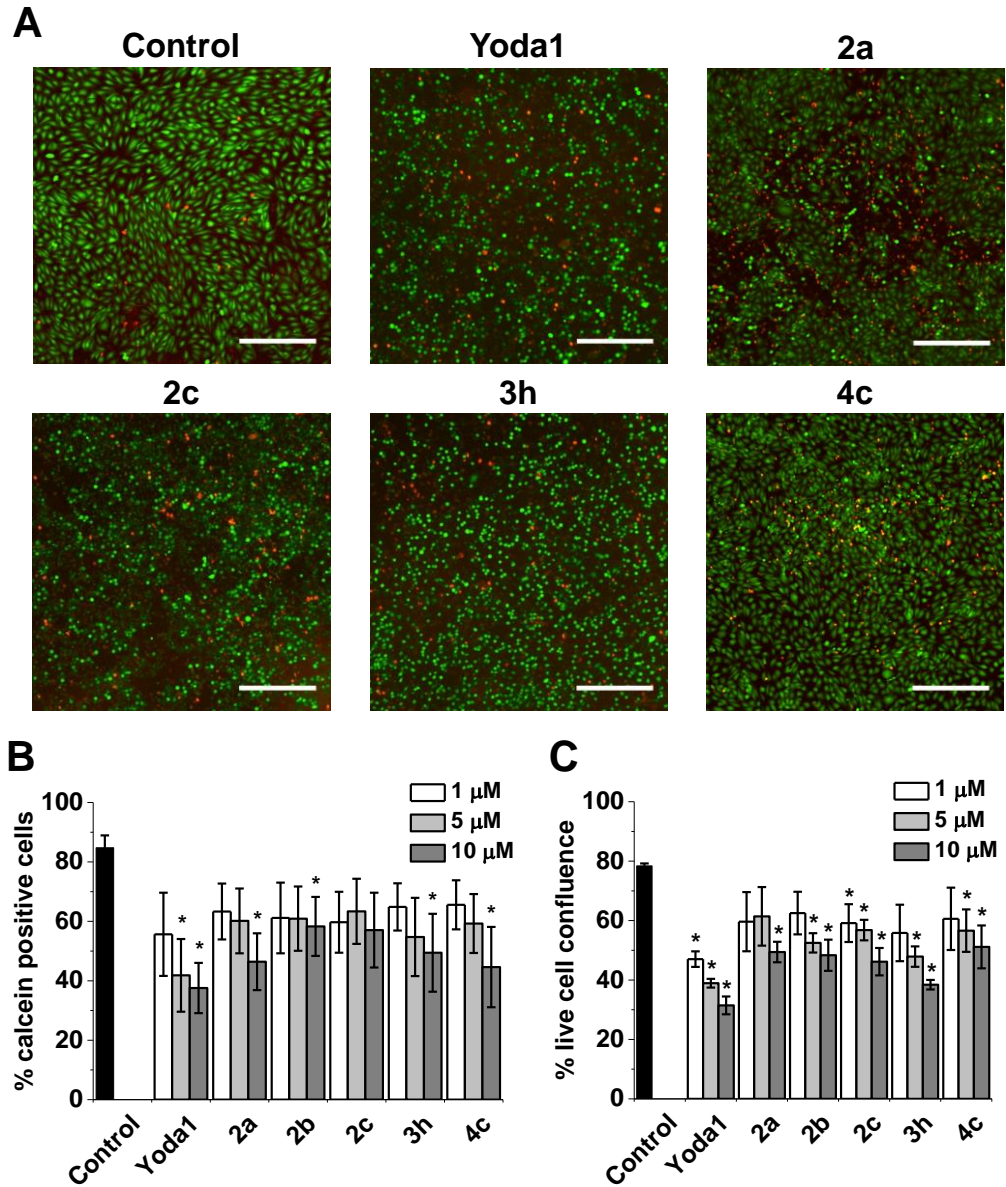


Figure 5.11: Yoda1 and its analogues caused cell death in HUVECs. **A**, HUVECs stained with calcein-AM (green) and ethidium homodimer-1 (red), treated with DMSO control, Yoda1, 4c, 3h, 2a or 2c as labelled at 1 μM . Scale bar 300 μm . **B**, Average data for calcein positive cells as a percentage of total cells. $n/N = 4/8$. * = $P < 0.05$. **C**, Percentage confluence of green calcein positive cells per well. $n/N = 4/8$. * = $P < 0.05$.

5.3 Discussion

In this study modification to the Yoda1 structure was made to determine structure activity relationship. Substitution of the chlorines in the dichlorophenyl ring with either methyl or methoxy groups retained activation of Yoda1 in analogues **2a**, **2b** and **2c**. Replacing the hydrogen bond accepting pyrazine with hydrogen bond donors abolished activation of Piezo1. However, substituting the pyrazine ring with a 4-benzoic acid ring retained activation of Piezo1 with analogue **3h**. Furthermore, substitution of the thiadiazole group for an oxadiazole retained activation of Yoda1 with analogue **4c**. These hit compounds did not have off-target effects or activate TRPC4, TRPC5 and TRPV4 channels. Analogue **3h** had greatly improved pharmacokinetic properties compared to Yoda1, which would make this an ideal candidate for compound development. However, Yoda1 and the hit analogues induced endothelial cell death and cell detachment in response to shear stress.

5.3.1 Yoda1 structure activity relationship

Currently no binding site for Yoda1 has been suggested in the Piezo1 protein. The original discovery of Yoda1 suggested that activation of Piezo1 was membrane delimited as Yoda1 activated Piezo1 reconstituted in an artificial membrane and activity was lost in modified Yoda1-like compounds. The structure-activity relationship of Yoda1 may help to reveal a binding site of Yoda1 to Piezo1.

In the initial discovery of Yoda1 the dichlorophenyl ring structure was suggested to be essential for Piezo1 activation. However, dichlorophenyl modifications were tolerated in compounds **2a**, **2b** and **2c** with increased potency compared to Yoda1. Retaining chlorine in the 2-position of the phenyl ring with either a 6-

methyl- or 6-methoxy- replacing the second chlorine maintained activation of Piezo1. Replacing both chlorines with methyl groups also retained activation of Piezo1. However, replacing the 2-chlorine with another halogen, fluorine, greatly reduced Piezo1 activation. Removal of the phenyl ring or replacing it with a different chemical structure almost abolished Piezo1 activation in all analogues. The reduction in activity of analogues **2g** and **2f** suggested that Yoda1 does not interact with Piezo1 by salt bridge or cation- π interactions. This suggests that chlorine and methyl groups may form similar interactions with the Piezo1 protein. This is most likely due to lipophilic interaction between these chemical groups and Piezo1.

The central ring and linker group of Yoda1 was also suggested to be essential for Yoda1 activity. Modifying the linker with the addition of a methyl group greatly reduced Piezo1 activation with slight inhibition of Yoda1 response. This suggested that modification to the linker region of Yoda1 cannot be tolerated as Syeda et al. (2015) suggested. However, modifying the central ring structure by replacing the sulphur with an oxygen in the ring retained Piezo1 activation but did not compete as efficiently as other analogues of Piezo1 that also activated Piezo1. Initial testing of compound **4c** suggested activation similar to that of Yoda1. However, when dose-response curves were made, **4c** had an EC₅₀ almost doubled compared to Yoda1. Additionally, initial test results were variable when tested as an agonist. This may have been due to the stability of **4c** under storage affecting the compounds efficacy.

Changes to the pyrazine ring structure of Yoda1 were not suggested to affect Yoda1 when first discovered. Modifications to the pyrazine ring generally reduced the activation of Piezo1. This suggests that the pyrazine ring structure may interact with Piezo1 and is important in the function of Yoda1.

Replacement of the hydrogen acceptor of pyrazine with pyrrole or 4-aminophenyl analogues reduced activation of compared to Yoda1. This suggests that hydrogen bonding may be important for interaction between the pyrazine ring of Yoda1 and Piezo1. However, one modification of the pyrazine ring well tolerated. Replacing the pyrazine ring with a benzoic acid ring produced an analogue of Yoda1 with equal activation in initial testing. Dose-response studies revealed **3h** to be more potent. However, the peak responses of **3h** were lower than those of Yoda1. The hydrophilic carboxylic acid modification of **3h** would reduce the compounds ability to diffuse through the plasma membrane of cells. This would suggest that **3h** is interacting with an exposed extracellular domain of the Piezo1 protein.

These results suggest that Yoda1 can be modified to produce more potent activators of Piezo1. Interaction sites of Yoda1 with the Piezo1 still remain unknown. With the crystal structure of mouse Piezo1 CED resolved computational docking of Yoda1 and active analogues may reveal sites in the protein where the drugs may interact. Site-directed mutagenesis and co-crystallisation of the drug would prove these interaction sites. This would allow a structure-based drug design method which may improve the efficiency of producing hit compounds. However, if the chemical activators of Piezo1 do not bind to the CED of Piezo1 this will not be achievable due to the remaining Piezo1 structure being resolved at a lower resolution.

5.3.2 Selectivity of Piezo1 activators

When discovered, Yoda1 was tested for selectivity against Piezo2 and as shown to activate purified Piezo1 protein in an artificial membrane. However, Yoda1 was not tested in other cell lines apart from Piezo1-null HEK293 cells. There is

a plethora of targets Yoda1 and its analogues may interact with. Here Yoda1 and hit analogues were tested for selectivity against other Ca^{2+} permeable ion channels overexpressed in different cell types. Additionally, the analogues were tested against HUVECs with Piezo1 depleted by siRNA treatment. Yoda1 and the hit analogues showed no activity against TRPC4 or TRPC5 channels. Additionally, Ca^{2+} flux was abolished in HUVECs treated with Piezo1 siRNA. This suggests that these compound were only activating Piezo1 in HUVECs and not other Ca^{2+} permeable ion channels. Ca^{2+} flux occurred in TRPV4 overexpressing CHO cells in response to Yoda1 and analogues except **4c**. This may have been due to native expression of Piezo1 in CHO cells, which has been suggested by McHugh et al. (2010). Therefore, Piezo1 siRNA was used to reduce Piezo1 expression. Responses from Yoda1 and its analogues was reduced and **4aPDD** responses were not affected. This suggests that Yoda1 and its analogues do not affect TRPV4. However, confirmation could be achieved by expressing TRPV4 in a TRPV4-null cell line and testing the compound or blocking the Yoda1 responses with a selective antagonist of Piezo1 if one was available.

5.3.3 Stability and solubility of Yoda1 analogues

Selected hit analogues were sent for solubility and stability analysis. **3h** showed greater solubility and mouse microsomal stability than Yoda1 and **2c**. These characteristics would make **3h** a more desirable drug to use in vivo due to solubility in solution and relative half-life. The increase in solubility occurred through replacement of the pyrazine ring to a benzoic acid. The increase in solubility may have occurred due to the carboxylic acid group being able to form hydrogen bonds with water. Additionally, this group may contribute to the reduced breakdown by P450 enzymes as measured in the microsomal stability

test as P450 enzymes favour lipophilic compounds (Lewis and Dickins, 2003). The improved solubility and stability properties of **3h** would make it a more ideal candidate for testing in vivo compared to Yoda1.

5.3.4 Piezo1 activators as a therapeutic agents

Activators of Yoda1 may be possible therapeutic agents to combat loss-of-function mutations of Piezo1 in congenital recessive lymphatic dysplasia and has been proposed to be an aid to mimic exercise by mimicking shunting of blood from the gut to muscles. Here, **4c** had a small effect on endothelial cell alignment in response to shear stress. This suggests that an activator of Piezo1 may have therapeutic potential in diseases where shear is involved in the pathophysiology, such as atherosclerosis. However, more investigation is required into the effects of activators of Piezo1 on shear stress-dependent functions of endothelial cells and whether Piezo1 activators function under low or disturbed shear stress conditions.

Furthermore, activating Piezo1 may not be a viable therapeutic option. Activators of Piezo1 caused death of HUVECs after treatment for 1 hour. However, HUVECs used in this investigation were seeded 24 hours and were still proliferating. In vivo, healthy endothelial cells become senescent and form tight cell-to-cell junctions. This may affect the activation of Piezo1 and the toxicity of Yoda1-like compounds in vivo. Conversely, activation may exacerbate apoptosis of endothelial cells that occurs in atherosclerotic plaques. This may result in acceleration of atherosclerotic cap thinning and rupture of the atheroma. A balance between the effects of Piezo1 activation as a therapeutic agent versus side effects would have to be determined.

5.3.5 Summary

Investigating the structure-activity relationship of Yoda1 has shown that modifications can be made to each ring structure of the compound and retain activation of Piezo1. These modifications have led to the development of more potent Yoda1-like compounds. Additionally, these modifications have been shown to have improved the solubility and stability compared to Yoda1 in the case of compound **3h**. This would make **3h** a desirable drug to use in vivo. However, caution must be taken at the dose of Piezo1 activating agents used in vivo as endothelial cell death may occur.

Chapter 6

Final summary and future work

The objective of this thesis was to identify mechanisms by which Ca^{2+} regulation by Piezo1 channels may be affected by endogenous and synthetic small molecules. This was achieved using Ca^{2+} measurements, cell function assays, computational analysis, and transfections of cells with mutant cDNAs. Chemical synthesis was performed by a collaborator.

In Results Chapter 3, cholesterol regulation of Piezo1 was investigated. The data suggested that cholesterol directly interacts with Piezo1 at cholesterol binding motifs that may modify the gating of the channel. Addition and depletion of membrane cholesterol reduced activation of Piezo1, suggesting cholesterol is essential for Piezo1 activity whilst also being able to suppress the channel. 15 highly conserved cholesterol binding motifs were discovered in Piezo1, 3 of which were shown to interact with cholesterol in molecular dynamics simulations. Mutations of predicted cholesterol interaction sites reduced inhibition by cholesterol. To further investigate these sites, further cumulative mutations of multiple amino acids should be performed. Additionally, in light of recent structural data, mutations should be made to determine the interactions between cholesterol and the proposed lipid-binding pocket in Piezo1 (Saotome et al., 2017). Additional biophysical assay may also show direct interaction such as FRET assay with fluorescent analogues of cholesterol, such as TopFluor Cholesterol. Interactions between Piezo1 and cholesterol could also be probed using sterol analogues to displace cholesterol.

The future challenges are to determine whether inhibition of Piezo1 by cholesterol contributes to pathophysiological events, such as reduced activation of eNOS in response to shear stress, which may contribute to atherosclerosis (Figure 6.1).

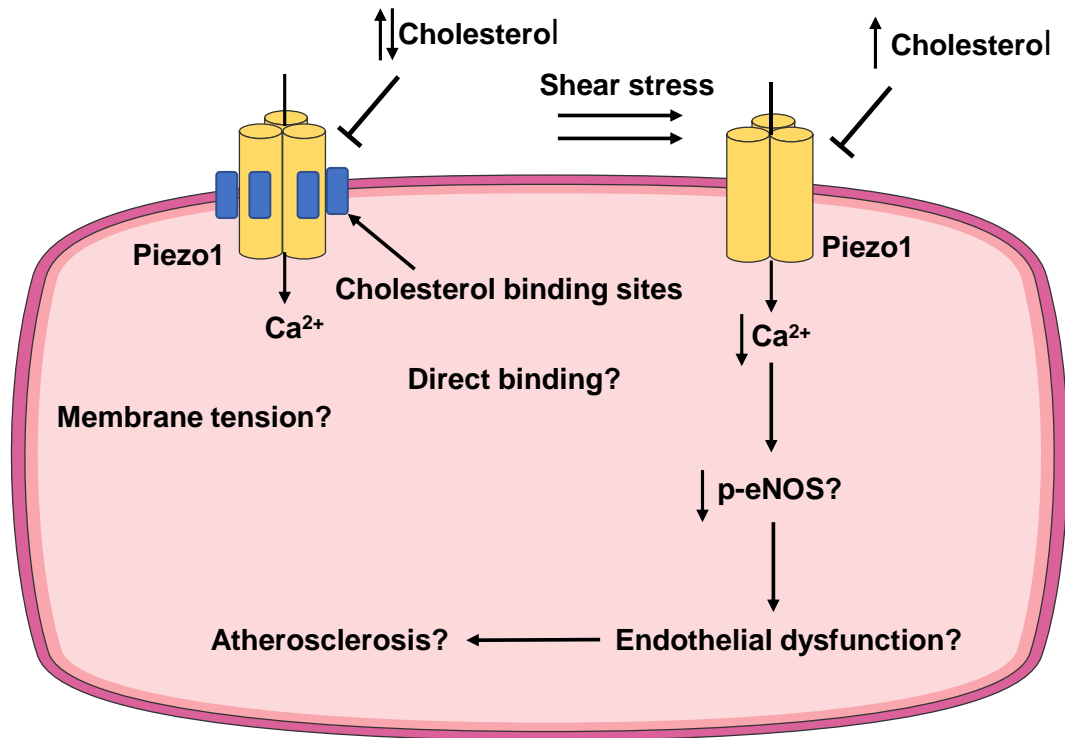


Figure 6.1: Cartoon summarising the data from Chapter 3 and new hypothesis based on the data. Piezo1-dependent Ca^{2+} entry is inhibited by addition or depletion of cholesterol to the cell membrane. Piezo1 contains cholesterol binding motifs. When they are mutated Piezo1 is less sensitive to addition of cholesterol. Further investigation is required to determine the direct binding of cholesterol to these sites. Additionally, changes in membrane tension caused by cholesterol needs to be investigated as a mechanism of regulating Piezo1. Due to the effects of cholesterol on Piezo1 and Piezo1's role in the vasculature further investigation is needed to understand whether cholesterol's inhibition of Piezo1 plays a role in the development of atherosclerosis.

In Results chapter 4, sphingomyelinase was shown to potentiate endothelial Piezo1 activation via production of sphingosine and subsequent inhibition of protein kinase C and activation of protein kinase D. Inhibiting sphingosine production abolished the potentiating effects of SMase on Piezo1 activation. Inhibiting PKC produced similar potentiating effects to SMase on Piezo1 activation. Additionally, activating PKC with SC-9 abolished potentiation of Piezo1 activation by SMase. Inhibition of PLC also potentiated Piezo1 activation. However, inhibition of PLC abolished SMase-induced increases in intracellular Ca^{2+} and SMase did not potentiate the effect of PLC further, suggesting that PLC activation may be involved in the potentiation of Piezo1 by SMase. PLC activation produces DAG which can activate PKD. PKD inhibition abolished the SMase-induced potentiation of Piezo1. Other mechanisms may also play a role in SMase, such as activation of phospholipase D by sphingosine. Therefore, more investigation into effects of protein kinase and the mechanism by which they affect Piezo1 are required.

Activation of native SMase often occurs in response to stress, inflammatory and infectious signalling pathways. Sphingomyelinase and sphingosine have also been suggested to contribute to endothelial dysfunction. Furthermore, endothelial cell death has been reported in response to SMase activation by TNF α (Yang et al., 2004). Piezo1 may contribute to these effects by modulation of sphingomyelinase activation (Figure 6.2). However, the effect of endogenous SMase activation needs to be investigated. Blocking the modulation of Piezo1 by SMase activation may provide new treatments for cardiovascular diseases.

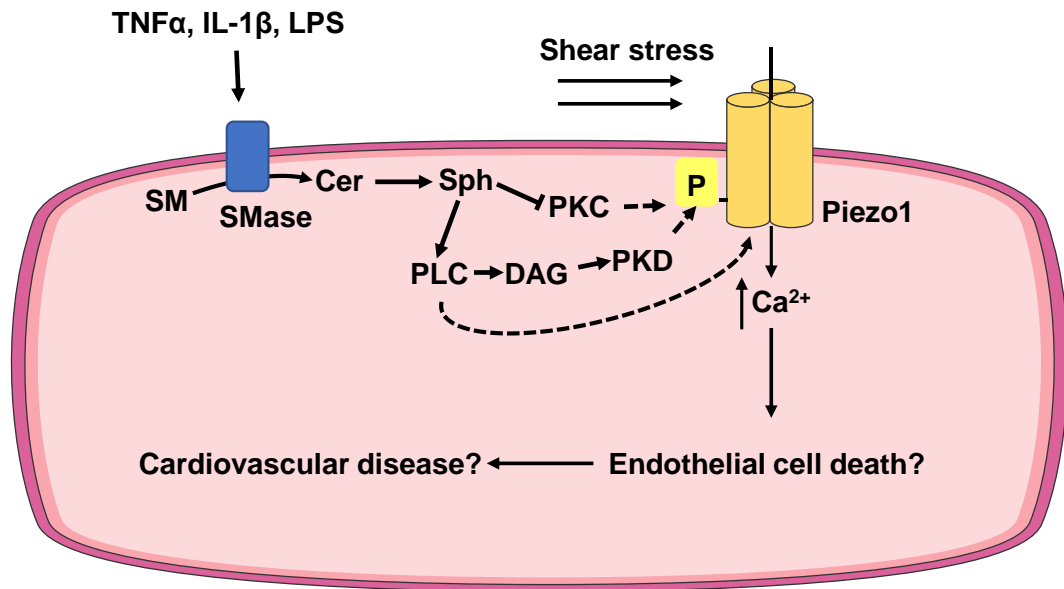


Figure 6.2: Cartoon summarising the data from Chapter 4 and new hypothesis based on the data. SMase induced potentiation of endothelial Piezo1 activation. The potentiation was due to production of sphingosine and subsequent inhibition of PKC, activation of PLC and activation of PKD. Further investigation is required into the mechanism which PKC and PKD modulate Piezo1 activity. Also, further investigation is required in the effects of activators of endogenous SMase, the role Piezo1 has on their functions and whether this may play a role in cardiovascular diseases.

In Results chapter 5, novel analogues of Piezo1 activator Yoda1 were discovered. Five new activators of Piezo1 were discovered with four showing greater potency in P1 HEK TReX cells. These analogues showed that each of the three chemical ring structures of Yoda1 may be altered and still maintain Piezo1. The structure-activity relationship may help to determine a Yoda1 binding site within the structure of Piezo1. Computational docking of these compounds and mutagenesis of potential interacting residues would need to be investigated. This would allow structure-based drug design to aid development of small molecule modulators of Piezo1. Furthermore, modifying the pyrazine ring of yoda1 improved the in vitro pharmacokinetic profile of the analogue **3h** compared to Yoda1 by improving aqueous solubility and clearance. This may make the drug favourable for use in vivo. However, before use in vivo a functional profile of this novel analogues must be obtained. Endothelial alignment experiments resulted in loss of cells after treated with Yoda1 and analogues. Additionally, endothelial cell death occurred in response to Yoda1 and its analogues. However, full dose-response curves for these phenomena need to be attained. Additionally, Yoda1 and analogues need to be tested on intact endothelium as the effects of cytotoxicity may be different between a pure cell culture and endothelial cell supported by other tissues. Ex vivo studies on freshly isolated vessels may be able to determine the effect of Piezo1 activators on endothelial cell function. Development of small molecule Piezo1 modulators may provide treatment options for diseases caused by loss- or gain-of-function mutations of Piezo1 and may provide treatment options for atherosclerosis by modulation of Piezo1 in endothelial cells.

In summary, this research has developed new knowledge and hypotheses about the modulation of Piezo1 activation by lipids and targeting Piezo1 using small molecules. These may help to develop new strategies to treat cardiovascular disease such as atherosclerosis.

References

- Abdullaev, I.F., Bisailon, J.M., Potier, M., Gonzalez, J.C., Motiani, R.K. and Trebak, M. 2008. Stim1 and Orai1 mediate CRAC currents and store-operated calcium entry important for endothelial cell proliferation. *Circulation research*. **103**(11),pp.1289–99.
- Abi-Char, J., Maguy, A., Coulombe, A., Balse, E., Ratajczak, P., Samuel, J.-L., Nattel, S. and Hatem, S.N. 2007. Membrane cholesterol modulates Kv1.5 potassium channel distribution and function in rat cardiomyocytes. *The Journal of Physiology*. **582**(3),pp.1205–1217.
- Absi, M., Burnham, M.P., Weston, A.H., Harno, E., Rogers, M. and Edwards, G. 2009. Effects of methyl β -cyclodextrin on EDHF responses in pig and rat arteries; association between SKCa channels and caveolin-rich domains. *British Journal of Pharmacology*. **151**(3),pp.332–340.
- Addona, G.H., Sandermann, H., Kloczewiak, M.A. and Miller, K.W. 2003. Low chemical specificity of the nicotinic acetylcholine receptor sterol activation site. *Biochimica et biophysica acta*. **1609**(2),pp.177–82.
- Akbulut, Y., Gaunt, H.J., Muraki, K., Ludlow, M.J., Amer, M.S., Bruns, A., Vasudev, N.S., Radtke, L., Willot, M., Hahn, S., Seitz, T., Ziegler, S., Christmann, M., Beech, D.J. and Waldmann, H. 2015. (–)-Englerin A is a Potent and Selective Activator of TRPC4 and TRPC5 Calcium Channels. *Angewandte Chemie International Edition*. **54**(12),pp.3787–3791.
- Albert, A.P., Piper, A.S. and Large, W.A. 2005. Role of phospholipase D and diacylglycerol in activating constitutive TRPC-like cation channels in rabbit ear artery myocytes. *The Journal of physiology*. **566**(Pt 3),pp.769–80.
- Albuisson, J., Murthy, S.E., Bandell, M., Coste, B., Louis-dit-Picard, H., Mathur, J., Fénéant-Thibault, M., Tertian, G., de Jaureguiberry, J.-P., Syfuss, P.-Y., Cahalan, S., Garçon, L., Toutain, F., Simon Rohrlich, P., Delaunay, J., Picard, V., Jeunemaitre, X. and Patapoutian, A. 2013. Dehydrated hereditary stomatocytosis linked to gain-of-function mutations in mechanically activated PIEZO1 ion channels. *Nature Communications*. **4**,p.1884.
- Allahverdian, S., Pannu, P.S. and Francis, G.A. 2012. Contribution of monocyte-derived macrophages and smooth muscle cells to arterial foam cell formation. *Cardiovascular Research*. **95**(2),pp.165–172.
- Alvarez, S.E., Harikumar, K.B., Hait, N.C., Allegood, J., Strub, G.M., Kim, E.Y., Maceyka, M., Jiang, H., Luo, C., Kordula, T., Milstien, S. and Spiegel, S. 2010. Sphingosine-1-phosphate is a missing cofactor for the E3 ubiquitin ligase TRAF2. *Nature*. **465**(7301),pp.1084–1088.
- Andolfo, I., Alper, S.L., De Franceschi, L., Auriemma, C., Russo, R., De Falco, L., Vallefuoco, F., Esposito, M.R., Vandorpe, D.H., Shmukler, B.E., Narayan, R., Montanaro, D., D'Armiento, M., Vetro, A., Limongelli, I., Zuffardi, O., Glader, B.E., Schrier, S.L., Brugnara, C., Stewart, G.W., Delaunay, J. and Iolascon, A. 2013. Multiple clinical forms of dehydrated hereditary stomatocytosis arise from mutations in PIEZO1. *Blood*. **121**(19),pp.3925–35, S1-12.
- Andolfo, I., Manna, F., De Rosa, G., Rosato, B.E., Gambale, A., Tomaiuolo, G., Carciati, A., Marra, R., De Franceschi, L., Iolascon, A. and Russo, R. 2017. PIEZO1-R1864H rare variant accounts for a genetic phenotype-modifier role in dehydrated hereditary stomatocytosis. *Haematologica*,p.haematol.2017.180687.

- Andolfo, I., Russo, R., Gambale, A. and Iolascon, A. 2016. New insights on hereditary erythrocyte membrane defects. *Haematologica*. **101**(11),pp.1284–1294.
- Arana, L., Gangoiti, P., Ouro, A., Trueba, M. and Gómez-Muñoz, A. 2010. Ceramide and ceramide 1-phosphate in health and disease. *Lipids in health and disease*. **9**,p.15.
- Augé, N., Andrieu, N., Nègre-Salvayre, A., Thiers, J.C., Levade, T. and Salvayre, R. 1996. The sphingomyelin-ceramide signaling pathway is involved in oxidized low density lipoprotein-induced cell proliferation. *The Journal of biological chemistry*. **271**(32),pp.19251–5.
- Auge, N., Garcia, V., Maupas-Schwalm, F., Levade, T., Salvayre, R. and Negre-Salvayre, A. 2002. Oxidized LDL-induced smooth muscle cell proliferation involves the EGF receptor/PI-3 kinase/Akt and the sphingolipid signaling pathways. *Arteriosclerosis, thrombosis, and vascular biology*. **22**(12),pp.1990–5.
- Auge, N., Maupas-Schwalm, F., Elbaz, M., Thiers, J.-C., Waysbort, A., Itohara, S., Krell, H.-W., Salvayre, R. and Nègre-Salvayre, A. 2004. Role for Matrix Metalloproteinase-2 in Oxidized Low-Density Lipoprotein-Induced Activation of the Sphingomyelin/Ceramide Pathway and Smooth Muscle Cell Proliferation. *Circulation*. **110**(5),pp.571–578.
- Bae, C., Gnanasambandam, R., Nicolai, C., Sachs, F. and Gottlieb, P.A. 2013. Xerocytosis is caused by mutations that alter the kinetics of the mechanosensitive channel PIEZO1. *Proceedings of the National Academy of Sciences*. **110**(12),pp.E1162–E1168.
- Bae, C., Gottlieb, P. and Sachs, F. 2013. Human PIEZO1: removing inactivation. *Biophysical journal*. **105**(4),pp.880–6.
- Bae, C., Sachs, F. and Gottlieb, P. 2011. The mechanosensitive ion channel Piezo1 is inhibited by the peptide GsMTx4. *Biochemistry*. **50**(29),pp.6295–6300.
- Bae, C., Sachs, F. and Gottlieb, P. a 2015. Protonation of Human PIEZO1 Ion Channel Stabilizes Inactivation. *The Journal of biological chemistry*. (716),pp.1–16.
- Balijepalli, R.C., Foell, J.D., Hall, D.D., Hell, J.W. and Kamp, T.J. 2006. Localization of cardiac L-type Ca²⁺ channels to a caveolar macromolecular signaling complex is required for beta2-adrenergic regulation. *Proceedings of the National Academy of Sciences*. **103**(19),pp.7500–7505.
- Balijepalli, R.C. and Kamp, T.J. 2008. Caveolae, ion channels and cardiac arrhythmias. *Progress in Biophysics and Molecular Biology*. **98**(2–3),pp.149–160.
- Balut, C., Steels, P., Radu, M., Ameloot, M., Driessche, W. Van and Jans, D. 2006. Membrane cholesterol extraction decreases Na⁺ transport in A6 renal epithelia. *American journal of physiology. Cell physiology*. **290**(1),pp.C87-94.
- Bandhuvula, P. and Saba, J.D. 2007. Sphingosine-1-phosphate lyase in immunity and cancer: silencing the siren. *Trends in Molecular Medicine*. **13**(5),pp.210–217.
- Bao, J.-X., Xia, M., Poklis, J.L., Han, W.-Q., Brimson, C. and Li, P.-L. 2010. Triggering role of acid sphingomyelinase in endothelial lysosome-membrane fusion and dysfunction in coronary arteries. *American Journal of Physiology-Heart and Circulatory Physiology*. **298**(3),pp.H992–H1002.

- Barenholz, Y. 2000. Liposomology. *Progress in Lipid Research*. **39**(1),pp.1–2.
- Barrantes, F.J. 2007. Cholesterol effects on nicotinic acetylcholine receptor. *Journal of Neurochemistry*. **103**(s1),pp.72–80.
- Bazzi, M.D. and Nelsestuen, G.L. 1987. Mechanism of protein kinase C inhibition by sphingosine. *Biochemical and Biophysical Research Communications*. **146**(1),pp.203–207.
- Beech, D.J., Bahnasi, Y.M., Dedman, A.M. and Al-Shawaf, E. 2009. TRPC channel lipid specificity and mechanisms of lipid regulation. *Cell calcium*. **45**(6),pp.583–8.
- Bennett, M.R., Sinha, S. and Owens, G.K. 2016. Vascular Smooth Muscle Cells in Atherosclerosis. *Circulation research*. **118**(4),pp.692–702.
- Berridge, M.J. 2002. The endoplasmic reticulum: a multifunctional signaling organelle. *Cell calcium*. **32**(5–6),pp.235–49.
- Berridge, M.J., Bootman, M.D. and Roderick, H.L. 2003. Calcium: Calcium signalling: dynamics, homeostasis and remodelling. *Nature Reviews Molecular Cell Biology*. **4**(7),pp.517–529.
- Berrier, C., Pozza, A., de Lacroix de Lavalette, A., Chardonnet, S., Mesneau, A., Jaxel, C., le Maire, M. and Ghazi, A. 2013. The purified mechanosensitive channel TREK-1 is directly sensitive to membrane tension. *The Journal of biological chemistry*. **288**(38),pp.27307–14.
- Bharath, L.P., Ruan, T., Li, Y., Ravindran, A., Wan, X., Nhan, J.K., Walker, M.L., Deeter, L., Goodrich, R., Johnson, E., Munday, D., Mueller, R., Kunz, D., Jones, D., Reese, V., Summers, S.A., Babu, P.V.A., Holland, W.L., Zhang, Q.-J., Abel, E.D. and Symons, J.D. 2015. Ceramide-Initiated Protein Phosphatase 2A Activation Contributes to Arterial Dysfunction In Vivo. *Diabetes*. **64**(11),pp.3914–26.
- Bielawski, J., Szulc, Z.M., Hannun, Y.A. and Bielawska, A. 2006. Simultaneous quantitative analysis of bioactive sphingolipids by high-performance liquid chromatography-tandem mass spectrometry. *Methods*. **39**(2),pp.82–91.
- Björkegren, J., Silveira, A., Boquist, S., Tang, R., Karpe, F., Bond, M.G., de Faire, U. and Hamsten, A. 2002. Postprandial enrichment of remnant lipoproteins with apoC-I in healthy normolipidemic men with early asymptomatic atherosclerosis. *Arteriosclerosis, thrombosis, and vascular biology*. **22**(9),pp.1470–4.
- Bleasdale, J.E., Thakur, N.R., Gremban, R.S., Bundy, G.L., Fitzpatrick, F.A., Smith, R.J. and Bunting, S. 1990. Selective inhibition of receptor-coupled phospholipase C-dependent processes in human platelets and polymorphonuclear neutrophils. *The Journal of pharmacology and experimental therapeutics*. **255**(2),pp.756–68.
- Bobryshev, Y. V. 2006. Monocyte recruitment and foam cell formation in atherosclerosis. *Micron*. **37**(3),pp.208–222.
- Bock, J., Szabó, I., Gamper, N., Adams, C. and Gulbins, E. 2003. Ceramide inhibits the potassium channel Kv1.3 by the formation of membrane platforms. *Biochemical and biophysical research communications*. **305**(4),pp.890–7.
- Bokoch, G.M., Reilly, A.M., Daniels, R.H., King, C.C., Olivera, A., Spiegel, S. and Knaus, U.G. 1998. A GTPase-independent mechanism of p21-activated kinase activation. Regulation by sphingosine and other biologically active lipids. *The Journal of biological chemistry*. **273**(14),pp.8137–44.
- Bolotina, V., Omelyanenko, V., Heyes, B., Ryan, U. and Bregestovski, P. 1989.

- Variations of membrane cholesterol alter the kinetics of Ca²⁺-dependent K⁺ channels and membrane fluidity in vascular smooth muscle cells. *Pflugers Archiv : European journal of physiology*. **415**(3),pp.262–8.
- Borbiro, I., Badheka, D. and Rohacs, T. 2015. Activation of TRPV1 channels inhibits mechanosensitive Piezo channel activity by depleting membrane phosphoinositides. *Science signaling*. **8**(363),p.ra15.
- Borén, J., Olin, K., Lee, I., Chait, A., Wight, T.N. and Innerarity, T.L. 1998. Identification of the principal proteoglycan-binding site in LDL. A single-point mutation in apo-B100 severely affects proteoglycan interaction without affecting LDL receptor binding. *Journal of Clinical Investigation*. **101**(12),pp.2658–2664.
- Borroni, V., Borroni, V., Baier, C.J., Lang, T., Bonini, I., White, M.M., Garbus, I. and Barrantes, F.J. 2007. Cholesterol depletion activates rapid internalization of submicron-sized acetylcholine receptor domains at the cell membrane. *Molecular Membrane Biology*. **24**(1),pp.1–15.
- Bossu, J.L., Elhamedani, A. and Feltz, A. 1992. Voltage-dependent calcium entry in confluent bovine capillary endothelial cells. *FEBS letters*. **299**(3),pp.239–42.
- Bossu, J.L., Elhamedani, A., Feltz, A., Tanzi, F., Aunis, D. and Thierse, D. 1992. Voltage-gated Ca entry in isolated bovine capillary endothelial cells: evidence of a new type of BAY K 8644-sensitive channel. *Pflugers Archiv : European journal of physiology*. **420**(2),pp.200–7.
- Bourbon, N.A., Sandrasegarane, L. and Kester, M. 2002. Ceramide-induced Inhibition of Akt Is Mediated through Protein Kinase C ζ . *Journal of Biological Chemistry*. **277**(5),pp.3286–3292.
- Brady, R.O., Kanfer, J.N., Mock, M.B. and Fredrickson, D.S. 1966. The metabolism of sphingomyelin. II. Evidence of an enzymatic deficiency in Niemann-Pick disease. *Proceedings of the National Academy of Sciences of the United States of America*. **55**(2),pp.366–9.
- Brini, M. and Carafoli, E. 2011. The plasma membrane Ca²⁺ ATPase and the plasma membrane sodium calcium exchanger cooperate in the regulation of cell calcium. *Cold Spring Harbor perspectives in biology*. **3**(2).
- Brohawn, S.G., Campbell, E.B. and MacKinnon, R. 2014. Physical mechanism for gating and mechanosensitivity of the human TRAAK K⁺ channel. *Nature*. **516**(7529),pp.126–130.
- Bukiya, A.N., Belani, J.D., Rychnovsky, S. and Dopico, A.M. 2011. Specificity of cholesterol and analogs to modulate BK channels points to direct sterol–channel protein interactions. *The Journal of General Physiology*. **137**(1),pp.93–110.
- Burnstock, G. and Ralevic, V. 2013. Purinergic Signaling and Blood Vessels in Health and Disease. *Pharmacological Reviews*. **66**(1),pp.102–192.
- Caffrey, D.R., Dana, P.H., Mathur, V., Ocano, M., Hong, E.-J., Wang, Y.E., Somaroo, S., Caffrey, B.E., Potluri, S., Huang, E.S., Edgar, R., Batzoglou, S., Thompson, J., Plewniak, F., Poch, O., Bentz, J., Baucom, A., Hansen, M., Gregoret, L., Clamp, M., Cuff, J., Searle, S., Barton, G., Deleage, G., Combet, C., Blanchet, C., Geourjon, C., Galtier, N., Gouy, M., Gautier, C., Nicholas, K., Parry-Smith, D., Payne, A., Michie, A., Attwood, T., Barton, G., Goodstadt, L., Ponting, C., Ilyin, V., Pieper, U., Stuart, A., Marti-Renom, M., McMahan, L., Sali, A., Li, W., Godzik, A., Wang, Y., Geer, L., Chappay, C., Kans, J., Bryant, S., Thompson, J., Muller, A., Waterhouse, A., Procter, J., Barton, G., Plewniak, F., Poch, O., Johnson, J., Mason, K.,

- Moallemi, C., Xi, H., Somaroo, S., Huang, E., Berman, H., Westbrook, J., Feng, Z., Gilliland, G., Bhat, T., Weissig, H., Shindyalov, I., Bourne, P., Saitou, N., Nei, M., Zmasek, C., Eddy, S., Lee, B., Richards, F., Morgan, D., Kristensen, D., Mittelman, D., Lichtarge, O. and Strang, G. 2007. PFAAT version 2.0: A tool for editing, annotating, and analyzing multiple sequence alignments. *BMC Bioinformatics*. **8**(1),p.381.
- Cahalan, S.M., Lukacs, V., Ranade, S.S., Chien, S., Bandell, M. and Patapoutian, A. 2015. Piezo1 links mechanical forces to red blood cell volume. *eLife*. **4**,p.e07370.
- Calaghan, S. and White, E. 2006. Caveolae modulate excitation-contraction coupling and beta2-adrenergic signalling in adult rat ventricular myocytes. *Cardiovascular research*. **69**(4),pp.816–24.
- Chae, S.-S., Paik, J.-H., Furneaux, H. and Hla, T. 2004. Requirement for sphingosine 1-phosphate receptor-1 in tumor angiogenesis demonstrated by in vivo RNA interference. *The Journal of clinical investigation*. **114**(8),pp.1082–9.
- Chalfant, C.E., Kishikawa, K., Mumby, M.C., Kamibayashi, C., Bielawska, A. and Hannun, Y.A. 1999. Long chain ceramides activate protein phosphatase-1 and protein phosphatase-2A. Activation is stereospecific and regulated by phosphatidic acid. *The Journal of biological chemistry*. **274**(29),pp.20313–7.
- Chapman, H., Ramström, C., Korhonen, L., Laine, M., Wann, K.T., Lindholm, D., Pasternack, M. and Törnquist, K. 2005. Downregulation of the HERG (KCNH2) K⁺ channel by ceramide: evidence for ubiquitin-mediated lysosomal degradation. *Journal of Cell Science*. **118**(22),pp.5325–5334.
- Cheng, H.-W., James, A.F., Foster, R.R., Hancox, J.C. and Bates, D.O. 2006. VEGF Activates Receptor-Operated Cation Channels in Human Microvascular Endothelial Cells. *Arteriosclerosis, Thrombosis, and Vascular Biology*. **26**(8),pp.1768–1776.
- Chiu, J. and Chien, S. 2011. Effects of disturbed flow on vascular endothelium: pathophysiological basis and clinical perspectives. *Physiological reviews*. **91**(1),pp.327–387.
- Chubinskiy-Nadezhdin, V.I., Negulyaev, Y.A. and Morachevskaya, E.A. 2011. Cholesterol depletion-induced inhibition of stretch-activated channels is mediated via actin rearrangement. *Biochemical and biophysical research communications*. **412**(1),pp.80–5.
- Cinar, E., Zhou, S., DeCoursey, J., Wang, Y., Waugh, R.E. and Wan, J. 2015. Piezo1 regulates mechanotransductive release of ATP from human RBCs. *Proceedings of the National Academy of Sciences of the United States of America*. **112**(38),pp.11783–8.
- Clapham, D.E.D.D.E. 2007. Calcium signaling. *Cell*. **131**(6),pp.1047–58.
- Combs, D.J. and Lu, Z. 2015. Sphingomyelinase D inhibits store-operated Ca²⁺ entry in T lymphocytes by suppressing ORAI current. *The Journal of General Physiology*. **146**(2),pp.161–172.
- Combs, D.J., Shin, H.-G., Xu, Y., Ramu, Y. and Lu, Z. 2013. Tuning voltage-gated channel activity and cellular excitability with a sphingomyelinase. *The Journal of general physiology*. **142**(4),pp.367–80.
- Coste, B., Mathur, J., Schmidt, M., Earley, T.J., Ranade, S., Petrus, M.J., Dubin, A.E. and Patapoutian, A. 2010. Piezo1 and Piezo2 are essential components of distinct mechanically activated cation channels. *Science (New York, N. Y.)*. **330**(6000),pp.55–60.

- Coste, B., Murthy, S.E., Mathur, J., Schmidt, M., Mechioukhi, Y., Delmas, P. and Patapoutian, A. 2015. Piezo1 ion channel pore properties are dictated by C-terminal region. *Nature communications*. **6**,p.7223.
- Coste, B., Xiao, B., Santos, J.S., Syeda, R., Grandl, J., Spencer, K.S., Kim, S.E., Schmidt, M., Mathur, J., Dubin, A.E., Montal, M. and Patapoutian, A. 2012. Piezo proteins are pore-forming subunits of mechanically activated channels. *Nature*. **483**(7388),pp.176–81.
- Cox, C.D., Bae, C., Ziegler, L., Hartley, S., Nikolova-Krstevski, V., Rohde, P.R., Ng, C.-A., Sachs, F., Gottlieb, P.A. and Martinac, B. 2016. Removal of the mechanoprotective influence of the cytoskeleton reveals PIEZO1 is gated by bilayer tension. *Nature communications*. **7**,p.10366.
- Czarny, M., Liu, J., Oh, P. and Schnitzer, J.E. 2003. Transient mechanoactivation of neutral sphingomyelinase in caveolae to generate ceramide. *The Journal of biological chemistry*. **278**(7),pp.4424–30.
- Czarny, M. and Schnitzer, J.E. 2004. Neutral sphingomyelinase inhibitor scyphostatin prevents and ceramide mimics mechanotransduction in vascular endothelium. *American journal of physiology. Heart and circulatory physiology*. **287**(3),pp.H1344–H1352.
- Dardik, A., Chen, L., Frattini, J., Asada, H., Aziz, F., Kudo, F. a and Sumpio, B.E. 2005. Differential effects of orbital and laminar shear stress on endothelial cells. *Journal of vascular surgery*. **41**(5),pp.869–80.
- Deng, Y., Rivera-Molina, F.E., Toomre, D.K. and Burd, C.G. 2016. Sphingomyelin is sorted at the trans Golgi network into a distinct class of secretory vesicle. *Proceedings of the National Academy of Sciences*. **113**(24),pp.6677–6682.
- Derler, I., Jardin, I., Stathopoulos, P.B., Muik, M., Fahrner, M., Zayats, V., Pandey, S.K., Poteser, M., Lackner, B., Absolonova, M., Schindl, R., Groschner, K., Ettrich, R., Ikura, M. and Romanin, C. 2016. Cholesterol modulates Orai1 channel function. *Science signaling*. **9**(412),p.ra10.
- Deshmane, S.L., Kremlev, S., Amini, S. and Sawaya, B.E. 2009. Monocyte chemoattractant protein-1 (MCP-1): an overview. *Journal of interferon & cytokine research : the official journal of the International Society for Interferon and Cytokine Research*. **29**(6),pp.313–26.
- Devlin, C.M., Leventhal, A.R., Kuriakose, G., Schuchman, E.H., Williams, K.J. and Tabas, I. 2008. Acid sphingomyelinase promotes lipoprotein retention within early atheromata and accelerates lesion progression. *Arteriosclerosis, thrombosis, and vascular biology*. **28**(10),pp.1723–30.
- Dinkla, S., Wessels, K., Verdurmen, W.P.R., Tomelleri, C., Cluitmans, J.C.A., Fransen, J., Fuchs, B., Schiller, J., Joosten, I., Brock, R. and Bosman, G.J.C.G.M. 2012. Functional consequences of sphingomyelinase-induced changes in erythrocyte membrane structure. *Cell Death & Disease*. **3**(10),pp.e410–e410.
- Dong, H., Jiang, Y., Triggler, C.R., Li, X. and Lytton, J. 2006. Novel role for K⁺ - dependent Na⁺ /Ca²⁺ exchangers in regulation of cytoplasmic free Ca²⁺ and contractility in arterial smooth muscle. *American Journal of Physiology-Heart and Circulatory Physiology*. **291**(3),pp.H1226–H1235.
- Dong, Y.Y., Pike, A.C.W., Mackenzie, A., McClenaghan, C., Aryal, P., Dong, L., Quigley, A., Grieben, M., Goubin, S., Mukhopadhyay, S., Ruda, G.F., Clausen, M. V., Cao, L., Brennan, P.E., Burgess-Brown, N.A., Sansom, M.S.P., Tucker, S.J. and Carpenter, E.P. 2015. K2P channel gating mechanisms revealed by structures of TREK-2 and a complex with Prozac.

- Science*. **347**(6227),pp.1256–1259.
- Draper, J.M., Xia, Z., Smith, R.A., Zhuang, Y., Wang, W. and Smith, C.D. 2011. Discovery and Evaluation of Inhibitors of Human Ceramidase. *Molecular Cancer Therapeutics*. **10**(11),pp.2052–2061.
- Duan, R. 2006. Alkaline sphingomyelinase: An old enzyme with novel implications. *Biochimica et Biophysica Acta (BBA) - Molecular and Cell Biology of Lipids*. **1761**(3),pp.281–291.
- Dubin, A.E., Murthy, S., Lewis, A.H., Brosse, L., Cahalan, S.M., Grandl, J., Coste, B. and Patapoutian, A. 2017. Endogenous Piezo1 Can Confound Mechanically Activated Channel Identification and Characterization. *Neuron*. **94**(2),p.266–270.e3.
- Dubin, A.E., Schmidt, M., Mathur, J., Petrus, M.J., Xiao, B., Coste, B. and Patapoutian, A. 2012. Inflammatory signals enhance piezo2-mediated mechanosensitive currents. *Cell reports*. **2**(3),pp.511–7.
- Eder, P. and Groschner, K. 2008. TRPC3/6/7: Topical aspects of biophysics and pathophysiology. *Channels (Austin, Tex.)*. **2**(2),pp.94–9.
- Eijkelkamp, N., Linley, J.E., Torres, J.M., Bee, L., Dickenson, A.H., Gringhuis, M., Minett, M.S., Hong, G.S., Lee, E., Oh, U., Ishikawa, Y., Zwartkuis, F.J., Cox, J.J. and Wood, J.N. 2013. A role for Piezo2 in EPAC1-dependent mechanical allodynia. *Nature Communications*. **4**,p.1682.
- Eiseler, T., Döppler, H., Yan, I.K., Kitatani, K., Mizuno, K. and Storz, P. 2009. Protein kinase D1 regulates cofilin-mediated F-actin reorganization and cell motility through slingshot. *Nature cell biology*. **11**(5),pp.545–56.
- Eisenhoffer, G.T., Loftus, P.D., Yoshigi, M., Otsuna, H., Chien, C.-B., Morcos, P.A. and Rosenblatt, J. 2012. Crowding induces live cell extrusion to maintain homeostatic cell numbers in epithelia. *Nature*. **484**(7395),pp.546–549.
- Endemann, D.H. and Schiffrin, E.L. 2004. Endothelial Dysfunction. *Journal of the American Society of Nephrology*. **15**(8),pp.1983–1992.
- Epand, R.M. 2006. Cholesterol and the interaction of proteins with membrane domains. *Progress in Lipid Research*. **45**(4),pp.279–294.
- Ertel, E.A., Campbell, K.P., Harpold, M.M., Hofmann, F., Mori, Y., Perez-Reyes, E., Schwartz, A., Snutch, T.P., Tanabe, T., Birnbaumer, L., Tsien, R.W. and Catterall, W.A. 2000. Nomenclature of voltage-gated calcium channels. *Neuron*. **25**(3),pp.533–5.
- Fang, Y., Mohler, E.R., Hsieh, E., Osman, H., Hashemi, S.M., Davies, P.F., Rothblat, G.H., Wilensky, R.L. and Levitan, I. 2006. Hypercholesterolemia Suppresses Inwardly Rectifying K⁺ Channels in Aortic Endothelium In Vitro and In Vivo. *Circulation Research*. **98**(8),pp.1064–1071.
- Fantini, J. and Barrantes, F.J. 2013. How cholesterol interacts with membrane proteins: an exploration of cholesterol-binding sites including CRAC, CARC, and tilted domains. *Frontiers in physiology*. **4**,p.31.
- Faucherre, A., Nargeot, J., Mangoni, M.E. and Jopling, C. 2013. Piezo2B Regulates Vertebrate Light Touch Response. *The Journal of neuroscience : the official journal of the Society for Neuroscience*. **33**(43),pp.17089–17094.
- Fiser, A. and Šali, A. 2003. Modeller: Generation and refinement of homology-based protein structure models. *Methods Enzymol*. **374**,pp.461–491.
- Fotiou, E., Martin-Almedina, S., Simpson, M.A., Lin, S., Gordon, K., Brice, G., Atton, G., Jeffery, I., Rees, D.C., Mignot, C., Vogt, J., Homfray, T., Snyder, M.P., Rockson, S.G., Jeffery, S., Mortimer, P.S., Mansour, S. and

- Ostergaard, P. 2015. Novel mutations in PIEZO1 cause an autosomal recessive generalized lymphatic dysplasia with non-immune hydrops fetalis. *Nature communications*. **6**,p.8085.
- Franz-Wachtel, M., Eisler, S.A., Krug, K., Wahl, S., Carpy, A., Nordheim, A., Pfizenmaier, K., Hausser, A. and Macek, B. 2012. Global Detection of Protein Kinase D-dependent Phosphorylation Events in Nocodazole-treated Human Cells. *Molecular & Cellular Proteomics*. **11**(5),pp.160–170.
- Ganapathi, S.B., Fox, T.E., Kester, M. and Elmslie, K.S. 2010. Ceramide modulates HERG potassium channel gating by translocation into lipid rafts. *American Journal of Physiology-Cell Physiology*. **299**(1),pp.C74–C86.
- Gangoiti, P., Granado, M.H., Wang, S.W., Kong, J.Y., Steinbrecher, U.P. and Gómez-Muñoz, A. 2008. Ceramide 1-phosphate stimulates macrophage proliferation through activation of the PI3-kinase/PKB, JNK and ERK1/2 pathways. *Cellular Signalling*. **20**(4),pp.726–736.
- Gatt, S. 1963. Enzymic hydrolysis and synthesis of ceramides. *The Journal of biological chemistry*. **238**,pp.3131–3.
- Gatt, S. 1976. Magnesium-dependent sphingomyelinase. *Biochemical and Biophysical Research Communications*. **68**(1),pp.235–241.
- Ge, J., Li, W., Zhao, Q., Li, N., Chen, M., Zhi, P., Li, R., Gao, N., Xiao, B. and Yang, M. 2015. Architecture of the mammalian mechanosensitive Piezo1 channel. *Nature*.
- Geng, Y.-J. and Libby, P. 2002. Progression of atheroma: a struggle between death and procreation. *Arteriosclerosis, thrombosis, and vascular biology*. **22**(9),pp.1370–80.
- Ghanam, K., Javellaud, J., Ea-Kim, L. and Oudart, N. 2000. Effects of treatment with 17beta-estradiol on the hypercholesterolemic rabbit middle cerebral artery. *Maturitas*. **34**(3),pp.249–60.
- Gimpl, G., Burger, K. and Fahrenholz, F. 1997. Cholesterol as Modulator of Receptor Function †. *Biochemistry*. **36**(36),pp.10959–10974.
- Gnanasambandam, R., Bae, C., Gottlieb, P.A. and Sachs, F. 2015. Ionic Selectivity and Permeation Properties of Human PIEZO1 Channels. S. Barnes, ed. *PLoS one*. **10**(5),p.e0125503.
- Goldschmidt-Clermont, P.J., Creager, M.A., Losordo, D.W., Lorsordo, D.W., Lam, G.K.W., Wassef, M. and Dzau, V.J. 2007. Subendothelial Lipoprotein Retention as the Initiating Process in Atherosclerosis: Update and Therapeutic Implications. *Circulation*. **116**,pp.1832–1844.
- Gomez-Muñoz, A., Duffy, P.A., Martin, A., O'Brien, L., Byun, H.S., Bittman, R. and Brindley, D.N. 1995. Short-chain ceramide-1-phosphates are novel stimulators of DNA synthesis and cell division: antagonism by cell-permeable ceramides. *Molecular pharmacology*. **47**(5),pp.833–9.
- Gomez-Muñoz, A., Frago, L.M., Alvarez, L. and Varela-Nieto, I. 1997. Stimulation of DNA synthesis by natural ceramide 1-phosphate. *The Biochemical journal*. **325 (Pt 2)**(Pt 2),pp.435–40.
- Gómez-Muñoz, A., Gangoiti, P., Granado, M.H., Arana, L. and Ouro, A. 2013. Ceramide 1-Phosphate in Cell Survival and Inflammatory Signaling.
- Gómez-Muñoz, A., Kong, J.Y., Salh, B. and Steinbrecher, U.P. 2004. Ceramide-1-phosphate blocks apoptosis through inhibition of acid sphingomyelinase in macrophages. *Journal of Lipid Research*. **45**(1),pp.99–105.
- Goñi, F.M. and Alonso, A. 2002. Sphingomyelinases: enzymology and membrane activity. *FEBS letters*. **531**(1),pp.38–46.

- Gottlieb, P.A., Bae, C. and Sachs, F. 2012. Gating the mechanical channel Piezo1: a comparison between whole-cell and patch recording. *Channels*. **6**(4),pp.282–289.
- Gottlieb, P.A. and Sachs, F. 2012. Piezo1: properties of a cation selective mechanical channel. *Channels*. **6**(4),pp.214–219.
- Gräler, M.H., Bernhardt, G. and Lipp, M. 1999. A lymphoid tissue-specific receptor, EDG6, with potential immune modulatory functions mediated by extracellular lysophospholipids. *Current topics in microbiology and immunology*. **246**,p.131–6; discussion 137.
- Gräler, M.H., Grosse, R., Kusch, A., Kremmer, E., Gudermann, T. and Lipp, M. 2003. The sphingosine 1-phosphate receptor S1P₄ regulates cell shape and motility via coupling to G_i and G_{12/13}. *Journal of Cellular Biochemistry*. **89**(3),pp.507–519.
- Grassme, H., Jekle, A., Riehle, A., Schwarz, H., Berger, J., Sandhoff, K., Kolesnick, R. and Gulbins, E. 2001. CD95 signaling via ceramide-rich membrane rafts. *The Journal of biological chemistry*. **276**(23),pp.20589–96.
- Gray, P.C., Scott, J.D. and Catterall, W.A. 1998. Regulation of ion channels by cAMP-dependent protein kinase and A-kinase anchoring proteins. *Current Opinion in Neurobiology*. **8**(3),pp.330–334.
- Grimm, C., Kraft, R., Schultz, G. and Harteneck, C. 2005. Activation of the melastatin-related cation channel TRPM3 by D-erythro-sphingosine [corrected]. *Molecular pharmacology*. **67**(3),pp.798–805.
- Gudipaty, S.A., Lindblom, J., Loftus, P.D., Redd, M.J., Edes, K., Davey, C.F., Krishnegowda, V. and Rosenblatt, J. 2017. Mechanical stretch triggers rapid epithelial cell division through Piezo1. *Nature*. **543**(7643),pp.118–121.
- Gulbins, E. 2003. Regulation of death receptor signaling and apoptosis by ceramide. *Pharmacological Research*. **47**(5),pp.393–399.
- Guo, Y.R. and MacKinnon, R. 2017. Structure-based membrane dome mechanism for Piezo mechanosensitivity. *eLife*. **6**,p.e33660.
- Hait, N.C., Allegood, J., Maceyka, M., Strub, G.M., Harikumar, K.B., Singh, S.K., Luo, C., Marmorstein, R., Kordula, T., Milstien, S. and Spiegel, S. 2009. Regulation of histone acetylation in the nucleus by sphingosine-1-phosphate. *Science (New York, N.Y.)*. **325**(5945),pp.1254–7.
- Hait, N.C., Oskeritzian, C.A., Paugh, S.W., Milstien, S. and Spiegel, S. 2006. Sphingosine kinases, sphingosine 1-phosphate, apoptosis and diseases. *Biochimica et Biophysica Acta (BBA) - Biomembranes*. **1758**(12),pp.2016–2026.
- Hait, N.C., Sarkar, S., Le Stunff, H., Mikami, A., Maceyka, M., Milstien, S. and Spiegel, S. 2005. Role of sphingosine kinase 2 in cell migration toward epidermal growth factor. *The Journal of biological chemistry*. **280**(33),pp.29462–9.
- Hajdú, P., Varga, Z., Pieri, C., Panyi, G. and Gáspár, R. 2003. Cholesterol modifies the gating of Kv1.3 in human T lymphocytes. *Pflügers Archiv : European journal of physiology*. **445**(6),pp.674–82.
- Hankins, J.L., Ward, K.E., Linton, S.S., Barth, B.M., Stahelin, R. V, Fox, T.E. and Kester, M. 2013. Ceramide 1-phosphate mediates endothelial cell invasion via the annexin a2-p11 heterotetrameric protein complex. *The Journal of biological chemistry*. **288**(27),pp.19726–38.
- Hannun, Y.A. and Obeid, L.M. 2008. Principles of bioactive lipid signalling:

- lessons from sphingolipids. *Nature Reviews Molecular Cell Biology*. **9**(2),pp.139–150.
- Harrington, L.S., Evans, R.J., Wray, J., Norling, L., Swales, K.E., Vial, C., Ali, F., Carrier, M.J. and Mitchell, J.A. 2007. Purinergic 2X1 Receptors Mediate Endothelial Dependent Vasodilation to ATP. *Molecular Pharmacology*. **72**(5),pp.1132–1136.
- Hartmannsgruber, V., Heyken, W.-T.T., Kacik, M., Kaistha, A., Grgic, I., Harteneck, C., Liedtke, W., Hoyer, J., Köhler, R. and Köhler, R. 2007. Arterial response to shear stress critically depends on endothelial TRPV4 expression. *PLoS ONE*. **2**(9),p.e827.
- Häse, C.C., Le Dain, A.C. and Martinac, B. 1995. Purification and functional reconstitution of the recombinant large mechanosensitive ion channel (MscL) of *Escherichia coli*. *The Journal of biological chemistry*. **270**(31),pp.18329–34.
- Heaps, C.L., Tharp, D.L. and Bowles, D.K. 2005. Hypercholesterolemia abolishes voltage-dependent K⁺ channel contribution to adenosine-mediated relaxation in porcine coronary arterioles. *American Journal of Physiology-Heart and Circulatory Physiology*. **288**(2),pp.H568–H576.
- Heinrich, M., Neumeyer, J., Jakob, M., Hallas, C., Tchikov, V., Winoto-Morbach, S., Wickel, M., Schneider-Brachert, W., Trauzold, A., Hethke, A. and Schütze, S. 2004. Cathepsin D links TNF-induced acid sphingomyelinase to Bid-mediated caspase-9 and -3 activation. *Cell death and differentiation*. **11**(5),pp.550–63.
- Hess, B., Kutzner, C., van der Spoel, D. and Lindahl, E. 2008. GROMACS 4: algorithms for highly efficient, load-balanced, and scalable molecular simulation. *J. Chem. Theory Comput.* **4**(3),pp.435–447.
- Hinkovska-Galcheva, V., Boxer, L.A., Kindzelskii, A., Hiraoka, M., Abe, A., Goparju, S., Spiegel, S., Petty, H.R. and Shayman, J.A. 2005. Ceramide 1-Phosphate, a Mediator of Phagocytosis. *Journal of Biological Chemistry*. **280**(28),pp.26612–26621.
- Hinkovska-Galcheva, V.T., Boxer, L.A., Mansfield, P.J., Harsh, D., Blackwood, A. and Shayman, J.A. 1998. The formation of ceramide-1-phosphate during neutrophil phagocytosis and its role in liposome fusion. *The Journal of biological chemistry*. **273**(50),pp.33203–9.
- Hofmann, K., Tomiuk, S., Wolff, G. and Stoffel, W. 2000. Cloning and characterization of the mammalian brain-specific, Mg²⁺-dependent neutral sphingomyelinase. *Proceedings of the National Academy of Sciences of the United States of America*. **97**(11),pp.5895–900.
- Hojjati, M.R., Li, Z., Zhou, H., Tang, S., Huan, C., Ooi, E., Lu, S. and Jiang, X.-C. 2005. Effect of myriocin on plasma sphingolipid metabolism and atherosclerosis in apoE-deficient mice. *The Journal of biological chemistry*. **280**(11),pp.10284–9.
- Horinouchi, K., Erlich, S., Perl, D.P., Ferlinz, K., Bisgaier, C.L., Sandhoff, K., Desnick, R.J., Stewart, C.L. and Schuchman, E.H. 1995. Acid sphingomyelinase deficient mice: a model of types A and B Niemann–Pick disease. *Nature Genetics*. **10**(3),pp.288–293.
- Hornbeck, P. V, Zhang, B., Murray, B., Kornhauser, J.M., Latham, V. and Skrzypek, E. 2015. PhosphoSitePlus, 2014: mutations, PTMs and recalibrations. *Nucleic Acids Research*. **43**.
- Hwang, Y., Tani, M., Nakagawa, T., Okino, N. and Ito, M. 2005. Subcellular localization of human neutral ceramidase expressed in HEK293 cells.

- Biochemical and Biophysical Research Communications*. **331**(1),pp.37–42.
- Ichikawa, S. and Hirabayashi, Y. 1998. Glucosylceramide synthase and glycosphingolipid synthesis. *Trends in cell biology*. **8**(5),pp.198–202.
- Igarashi, Y., Hakomori, S., Toyokuni, T., Dean, B., Fujita, S., Sugimoto, M., Ogawa, T., El-Ghendy, K. and Racker, E. 1989. Effect of chemically well-defined sphingosine and its N-methyl derivatives on protein kinase C and src kinase activities. *Biochemistry*. **28**(17),pp.6796–6800.
- Im, D.S., Heise, C.E., Ancellin, N., O'Dowd, B.F., Shei, G.J., Heavens, R.P., Rigby, M.R., Hla, T., Mandala, S., McAllister, G., George, S.R. and Lynch, K.R. 2000. Characterization of a novel sphingosine 1-phosphate receptor, Edg-8. *The Journal of biological chemistry*. **275**(19),pp.14281–6.
- Ittaman, S. V, VanWormer, J.J. and Rezkalla, S.H. 2014. The role of aspirin in the prevention of cardiovascular disease. *Clinical medicine & research*. **12**(3–4),pp.147–54.
- Jackson, W.F. 2000. Ion channels and vascular tone. *Hypertension (Dallas, Tex. : 1979)*. **35**(1 Pt 2),pp.173–8.
- Jacobs, E.R., Cheliakine, C., Gebremedhin, D., Birks, E.K., Davies, P.F. and Harder, D.R. 1995. Shear activated channels in cell-attached patches of cultured bovine aortic endothelial cells. *Pflügers Archiv : European journal of physiology*. **431**(1),pp.129–131.
- Jacobson, K., Sheets, E.D. and Simson, R. 1995. Revisiting the fluid mosaic model of membranes. *Science (New York, N. Y.)*. **268**(5216),pp.1441–2.
- Jefferson, A.B. and Schulman, H. 1988. Sphingosine inhibits calmodulin-dependent enzymes. *The Journal of biological chemistry*. **263**(30),pp.15241–4.
- Jeremy, R.W. and McCarron, H. 2000. Effect of hypercholesterolemia on Ca²⁺-dependent K⁺ channel-mediated vasodilatation in vivo. *American Journal of Physiology-Heart and Circulatory Physiology*. **279**(4),pp.H1600–H1608.
- Jia, S.-J., Jin, S., Zhang, F., Yi, F., Dewey, W.L. and Li, P.-L. 2008. Formation and function of ceramide-enriched membrane platforms with CD38 during M₁-receptor stimulation in bovine coronary arterial myocytes. *American Journal of Physiology-Heart and Circulatory Physiology*. **295**(4),pp.H1743–H1752.
- Jiang, J., Thorén, P., Caligiuri, G., Hansson, G.K. and Pernow, J. 1999. Enhanced phenylephrine-induced rhythmic activity in the atherosclerotic mouse aorta via an increase in opening of K_{Ca} channels: relation to K_v channels and nitric oxide. *British Journal of Pharmacology*. **128**(3),pp.637–646.
- Jiang, L.H., Gamper, N. and Beech, D.J. 2011. Properties and therapeutic potential of transient receptor potential channels with putative roles in adversity: focus on TRPC5, TRPM2 and TRPA1. *Current drug targets*. **12**(5),pp.724–36.
- Jiang, L.I., Collins, J., Davis, R., Lin, K.-M., DeCamp, D., Roach, T., Hsueh, R., Rebres, R.A., Ross, E.M., Taussig, R., Fraser, I. and Sternweis, P.C. 2007. Use of a cAMP BRET sensor to characterize a novel regulation of cAMP by the sphingosine 1-phosphate/G13 pathway. *The Journal of biological chemistry*. **282**(14),pp.10576–84.
- Jiao, J., Garg, V., Yang, B., Elton, T.S. and Hu, K. 2008. Protein Kinase C- Induces Caveolin-Dependent Internalization of Vascular Adenosine 5'-Triphosphate-Sensitive K⁺ Channels. *Hypertension*. **52**(3),pp.499–506.
- Jin, S., Yi, F., Zhang, F., Poklis, J.L. and Li, P.-L. 2008. Lysosomal targeting

- and trafficking of acid sphingomyelinase to lipid raft platforms in coronary endothelial cells. *Arteriosclerosis, thrombosis, and vascular biology*. **28**(11),pp.2056–62.
- Johnson, K.R., Johnson, K.Y., Becker, K.P., Bielawski, J., Mao, C. and Obeid, L.M. 2003. Role of Human Sphingosine-1-phosphate Phosphatase 1 in the Regulation of Intra- and Extracellular Sphingosine-1-phosphate Levels and Cell Viability. *Journal of Biological Chemistry*. **278**(36),pp.34541–34547.
- de Jong, D.H., Singh, G., Bennett, W.F.D., Arnarez, C., Wassenaar, T.A., Schäfer, L. V, Periole, X., Tieleman, D.P. and Marrink, S.J. 2012. Improved parameters for the martini coarse-grained protein force field. *J. Chem. Theory Comput.* **9**(1),pp.687–697.
- Kanfer, J.N., Young, O.M., Shapiro, D. and Brady, R.O. 1966. The metabolism of sphingomyelin. I. Purification and properties of a sphingomyelin-cleaving enzyme from rat liver tissue. *The Journal of biological chemistry*. **241**(5),pp.1081–4.
- Katta, S., Krieg, M. and Goodman, M.B. 2015. Feeling Force: Physical and Physiological Principles Enabling Sensory Mechanotransduction. *Annual Review of Cell and Developmental Biology*. **31**(1),pp.347–371.
- Khan, B. V, Harrison, D.G., Olbrych, M.T., Alexander, R.W. and Medford, R.M. 1996. Nitric oxide regulates vascular cell adhesion molecule 1 gene expression and redox-sensitive transcriptional events in human vascular endothelial cells. *Proceedings of the National Academy of Sciences of the United States of America*. **93**(17),pp.9114–9.
- Khan, W.A., Mascarella, S.W., Lewin, A.H., Wyrick, C.D., Carroll, F.I. and Hannun, Y.A. 1991. Use of D-erythro-sphingosine as a pharmacological inhibitor of protein kinase C in human platelets. *The Biochemical journal*. **278 (Pt 2)**(Pt 2),pp.387–92.
- Kim, S., Coste, B., Chadha, A., Cook, B. and Patapoutian, A. 2012. The role of Drosophila Piezo in mechanical nociception. *Nature*. **483**(7388),pp.209–212.
- King, C.C., Zenke, F.T., Dawson, P.E., Dutil, E.M., Newton, A.C., Hemmings, B.A. and Bokoch, G.M. 2000. Sphingosine is a novel activator of 3-phosphoinositide-dependent kinase 1. *The Journal of biological chemistry*. **275**(24),pp.18108–13.
- Kirichok, Y., Krapivinsky, G. and Clapham, D.E. 2004. The mitochondrial calcium uniporter is a highly selective ion channel. *Nature*. **427**(6972),pp.360–364.
- Köhler, R. and Hoyer, J. 2007. Role of TRPV4 in the Mechanotransduction of Shear Stress in Endothelial Cells.
- Koldsø, H., Shorthouse, D., Hélie, J. and Sansom, M.S.P. 2014. Lipid Clustering Correlates with Membrane Curvature as Revealed by Molecular Simulations of Complex Lipid Bilayers C. Fradin, ed. *PLoS Computational Biology*. **10**(10),p.e1003911.
- Kolmakova, A., Kwiterovich, P., Virgil, D., Alaupovic, P., Knight-Gibson, C., Martin, S.F. and Chatterjee, S. 2004. Apolipoprotein C-I Induces Apoptosis in Human Aortic Smooth Muscle Cells via Recruiting Neutral Sphingomyelinase. *Arteriosclerosis, Thrombosis, and Vascular Biology*. **24**(2),pp.264–269.
- Kono, M., Mi, Y., Liu, Y., Sasaki, T., Allende, M.L., Wu, Y.-P., Yamashita, T. and Proia, R.L. 2004. The sphingosine-1-phosphate receptors S1P1, S1P2, and S1P3 function coordinately during embryonic angiogenesis.

- The Journal of biological chemistry*. **279**(28),pp.29367–73.
- Krause, M.R. and Regen, S.L. 2014. The Structural Role of Cholesterol in Cell Membranes: From Condensed Bilayers to Lipid Rafts. *Accounts of Chemical Research*. **47**(12),pp.3512–3521.
- Krut, O., Wiegmann, K., Kashkar, H., Yazdanpanah, B. and Krönke, M. 2006. Novel Tumor Necrosis Factor-responsive Mammalian Neutral Sphingomyelinase-3 Is a C-tail-anchored Protein. *Journal of Biological Chemistry*. **281**(19),pp.13784–13793.
- Kung, C. 2005. A possible unifying principle for mechanosensation. *Nature*. **436**(7051),pp.647–54.
- Ledoux, J., Werner, M.E., Brayden, J.E. and Nelson, M.T. 2006. Calcium-Activated Potassium Channels and the Regulation of Vascular Tone. *Physiology*. **21**(1),pp.69–78.
- Lee, I.-H., Campbell, C.R., Song, S.-H., Day, M.L., Kumar, S., Cook, D.I. and Dinudom, A. 2009. The Activity of the Epithelial Sodium Channels Is Regulated by Caveolin-1 via a Nedd4-2-dependent Mechanism. *Journal of Biological Chemistry*. **284**(19),pp.12663–12669.
- Lee, M.J., Van Brocklyn, J.R., Thangada, S., Liu, C.H., Hand, A.R., Menzeleev, R., Spiegel, S. and Hla, T. 1998. Sphingosine-1-phosphate as a ligand for the G protein-coupled receptor EDG-1. *Science (New York, N.Y.)*. **279**(5356),pp.1552–5.
- Lee, M.J., Thangada, S., Claffey, K.P., Ancellin, N., Liu, C.H., Kluk, M., Volpi, M., Sha'afi, R.I. and Hla, T. 1999. Vascular endothelial cell adherens junction assembly and morphogenesis induced by sphingosine-1-phosphate. *Cell*. **99**(3),pp.301–12.
- Levade, T., Gatt, S., Maret, A. and Salvayre, R. 1991. Different pathways of uptake and degradation of sphingomyelin by lymphoblastoid cells and the potential participation of the neutral sphingomyelinase. *The Journal of biological chemistry*. **266**(21),pp.13519–29.
- Lewis, A.H. and Grandl, J. 2015. Mechanical sensitivity of Piezo1 ion channels can be tuned by cellular membrane tension. *eLife*. **4**.
- Lewis, D.F. V and Dickins, M. 2003. Baseline lipophilicity relationships in human cytochromes P450 associated with drug metabolism. *Drug metabolism reviews*. **35**(1),pp.1–18.
- Lewis, R.S. 2011. Store-Operated Calcium Channels: New Perspectives on Mechanism and Function. *Cold Spring Harbor Perspectives in Biology*. **3**(12),pp.a003970–a003970.
- Li, C., Reznia, S., Kammerer, S., Sokolowski, A., Devaney, T., Gorischek, A., Jahn, S., Hackl, H., Groschner, K., Windpassinger, C., Malle, E., Bauernhofer, T. and Schreibmayer, W. 2015. Piezo1 forms mechanosensitive ion channels in the human MCF-7 breast cancer cell line. *Scientific reports*. **5**(1),p.8364.
- Li, H. and Papadopoulos, V. 1998. Peripheral-Type Benzodiazepine Receptor Function in Cholesterol Transport. Identification of a Putative Cholesterol Recognition/Interaction Amino Acid Sequence and Consensus Pattern ¹. *Endocrinology*. **139**(12),pp.4991–4997.
- Li, J., Cubbon, R.M., Wilson, L.A., Amer, M.S., McKeown, L., Hou, B., Majeed, Y., Tumova, S., Seymour, V.A.L., Taylor, H., Stacey, M., O'Regan, D., Foster, R., Porter, K.E., Kearney, M.T. and Beech, D.J. 2011. Orai1 and CRAC Channel Dependence of VEGF-Activated Ca²⁺ Entry and Endothelial Tube Formation. *Circulation Research*. **108**(10),pp.1190–1198.

- Li, J., Hou, B., Tumova, S., Muraki, K., Bruns, A., Ludlow, M.J.M.J., Sedo, A., Hyman, A.J.A.J., McKeown, L., Young, R.S.R.S., Yuldasheva, N.Y.N.Y., Majeed, Y., Wilson, L.A.L.A., Rode, B., Bailey, M.A.M.A., Kim, H.R.H.R., Fu, Z., Carter, D.A.L.D.A.L., Bilton, J., Imrie, H., Ajuh, P., Dear, T.N.N., Cubbon, R.M.R.M., Kearney, M.T.M.T., Prasad, R.K., Evans, P.C.P.C., Ainscough, J.F.X.J.F.X., Beech, D.J.D.J., Prasad, K.R., Evans, P.C.P.C., Ainscough, J.F.X.J.F.X. and Beech, D.J.D.J. 2014. Piezo1 integration of vascular architecture with physiological force. *Nature*. **515**(7526).
- Li, J., Sukumar, P., Milligan, C.J., Kumar, B., Ma, Z.-Y., Munsch, C.M., Jiang, L.-H., Porter, K.E. and Beech, D.J. 2008. Interactions, functions, and independence of plasma membrane STIM1 and TRPC1 in vascular smooth muscle cells. *Circulation research*. **103**(8),pp.e97-104.
- Libby, P. 2012. Inflammation in Atherosclerosis. *Arteriosclerosis, Thrombosis, and Vascular Biology*. **32**(9),pp.2045–2051.
- Limaye, V. 2008. The Role of Sphingosine Kinase and Sphingosine-1-Phosphate in the Regulation of Endothelial Cell Biology. *Endothelium*. **15**(3),pp.101–112.
- Lin, S., Fagan, K.A., Li, K.X., Shaul, P.W., Cooper, D.M. and Rodman, D.M. 2000. Sustained endothelial nitric-oxide synthase activation requires capacitative Ca²⁺ entry. *The Journal of biological chemistry*. **275**(24),pp.17979–85.
- Liu, B., Hassler, D.F., Smith, G.K., Weaver, K. and Hannun, Y.A. 1998. Purification and characterization of a membrane bound neutral pH optimum magnesium-dependent and phosphatidylserine-stimulated sphingomyelinase from rat brain. *The Journal of biological chemistry*. **273**(51),pp.34472–9.
- Liu, C. and Montell, C. 2015. Forcing open TRP channels: Mechanical gating as a unifying activation mechanism. *Biochemical and biophysical research communications*. **460**(1),pp.22–5.
- Liu, F., Li, X., Lu, C., Bai, A., Bielawski, J., Bielawska, A., Marshall, B., Schoenlein, P. V., Lebedyeva, I.O. and Liu, K. 2016. Ceramide activates lysosomal cathepsin B and cathepsin D to attenuate autophagy and induces ER stress to suppress myeloid-derived suppressor cells. *Oncotarget*. **7**(51),pp.83907–83925.
- Liu, Y., Wada, R., Yamashita, T., Mi, Y., Deng, C.X., Hobson, J.P., Rosenfeldt, H.M., Nava, V.E., Chae, S.S., Lee, M.J., Liu, C.H., Hla, T., Spiegel, S. and Proia, R.L. 2000. Edg-1, the G protein-coupled receptor for sphingosine-1-phosphate, is essential for vascular maturation. *The Journal of clinical investigation*. **106**(8),pp.951–61.
- Lopes Pinheiro, M.A., Kroon, J., Hoogenboezem, M., Geerts, D., van het Hof, B., van der Pol, S.M.A., van Buul, J.D. and de Vries, H.E. 2016. Acid Sphingomyelinase–Derived Ceramide Regulates ICAM-1 Function during T Cell Transmigration across Brain Endothelial Cells. *The Journal of Immunology*. **196**(1),pp.72–79.
- López-Montero, I., Rodríguez, N., Cribier, S., Pohl, A., Vélez, M. and Devaux, P.F. 2005. Rapid Transbilayer Movement of Ceramides in Phospholipid Vesicles and in Human Erythrocytes. *Journal of Biological Chemistry*. **280**(27),pp.25811–25819.
- Lukacs, V., Mathur, J., Mao, R., Bayrak-Toydemir, P., Procter, M., Cahalan, S.M., Kim, H.J., Bandell, M., Longo, N., Day, R.W., Stevenson, D.A., Patapoutian, A. and Krock, B.L. 2015. Impaired PIEZO1 function in

- patients with a novel autosomal recessive congenital lymphatic dysplasia. *Nature communications*. **6**,p.8329.
- Lukacs, V., Thyagarajan, B., Varnai, P., Balla, A., Balla, T. and Rohacs, T. 2007. Dual Regulation of TRPV1 by Phosphoinositides. *Journal of Neuroscience*. **27**(26),pp.7070–7080.
- Lukacs, V., Yudin, Y., Hammond, G.R., Sharma, E., Fukami, K. and Rohacs, T. 2013. Distinctive changes in plasma membrane phosphoinositides underlie differential regulation of TRPV1 in nociceptive neurons. *The Journal of neuroscience : the official journal of the Society for Neuroscience*. **33**(28),pp.11451–63.
- Lundbæk, J.A. and Andersen, O.S. 1999. Spring Constants for Channel-Induced Lipid Bilayer Deformations Estimates Using Gramicidin Channels. *Biophysical Journal*. **76**(2),pp.889–895.
- Lundbæk, J.A., Birn, P., Girshman, J., Hansen, A.J. and Andersen, O.S. 1996. Membrane Stiffness and Channel Function †. *Biochemistry*. **35**(12),pp.3825–3830.
- Lundbæk, J.A., Birn, P., Hansen, A.J., Søgaard, R., Nielsen, C., Girshman, J., Bruno, M.J., Tape, S.E., Egebjerg, J., Greathouse, D. V., Mattice, G.L., Koeppe, R.E. and Andersen, O.S. 2004. Regulation of Sodium Channel Function by Bilayer Elasticity. *The Journal of General Physiology*. **123**(5),pp.599–621.
- Lundbaek, J.A., Koeppe, R.E. and Andersen, O.S. 2010. Amphiphile regulation of ion channel function by changes in the bilayer spring constant. *Proceedings of the National Academy of Sciences*. **107**(35),pp.15427–15430.
- Lusis, A.J. 2000. Atherosclerosis. *Nature* **2000** 407:6801.
- Ma, Y., Pitson, S., Hercus, T., Murphy, J., Lopez, A. and Woodcock, J. 2005. Sphingosine activates protein kinase A type II by a novel cAMP-independent mechanism. *The Journal of biological chemistry*. **280**(28),pp.26011–7.
- Maceyka, M., Harikumar, K.B., Milstien, S. and Spiegel, S. 2012. Sphingosine-1-phosphate signaling and its role in disease. *Trends in cell biology*. **22**(1),pp.50–60.
- Maingret, F., Patel, A.J., Lesage, F., Lazdunski, M. and Honoré, E. 2000. Lysophospholipids open the two-pore domain mechano-gated K(+) channels TREK-1 and TRAAK. *The Journal of biological chemistry*. **275**(14),pp.10128–33.
- Maiolino, G., Rossitto, G., Caielli, P., Bisogni, V., Rossi, G.P. and Calò, L.A. 2013. The role of oxidized low-density lipoproteins in atherosclerosis: the myths and the facts. *Mediators of inflammation*. **2013**,p.714653.
- Malek, R.L., Toman, R.E., Edsall, L.C., Wong, S., Chiu, J., Letterle, C.A., Van Brocklyn, J.R., Milstien, S., Spiegel, S. and Lee, N.H. 2001. Nrg-1 belongs to the endothelial differentiation gene family of G protein-coupled sphingosine-1-phosphate receptors. *The Journal of biological chemistry*. **276**(8),pp.5692–9.
- Mandon, E.C., Ehse, I., Rother, J., van Echten, G. and Sandhoff, K. 1992. Subcellular localization and membrane topology of serine palmitoyltransferase, 3-dehydrosphinganine reductase, and sphinganine N-acyltransferase in mouse liver. *The Journal of biological chemistry*. **267**(16),pp.11144–8.
- Mao, C. and Obeid, L.M. 2008. Ceramidases: regulators of cellular responses

- mediated by ceramide, sphingosine, and sphingosine-1-phosphate. *Biochimica et biophysica acta*. **1781**(9),pp.424–34.
- Marathe, S., Kuriakose, G., Williams, K.J. and Tabas, I. 1999. Sphingomyelinase, an enzyme implicated in atherogenesis, is present in atherosclerotic lesions and binds to specific components of the subendothelial extracellular matrix. *Arteriosclerosis, thrombosis, and vascular biology*. **19**(11),pp.2648–58.
- Marathe, S., Schissel, S.L., Yellin, M.J., Beatini, N., Mintzer, R., Williams, K.J. and Tabas, I. 1998. Human vascular endothelial cells are a rich and regulatable source of secretory sphingomyelinase. Implications for early atherogenesis and ceramide-mediated cell signaling. *The Journal of biological chemistry*. **273**(7),pp.4081–8.
- Marchesini, N. and Hannun, Y.A. 2004. Acid and neutral sphingomyelinases: roles and mechanisms of regulation. *Biochemistry and Cell Biology*. **82**(1),pp.27–44.
- Marrink, S.J. and Tieleman, D.P. 2013. Perspective on the Martini model. *Chem. Soc. Rev.* **42**(16),pp.6801–6822.
- Marsh, D. and Barrantes, F.J. 1978. Immobilized lipid in acetylcholine receptor-rich membranes from *Torpedo marmorata*. *Proceedings of the National Academy of Sciences of the United States of America*. **75**(9),pp.4329–33.
- Martinac, B., Adler, J. and Kung, C. 1990. Mechanosensitive ion channels of *E. coli* activated by amphipaths. *Nature*. **348**(6298),pp.261–263.
- Matecki, A. and Pawelczyk, T. 1997. Regulation of phospholipase C δ 1 by sphingosine. *Biochimica et Biophysica Acta (BBA) - Biomembranes*. **1325**(2),pp.287–296.
- Mathes, C., Fleig, A. and Penner, R. 1998. Calcium release-activated calcium current (ICRAC) is a direct target for sphingosine. *The Journal of biological chemistry*. **273**(39),pp.25020–30.
- McDonald, O.B., Hannun, Y.A., Reynolds, C.H. and Sahyoun, N. 1991. Activation of casein kinase II by sphingosine. *The Journal of biological chemistry*. **266**(32),pp.21773–6.
- McHugh, B.J., Buttery, R., Lad, Y., Banks, S., Haslett, C. and Sethi, T. 2010. Integrin activation by Fam38A uses a novel mechanism of R-Ras targeting to the endoplasmic reticulum. *Journal of cell science*. **123**(Pt 1),pp.51–61.
- McHugh, B.J., Murdoch, A., Haslett, C. and Sethi, T. 2012. Loss of the integrin-activating transmembrane protein Fam38A (Piezo1) promotes a switch to a reduced integrin-dependent mode of cell migration. *PloS one*. **7**(7),p.e40346.
- Meacci, E., Vasta, V., Neri, S., Farnararo, M. and Bruni, P. 1996. Activation of Phospholipase D in Human Fibroblasts by Ceramide and Sphingosine: Evaluation of Their Modulatory Role in Bradykinin Stimulation of Phospholipase D. *Biochemical and Biophysical Research Communications*. **225**(2),pp.392–399.
- van Meer, G., Voelker, D.R. and Feigenson, G.W. 2008. Membrane lipids: where they are and how they behave. *Nature Reviews Molecular Cell Biology*. **9**(2),pp.112–124.
- Megha and London, E. 2004. Ceramide selectively displaces cholesterol from ordered lipid domains (rafts): implications for lipid raft structure and function. *The Journal of biological chemistry*. **279**(11),pp.9997–10004.
- Michel, C. and van Echten-Deckert, G. 1997. Conversion of dihydroceramide to ceramide occurs at the cytosolic face of the endoplasmic reticulum. *FEBS*

- letters*. **416**(2),pp.153–5.
- Mickus, D.E., Levitt, D.G. and Rychnovsky, S.D. 1992. Enantiomeric cholesterol as a probe of ion-channel structure. *Journal of the American Chemical Society*. **114**(1),pp.359–360.
- Milescu, M., Bosmans, F., Lee, S., Alabi, A.A., Kim, J. II and Swartz, K.J. 2009. Interactions between lipids and voltage sensor paddles detected with tarantula toxins. *Nature Structural & Molecular Biology*. **16**(10),pp.1080–1085.
- Mitsutake, S., Kim, T.-J., Inagaki, Y., Kato, M., Yamashita, T. and Igarashi, Y. 2004. Ceramide Kinase Is a Mediator of Calcium-dependent Degranulation in Mast Cells. *Journal of Biological Chemistry*. **279**(17),pp.17570–17577.
- Miyamoto, T., Mochizuki, T., Nakagomi, H., Kira, S., Watanabe, M., Takayama, Y., Suzuki, Y., Koizumi, S., Takeda, M. and Tominaga, M. 2014. Functional role for Piezo1 in stretch-evoked Ca²⁺ influx and ATP release in urothelial cell cultures. *The Journal of biological chemistry*. **289**(23),pp.16565–16575.
- Mogami, K., Kishi, H. and Kobayashi, S. 2005. Sphingomyelinase causes endothelium-dependent vasorelaxation through endothelial nitric oxide production without cytosolic Ca²⁺ elevation. *FEBS Letters*. **579**(2),pp.393–397.
- Monticelli, L., Kandasamy, S.K., Periole, X., Larson, R.G., Tieleman, D.P. and Marrink, S.-J. 2008. The MARTINI coarse-grained force field: extension to proteins. *J. Chem. Theory Comput.* **4**(5),pp.819–834.
- Moore, K.J. and Tabas, I. 2011. Macrophages in the Pathogenesis of Atherosclerosis. *Cell*. **145**(3),pp.341–355.
- Morachevskaya, E., Sudarikova, A. and Negulyaev, Y. 2007. Mechanosensitive channel activity and F-actin organization in cholesterol-depleted human leukaemia cells. *Cell biology international*. **31**(4),pp.374–81.
- Morello, F., Perino, A. and Hirsch, E. 2008. Phosphoinositide 3-kinase signalling in the vascular system. *Cardiovascular Research*. **82**(2),pp.261–271.
- Müller, G., Ayoub, M., Storz, P., Rennecke, J., Fabbro, D. and Pfizenmaier, K. 1995. PKC zeta is a molecular switch in signal transduction of TNF-alpha, bifunctionally regulated by ceramide and arachidonic acid. *The EMBO journal*. **14**(9),pp.1961–9.
- Munaron, L. and Fiorio Pla, A. 2009. Endothelial calcium machinery and angiogenesis: understanding physiology to interfere with pathology. *Current medicinal chemistry*. **16**(35),pp.4691–703.
- Münzel, T., Sinning, C., Post, F., Warnholtz, A. and Schulz, E. 2008. Pathophysiology, diagnosis and prognostic implications of endothelial dysfunction. *Annals of Medicine*. **40**(3),pp.180–196.
- Muramatsu, M., Tyler, R.C., Rodman, D.M. and McMurtry, I.F. 1997. Possible role of T-type Ca²⁺ channels in L-NNA vasoconstriction of hypertensive rat lungs. *American Journal of Physiology-Heart and Circulatory Physiology*. **272**(6),pp.H2616–H2621.
- Murohara, T., Kugiyama, K., Ohgushi, M., Sugiyama, S., Ohta, Y. and Yasue, H. 1996. Effects of sphingomyelinase and sphingosine on arterial vasomotor regulation. *Journal of lipid research*. **37**(7),pp.1601–8.
- Najibi, S. and Cohen, R.A. 1995. Enhanced role of K⁺ channels in relaxations of hypercholesterolemic rabbit carotid artery to NO. *American Journal of Physiology-Heart and Circulatory Physiology*. **269**(3),pp.H805–H811.

- Najibi, S., Cowan, C.L., Palacino, J.J. and Cohen, R.A. 1994. Enhanced role of potassium channels in relaxations to acetylcholine in hypercholesterolemic rabbit carotid artery. *American Journal of Physiology-Heart and Circulatory Physiology*. **266**(5),pp.H2061–H2067.
- Nakamura, H., Wakita, S., Yasufuku, K., Makiyama, T., Waraya, M., Hashimoto, N. and Murayama, T. 2015. Sphingomyelin Regulates the Activity of Secretory Phospholipase A₂ in the Plasma Membrane. *Journal of Cellular Biochemistry*. **116**(9),pp.1898–1907.
- Nakazono, M., Nanbu, S., Uesaki, A., Kuwano, R., Kashiwabara, M. and Zaito, K. 2007. Bisindolylmaleimides with Large Stokes Shift and Long-Lasting Chemiluminescence Properties. *Organic Letters*. **9**(18),pp.3583–3586.
- Natarajan, V., Jayaram, H.N., Scribner, W.M. and Garcia, J.G. 1994. Activation of endothelial cell phospholipase D by sphingosine and sphingosine-1-phosphate. *American Journal of Respiratory Cell and Molecular Biology*. **11**(2),pp.221–229.
- Navar, L.G., Inscho, E.W., Majid, S.A., Imig, J.D., Harrison-Bernard, L.M. and Mitchell, K.D. 1996. Paracrine regulation of the renal microcirculation. *Physiological reviews*. **76**(2),pp.425–536.
- Niaudet, C., Bonnaud, S., Guillonnet, M., Gouard, S., Gaugler, M.-H., Dutoit, S., Ripoche, N., Dubois, N., Trichet, V., Corre, I. and Paris, F. 2017. Plasma membrane reorganization links acid sphingomyelinase/ceramide to p38 MAPK pathways in endothelial cells apoptosis. *Cellular Signalling*. **33**,pp.10–21.
- Nichols, M., Townsend, N. and Luengo-Fernandez, R. 2012. European Cardiovascular Disease Statistics: 2012 edition. *Brussels: European Heart Network*.
- Nishino, H., Kitagawa, K., Iwashima, A., Ito, M., Tanaka, T. and Hidaka, H. 1986. N-(6-Phenylhexyl)-5-chloro-1-naphthalenesulfonamide is one of a new class of activators for Ca²⁺-activated, phospholipid-dependent protein kinase. *Biochimica et Biophysica Acta (BBA) - Molecular Cell Research*. **889**(2),pp.236–239.
- Noda, M., Shimizu, S., Tanabe, T., Takai, T., Kayano, T., Ikeda, T., Takahashi, H., Nakayama, H., Kanaoka, Y., Minamino, N., Kangawa, K., Matsuo, H., Raftery, M.A., Hirose, T., Inayama, S., Hayashida, H., Miyata, T. and Numa, S. 1984. Primary structure of Electrophorus electricus sodium channel deduced from cDNA sequence. *Nature*. **312**(5990),pp.121–127.
- Norum, J.H., Méthi, T., Mattingly, R.R. and Levy, F.O. 2005. Endogenous expression and protein kinase A-dependent phosphorylation of the guanine nucleotide exchange factor Ras-GRF1 in human embryonic kidney 293 cells. *FEBS Journal*. **272**(9),pp.2304–2316.
- Nourse, J.L. and Pathak, M.M. 2017. How cells channel their stress: Interplay between Piezo1 and the cytoskeleton. *Seminars in Cell & Developmental Biology*. **71**,pp.3–12.
- Numazaki, M., Tominaga, T., Toyooka, H. and Tominaga, M. 2002. Direct phosphorylation of capsaicin receptor VR1 by protein kinase Cepsilon and identification of two target serine residues. *The Journal of biological chemistry*. **277**(16),pp.13375–8.
- Ohta, H., Sweeney, E.A., Masamune, A., Yatomi, Y., Hakomori, S. and Igarashi, Y. 1995. Induction of apoptosis by sphingosine in human leukemic HL-60 cells: a possible endogenous modulator of apoptotic DNA

- fragmentation occurring during phorbol ester-induced differentiation. *Cancer research*. **55**(3),pp.691–7.
- Olesen, S., Clapham, D. and Davies, P. 1988. Haemodynamic shear stress activates a K⁺ current in vascular endothelial cells. *Nature*. **331**(6152),pp.168–170.
- Ozkor, M.A. and Quyyumi, A.A. 2011. Endothelium-derived hyperpolarizing factor and vascular function. *Cardiology research and practice*. **2011**,p.156146.
- Padera, T.P., Meijer, E.F.J. and Munn, L.L. 2016. The Lymphatic System in Disease Processes and Cancer Progression. *Annual Review of Biomedical Engineering*. **18**(1),pp.125–158.
- Paik, J.H., Chae Ss, S., Lee, M.J., Thangada, S. and Hla, T. 2001. Sphingosine 1-phosphate-induced endothelial cell migration requires the expression of EDG-1 and EDG-3 receptors and Rho-dependent activation of alpha vbeta3- and beta1-containing integrins. *The Journal of biological chemistry*. **276**(15),pp.11830–7.
- Parthasarathy, S., Raghavamenon, A., Garelnabi, M.O. and Santanam, N. 2010. Oxidized low-density lipoprotein. *Methods in molecular biology (Clifton, N.J.)*. **610**,pp.403–17.
- Patel, H.H., Murray, F. and Insel, P.A. 2008. Caveolae as Organizers of Pharmacologically Relevant Signal Transduction Molecules. *Annual Review of Pharmacology and Toxicology*. **48**(1),pp.359–391.
- Patel, S. and Docampo, R. 2010. Acidic calcium stores open for business: expanding the potential for intracellular Ca²⁺ signaling. *Trends in Cell Biology*. **20**(5),pp.277–286.
- Pathak, M.M., Nourse, J.L., Tran, T., Hwe, J., Arulmoli, J., Le, D.T.T., Bernardis, E., Flanagan, L.A. and Tombola, F. 2014. Stretch-activated ion channel Piezo1 directs lineage choice in human neural stem cells. *Proceedings of the National Academy of Sciences of the United States of America*. **111**(45),pp.16148–53.
- Pavoine, C. and Pecker, F. 2009. Sphingomyelinases: their regulation and roles in cardiovascular pathophysiology. *Cardiovascular research*. **82**(2),pp.175–83.
- Pérez-Cañamás, A., Benvegnù, S., Rueda, C.B., Rábano, A., Satrústegui, J. and Ledesma, M.D. 2017. Sphingomyelin-induced inhibition of the plasma membrane calcium ATPase causes neurodegeneration in type A Niemann–Pick disease. *Molecular Psychiatry*. **22**(5),pp.711–723.
- Perk, J., De Backer, G., Gohlke, H., Graham, I., Reiner, Z., Verschuren, M., Albus, C., Benlian, P., Boysen, G., Cifkova, R., Deaton, C., Ebrahim, S., Fisher, M., Germano, G., Hobbs, R., Hoes, A., Karadeniz, S., Mezzani, A., Prescott, E., Ryden, L., Scherer, M., Syvanne, M., Scholte Op Reimer, W.J.M., Vrints, C., Wood, D., Zamorano, J.L., Zannad, F., Cooney, M.T., Bax, J., Baumgartner, H., Ceconi, C., Dean, V., Deaton, C., Fagard, R., Funck-Brentano, C., Hasdai, D., Hoes, A., Kirchhof, P., Knuuti, J., Kolh, P., McDonagh, T., Moulin, C., Popescu, B.A., Reiner, Z., Sechtem, U., Sirnes, P.A., Tendera, M., Torbicki, A., Vahanian, A., Windecker, S., Funck-Brentano, C., Sirnes, P.A., Aboyans, V., Ezquerra, E.A., Baigent, C., Brotons, C., Burell, G., Ceriello, A., De Sutter, J., Deckers, J., Del Prato, S., Diener, H.-C., Fitzsimons, D., Fras, Z., Hambrecht, R., Jankowski, P., Keil, U., Kirby, M., Larsen, M.L., Mancía, G., Manolis, A.J., McMurray, J., Pajak, A., Parkhomenko, A., Rallidis, L., Rigo, F., Rocha, E., Ruilope, L.M.,

- van der Velde, E., Vanuzzo, D., Viigimaa, M., Volpe, M., Wiklund, O. and Wolpert, C. 2012. European Guidelines on cardiovascular disease prevention in clinical practice (version 2012): The Fifth Joint Task Force of the European Society of Cardiology and Other Societies on Cardiovascular Disease Prevention in Clinical Practice (constituted by representatives of nine societies and by invited experts) * Developed with the special contribution of the European Association for Cardiovascular Prevention & Rehabilitation (EACPR). *European Heart Journal*. **33**(13),pp.1635–1701.
- Pettus, B.J., Bielawska, A., Spiegel, S., Roddy, P., Hannun, Y.A. and Chalfant, C.E. 2003. Ceramide Kinase Mediates Cytokine- and Calcium Ionophore-induced Arachidonic Acid Release. *Journal of Biological Chemistry*. **278**(40),pp.38206–38213.
- Pettus, B.J., Bielawska, A., Subramanian, P., Wijesinghe, D.S., Maceyka, M., Leslie, C.C., Evans, J.H., Freiberg, J., Roddy, P., Hannun, Y.A. and Chalfant, C.E. 2004. Ceramide 1-Phosphate Is a Direct Activator of Cytosolic Phospholipase A₂. *Journal of Biological Chemistry*. **279**(12),pp.11320–11326.
- Peyronnet, R., Martins, J.R., Duprat, F., Demolombe, S., Arhatte, M., Jodar, M., Tauc, M., Duranton, C., Paulais, M., Teulon, J., Honoré, E. and Patel, A. 2013. Piezo1-dependent stretch-activated channels are inhibited by Polycystin-2 in renal tubular epithelial cells. *EMBO reports*. **14**(12),pp.1143–8.
- Picazo-Juarez, G., Romero-Suarez, S., Nieto-Posadas, A., Llorente, I., Jara-Oseguera, A., Briggs, M., McIntosh, T.J., Simon, S.A., Ladrón-de-Guevara, E., Islas, L.D. and Rosenbaum, T. 2011. Identification of a Binding Motif in the S5 Helix That Confers Cholesterol Sensitivity to the TRPV1 Ion Channel. *Journal of Biological Chemistry*. **286**(28),pp.24966–24976.
- Picazo-Juárez, G., Romero-Suárez, S., Nieto-Posadas, A., Llorente, I., Jara-Oseguera, A., Briggs, M., McIntosh, T.J., Simon, S.A., Ladrón-de-Guevara, E., Islas, L.D. and Rosenbaum, T. 2011. Identification of a Binding Motif in the S5 Helix That Confers Cholesterol Sensitivity to the TRPV1 Ion Channel. *Journal of Biological Chemistry*. **286**(28),pp.24966–24976.
- Piepoli, M.F., Hoes, A.W., Agewall, S., Albus, C., Brotons, C., Catapano, A.L., Cooney, M.-T., Corrà, U., Cosyns, B., Deaton, C., Graham, I., Hall, M.S., Hobbs, F.D.R., Løchen, M.-L., Löllgen, H., Marques-Vidal, P., Perk, J., Prescott, E., Redon, J., Richter, D.J., Sattar, N., Smulders, Y., Tiberi, M., van der Worp, H.B., van Dis, I., Verschuren, W.M.M., Binno, S., De Backer, G., Roffi, M., Aboyans, V., Bachl, N., Bueno, H., Carerj, S., Cho, L., Cox, J., De Sutter, J., Egidi, G., Fisher, M., Fitzsimons, D., Franco, O.H., Guenoun, M., Jennings, C., Jug, B., Kirchhof, P., Kotseva, K., Lip, G.Y.H., Mach, F., Mancía, G., Bermudo, F.M., Mezzani, A., Niessner, A., Ponikowski, P., Rauch, B., Rydén, L., Stauder, A., Turc, G., Wiklund, O., Windecker, S., Zamorano, J.L., Zamorano, J.L., Aboyans, V., Achenbach, S., Agewall, S., Badimon, L., Barón-Esquivias, G., Baumgartner, H., Bax, J.J., Bueno, H., Carerj, S., Dean, V., Erol, Ç., Fitzsimons, D., Gaemperli, O., Kirchhof, P., Kolh, P., Lancellotti, P., Lip, G.Y.H., Nihoyannopoulos, P., Piepoli, M.F., Ponikowski, P., Roffi, M., Torbicki, A., Carneiro, A.V., Windecker, S., Metzler, B., Najafov, R., Stelmashok, V., De Maeyer, C., Dilić, M., Gruev, I., Miličić, D., Vaverkova, H., Gustafsson, I., Attia, I., Duishvili, D., Ferrières, J., Kostova, N., Klimiashvili, Z., Hambrecht, R.,

- Tsioufis, K., Szabados, E., Andersen, K., Vaughan, C., Zafrir, B., Novo, S., Davletov, K., Jashari, F., Kerimkulova, A., Mintale, I., Saade, G., Petrulioniene, Z., Delagardelle, C., Magri, C.J., Rudi, V., Oukerraj, L., Çölkesen, B.E., Schirmer, H., dos Reis, R.P., Gherasim, D., Nedogoda, S., Zavatta, M., Giga, V., Filipova, S., Padial, L.R., Kiessling, A., Mach, F., Mahdhaoui, A., Ural, D., Nesukay, E. and Gale, C. 2016. 2016 European Guidelines on cardiovascular disease prevention in clinical practice: The Sixth Joint Task Force of the European Society of Cardiology and Other Societies on Cardiovascular Disease Prevention in Clinical Practice (constituted by representati. *European Heart Journal*. **37**(29),pp.2315–2381.
- Pike, L.J. 2003. Lipid rafts: bringing order to chaos. *Journal of lipid research*. **44**(4),pp.655–67.
- Pitman, M.R., Costabile, M. and Pitson, S.M. 2016. Recent advances in the development of sphingosine kinase inhibitors. *Cellular Signalling*. **28**(9),pp.1349–1363.
- Poole, K., Herget, R., Lapatsina, L., Ngo, H.-D. and Lewin, G.R. 2014. Tuning Piezo ion channels to detect molecular-scale movements relevant for fine touch. *Nature Communications*. **5**,p.3520.
- Prendergast, C., Quayle, J., Burdyga, T. and Wray, S. 2014a. Atherosclerosis affects calcium signalling in endothelial cells from apolipoprotein E knockout mice before plaque formation. *Cell calcium*. **55**(3),pp.146–54.
- Prendergast, C., Quayle, J., Burdyga, T. and Wray, S. 2014b. Atherosclerosis differentially affects calcium signalling in endothelial cells from aortic arch and thoracic aorta in Apolipoprotein E knockout mice. *Physiological reports*. **2**(10).
- Qi, Y., Andolfi, L., Frattini, F., Mayer, F., Lazzarino, M. and Hu, J. 2015. Membrane stiffening by STOML3 facilitates mechanosensation in sensory neurons. *Nature communications*. **6**,p.8512.
- Qin, X., Yue, Z., Sun, B., Yang, W., Xie, J., Ni, E., Feng, Y., Mahmood, R., Zhang, Y. and Yue, L. 2013. Sphingosine and FTY720 are potent inhibitors of the transient receptor potential melastatin 7 (TRPM7) channels. *British Journal of Pharmacology*. **168**(6),pp.1294–1312.
- Ralevic, V. 2012. P2X receptors in the cardiovascular system. *Wiley Interdisciplinary Reviews: Membrane Transport and Signaling*. **1**(5),pp.663–674.
- Ramström, C., Chapman, H., Ekokoski, E., Tuominen, R.K., Pasternack, M. and Törnquist, K. 2004. Tumor necrosis factor α and ceramide depolarise the resting membrane potential of thyroid FRTL-5 cells via a protein kinase C ζ -dependent regulation of K⁺ channels. *Cellular Signalling*. **16**(12),pp.1417–1424.
- Ramu, Y., Xu, Y. and Lu, Z. 2006. Enzymatic activation of voltage-gated potassium channels. *Nature*. **442**(7103),pp.696–699.
- Ranade, S.S., Qiu, Z., Woo, S.-H., Hur, S.S., Murthy, S.E., Cahalan, S.M., Xu, J., Mathur, J., Bandell, M., Coste, B., Li, Y.-S.J., Chien, S. and Patapoutian, A. 2014. Piezo1, a mechanically activated ion channel, is required for vascular development in mice. *Proceedings of the National Academy of Sciences of the United States of America*. **111**(28),pp.10347–52.
- Ranade, S.S., Syeda, R. and Patapoutian, A. 2015. Mechanically Activated Ion Channels. *Neuron*. **87**(6),pp.1162–1179.

- Rao, B.G. and Spence, M.W. 1976. Sphingomyelinase activity at pH 7.4 in human brain and a comparison to activity at pH 5.0. *Journal of lipid research*. **17**(5),pp.506–15.
- Retailleau, K., Duprat, F., Arhatte, M., Ranade, S.S., Peyronnet, R., Martins, J.R., Jodar, M., Moro, C., Offermanns, S., Feng, Y., Demolombe, S., Patel, A. and Honoré, E. 2015. Piezo1 in Smooth Muscle Cells Is Involved in Hypertension-Dependent Arterial Remodeling. *Cell Reports*. **13**(6),pp.1161–1171.
- Rezakhaniha, R., Ajianniotis, A., Schrauwen, J.T.C., Griffa, A., Sage, D., Bouten, C.V.C., van de Vosse, F.N., Unser, M. and Stergiopoulos, N. 2012. Experimental investigation of collagen waviness and orientation in the arterial adventitia using confocal laser scanning microscopy. *Biomechanics and Modeling in Mechanobiology*. **11**(3–4),pp.461–473.
- Riboni, L., Bassi, R., Caminiti, A., Prinetti, A., Viani, P. and Tettamanti, G. 1998. Metabolic fate of exogenous sphingosine in neuroblastoma neuro2A cells. Dose-dependence and biological effects. *Annals of the New York Academy of Sciences*. **845**,pp.46–56.
- Rizzo, V., McIntosh, D.P., Oh, P. and Schnitzer, J.E. 1998. In situ flow activates endothelial nitric oxide synthase in luminal caveolae of endothelium with rapid caveolin dissociation and calmodulin association. *The Journal of biological chemistry*. **273**(52),pp.34724–9.
- Robinson, J.G., Farnier, M., Krempf, M., Bergeron, J., Luc, G., Aversa, M., Stroes, E.S., Langslet, G., Raal, F.J., El Shahawy, M., Koren, M.J., Lepor, N.E., Lorenzato, C., Pordy, R., Chaudhari, U. and Kastelein, J.J.P. 2015. Efficacy and Safety of Alirocumab in Reducing Lipids and Cardiovascular Events. *New England Journal of Medicine*. **372**(16),pp.1489–1499.
- Rode, B., Shi, J., Endesh, N., Drinkhill, M.J., Webster, P.J., Lotteau, S.J., Bailey, M.A., Yuldasheva, N.Y., Ludlow, M.J., Cubbon, R.M., Li, J., Futers, T.S., Morley, L., Gaunt, H.J., Marszalek, K., Viswambharan, H., Cuthbertson, K., Baxter, P.D., Foster, R., Sukumar, P., Weightman, A., Calaghan, S.C., Wheatcroft, S.B., Kearney, M.T. and Beech, D.J. 2017. Piezo1 channels sense whole body physical activity to reset cardiovascular homeostasis and enhance performance. *Nature Communications*. **8**(1),p.350.
- Rodman, D.M., Reese, K., Harral, J., Fouty, B., Wu, S., West, J., Hoedt-Miller, M., Tada, Y., Li, K.-X., Cool, C., Fagan, K. and Cribbs, L. 2005. Low-Voltage-Activated (T-Type) Calcium Channels Control Proliferation of Human Pulmonary Artery Myocytes. *Circulation Research*. **96**(8),pp.864–872.
- Rohacs, T. 2014. Phosphoinositide Regulation of TRP Channels *In: Springer, Cham*, pp. 1143–1176.
- Romanenko, V.G., Rothblat, G.H. and Levitan, I. 2002. Modulation of endothelial inward-rectifier K⁺ current by optical isomers of cholesterol. *Biophysical journal*. **83**(6),pp.3211–22.
- Romanenko, V.G., Rothblat, G.H. and Levitan, I. 2004. Sensitivity of Volume-regulated Anion Current to Cholesterol Structural Analogues. *The Journal of General Physiology*. **123**(1),pp.77–88.
- Romiti, E., Meacci, E., Tanzi, G., Becciolini, L., Mitsutake, S., Farnararo, M., Ito, M. and Bruni, P. 2001. Localization of neutral ceramidase in caveolin-enriched light membranes of murine endothelial cells. *FEBS letters*. **506**(2),pp.163–8.

- Rosen, H., Stevens, R.C., Hanson, M., Roberts, E. and Oldstone, M.B.A. 2013. Sphingosine-1-Phosphate and Its Receptors: Structure, Signaling, and Influence. *Annual Review of Biochemistry*. **82**(1),pp.637–662.
- Rosenhouse-Dantsker, A., Mehta, D. and Levitan, I. 2012. Regulation of ion channels by membrane lipids. *Comprehensive Physiology*. **2**(1),pp.31–68.
- Rosenhouse-Dantsker, A., Noskov, S., Durdagi, S., Logothetis, D.E. and Levitan, I. 2013. Identification of Novel Cholesterol-binding Regions in Kir2 Channels. *Journal of Biological Chemistry*. **288**(43),pp.31154–31164.
- Rosenson, R.S. 2004. Statins in atherosclerosis: lipid-lowering agents with antioxidant capabilities. *Atherosclerosis*. **173**(1),pp.1–12.
- Rychnovsky, S.D. and Mickus, D.E. 1992. Synthesis of ent-cholesterol, the unnatural enantiomer. *The Journal of Organic Chemistry*. **57**(9),pp.2732–2736.
- Salido, G.M., Sage, S.O. and Rosado, J.A. 2009. TRPC channels and store-operated Ca²⁺ entry. *Biochimica et Biophysica Acta (BBA) - Molecular Cell Research*. **1793**(2),pp.223–230.
- Saotome, K., Murthy, S.E., Kefauver, J.M., Whitwam, T., Patapoutian, A. and Ward, A.B. 2017. Structure of the mechanically activated ion channel Piezo1. *Nature*.
- Sathyanarayana, P., Barthwal, M.K., Kundu, C.N., Lane, M.E., Bergmann, A., Tzivion, G. and Rana, A. 2002. Activation of the Drosophila MLK by ceramide reveals TNF-alpha and ceramide as agonists of mammalian MLK3. *Molecular cell*. **10**(6),pp.1527–33.
- Sawai, H., Domae, N., Nagan, N. and Hannun, Y.A. 1999. Function of the cloned putative neutral sphingomyelinase as lyso-platelet activating factor-phospholipase C. *The Journal of biological chemistry*. **274**(53),pp.38131–9.
- Schissel, S.L., Jiang, X., Tweedie-Hardman, J., Jeong, T., Camejo, E.H., Najib, J., Rapp, J.H., Williams, K.J. and Tabas, I. 1998. Secretory sphingomyelinase, a product of the acid sphingomyelinase gene, can hydrolyze atherogenic lipoproteins at neutral pH. Implications for atherosclerotic lesion development. *The Journal of biological chemistry*. **273**(5),pp.2738–46.
- Schissel, S.L., Schuchman, E.H., Williams, K.J. and Tabas, I. 1996. Zn²⁺-stimulated sphingomyelinase is secreted by many cell types and is a product of the acid sphingomyelinase gene. *The Journal of biological chemistry*. **271**(31),pp.18431–6.
- Schuchman, E.H., Levrán, O., Pereira, L. V and Desnick, R.J. 1992. Structural organization and complete nucleotide sequence of the gene encoding human acid sphingomyelinase (SMPD1). *Genomics*. **12**(2),pp.197–205.
- Scull, C.M. and Tabas, I. 2011. Mechanisms of ER Stress-Induced Apoptosis in Atherosclerosis. *Arteriosclerosis, Thrombosis, and Vascular Biology*. **31**(12),pp.2792–2797.
- Sezgin, E., Can, F.B., Schneider, F., Clausen, M.P., Galiani, S., Stanly, T.A., Waithe, D., Colaco, A., Honigmann, A., Wüstner, D., Platt, F. and Eggeling, C. 2016. A comparative study on fluorescent cholesterol analogs as versatile cellular reporters. *Journal of lipid research*. **57**(2),pp.299–309.
- Singh, A.K., McMillan, J., Bukiya, A.N., Burton, B., Parrill, A.L. and Dopico, A.M. 2012. Multiple Cholesterol Recognition/Interaction Amino Acid Consensus (CRAC) Motifs in Cytosolic C Tail of Slo1 Subunit Determine Cholesterol Sensitivity of Ca²⁺ - and Voltage-gated K⁺ (BK) Channels.

- Journal of Biological Chemistry*. **287**(24),pp.20509–20521.
- Singleton, P.A., Dudek, S.M., Chiang, E.T. and Garcia, J.G.N. 2005. Regulation of sphingosine 1-phosphate-induced endothelial cytoskeletal rearrangement and barrier enhancement by S1P₁ receptor, PI3 kinase, Tiam1/Rac1, and α -actinin. *The FASEB Journal*. **19**(12),pp.1646–1656.
- Smith, A.R., Visioli, F., Frei, B. and Hagen, T.M. 2006. Age-related changes in endothelial nitric oxide synthase phosphorylation and nitric oxide dependent vasodilation: evidence for a novel mechanism involving sphingomyelinase and ceramide-activated phosphatase 2A. *Aging Cell*. **5**(5),pp.391–400.
- Smith, E.L. and Schuchman, E.H. 2008. The unexpected role of acid sphingomyelinase in cell death and the pathophysiology of common diseases. *FASEB journal : official publication of the Federation of American Societies for Experimental Biology*. **22**(10),pp.3419–31.
- Smith, E.R., Merrill Jr., A.H. and Obeid, L.M. 2000. Effects of Sphingosine and Other Sphingolipids on Protein Kinase C. *Methods in Enzymology*. **312**,pp.361–373.
- Smith, R.J., Sam, L.M., Justen, J.M., Bundy, G.L., Bala, G.A. and Bleasdale, J.E. 1990. Receptor-coupled signal transduction in human polymorphonuclear neutrophils: effects of a novel inhibitor of phospholipase C-dependent processes on cell responsiveness. *The Journal of pharmacology and experimental therapeutics*. **253**(2),pp.688–97.
- Sooksawate, T. and Simmonds, M.A. 2001. Effects of membrane cholesterol on the sensitivity of the GABA(A) receptor to GABA in acutely dissociated rat hippocampal neurones. *Neuropharmacology*. **40**(2),pp.178–84.
- Spiegel, S. and Milstien, S. 2003. Sphingosine-1-phosphate: an enigmatic signalling lipid. *Nature Reviews Molecular Cell Biology*. **4**(5),pp.397–407.
- Stansfeld, P. and Sansom, M.P. 2011. Molecular simulation approaches to membrane proteins. *Structure*. **19**(11),pp.1562–1572.
- Steen, H., Kolmakova, A., Stuber, M., Rodriguez, E.R., Gao, F., Chatterjee, S. and Lima, J.A. 2007. MRI visualized neo-intimal dissection and co-localization of novel apoptotic markers apolipoprotein C-1, ceramide and caspase-3 in a Watanabe hyperlipidemic rabbit model. *Atherosclerosis*. **191**(1),pp.82–89.
- Steinberg, H.O., Bayazeed, B., Hook, G., Johnson, A., Cronin, J. and Baron, A.D. 1997. Endothelial dysfunction is associated with cholesterol levels in the high normal range in humans. *Circulation*. **96**(10),pp.3287–93.
- Stewart, J., Manmathan, G. and Wilkinson, P. 2017. Primary prevention of cardiovascular disease: A review of contemporary guidance and literature. *JRSM Cardiovascular Disease*. **6**,p.204800401668721.
- Stoffel, W., Knifka, J., Koebke, J., Niehoff, A., Jenke, B., Holz, B., Binczek, E. and Günter, R.H. 2007. Neutral Sphingomyelinase (SMPD3) Deficiency Causes a Novel Form of Chondrodysplasia and Dwarfism That Is Rescued by Col2A1-Driven smpd3 Transgene Expression. *The American Journal of Pathology*. **171**(1),pp.153–161.
- Streets, A.J., Needham, A.J., Gill, S.K. and Ong, A.C.M. 2010. Protein kinase D-mediated phosphorylation of polycystin-2 (TRPP2) is essential for its effects on cell growth and calcium channel activity. *Molecular biology of the cell*. **21**(22),pp.3853–65.
- Strub, G.M., Paillard, M., Liang, J., Gomez, L., Allegood, J.C., Hait, N.C.,

- Maceyka, M., Price, M.M., Chen, Q., Simpson, D.C., Kordula, T., Milstien, S., Lesnefsky, E.J. and Spiegel, S. 2011. Sphingosine-1-phosphate produced by sphingosine kinase 2 in mitochondria interacts with prohibitin 2 to regulate complex IV assembly and respiration. *FASEB journal : official publication of the Federation of American Societies for Experimental Biology*. **25**(2),pp.600–12.
- Subramanian, P., Stahelin, R. V., Szulc, Z., Bielawska, A., Cho, W. and Chalfant, C.E. 2005. Ceramide 1-Phosphate Acts as a Positive Allosteric Activator of Group IVA Cytosolic Phospholipase A₂ α and Enhances the Interaction of the Enzyme with Phosphatidylcholine. *Journal of Biological Chemistry*. **280**(18),pp.17601–17607.
- Suchyna, T., Johnson, J., Hamer, K., Leykam, J., Gage, D., Clemoc, H., Baumgarten, C. and Sachs, F. 2000. Identification of a Peptide Toxin from *Grammostola spatulata* Spider Venom that Blocks Cation-selective Stretch-activated Channels. *The Journal of general physiology*. **115**(5),pp.583–598.
- Suchyna, T.M.T., Tape, S.E.S., Koeppe, R.R.E., Andersen, O.S., Sachs, F. and Gottlieb, P.A. 2004. Bilayer-dependent inhibition of mechanosensitive channels by neuroactive peptide enantiomers. *Nature*. **430**(6996),pp.235–240.
- Sugiura, M., Kono, K., Liu, H., Shimizugawa, T., Minekura, H., Spiegel, S. and Kohama, T. 2002. Ceramide kinase, a novel lipid kinase. Molecular cloning and functional characterization. *The Journal of biological chemistry*. **277**(26),pp.23294–300.
- Sukriti, S., Tauseef, M., Yazbeck, P. and Mehta, D. 2014. Mechanisms regulating endothelial permeability. *Pulmonary circulation*. **4**(4),pp.535–51.
- Syeda, R., Florendo, M.N., Cox, C.D., Kefauver, J.M., Santos, J.S., Martinac, B., Correspondence, A.P. and Patapoutian, A. 2016. Piezo1 Channels Are Inherently Mechanosensitive. *CellReports*. **17**,pp.1739–1746.
- Syeda, R., Xu, J., Dubin, A.E., Coste, B., Mathur, J., Huynh, T., Matzen, J., Lao, J., Tully, D.C., Engels, I.H., Petrassi, H.M., Schumacher, A.M., Montal, M., Bandell, M. and Patapoutian, A. 2015. Chemical activation of the mechanotransduction channel Piezo1. *eLife*. **4**.
- Szente, L. and Fenyvesi, É. 2017. Cyclodextrin-Lipid Complexes: Cavity Size Matters. *Structural Chemistry*. **28**(2),pp.479–492.
- Szewczyk, M.M., Davis, K.A., Samson, S.E., Simpson, F., Rangachari, P.K. and Grover, A.K. 2007. Ca²⁺-pumps and Na⁺?Ca²⁺-exchangers in coronary artery endothelium versus smooth muscle. *Journal of Cellular and Molecular Medicine*. **11**(1),pp.129–138.
- Tabas, I. 1999. Secretory sphingomyelinase. *Chemistry and Physics of Lipids*. **102**(1–2),pp.123–130.
- Tafesse, F.G., Ternes, P. and Holthuis, J.C.M. 2006. The Multigenic Sphingomyelin Synthase Family. *Journal of Biological Chemistry*. **281**(40),pp.29421–29425.
- Takashima, S., Sugimoto, N., Takuwa, N., Okamoto, Y., Yoshioka, K., Takamura, M., Takata, S., Kaneko, S. and Takuwa, Y. 2008. G12/13 and Gq mediate S1P2-induced inhibition of Rac and migration in vascular smooth muscle in a manner dependent on Rho but not Rho kinase. *Cardiovascular Research*. **79**(4),pp.689–697.
- Takuwa, Y., Okamoto, Y., Yoshioka, K. and Takuwa, N. 2008. Sphingosine-1-phosphate signaling and biological activities in the cardiovascular system.

- Biochimica et Biophysica Acta (BBA) - Molecular and Cell Biology of Lipids*. **1781**(9),pp.483–488.
- Tettamanti, G. 2003. Ganglioside/glycosphingolipid turnover: New concepts. *Glycoconjugate Journal*. **20**(5),pp.301–317.
- Thannhauser, S.J. and Reichel, M. 1940. Studies on animal lipids. XVI. The occurrence of sphingomyelin as a mixture of sphingomyelin fatty acid ester and free sphingomyelin, demonstrated by enzymatic hydrolysis and mild saponification. *Journal of Biological Chemistry*. **135**,pp.1–13.
- Tomiuk, S., Hofmann, K., Nix, M., Zumbansen, M. and Stoffel, W. 1998. Cloned mammalian neutral sphingomyelinase: functions in sphingolipid signaling? *Proceedings of the National Academy of Sciences of the United States of America*. **95**(7),pp.3638–43.
- Toyama, K., Wulff, H., Chandy, K.G., Azam, P., Raman, G., Saito, T., Fujiwara, Y., Mattson, D.L., Das, S., Melvin, J.E., Pratt, P.F., Hatoum, O.A., Gutterman, D.D., Harder, D.R. and Miura, H. 2008. The intermediate-conductance calcium-activated potassium channel KCa3.1 contributes to atherogenesis in mice and humans. *Journal of Clinical Investigation*. **118**(9),pp.3025–3037.
- Tsoukias, N.M. 2011. Calcium dynamics and signaling in vascular regulation: computational models. *Wiley interdisciplinary reviews. Systems biology and medicine*. **3**(1),pp.93–106.
- Vial, C. and Evans, R.J. 2002. P2X(1) receptor-deficient mice establish the native P2X receptor and a P2Y6-like receptor in arteries. *Molecular pharmacology*. **62**(6),pp.1438–45.
- Villani, M., Subathra, M., Im, Y.-B., Choi, Y., Signorelli, P., Del Poeta, M. and Luberto, C. 2008. Sphingomyelin synthases regulate production of diacylglycerol at the Golgi. *The Biochemical journal*. **414**(1),pp.31–41.
- de Villiers, W.J. and Smart, E.J. 1999. Macrophage scavenger receptors and foam cell formation. *Journal of leukocyte biology*. **66**(5),pp.740–6.
- Wang, G., Silva, J., Krishnamurthy, K., Tran, E., Condie, B.G. and Bieberich, E. 2005. Direct binding to ceramide activates protein kinase C ζ before the formation of a pro-apoptotic complex with PAR-4 in differentiating stem cells. *The Journal of biological chemistry*. **280**(28),pp.26415–24.
- Wang, Q.J. 2006. PKD at the crossroads of DAG and PKC signaling. *Trends in Pharmacological Sciences*. **27**(6),pp.317–323.
- Wang, S., Chennupati, R., Kaur, H., Iring, A., Wettschureck, N. and Offermanns, S. 2016. Endothelial cation channel PIEZO1 controls blood pressure by mediating flow-induced ATP release. *Journal of Clinical Investigation*. **126**(12),pp.4527–4536.
- Wang, X.-L., Ye, D., Peterson, T.E., Cao, S., Shah, V.H., Katusic, Z.S., Sieck, G.C. and Lee, H.-C. 2005. Caveolae Targeting and Regulation of Large Conductance Ca²⁺-activated K⁺ Channels in Vascular Endothelial Cells. *Journal of Biological Chemistry*. **280**(12),pp.11656–11664.
- Warboys, C., de Luca, A., Amini, N., Luong, L., Duckles, H., Hsiao, S., White, A., Biswas, S., Khamis, R., Chong, C., Cheung, W., Sherwin, S., Bennett, M., Gil, J., Mason, J., Haskard, D. and Evans, P. 2014. Disturbed Flow Promotes Endothelial Senescence via a p53-Dependent Pathway. *Arteriosclerosis, thrombosis, and vascular biology*. **34**(5),pp.585–595.
- Watanabe, N. and Ikeda, U. 2004. Matrix metalloproteinases and atherosclerosis. *Current atherosclerosis reports*. **6**(2),pp.112–20.
- Weiss, R.H., Huang, C.-L. and Ives, H.E. 1991. Sphingosine reverses growth

- inhibition caused by activation of protein kinase c in vascular smooth muscle cells. *Journal of Cellular Physiology*. **149**(2),pp.307–312.
- Westover, E.J. and Covey, D.F. 2004. The Enantiomer of Cholesterol. *The Journal of Membrane Biology*. **202**(2),pp.61–72.
- WHO 2017. Cardiovascular diseases (CVDs). WHO.
- WHO 2018. The challenge of cardiovascular disease – quick statistics.
- Windh, R.T., Lee, M.J., Hla, T., An, S., Barr, A.J. and Manning, D.R. 1999. Differential coupling of the sphingosine 1-phosphate receptors Edg-1, Edg-3, and H218/Edg-5 to the G(i), G(q), and G(12) families of heterotrimeric G proteins. *The Journal of biological chemistry*. **274**(39),pp.27351–8.
- Winn, R.K. and Harlan, J.M. 2005. The role of endothelial cell apoptosis in inflammatory and immune diseases. *Journal of Thrombosis and Haemostasis*. **3**(8),pp.1815–1824.
- Wong, C.-O. and Yao, X. 2011. TRP Channels in Vascular Endothelial Cells *In: Springer, Dordrecht*, pp. 759–780.
- Woodcock, J. 2006. Sphingosine and ceramide signalling in apoptosis. *IUBMB Life (International Union of Biochemistry and Molecular Biology: Life)*. **58**(8),pp.462–466.
- Wu, C.-C., Su, M.-J., Chi, J.-F., Chen, W.-J., Hsu, H.-C. and Lee, Y.-T. 1995. The effect of hypercholesterolemia on the sodium inward currents in cardiac myocyte. *Journal of Molecular and Cellular Cardiology*. **27**(6),pp.1263–1269.
- Xia, P., Wang, L., Moretti, P.A.B., Albanese, N., Chai, F., Pitson, S.M., D'Andrea, R.J., Gamble, J.R. and Vadas, M.A. 2002. Sphingosine kinase interacts with TRAF2 and dissects tumor necrosis factor-alpha signaling. *The Journal of biological chemistry*. **277**(10),pp.7996–8003.
- Xu, F., Satoh, E. and Iijima, T. 2003. Protein kinase C-mediated Ca²⁺ entry in HEK 293 cells transiently expressing human TRPV4. *British journal of pharmacology*. **140**(2),pp.413–21.
- Xu, X. and London, E. 2000. The effect of sterol structure on membrane lipid domains reveals how cholesterol can induce lipid domain formation. *Biochemistry*. **39**(5),pp.843–9.
- Xu, Y., Ramu, Y. and Lu, Z. 2008. Removal of phospho-head groups of membrane lipids immobilizes voltage sensors of K⁺ channels. *Nature*. **451**(7180),pp.826–829.
- Yamaji, T., Kumagai, K., Tomishige, N. and Hanada, K. 2008. Two sphingolipid transfer proteins, CERT and FAPP2: Their roles in sphingolipid metabolism. *IUBMB Life*. **60**(8),pp.511–518.
- Yamamoto, K., Sokabe, T., Matsumoto, T., Yoshimura, K., Shibata, M., Ohura, N., Fukuda, T., Sato, T., Sekine, K., Kato, S., Isshiki, M., Fujita, T., Kobayashi, M., Kawamura, K., Masuda, H., Kamiya, A. and Ando, J. 2006. Impaired flow-dependent control of vascular tone and remodeling in P2X4-deficient mice. *Nature medicine*. **12**(1),pp.133–7.
- Yang, D.-I., Yeh, C.-H., Chen, S., Xu, J. and Hsu, C.Y. 2004. Neutral sphingomyelinase activation in endothelial and glial cell death induced by amyloid beta-peptide. *Neurobiology of Disease*. **17**(1),pp.99–107.
- Yang, X.-N., Lu, Y.-P., Liu, J.-J., Huang, J.-K., Liu, Y.-P., Xiao, C.-X., Jazag, A., Ren, J.-L. and Guleng, B. 2014. Piezo1 Is a Novel Trefoil Factor Family 1 Binding Protein that Promotes Gastric Cancer Cell Mobility In Vitro. *Digestive Diseases and Sciences*. **59**(7),pp.1428–1435.
- Yusuf, S., Hawken, S., Ôunpuu, S., Dans, T., Avezum, A., Lanan, F.,

- McQueen, M., Budaj, A., Pais, P., Varigos, J. and Lisheng, L. 2004. Effect of potentially modifiable risk factors associated with myocardial infarction in 52 countries (the INTERHEART study): case-control study. *The Lancet*. **364**(9438),pp.937–952.
- Zarychanski, R., Schulz, V.P., Houston, B.L., Maksimova, Y., Houston, D.S., Smith, B., Rinehart, J. and Gallagher, P.G. 2012. Mutations in the mechanotransduction protein PIEZO1 are associated with hereditary xerocytosis. *Blood*. **120**(9),pp.1908–15.
- Zeidan, Y.H., Wu, B.X., Jenkins, R.W., Obeid, L.M. and Hannun, Y.A. 2008. A novel role for protein kinase C δ -mediated phosphorylation of acid sphingomyelinase in UV light-induced mitochondrial injury. *The FASEB Journal*. **22**(1),pp.183–193.
- Zhang, A.Y., Yi, F., Jin, S., Xia, M., Chen, Q., Gulbins, E. and Li, P. 2007. Acid Sphingomyelinase and Its Redox Amplification in Formation of Lipid Raft Redox Signaling Platforms in Endothelial Cells. *Antioxidants & Redox Signaling*. **9**(7),pp.817–828.
- Zhang, T., Chi, S., Jiang, F., Zhao, Q. and Xiao, B. 2017. A protein interaction mechanism for suppressing the mechanosensitive Piezo channels. *Nature communications*. **8**(1),p.1797.
- Zhang, W., Cheng, L.E., Kittelmann, M., Li, J., Petkovic, M., Cheng, T., Jin, P., Guo, Z., Göpfert, M.C., Jan, L.Y. and Jan, Y.N. 2015. Ankyrin Repeats Convey Force to Gate the NOMPC Mechanotransduction Channel. *Cell*. **162**(6),pp.1391–403.
- Zhang, Y., Yao, B., Delikat, S., Bayoumy, S., Lin, X.-H., Basu, S., McGinley, M., Chan-Hui, P.-Y., Lichenstein, H. and Kolesnick, R. 1997. Kinase Suppressor of Ras Is Ceramide-Activated Protein Kinase. *Cell*. **89**(1),pp.63–72.
- Zhao, Q., Wu, K., Geng, J., Chi, S., Wang, Y., Zhi, P., Zhang, M. and Xiao, B. 2016. Ion Permeation and Mechanotransduction Mechanisms of Mechanosensitive Piezo Channels. *Neuron*. **89**(6),pp.1248–63.
- Zhao, Q., Zhou, H., Chi, S., Wang, Y., Wang, J., Geng, J., Wu, K., Liu, W., Zhang, T., Dong, M.-Q., Wang, J., Li, X. and Xiao, B. 2018. Structure and mechanogating mechanism of the Piezo1 channel. *Nature* 2018.
- Zhou, C., Chen, H., King, J.A., Sellak, H., Kuebler, W.M., Yin, J., Townsley, M.I., Shin, H.-S. and Wu, S. 2010. α_{1G} T-type calcium channel selectively regulates P-selectin surface expression in pulmonary capillary endothelium. *American Journal of Physiology-Lung Cellular and Molecular Physiology*. **299**(1),pp.L86–L97.
- Zhou, C. and Wu, S. 2006. T-type Calcium Channels in Pulmonary Vascular Endothelium. *Microcirculation*. **13**(8),pp.645–656.
- Zumbansen, M. and Stoffel, W. 2002. Neutral sphingomyelinase 1 deficiency in the mouse causes no lipid storage disease. *Molecular and cellular biology*. **22**(11),pp.3633–8.

Appendix A

Table 8: Cholesterol binding motifs in human Piezo1. The position, sequence, average conservation of amino acids (AA) in the motif, motif type and predicted location based on the most recent structure from Zhao et al. (2018).

Position	Sequence	hPiezo1		
		Average AA conservation	Motif type	Predicted location
183 - 190	RLAARFRV	0.24	CARC	Alpha helix before TH5
243 - 250	RGFSRLCV	0.31	CARC	TH7
318 - 330	VLLLLCYATASLRK	0.31	CRAC	TH8
329 - 341	LRKLRAYRPSGQR	0.21	CRAC	Exiting TH8
531 - 539	RQFVKEKLL	0.64	CARC	TH12
573 - 583	KGVYAKYWIYV	0.62	CARC	Alpha helix before TH13
571 - 578	LVKGVYAK	0.57	CRAC	Alpha helix before TH13
596 - 603	RLVVKIV	0.69	CARC	Going into TH14/TH14
601 - 610	KIVYMFLFLL	0.73	CARC	TH14
612 - 624	LTLFQVYYSLWRK	0.68	CRAC	Exiting TH14
623 - 634	RKLLKAFWWLVV	0.69	CARC	Going into TH15
657 - 667	RNLTGFTDEQL	0.67	CARC	Between TH15 - TH16
696 - 703	LQLHYFHR	0.70	CRAC	Exiting TH16
703 - 708	RPFMQL	0.59	CARC	Between TH16 - TH17
801 - 810	RVQVFLRRL	0.63	CARC	TH17
816 - 827	KLVALYTVWVAL	0.72	CARC	TH17
845 - 851	LPYPRFR	0.65	CRAC	Between TH18 - TH19
867 - 875	VCKMLYQLK	0.73	CRAC	TH19
869 - 877	KMLYQLKVV	0.72	CARC	TH19
920 - 926	RKGFPNL	0.61	CARC	Between TH19 - TH20
940 - 948	VFEAIVYRR	0.68	CRAC	TH20
947 - 958	RRQEHYRRQHQL	0.59	CARC	TH20
984 - 996	KYFINFFFYKFGL	0.72	CARC	TH21
1010 - 1017	RMNFLVTL	0.73	CARC	TH22
1036 - 1047	RLWPNYCLFLAL	0.73	CARC	TH23
1063 - 1073	LCIDYPWRWSR	0.74	CRAC	Between TH23 - TH24
1081 - 1092	LIKWLYLPDFFR	0.76	CRAC	Between TH23 - TH24
1152 - 1160	RSYLDMLKV	0.79	CARC	Alpha helix 2 before TM25
1159 - 1171	KVAVFRYLFWLVL	0.78	CARC	Alpha helix 2 before TM25/TM25
1181 - 1191	RISIFGLGYLL	0.81	CARC	Going into TH26
1257 - 1267	VCTVKGYDDPK	0.64	CRAC	Between TH27 - TH28
1300 - 1310	RVFLSHYYLHV	0.81	CARC	TH28 - Pre-beam
1301 - 1311	VFLSHYYLHVR	0.76	CRAC	TH28 - Pre-beam
1323 - 1333	RGFALYNAANL	0.63	CARC	Beam
1544 - 1554	RAERYLLTQEL	0.61	CARC	Between Beam - TH29
1611 - 1618	LSTGYHTR	0.40	CRAC	Between Beam - TH29

hPiezo1				
Position	Sequence	Average AA conservation	Motif type	Predicted location
1674 - 1683	RLLRAVYQCV	0.62	CARC	Alpha2 before TH29
1724 - 1735	RPSKRFWMTAIV	0.76	CARC	Going into TH31
1758 - 1766	VVLRRYENK	0.57	CRAC	Between TH31 - TH32
1762 - 1774	RYENKPYFPPRIL	0.71	CARC	Between TH31 - TH32
1776 - 1784	LEKTDGYIK	0.68	CRAC	Going into TH32
1778 - 1788	KTDGYIKYDLV	0.68	CARC	Going into TH32
1797 - 1805	RSQLLCYGL	0.72	CARC	Leaving TH32
1925 - 1934	RRLQGFCLSL	0.32	CARC	Between TH32 - TH33
1934 - 1944	LAQGTYRPLRR	0.54	CRAC	Between TH32 - TH33
1940 - 1950	RPLRRFFHDIL	0.63	CARC	Between TH32 - TH33
1955 - 1966	RAATDVYALMFL	0.81	CARC	Between TH32 - TH33
2016 - 2025	VVDRALYLRK	0.85	CRAC	TH34
2019 - 2028	RALYLRKTVL	0.85	CARC	TH34
2030 - 2039	KLAFQVALVL	0.78	CARC	TH35
2055 - 2062	RMFNQNVV	0.72	CARC	Between TH35 - TH36
2061 - 2070	VVAQLWYFVK	0.80	CRAC	TH36
2070 - 2076	KCIYFAL	0.81	CARC	TH36
2076 - 2082	LSAYQIR	0.86	CRAC	TH36
2082 - 2090	RCGYPTRIL	0.85	CARC	Between TH36 - Anchor alpha1
2096 - 2103	KKYNHLNL	0.80	CARC	Entering Anchor alpha1
2110 - 2118	RLVPFLVEL	0.85	CARC	Anchor alpha1 - alpha2
2167 - 2178	KKKIVKYGMGGL	0.85	CARC	Entering OH
2215 - 2222	KLGGYEPL	0.86	CARC	CED
2245 - 2252	RQFDPQPL	0.55	CARC	CED
2302 - 2311	RFTWNFQRDL	0.76	CARC	CED
2317 - 2323	VEYANEK	0.66	CRAC	CED
2355 - 2361	LFPKYIR	0.78	CRAC	CED
2479 - 2487	KLCQDIFLV	0.83	CARC	CTD alpha1
2495 - 2502	LEEELYAK	0.82	CRAC	Between CTD alpha1-alpha2

Table 9: Cholesterol binding motifs in mouse Piezo1. The position, sequence, average conservation of amino acids (AA) in the motif, motif type and predicted location based on the most recent structure from Zhao et al. (2018).

mPiezo1				
Position	Sequence	Average AA conservation	Motif type	Predicted location
113 - 122	KDIFNTRLV	0.27	CARC	Between TH3 - TH4
290 - 298	RLFGLKNFV	0.36	CARC	Between TH7 - TH8
295 - 300	KNFVDL	0.27	CARC	Between TH7 - TH8
314 - 326	KHAWPIYVSPGIL	0.32	CARC	Between TH7 - TH8/TH8
537 - 545	RQFVKEKL	0.66	CARC	TH12
577 - 584	LVTGIYVK	0.57	CRAC	Alpha helix before TH13
602 - 609	RLVVYKIV	0.69	CARC	Going into TH14/TH14
607 - 618	KIVYMFLFLCL	0.73	CARC	TH14
618 - 630	LTLFQVYYTLWR	0.68	CRAC	Exiting TH14
629 - 640	RKLLRVFWWLVV	0.69	CARC	Going into TH15
663 - 673	RNLTGFTDEQL	0.67	CARC	Between TH15 - TH16
702 - 709	LQLHYFHR	0.70	CRAC	Exiting TH16
709 - 717	RPFMQLTDL	0.60	CARC	Between TH16 - TH17
796 - 805	RIQVFVRRLL	0.63	CARC	TH17
811 - 822	KLVALYTVWVAL	0.72	CARC	TH17
840 - 846	LPYPRFR	0.65	CRAC	Between TH18 - TH19
862 - 870	VCKMLYQLK	0.73	CRAC	TH19
864 - 872	KMLYQLKIV	0.72	CARC	TH19
915 - 921	RKGYPNL	0.54	CARC	Between TH19 - TH20
935 - 943	VFEAVVYRR	0.68	CRAC	TH20
979 - 991	KYFINFFFYKFGI	0.72	CARC	TH21
1005 - 1012	RMNFMVIL	0.73	CARC	TH22
1031 - 1042	RLWPNYCLFTL	0.73	CARC	TH23
1058 - 1068	LCIDYPWRWSK	0.74	CRAC	Between TH23 - TH24
1076 - 1087	LIKWLYLPDFFR	0.76	CRAC	Between TH23 - TH24
1147 - 1155	RSYLDMLKV	0.79	CARC	Alpha helix 2 before TM25
1154 - 1168	KVAVFRYLFWLVLVV	0.78	CARC	Alpha helix 2 before TM25/TM25
1176 - 1186	RISIFGLGYLL	0.81	CARC	Going into TH26
1252 - 1262	LVCTVKGYDDPK	0.66	CRAC	Between TH27 - TH28
1295 - 1305	RIFLSHYFLHV	0.81	CARC	TH28 - Pre-beam
1318 - 1328	RGFALYNAANL	0.63	CARC	Beam
1602 - 1609	LSTGYNTR	0.40	CRAC	Between Beam - TH29
1674 - 1683	RLLRAGYQCV	0.62	CARC	Alpha2 before TH29
1724 - 1735	RPSKRFWMTAIV	0.76	CARC	Going into TH31
1758 - 1766	VVLRRYENK	0.57	CRAC	Between TH31 - TH32
1762 - 1774	RYENKPYFPRL	0.71	CARC	Between TH31 - TH32
1776 - 1784	LEKTDSEYIK	0.68	CRAC	Going into TH32

mPiezo1				
Position	Sequence	Average AA conservation	Motif type	Predicted location
1778 - 1788	KTDSYIKYDLV	0.68	CARC	Going into TH32
1797 - 1805	RSQLLCYGL	0.72	CARC	Leaving TH32
1941 - 1950	RRLQSFCVSL	0.33	CARC	Between TH32 - TH33
1950 - 1960	LAQSFYQPLQR	0.54	CRAC	Between TH32 - TH33
1960 - 1966	RFFHDIL	0.66	CARC	Between TH32 - TH33
1971 - 1982	RAATDVYALMFL	0.81	CARC	Between TH32 - TH33
2032 - 2041	VIDRALYLRK	0.85	CRAC	TH34
2035 - 2044	RALYLRKTVL	0.85	CARC	TH34/Lipid pocket
2046 - 2055	KLAFQVVLVV	0.78	CARC	TH35
2071 - 2078	RMFSQNAV	0.72	CARC	Between TH35 - TH36
2078 - 2086	VAQLWYFVK	0.84	CRAC	TH36
2086 - 2092	KCIYFAL	0.81	CARC	TH36
2092 - 2098	LSAYQIR	0.86	CRAC	TH36
2098 - 2106	RCGYPTRIL	0.85	CARC	Between TH36 - Anchor alpha1
2112 - 2119	KKYNHLNL	0.80	CARC	Entering Anchor alpha1
2127 - 2135	LVPFLVELR	0.85	CARC	Anchor alpha1 - alpha2/Lipid pocket
2183 - 2194	KKKIVKYGMGGL	0.85	CARC	Entering OH
2231 - 2238	KLGGYEPL	0.86	CARC	CED
2318 - 2327	RFTWNFQRDL	0.76	CARC	CED
2333 - 2339	VEYTNEK	0.66	CRAC	CED
2371 - 2377	LFPKYIR	0.78	CRAC	CED
2422 - 2431	KASDFLEWVV	0.34	CARC	CED
2505 - 2513	LKLCQDIFLV	0.83	CARC	CTD alpha1
2521 - 2528	LEEELYAK	0.82	CRAC	Between CTD alpha1-alpha2

hPiezol	1	MEPHVLGAVLYWLLLPCALLAACLLRFSGLSLVYLLFLLLLPWFPGPTRC
mPiezol	1	MEPHVLGAGLYWLLLPCSTLLAASLLRFNALSIVYLLFLLLLPWLPGPSRH
hPiezol	51	GLQGHTGRLLRALLGLSLLFLVAHLALQICLHIVPRLDQLLGPSCSRWET
mPiezol	51	SIPGHTGRLLRALLCLSLLFLVAHLAFQICLHTVPHLDQFLGQNGSLWVK
hPiezol	101	LSRHIGVTRLDLKDIPNAIRLVAPDLGILVVSSVCLGICGRLARNTRQSP
mPiezol	101	VSQHIGVTRLDLKDIFNTRLVAPDLGVLLASSLCLGLCGRLTRKAGQSR
hPiezol	151	HPREL-----DDDERDVASPTAGLQEAATLAPTRRSRLAARFRVTAH
mPiezol	151	RTQELQDDDDDDDDDEDIDAAPAVGLKGAPALATKRRLWLASRFRVTAH
hPiezol	194	WLLVAAGRVLAVTLLALAGIAHPSALSSVYLLLFALCTWWACHFPISTR
mPiezol	201	WLLMTSGRTLIVIVLLALAGIAHPSAFSSIYLVVFLAICTWWSCHFPLSPL
hPiezol	244	GFSRLCVAVGCFGAGHLICLYCYQMPLAQALLPPAGIWARVLGLKDFVGP
mPiezol	251	GFNTLCVMVSCFGAGHLICLYCYQTPFIQDMLPPGNIWARLFGLKNFVDL
hPiezol	294	TNCSSPHALVLNTGLDWPVYASPGVLLLLCYATASLRKLRAYRPSGQRKE
mPiezol	301	PNYSSPNALVLNTKHAWPIYVSPGILLLLYTATSLLKLHKSCPSELRKE
hPiezol	344	AAKGYEARELELAELDQWPQERESDQHVVPTAPDTEADNCIVHELTTGQSS
mPiezol	351	TPREDEEHELELDHLEPEPQARDATQGEMPMTEPDLDNCTVHVLTSSQSP
hPiezol	394	VLRRPVRPKRAEPREASPLHSLGHLIMDQSYVCALIAMMVWSITYHSWLT
mPiezol	401	VRQRPVRPRLAELKEMSPLHGLGHLIMDQSYVCALIAMMVWSIMYHSWLT
hPiezol	444	FVLLLWACLIWTVRSRHLAMLCSPCILLYGMTLCCCLRYVWAMDLRPELP
mPiezol	451	FVLLLWACLIWTVRSRHLAMLCSPCILLYGLTLCCCLRYVWAMEL-PELP
hPiezol	494	TTLGPVSLRQLGLEHTRYPCDLGAMLLYTLTFWLLLRQFVKEKLLKWAE
mPiezol	500	TTLGPVSLHQLGLEHTRYPCDLGAMLLYLLTFWLLLRQFVKEKLLKKQK
hPiezol	544	SPAALTEVTVADTEPTRTQTLLQSLGELVKGVIYAKYWIYVCAGMFIVVSF
mPiezol	550	VPAALLEVTVADTEPTQTQTLLRSLGELVTGIYVKYWIYVCAGMFIVVSF
hPiezol	594	AGRLVVYKIVYMFLFLLCLTLFQVYYSLWRKLLKAFWWLVVAYTMLVLIA
mPiezol	600	AGRLVVYKIVYMFLFLLCLTLFQVYYSLWRKLLRVFWWLVVAYTMLVLIA
hPiezol	644	VYTFQFQDFPAYWRNLTGFTDEQLGDLGLEQFSVSELSILVPGFFLLA
mPiezol	650	VYTFQFQDFPTYWRNLTGFTDEQLGDLGLEQFSVSELSILIPGFFLLA
hPiezol	694	CILQLHYFHRPFMQLTDMHVSLPGTRLPRWAHRQDAVSGTPLLREEQQE

mPiezo1 700 CILQLHYFHRPFMQLTDLVHVPVPPGTRHPRWAHRQDAVSEAPLL-----

hPiezo1 744 HQQQQQEEEEEEEDSRDEGLGVATPHQATQVPEG-AAKWGLVAERLLELA
mPiezo1 744 -----EHQEEVEVFREDGQSMGPHQATQVPEGTASKWGLVADRLLDLA

hPiezo1 793 AGFSDVLSRVQVFLRRLLELHVFKLVALYTVVVALKEVSVMNLLLVLVLA
mPiezo1 788 ASFSAVLTRIQVFVRRLELHVFKLVALYTVVVALKEVSVMNLLLVLVLA

hPiezo1 843 FALPYPRFRPMASCLSTVWTCVIVCKMLYQLKVVNPQEYSSNCTEPPFN
mPiezo1 838 FALPYPRFRPMASCLSTVWTCIIIVCKMLYQLKIVNPHEYSSNCTEPPFN

hPiezo1 893 STNLLPTEISQSLLYRGPVDPANWFGVRKGFNLYGIQNHLQVLLLLVFE
mPiezo1 888 NTNLPLEINQSLLYRGPVDPANWFGVRKGYPNLYGIQNHLQIILLLVFE

hPiezo1 943 AIVYRRQEHYRRQHQLAPLPAQAVFASGTRQQLDQDLLGCLKYFINFFFY
mPiezo1 938 AVVYRRQEHYRRQHQQAPLPAQAVCADGTRQRLDQDLLSCLKYFINFFFY

hPiezo1 993 KFGLEICFLMAVNVIGQRMNFLT LHGCWLVAAILTRRHRQAIARLWPNYC
mPiezo1 988 KFGLEICFLMAVNVIGQRMNFMVILHGCWLVAAILTRRRREAIARLWPNYC

hPiezo1 1043 LFLALFLLYQYLLCLGMPPALCIDYPWRWSRAVPMNSALIKWLYLPDFFR
mPiezo1 1038 LFLTFLLYQYLLCLGMPPALCIDYPWRWSKAIIPMNSALIKWLYLPDFFR

hPiezo1 1093 APNSTNLISDFLLLLCASQQWQVFSAEERTEEWQRMAGVNTDRLEPLRGE
mPiezo1 1088 APNSTNLISDFLLLLCASQQWQVFSAEERTEEWQRMAGINTDHLEPLRGE

hPiezo1 1143 NPVPNFHICRSYLDMLKVAVFRYLFWLVLVVVFVGTGAT **RISIFGLGYLLA**
mPiezo1 1138 NPVPNFHICRSYLDMLKVAVFRYLFWLVLVVVFVAGAT **RISIFGLGYLLA**

hPiezo1 1193 CFYLLLFGTALLQRDTRARLVLDCLILYNVTVVIISKNMLSLLACVFVEQ
mPiezo1 1188 CFYLLLFGTLLQKDTRAQLVLDCLILYNVTVVIISKNMLSLLSCVFVEQ

hPiezo1 1243 MQTGFCWVIQLFSLVCTVKGYDPKEMMDRDQDCLLPVEEAGIIWDSVCF
mPiezo1 1238 MQSNFCWVIQLFSLVCTVKGYDPKEMMTRDRDCLLPVEEAGIIWDSICF

hPiezo1 1293 FFLLLQR **RVFLSHYYLHV** RADLQATALLASRGFALYNAANLKSIDFHRRRI
mPiezo1 1288 FFLLLQR **RIFLSHYFLHV** SADLKATALQASRGFALYNAANLKSINFHRQI

hPiezo1 1343 EEKSLAQLKRQMERIRAKQEKHRQGRVDRSRPQDTLGPDKPGLPEPDPSP
mPiezo1 1338 EEKSLAQLKRQMKRIRAKQEKYRQSQASRGQLQSK-DPQDPSQEPDPSP

hPiezo1 1393 GGSSPPRRQWWRPWL DHA TVIHSGDYFLFESDSEEEEEAVPEDPRPSAQS
mPiezo1 1387 GGSSPPRRQWWRPWL DHA TVIHSGDYFLFESDSEEEEEALPEDPRPAAQS

hPiezo1 1443 AFQLAYQAWVTNAQAVLRRRQQEQEQARQEQAGQLPTGGGSPSQEVEPAEG
mPiezo1 1437 AFQMAYQAWVTNAQTVLRQR---RERARQERAEQLASGGDLNPDVEPV DV

hPiezo1 1493 PEEAAAGRSHVVQRVLSTAQFLWMLGQALVDELTRWLQEFTRHHGTMSDV
mPiezo1 1484 PEDEMAGRSHMMQRVLSTMQFLWVLGQATVDGLTRWLRAFTKHHRTMSDV

hPiezo1 1543 LRAERYLLTQELLQGGEVHRGVLDQLYTSQAEATLPGPTEAPNAPSTVSS
mPiezo1 1534 LCAERYLLTQELLRVGEVRRGVLDQLYVGEDEATLSGPGVETRDGPSTASS

hPiezo1 1593 GLGAEELPSSMTDDMGSPSTGYHTRSGSEEAVTDPGEREAGASLY----
mPiezo1 1584 GLGAEELPSSMTDDTSSPLSTGYNTRSGSEEIVTDAGDLQAGTSLHGSQE

hPiezo1 1639 -----QGLMRTASELLLDRLRIPELEEAELFAEQGRALRLLRAVYQCV
mPiezo1 1634 LLANARTRMRTASELLLDRLHIPELEEAERFEAQGRTLRLLRAGYQCV

hPiezo1 1684 AAHSELLEYFIIILNHMVTASAGSLVLPVLVFLWAMLSIPRPSKRFWMTA
mPiezo1 1684 AAHSELLEYFIIILNHMVTASAASLVLPVLVFLWAMLTIPRPSKRFWMTA

hPiezo1 1734 IVFTEIAVVVKYLFQFGFFPWNSHVVLRRYENKPYFPPRILGLEKTDGYI
mPiezo1 1734 IVFTEVMVVTKYLFQFGFFPWNSYVVLRRYENKPYFPPRILGLEKTD SYI

hPiezo1 1784 KYDLVQLMALFFHRSQLLCYGLWDHEEDSPSKEHDKSGEEEQGAEEGP--
mPiezo1 1784 KYDLVQLMALFFHRSQLLCYGLWDHEEDRYPKDHCRSSVKDREAKEEPEA

hPiezo1 1832 -----GVP-----AATTEDHIQVEARVGPTDGTPEPQVELRPRDT
mPiezo1 1834 KLESQSETGTGHPKEPVLAGTTPRDHIQGGKSIRSKDVIQDPPEDLKRPT

hPiezo1 1867 RRISLRFRRRKKEGPARKGAAAIEAEDREEEEGEE--EKEAPTGREKRPS
mPiezo1 1884 RHISIRFRRR-KETPGPKGTAVMETE-HEEGEGKETTERKRPRHTQEK-S

hPiezo1 1915 RSGGRVRAAGRRLQGFCLSLAQGTYRPLRRFFHDILHTKY **RAATDVYALM**
mPiezo1 1931 KFRERMKAAGRRLQSFCVSLAQSFYQPLQRFFHDILHTKY **RAATDVYALM**

hPiezo1 1965 **FL**ADVVD FIIIIIFGFWAFGKHSAAATDITSSLSDDQVPEAFVMLLIQFST
mPiezo1 1981 **FL**ADIVDIIIIIFGFWAFGKHSAAATDIASSLSDDQVPQAFVFLMLLVQFGT

hPiezo1 2015 **MVDRALYLRKTVL**GKLA FQVALVLA IHLWMFFILPAVTERMFNQNVVAQ
mPiezo1 2031 **MVIDRALYLRKTVL**GKLA FQVVLVVA IHIWMFFILPAVTERMF SQNAVVAQ

hPiezo1 2065 **LWYFVKCIYFALSAYQIRCGYPTRI**LGNF LT **KKYNHLNL**FLFQGF **RLVPE**
mPiezo1 2081 **LWYFVKCIYFALSAYQIRCGYPTRI**LGNF LT **KKYNHLNL**FLFQGF **RLVPE**

hPiezo1 2115 **LVEL**RAVMDWVWTDTTLSLS S WMCVEDIYANIFI I KCSRETEKKYPQPKG
mPiezo1 2131 **LVEL**RAVMDWVWTDTTLSLS N WMCVEDIYANIFI I KCSRETEKKYPQPKG

hPiezo1 2165 QK**KKKIVKYGMGGL**IILFLIAIIWFPLLFMSLVRSVVGVVNQPIDVTVTL
mPiezo1 2181 QK**KKKIVKYGMGGL**IILFLIAIIWFPLLFMSLIRS SVVGVVNQPIDVTVTL

hPiezo1 2215 **KLGGYEPL**FTMSAQQPSIIPFFTAQAYEELSRQFDPQPLAMQFISQYSPED
mPiezo1 2231 **KLGGYEPL**FTMSAQQPSIVPFTPQAYEELSQQFDPYPLAMQFISQYSPED

hPiezo1 2265 IVTAQIEGSSGALWRISPPSRAQMKRELYNGTADITLRF'TWNFQORDLAKG
mPiezo1 2281 IVTAQIEGSSGALWRISPPSRAQMKQELYNGTADITLRF'TWNFQORDLAKG

hPiezo1 2315 GTVEYANEKHMLALAPNSTARRQLASLLEGTSDQSVVIPNLFPKYIRAPN
mPiezo1 2331 GTVEYTNEKHTLELAPNSTARRQLAQLLEGRPDQSVVIPHLPKYIRAPN

hPiezo1 2365 GPEANPVKQLQPNEEADYLGVRIQLRREQ-GAGATG-----FLEWW
mPiezo1 2381 GPEANPVKQLQPDEEEDYLGVRIQLRREQVGTGASGEQAGTKASDFLEWW

hPiezo1 2405 VIELQECRTDCNLLPMVIFSDKVSPPSLGFLAGYGIMGLYVSIVLVIGKF
mPiezo1 2431 VIELQDCKADCNLLPMVIFSDKVSPPSLGFLAGYGIVGLYVSIVLVVGKF

hPiezo1 2455 VRGFFSEISHSIMFEELPCVDRIL**KLCQDIFLV**RETRELE**LEEELYAKLI**
mPiezo1 2481 VRGFFSEISHSIMFEELPCVDRIL**KLCQDIFLV**RETRELE**LEEELYAKLI**

hPiezo1 2505 FLYRSPETMIKWTRERE
mPiezo1 2531 FLYRSPETMIKWTRERE

Figure 6.3: Alignment of human and mouse Piezo1 with highlighted highly conserved cholesterol binding motifs. CRAC domains are highlighted in blue and CARC domains are highlighted in green. Where they overlap the corresponding colour is highlighted above or below.